University of Udine
Department of Medicine (DAME)

PhD Course in Biomedical Science and Biotechnologies XXXI cycle

Oncogenic *KRAS* controls the redox homeostasis and survival/apoptosis pathways in pancreatic cancer cells: mechanistic and therapeutic aspects

PhD student: Annalisa Ferino

Supervisor: Prof. Luigi E. Xodo

Academic year 2018-2019

UNIVERSITÀ DEGLI STUDI DI UDINE
hic sunt futura

www.uniud.it

PhD course in Biomedical Science and Biotechnologies

University of Udine

XXXI cycle

Oncogenic *KRAS* controls the redox homeostasis and survival/apoptosis pathways in pancreatic cancer cells: mechanistic and therapeutic aspects

PhD student: Annalisa Ferino

Supervisor: Prof. Luigi E. Xodo

2018

Ma lei era di quel mondo dove le più belle cose

hanno il peggior destino,

e Rosa, lei ha vissuto quel che vivono le rose

lo spazio d'un mattino.

(*Francois de Malherbe*)

A Susanna

Sommario

1. ABSTRACT

Mutations in the *ras* genes are present in about 30% of all human cancers, but more than 90% of pancreatic ductal adenocarcinomas (PDACs) carry mutations in exon 1 of the *KRAS* gene: a genetic lesion that drives the malignant transformation of the cells. The main function of mutant *KRAS* in PDAC is to reprogram the metabolism in order to generate, from glucose and glutamine, the biomass and the reducing power necessary to fuel a high rate of proliferation.

As pancreatic cancer cells are addicted to *KRAS*, this oncogene is considered the main target for the design of new and innovative therapeutic strategies.

Recent studies have demonstrated that the promoter of *KRAS* contains a G- rich sequence motif located immediately upstream of the transcription start site (TSS). This sequence contains a non-canonical DNA structure, called G-quadruplex (G4).

This discovery, which was carried out in our laboratory in 2006 [1], raised many questions about the capacity of the G4 motif to form, under physiological conditions, a stable G4 structure. As the G4 motif is located near to TSS, a challenging question is to know if this folded DNA conformation is somehow implicated in transcription regulation. Although this issue has been addressed by many studies, the role of the G4 DNA in gene expression is not yet clear. However, in our laboratory we found that the G4 of *KRAS* is recognized by several transcription factors (TFs), including MAZ, hnRNP A1, PARP-1 and OGG1.

As PDAC cells have a high metabolic rate, they produce more reactive oxygen species (ROS) than healthy cells. A high intracellular level of ROS is toxic and oxidize lipids, proteins and DNA. These chemical modifications of the macromolecules, impair their function leading to cancer cells death by apoptosis. To avoid this unfavourable outcome, cancer cells have developed specific metabolic pathways, in order to control the redox homeostasis. The protein that behaves as a master regulator of oxidative stress is Nrf2, a transcription factor that, when ROS increases, migrates from the cytoplasm to the nucleus where it binds to a specific sequence of DNA, corresponding to the antioxidant response element (ARE). This stimulates the expression of several antioxidant genes that bring down ROS to levels suitable for optimal proliferation.

We found that in PDAC cells the ectopic expression of mutant *KRAS* G12D or G12V results in the upregulation of Nrf2, suggesting that the oncogenic *KRAS* controls the redox homeostasis through Nrf2 expression. Therefore, we also found that an increase of ROS upregulates *KRAS*.

So, all the results taken together show that the redox balance in PDAC cells is maintained by an axis composed by ROS, *KRAS* and Nrf2. This axis has a function that goes beyond the control of the redox homeostasis, as it affects also the survival and apoptosis pathways involving Nf-κB, Snail and RKIP. Our data show that low ROS levels result in the upregulation of NF-κB and pro-survival Snail and the simultaneously downregulation of pro-apoptotic RKIP: this gene expression pattern favours cell proliferation. By contrast, high ROS favour apoptosis by upregulating pro-apoptotic RKIP and downregulating NF- κB and pro-survival Snail.

We then addressed the issue of how ROS upregulate *KRAS*. Evidence that ROS stimulate *KRAS* through a mechanism involving guanine oxidation in the G4 motif is provided. It should be noted that among the four DNA bases, guanine, having the lowest redox potential, is prone to oxidation to 7,8-dihydro-8-oxo-guanine (8OG). ChIP and qPCR-Real Time experiments showed that 8OG is more abundant in the G4 motif region of *KRAS* than in non-G4 regions, suggesting that the critical G4 motif is a hotspot for guanine oxidation. We hypothesised that this epigenetic modification plays a critical role in regulating the expression of *KRAS*.

We moreover asked if 8OG affects the quadruplex structure formed in the promoter of the *KRAS* gene. In order to answer to this question, we designed a series of oligonucleotides mimicking the G4 motif, hosting 8OG in specific positions. By DMS footprinting, UV-spectroscopy and circular dichroism experiments, we analysed their capacity to fold into a stable G4. We found that 8OG has a strong impact on G4. When 8OG is located in a loop of the G4, both topology and stability of the G4 structure do not change. In contrast, when it is located in a G-run forming a G-tetrad, the G4 motif folds in an alternative way and replaces the oxidized G-run with the extra G-run present in the G4 motif sequence. The resulting G4 has a different topology and a T_M 10 °C lower than the T_M of the wild type G4.

Interestingly, we also found that the transcription factors MAZ, hnRNP A1 and PARP1 are recruited more efficiently to the G4 motif when it hosts oxidized guanines. Thanks to the binding to G4, MAZ and hnRNP A1 unfold the structure and induce the G4 motif to assume the duplex conformation. Besides TFs, hOGG1 is also recruited to the oxidized G4 motif. This glycosylase recognizes the G4 motif in duplex and excises 8OG though the base excision repair (BER) process. The free-excised 8OG binds to hOGG1 and the complex behaves as guanine exchange factor activating the *KRAS* protein by transforming KRAS-GDP into KRAS-GTP.

In the light of our findings, we have designed two anticancer strategies to inhibit *KRAS* in PDAC cells.

The first is based on the use of photosensitizers generating ROS together with Nrf2 inhibitors. Under these conditions, the photosensitizer produces high levels of ROS that trigger apoptosis.

The second considers that in pancreatic cancer several microRNAs are aberrantly downregulated. We discovered that miR-216b is one of this microRNA aberrantly downregulated in PDAC. We thus designed miR-216b mimics with unlocked nucleic acids (UNA) modifications to make it more resistant to endogenous nucleases. We found that the designed UNA-modified miRNAs strongly suppressed KRAS gene in an AGO2- dependent manner.

To conclude, although the research in oncology has made important achievements in the treatment of many human tumours, PDAC remains one of the deadliest disease with a poor prognosis. We think that our research may be useful in the rationale design of new and innovative anticancer strategies against PDAC.

2. INTRODUCTION

2.1 Pancreatic Cancer

Pancreatic ductal adenocarcinoma (PDAC) is an aggressive disease which represents one of the main causes of death in western countries [2]. There are many risk factors leading to this malignant disease, including cigarette smoking, family history of pancreatic cancer and chronic pancreatitis [3,4]. Generally, this type of tumour is asymptomatic and often, when diagnosed, it is untreatable, leading to a 5-year survival rate of only 5% [5,6]. Since PDAC shows a little response to conventional chemotherapy, tumour resection remains the main option. Unfortunately, many patients are not eligible for resection and, even when the latter is carried out, the patients face problems of recurrence.

PDAC is the most common form of pancreatic cancer, it arises in the exocrine part of the organ and starts from small non-invasive precursor lesions known as PanIN (Pancreatic Intraepithelial Neoplasia).

As already known, cancer is a genetic disease due to accumulation of somatic mutations in both oncogenes and tumour suppressor genes. Four genes resulted to be directly involved in the development of PDAC and the activation or suppression of their downstream signals play an important role in the initiation and progression of the malignancy. These critical genes are *KRAS*, *CDKN2A*, *TP53* and *SMAD4*.

KRAS is a proto-oncogene and it is found to be altered in more than 90% of PDAC patients. Point mutations, occurring mainly at codon 12 or 13, result in the production of an activated protein that controls several signalling pathways. The other three critical genes are tumour suppressor genes implicated in the control of cell cycle regulation (*CDKN2A*), in cellular stress response (*TP53*) and in signalling mediated by transforming growth factor β, TGFβ (*SMAD4*) [3,4].

2.2 RAS family

The role of the *ras* genes in the development of cancer was discovered in the mid-1960s, laying the molecular basis for cancer studies.

By investigating transforming retroviruses isolated from mice, rats, monkeys or chickens, scientists found that these viruses were able to cause a rapid onset of sarcoma in infected animals and transformation of cultured cells [7]. The first two viruses were discovered in rats by Jennifer Harvey [8] and Werner Kirsten [9] and were therefore called Harvey and Kirsten murine sarcoma viruses [8,10,11]. The ability of these genes to cause sarcoma in rats is the reason of their name (RAS derives from RAT Sarcoma), but at the beginning *ras* genes were considered variants of *src* genes [12,13]. In 1974, Scolnick and his collaborators speculated that the oncogenic potential of the sarcoma viruses were linked to their capacity to transduce normal cellular rat sequences into their own genomes [14], but years later other studies found out that tumours can be caused by mutations occurring in proto-oncogenes. In 1982, Geoffrey Cooper and his group published a study on human bladder and human lung carcinoma cell lines in which they found that the transforming genes in these cell lines were homologs of the *ras* genes of Harvey and Kirsten sarcoma viruses [15], and other works reported the presence of other homologous genes in human genome [16].

2.2.1 RAS proteins

The *ras* genes encode for low molecular weight GTPases (guanosine triphosphatesis) involved in signal transduction pathways which control proliferation, survival, growth, differentiation and other related important functions. The ras family includes three genes *HRAS*, *KRAS* and *NRAS*, encoding for highly homologous proteins of 21 KDa. There are two different isoforms for the KRAS protein, namely KRAS4A and KRAS4B, which derive from alternative splicing.

These proteins contain two functional domains: the membrane targeting domain and the G domain.

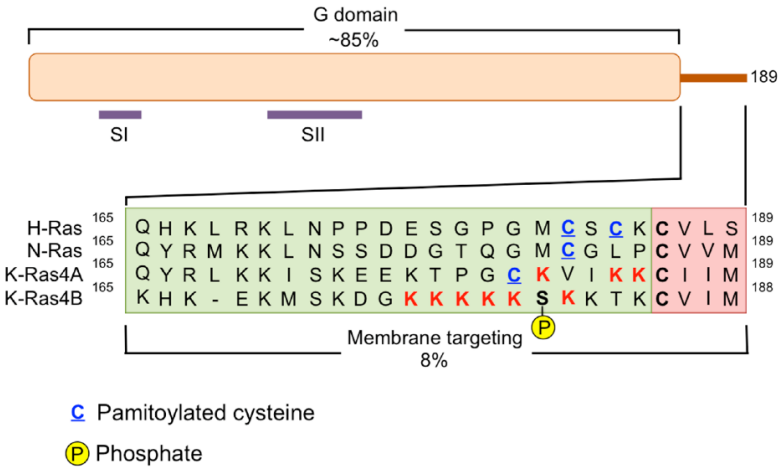

Figure 1. Representation of the two functional domains of RAS proteins: the G-domain shows a high similarity between different RAS isoforms and contains the two regions Switch I (SI) and Switch II (SII) important for the binding with protein effectors; the membrane targeting domain is the hypervariable region. (*Zeitouni D., 2016*)

The membrane targeting domain, located in the C-terminal domain of the protein, is a hypervariable region (HVR) and the three RAS isoforms show in this region the greatest diversity in amino acid sequence [17]. The C-terminal domain undergoes post-translational modifications, which make the RAS proteins functionally active. The first step consists in the lipid modification of the Cys186 in the "CAAX box", that is an important process driving the RAS localization [18]. In the CAAX motif, C represent cysteine, A is an aliphatic amino acid and X denote the terminal amino acid, which can be serine, methionine, glutamine or leucine and plays an important role in determining the type of lipid modification: farnesylation or geranylgeranylation. The farnesylation process consists in the binding of 15-carbon farnesyl group by the enzyme farnesyl transferase (FTase), whereas in the geranylgeranylation process, the Leu in CAAL allows the linkage of a 20- carbon geranylgeranyl chain by geranylgeranyl transferase [7,19,20]. Thanks to these modifications the immature proteins become more hydrophobic and show a higher affinity for the endoplasmic reticulum (ER) membrane [18]. In ER, the last three amino acids of either CAAX or CAAL are proteolytically cleaved by the RAS - converting enzyme 1 (Rce1) and the carboxyl terminal group is methylated. The final modification consists in the palmitoylation, which increases biological activity and membrane affinity of the mature RAS protein and allows its translocation to the plasma membrane [7,19].

The catalytic G-domain of 164 residues contains the regions of the protein responsible for binding to GTP and its hydrolysis to GDP. This domain is highly conserved in the three different isoforms (80% of sequence homology), even when the RAS mutations, that are critical for the catalytic activity of the protein, occur in the residues 12, 13 or 61 of this domain [21].

RAS proteins' activity is controlled by an on-off mechanism depending on GTP - GDP binding. The binding of GTP to the phosphate-binding loop present in the catalytic domain causes a conformational change in other two regions called Switch I and Switch II and permits the interaction with effectors molecules [17]. RAS proteins have a rather weak intrinsic capacity to hydrolyse GTP to GDP and their inactivation is mediated by a class of proteins called GAPs (GTPase activating proteins), which are able to speed up the hydrolysis. The two most studied GAPs proteins are $p120^{GAP}$ and NF1 [10].

$p120^{GAP}$ was the first identified RAS regulator and shows a catalytic domain that binds to the RAS effector domain in order to stop the RAS signalling. NF1 represents the tumour suppressor gene neurofibromatosis type I and contains a sequence homologous to $p120^{GAP}$: this factor encodes for a protein that is responsible for the RAS inhibition, favouring the GTP hydrolysis. It has been reported that mutations or deletions of the NF1 gene are associated to an increased risk of cancer development [22–24].

As RAS mutations are generally related to the loss of interaction between GAPs and RAS, these proteins are very important for the regulation of RAS hyperactivation and therefore for tumorigenesis prevention.

Other important RAS regulators are represented by a group of proteins called GEFs, or guanine nucleotide exchange factors, which control the switch between the GDP- bound inactive state and the GTP-bound active state, catalysing the exchange of GDP with GTP [22]. Since RAS proteins show a high affinity for both GDP and GTP, the nucleotide dissociation rate is slow and GEFs proteins play an important role, as the exchange of GDP for GTP is a rather fast process taking place within minutes or even less [25]. These proteins are reported to increase the exchanging rate by several orders of magnitude [26]. Three classes of GEF effectors containing the CDC25 catalytic domain and the N- terminal RAS exchange factor domain have been discovered: SOS, RAS-GRF and RAS- GRP. The SOS family consists of two proteins, SOS1 and SOS2, and their action on

nucleotide binding is due to their capacity to modify Switch I and Switch II residues on RAS proteins, leading to GDP release and favouring GTP replacement [27] (*Figure 2*).

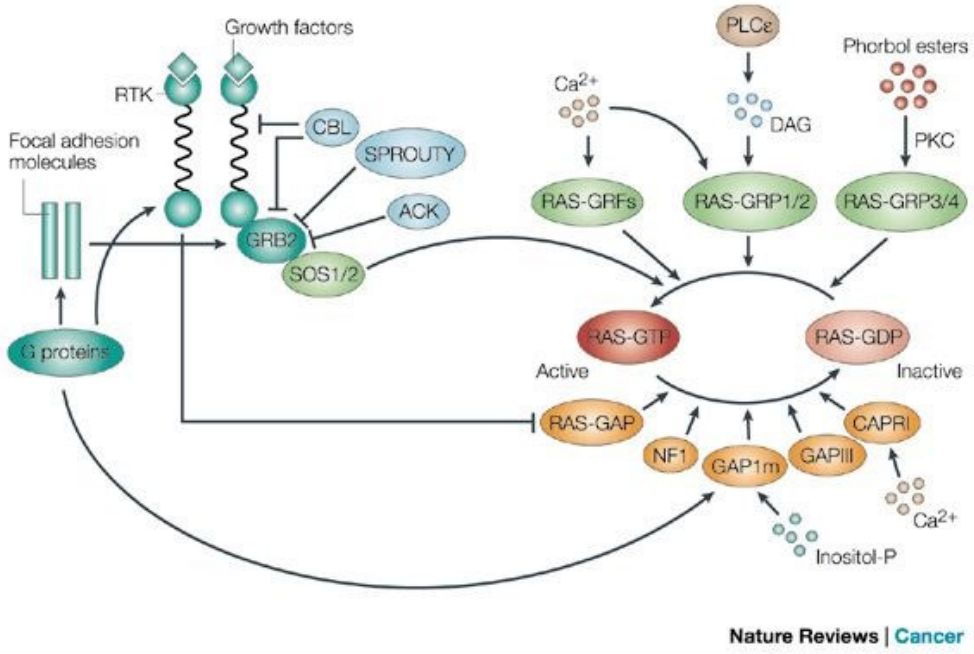

Figure 2. RAS regulation mediated by GAPs and GEFs effectors (*Malumbres M, 2003*)

2.2.2 KRAS and pancreatic cancer

As before mentioned, the most frequent type of tumour in human pancreas is pancreatic ductal adenocarcinoma and the principal cause of its development and progression is represented by activating mutations in the *KRAS* oncogene. It has been found that human pancreatic cancers present predominantly three specific single point mutations in exon 1 at residues G12, G13 and Q61. In particular, mutations at G12 or G13 create steric hindrance that avoids the interaction between RAS and GAPs and leads to a constitutive RAS activation. On the other hand, substitutions at residue Q61 block the critical coordination of a water molecule for nucleotide hydrolysis [28].

As all the mutations give RAS proteins constitutively active, the final result is the stimulation of downstream signalling pathways, leading to the increase of cell proliferation and survival, suppression of apoptosis, production of changes in tumour microenvironment, promotion of metabolic alterations and metastasis development (*Figure 3*).

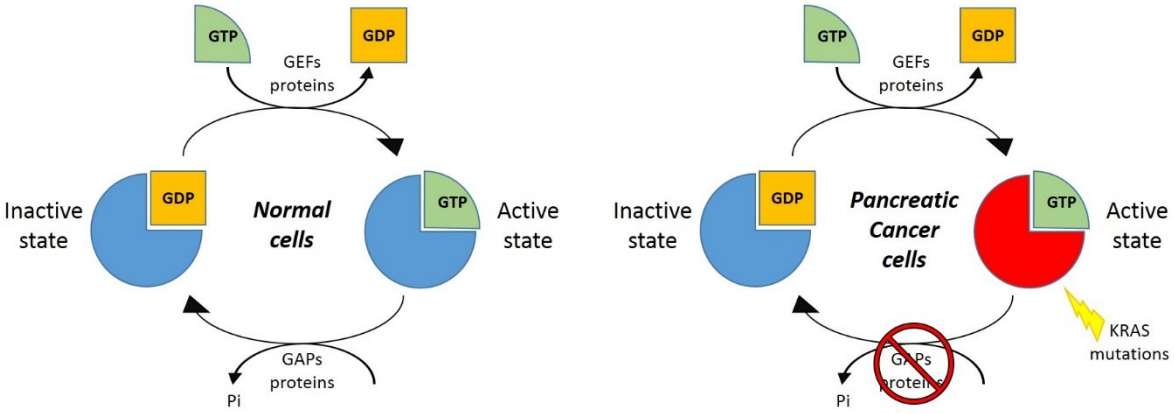

Figure 3. KRAS regulation in normal cells (left) and in pancreatic cancer cells (right).

In past years it has been shown that KRAS G12D plays a critical role in the progression of pancreatic cancer and, using experimental models, it has been demonstrated that this particular mutation is fundamental for tumour cell survival [29–31]. This point mutation consists in the substitution of glycine (G) with an aspartic acid (D) residue in exon 1, codon 12, leading to a constitutively active protein. As a result, constant KRAS G12D signalling brings to aberrant proliferation and increases the survival of cancer cells through the activation of downstream signalling pathways, as MAPK and PI3K- mTOR (*Figure 4*).

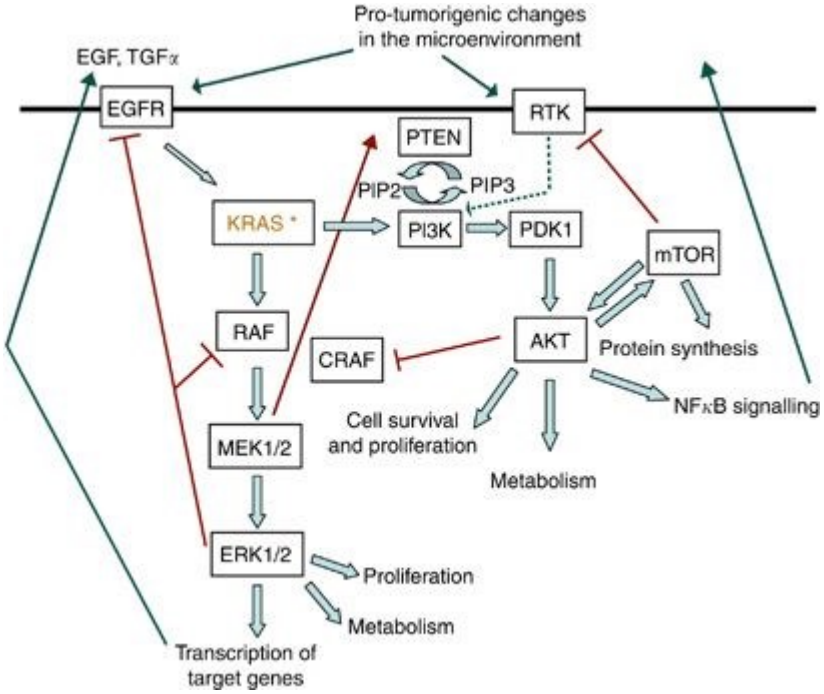

Figure 4. KRAS downstream signalling pathways. (*Eser S, 2014*)

Starting from the observation that cancer is a genetic disease caused by alterations occurring in cells, we can affirm that pancreatic ductal adenocarcinoma development is the result of several mutagenic events occurring in normal pancreatic cells.

In particular, *KRAS* mutations cause PanIN lesions that are small non- invasive precursor lesions. Then additional genetic alterations lead to the progression of the malignancy. Di Magliano and Logsdon, by studying the role of *KRAS* oncogene in pancreatic tumour development and progression, found that the effect of KRAS inactivation is time dependent [32]. Oncogenic *KRAS* is important at early stages of lesion formation: indeed, the inactivation of the protein leads to apoptosis or cancer regression [33]. Despite this, the transformation of PanIN lesions into adenocarcinoma requires additional mutations, such as loss of function of several tumour suppressor genes (p53 or p16) [34]. Moreover, to highlight the critical role of the *KRAS* gene in PDAC, it has been reported that its inactivation in the advanced disease causes tumour regression but the specific mechanisms have not been yet identified. However, a small fraction of tumour cells, which conserves the mutations in *KRAS* gene and in other related genes, continues to proliferate leading to metastasis [32]. These findings let to think that PDAC is closely related to *KRAS* activation.

Other recent data have demonstrated that pancreatic cancer cells are addicted to oncogenic *KRAS*. This means that the cells, in order to support their enhanced metabolic rate, require a constitutive expression of KRAS. Cells with a high rate of division need energy and biomass (biosynthetic precursors): this is obtained by modifying the metabolism which is reprogrammed by oncogenes [31,35]. In fact, DePinho and his group have recently found that oncogenic KRAS reprograms the glucose and glutamine (Gln) metabolism in PDAC, so as satisfy the high anabolic request typical of dividing cells. In particular they found that, when the KRAS activity is abolished in PDAC cells, a significant decrease of some glycolytic components is observed, such as glucose-6- phosphate (G6P), fructose-6-phospate (F6P) and fructose-1,6-bisphosphate (FBP). Authors also found that oncogenic *KRAS* increases the glycolytic flux, affecting glucose uptake and lactate production [31]. Together, these metabolic changes are responsible for the so- called Warburg effect, according to which cancer cells consume big amount of glucose even in the presence of oxygen: an apparent metabolic paradox considering

that, in the presence of oxygen, cells can efficiently produce energy with a high ATP/glucose yield through the aerobic mitochondrial metabolism [36,37].

So, why do cancer cells require glucose more than healthy cells? The answer to this question is quite simple: cancer cells require biomass to sustain a high rate of cell division. A high glycolytic flux provides the cells carbon atoms for the synthesis of essential molecules such as ribose, nucleotides, amino acids, phospholipids and many other essential compounds (*Figure 5A*) [38]. As illustrated in *Figure 5B*, Serine plays a critical role in the generation of amino acids and nucleotides. KRAS increases the activity of enzyme phosphoglycerate dehydrogenase (PHGDH), which substracts 3- phosphoglycerate (3PG) to the glycolytic flux, directing it towards the synthesis of Serine (Ser). This amino acid is essential for several anabolic pathways. For example, it is transformed into glycine (Gly) by providing a methyl group to folic acid (FA). By interacting with methionine, Ser can also provide cysteine (Cys). Methyl-THF is then involved in the synthesis of nucleotides.

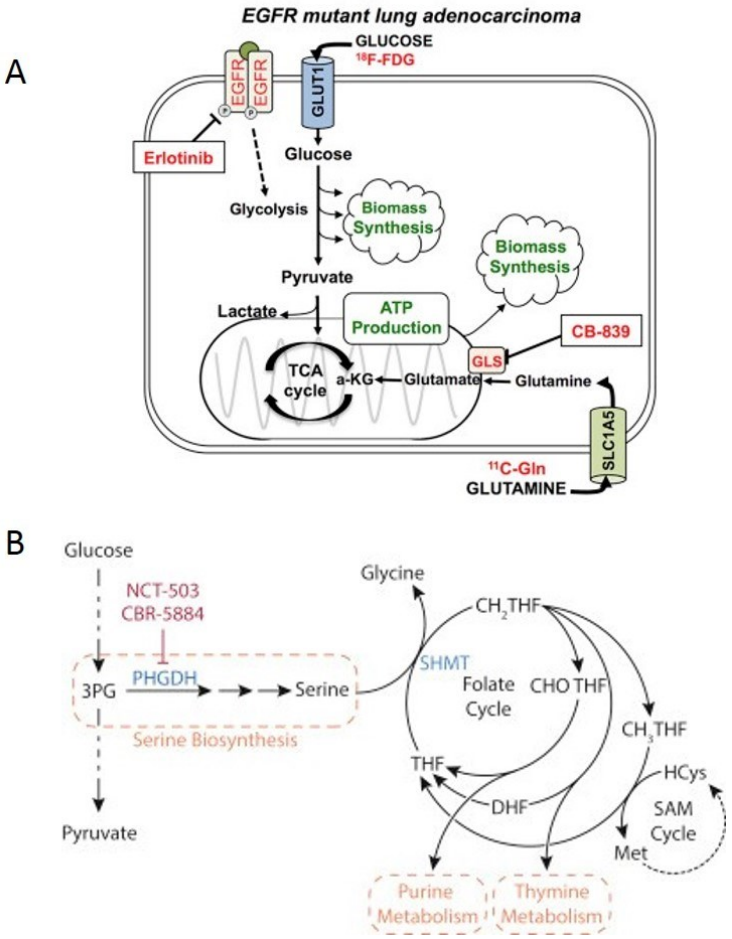

Figure 5. (A) The enhanced glycolytic flux in cancer cells fosters the synthesis of essential molecules. (*Cell Rep*. 2017 Jan 17; 18(3): 601–610.) (B) Serine biosynthesis and folate cycle are important pathways for the generation of amino acids and nucleotides (*Luengo A, 2017*)

In addition to glycolysis, the metabolic rewiring caused by KRAS affects also the Gln fate, which does not follow the canonical oxidative pathway through the tricarboxylic acid (TCA) cycle [39,40]. Gln is transformed into aspartate (Asp), and then translocated in the cytoplasm where it is converted to oxaloacetate (OOA). OOA is reduced to malate which is then decarboxylated to pyruvate: a process associated with the increase of NADPH/$NADP^+$ ratio, i.e. an increasing of reductive power, which is important for the maintenance of the redox homeostasis [39]. Moreover, Gln in PDAC is essential not only because it functions as a carbon source for the TCA cycle, but also because it supplies nitrogen for nucleotides, nonessential amino acids and hexosamine biosynthesis [41] (*Figure 6*).

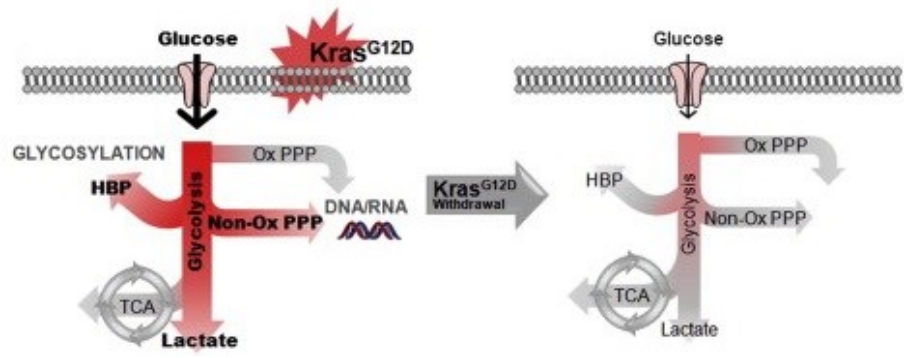

Figure 6. Effect of mutated KRAS on glucose metabolism and changes that happen upon $KRAS^{G12D}$ withdrawal. (*Ying H,2012*)

2.2.3 Targeting RAS as a therapeutic strategy

As RAS proteins play a central role in the malignant transformation and progression of PDAC, it is of great therapeutic significance to find strategies for targeting these proteins in order to cure PDAC. It is known that *ras* are the most mutated genes in human cancer [42]. The three *ras* isoforms are not equally mutated in human tumours: *KRAS* mutations are present in about 86% of human tumours, *NRAS* mutations in 11% of tumours and *HRAS* mutations only in about 3% of tumours. There are specific correlations between cancer and mutated *ras* isoforms: for example, PDAC and lung adenocarcinoma show preferentially *KRAS* mutations, whereas cutaneous melanoma and acute myelogenous leukaemias show preferentially mutations in *NRAS* gene. Mutations in both *KRAS* and *NRAS* can be found in colon and rectal carcinoma and also in multiple myeloma. Bladder cancer and head-neck squamous cell carcinoma show preferentially *HRAS* mutations [43].

These different isoform mutations observed in human cancer suggest that every tumour may need to be targeted in a different way. Efforts done up to now by the scientific community and by private pharmaceutical industries have not produced effective anti- *ras* therapeutics. Target therapy against RAS protein did not give the expected results and the opinion that *ras* is "undruggable" has become widespread in the research field. Because of this, the search for new targets to cure PDAC is one of the biggest challenges in therapy [17,43].Considering that KRAS is responsible for the initiation and

maintenance of PDAC, this critical oncogene remains the main target for the rational design of new therapeutic strategies.

Several types of anti KRAS approaches have been tested: (i) development of inhibitors binding to the RAS protein; (ii) inhibitors against the RAS membrane association; (iii) inhibitors capable to target downstream effectors of RAS signalling; (iv) synthetic lethality approach; (v) inhibitors against metabolic target; (vi) strategies against KRAS DNA and KRAS mRNA (*Figure 7*).

The first approach, based on the development of inhibitors binding to the RAS protein, showed to be rather difficult to apply. Computational studies allow to identify potential binding sites, but the hydrophobic pockets on the surface of the RAS protein are not deep enough to host a therapeutic molecule [43–45]. Several compounds were tested but all failed to give interesting results and showed in vivo toxicity. SCH-53239 was designed to compete with the binding of GDP [46] while other compounds based on non-steroidal anti-inflammatory drug (sulindac sulphide) were anticipated to inhibit RAS/RAF complex formation [47].

In addition, other molecules have been developed to inhibit the interaction between RAS and other cellular factors. The RAS/RAF interaction is one of the most targeted: MCP1 and derivatives, in addition to the inhibition of RAS/RAF binding, showed the capacity to revert the malignant phenotype, even if they did not result strong enough [48,49]. Genentech developed a compound called DCAI, which inhibits SOS- mediated nucleotide exchange by preventing the interaction between RAS and SOS [50]. Unfortunately, this molecule binds weakly to KRAS.

Because this first approach based on molecules designed to inhibit RAS proteins did not give promising results, the research concentrate the efforts to develop inhibitors against the RAS membrane association. The attention was focused on farnesyl transferase inhibitors (FITs) [51,52]. FTase is the enzyme that catalyses the addiction of a 15-carbon farnesyl group to immature RAS protein. With this modification, the RAS protein become more hydrophobic and it is targeted to endoplasmic reticulum for the final modifications. FITs can prevent RAS protein activation and several studies showed that there are effective therapeutic molecules but they are not useful against all RAS isoforms. As a matter of fact, some FITs compounds, such as lonafarnib or tipifarnib, have been tested in clinical trial and showed activity only in *HRAS*-mutant cancers [53].

This happens because if FTase activity is blocked, KRAS and NRAS proteins become substrates for geranylgeranyltransferase, another enzyme that add a C-20 geranylgeranyl isoprenoid group allowing the protein membrane association [53–55].

To overcome the problems related to differences in the RAS maturation process, researchers focus their attention on another strategy to obtain RAS inhibition, designing molecules capable to target downstream effectors of RAS signalling. Many drugs targeting RAS effectors were developed and tested in clinical trials, but until now, all these compounds remain only in early phase trials [56,57]. This strategy seems to be promising, but there are some problems to face: for example the cells are able to display some compensatory mechanisms when an important pathway is blocked, decreasing the efficacy of the treatment. Moreover, it could be necessary to inhibit not only one but several pathways that normally cross talk. This leads to the development of combining inhibitors against RAF and PI3K effectors that allow to obtain a greater outcome in terms of inhibition of RAS activity [57,58]. However, this method shows an important side effect related to increased toxicity in normal cells [43].

Because all these approaches, which target RAS proteins or their effectors, show several issues that need to be addressed and result to be a challenge for many reasons, it may be necessary to move to other directions.

The fourth anti KRAS approach deals with the concept of synthetic lethality. This method suggests that the identification of specific targets showing synthetic lethal interaction with RAS could increase therapeutic selectivity. The synthetic lethality is described as the co-occurrence of two genetic events that can bring to cell death [59]. The application of this approach is based on the discovery of genes whose inhibition would be lethal only when RAS is mutated [17,43]. Although this approach has not been yet tested in human cancer therapy, several synthetic lethal targets have been identified and this strategy seems to provide a new therapeutic framework.

In order to sustain the high metabolic rate, cancer cells enhance their metabolism and KRAS has been reported to be a key factor in promoting metabolic rewiring. Starting from this observation, it is easy to identify another anti KRAS approach based on the use of inhibitors directed against metabolic targets. Targeting metabolic pathways would be an interestingly anti-cancer strategy because normal cells, which are not KRAS-addicted, may be not affected by the treatment [43]. To sustain this hypothesis, Glutaminase

inhibitors have been tested in early phase clinical trials [60]. These molecules are able to alter the redox balance in pancreatic cancer cells blocking the action of glutaminase, an enzyme that catalyses the conversion of glutamine to glutamate. Moreover, if in combination with treatments that increase ROS, the glutaminase inhibitors are able to reduce pancreatic cancer growth [39].

Other drugs are used to obtain the inhibition of autophagy and macropynocitosis (HCQ), or to reduce glucose metabolism by blocking the mitochondrial complex I or MEK (phenformin / metformin) [39,60,61].

Findings demonstrating the importance of redox balance and the role of KRAS in maintaining ROS homeostasis through Nrf2 stimulation, suggest an interesting scenario: if controlled level of ROS promotes tumour development, the modification of redox balance in KRAS-driven tumours may represent an efficacy strategy to inhibit PDAC development [43,62].

Even if these three decades of research have not given amazing results in the field of RAS-targeting molecules and pancreatic tumour strategies yet, a greater knowledge about RAS proteins, differences between three RAS isoforms, processes mediated by these proteins and implication of mutated RAS in the regulation of metabolism have been achieved.

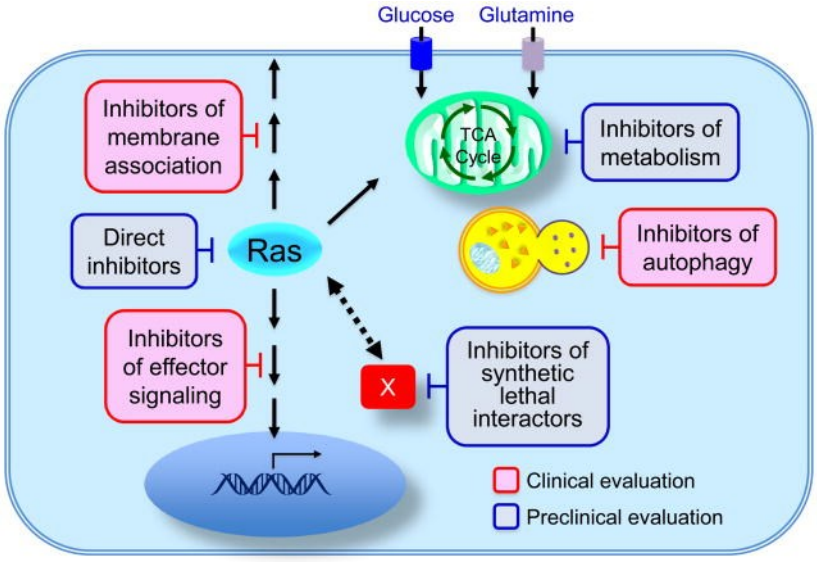

Figure 7. Representation of RAS inhibitors classes. (*Cox A D, 2014*)

Finally, based on the fact that target therapy against the RAS proteins did not give the expected results, many scientists focused on the gene itself and hypothesised several strategies to directly suppress KRAS in PDAC cells [63–65]. These strategies are based on the experimental findings that the suppression of KRAS in PDAC triggers a cell response, leading to apoptosis.

To design molecular approaches aiming at the inhibition of gene expression at transcriptional or translational level, it is important to know the mechanisms of transcription and translation. The research so far done in this field, to which also the laboratory where I have worked for my PhD has contributed, has put in evidence that the *ras* gene has promoters characterized by a high C+G regions, in particular upstream of the transcription start site (TSS). These G-rich regions have two important characteristics: first, they are structurally polymorphic and can form unusual G- quadruplex structures; second, guanines present in clusters can easily undergo oxidation to 8-oxoguanine (8OG). As reported in the results of this PhD work, G- quadruplex and 8OG play a crucial role in the biology of KRAS in PDAC cells.

Moreover, new therapeutic strategies are represented by microRNAs (miRNAs), which are small non-coding RNAs of approximately 20-22 nucleotides and act as post- transcriptional regulators. Immature miRNAs are initially transcribed as pre- miRNAs, then processed by Drosha in the nucleus and Dicer in the cytoplasm [66]. MicroRNAs are not able to act by themselves and need to be incorporated with Argonaute (AGO) family of proteins in a complex called RISC (RNA-induced silencing complex) [67,68]. Mature miRNAs in the RISC complex recognize complementary sequences on mRNA and cause mRNA degradation leading to the inhibition of translation. So, miRNAs can act as tumour suppressors.

It was reported from several studies that different miRNAs resulted deregulated in tumours bearing *ras* mutated oncogenes. For example, it was found that *let-7* miRNA family is implicated in the negative regulation of *ras*, both in *C. Elegans* tissues and in human cell lines [69]. Moreover, its expression is higher in normal adult lung tissue than lung cancer tissue, suggesting a possible role of this miRNA as tumour suppressor.

A Chinese group demonstrated that miR-96 targets the KRAS oncogene and acts as tumour suppressor gene in pancreatic cancer, leading human cells to apoptosis [63]. Furthermore, studying miRNA incidence in nasopharyngeal carcinoma (NCP), Guiyuan Li

and his collaborators found out that miR-216b is downregulated in NCP cell lines. They demonstrated that miR-216b binds to the 3'-UTR of KRAS mRNA and inhibits the expression of the gene leading to the suppression of tumour growth and invasion [70].

As microRNAs act as tumour suppressors, they can be used as anti *ras* agents and may represent drug targets for anticancer drug development [71].

2.3 Quadruplex DNA: a non-canonical structure

The common structure of DNA is a double helix, called B-DNA, which was discovered in 1953 by James Watson and Francis Crick. In addition to the canonical structure, DNA can assume several other conformations called non-canonical DNA structures, which include G- quadruplexes, triplexes, cruciforms, hairpins, Z-DNA, i-motifs and RNA:DNA hybrids (*Figure 8*) [72–74]. Recent studies showed that these structures can interact with specific proteins involved in transcription, translation, replication or recombination [75–78]. Unusual DNA structures can have a role also on DNA damage and repair [75,79,80]. In this work, as non- canonical DNA conformation, we focus on G- quadruplex DNA, since this structure has drawn the attention of many scientist in the last two decades and evidences that it occurs under in vivo conditions have been provided.

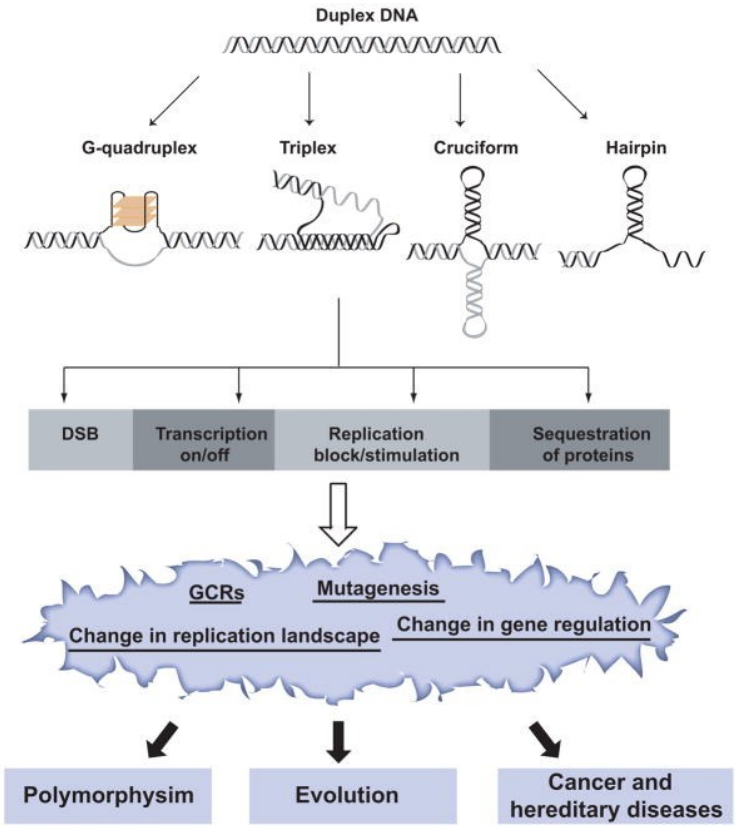

Figure 8. Possible non-canonical conformations of B-DNA and their effects on DNA stability and regulation. (*Saini N, 2013*)

2.3.1 DNA G-quadruplex

The discovery that DNA can assume structures that differ from the canonical double helix started in 1910 when Bang reported a study about a jelly- like substance formed by a concentrated solution of guanylic acid. He observed that a concentrated solution of guanylic acid (25 mg/ml) at pH 5 becomes viscous and forms a gel, suggesting the formation of a high-order structure [81]. The same author investigated the optical features of the gel and the structure of the fibres obtained from dried gel. He postulated that guanylic acid forms a helix type structure. About 50 years later, Gellert and collaborators reanalysed the fibres by X-ray diffraction and proposed the formation of a planar tetrameric structure, namely four guanines associated to form a planar structure called G-tetrad, stabilized by Hoogsteen hydrogen bonds [82].

As illustrated in *Figure 9*, each guanine in the G-tetrad forms two H-bonds with the neighbouring bases: N1-H····O6 and N2-H····N7. Two or more G-tetrads can stack on top of each other allowing the formation of a G-quadruplex, characterized by a central cavity where free metal cations can locate: preferentially monovalent cations such as K^+ (the major monovalent cation in the cells), Na^+ or NH_4^+, but also bivalent cations like Mg^{2+} or Ca^{2+}. The metal cations stabilize the structure by interacting with the O6 atoms of the four guanines of a G-tetrad. G4 structures can form spontaneously in physiological conditions and they are stabilized by K^+ concentrations lower than that of mammalian cells (140 mM).

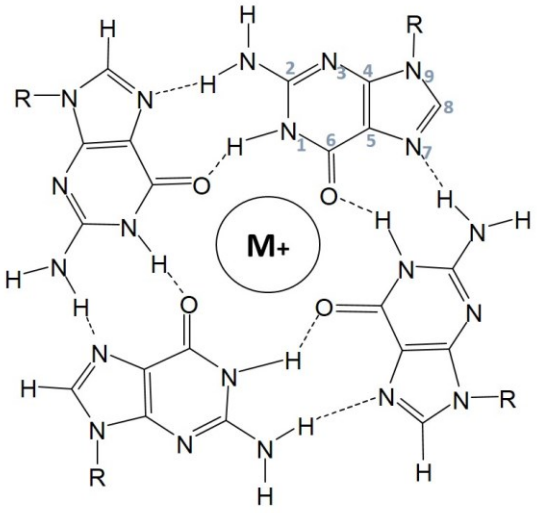

Figure 9. G tetrad structure showing the atoms involved in Hoogsteen hydrogen bonds (N_1, N_7, O_6 and N_2).

Intramolecular G4 is obtained by the stacking of two or more G-tetrads kept together by loops constituted by nucleotides that are not involved in G-tetrad formation. The number of the stacks, the length and the nature of the loops are the key elements in influencing the thermal stability: it is reported that is possible to obtain G4 structures *in vitro* that are more thermodynamically stable than the duplex DNA, but the thermal stability *in vitro* may not correlate with effects obtained *in vivo* [83–85]. G4 can have different topologies depending on the number of G-tetrads, the strand direction, the length of the loops, the sequence of the G4 motifs. It is possible to classify G- quadruplexes into: (i) intramolecular, when the quadruplex formation requires the presence of blocks of guanines in only one strand; (ii) intermolecular if the folding arise from two or more strands. G-quadruplex structures can be parallel, antiparallel or mixed parallel/antiparallel, depending on the direction of the strands: (i) in parallel G4 the strands run in the same direction; (ii) in antiparallel G4 at least one of the four stranded runs in the opposite direction compared to the others (*Figure 10*) [86,87].

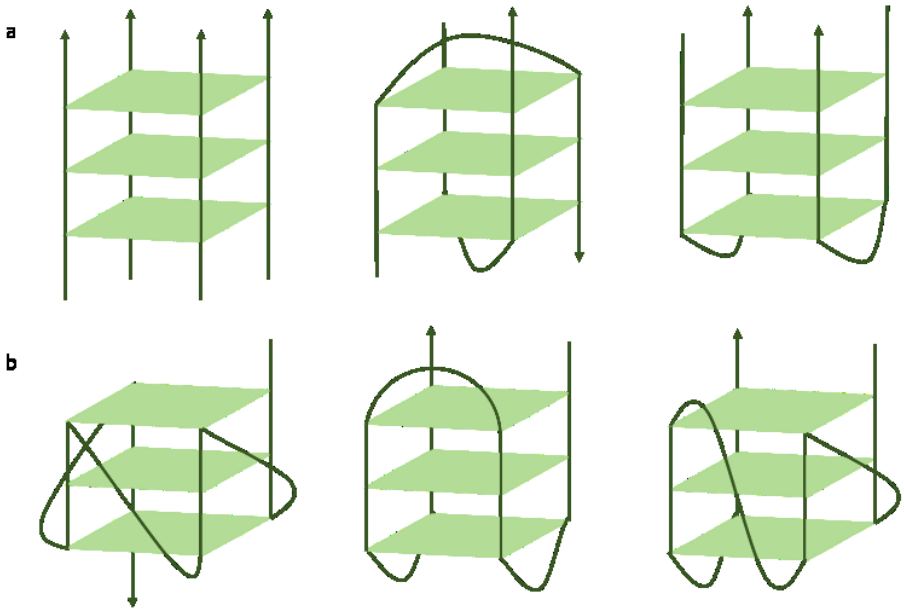

Figure 10. Schematic illustration of G-quadruplex structures. (a) Representation of intermolecular quadruplexes; (b) Representation of intramolecular quadruplexes and different types of DNA folding: parallel, antiparallel and mixed parallel/antiparallel.

The 3D-conformation of G- quadruplex is useful for the design of molecules capable of binding to these non-canonical structures in order to inhibit cellular processes, such as

replication and transcription [83,88]. In human genome there are more than 300.000 different G4-motifs that can potentially fold into a G4, but not all G-rich regions of the genome are able to assume the G4 conformation [89].

2.3.2 G-quadruplex in the genome

Bioinformatics analyses show that in human genome there are many sites which can fold into G-quadruplex structure [90,91]. The most studied G4 conformation is the one formed by a single DNA strand (intramolecular G4). It has been reported that this structure is common in eukaryotic genomes and growing evidences indicate that it might have a role in transcription regulation, as oncogene promoters are rich in G-rich sequences [92–94]. G4 is present also in telomeres and other biologically relevant genome regions [95–97].

In the past years, several bioinformatics tools have been developed to predict the tendency of genome sequences to form a G-quadruplex. The consensus sequence for quadruplex formation commonly accepted is $G_{3+}N_{1-7}G_{3+}N_{1-7}G_{3+}N_{1-7}G_{3+}$ but several variations have been proposed [89,98]. Guanine runs are generally formed by 2-to-5 consecutive guanines, whereas the loops comprise a number of nucleotides varying from 1 to 7 or more, but also longer loops have been found in G4 DNA. In general, the presence of a loop of 1 nucleotide increases the stability of the G4 [99–101]. Using algorithms scientists have predicted that in the human genome there are more than 360.000 sequences capable of folding into a G-quadruplex.

G-quadruplex structures are not randomly distributed, but often located in specific regions such as promoters, telomeres and 5'-UTRs, near or over transcription factor binding sites and in proximity of TSS [97,102].

The presence of G4 forming sequence has been detected not only in human genome, but also in plants [103–105], viruses [106] and bacteria [107]. Moreover, there are sequences in yeast which have the capability to fold into quadruplex and can be implicated in transcription regulation [108].

The group of Li Ning performed experiments to analyse the distribution of quadruplex motifs in genomic regions flanking transcription start sites across 13 animal species, and

found a significant enrichment of G4 structures in transcriptional regulatory regions of warm-blooded animals [109].

As these unusual folded DNA structures modulate transcription and translation, it is important to know their localization and their abundance inside the human genome. A significant step forward to the establishing of the location of G4 structures *in vivo* was obtained through the development of specific antibodies directed against telomeric G- quadruplex. One of these antibodies was selected from a synthetic library and used in an immunofluorescent assay showing the presence of G4 in a cellular contest [110]. After these results, other antibodies were used to map the localization of G4 in the human genomic DNA. In particular, the antibody BG4, with a very high specificity for G4 structures, was developed by the Balasubramanian's group [111]. Tests on human cells gave interesting results. BG4 confirmed the presence of G-quadruplexes in telomeric regions of chromosomes isolated from Hela cells, but some foci disseminated across the chromosomes were also detected, suggesting that G4 structures folds also in regions different from telomeres [111].

New insights in detecting G4 localization in human genome were achieved using polymerase stop assay, which is used to measure the polymerase stalling at G4 sites, with the Illumina next-generation sequencing [112]. This new method was called G4- seq and permitted to obtain a genome-wide distribution of G4s. The same group that developed the G4-seq experimental model, implemented the obtained results using the BG4 specific antibody as a probe to perform a G4-specific ChIP-seq, an antibody- dependent chromatin immunoprecipitation based on a high-throughput sequencing approach [113]. Using this method, Balasubramanian and co-workers demonstrated the existence of 10.000 G4 structures in human chromatin, localized in regulatory regions (including the promoter of the *c-MYC* and *KRAS* genes). They reported that the number of G4 structures is lower compared to the predictions made by computational analyses or to the results obtained with G4-seq. This was explained by proposing a possible suppressive role played by heterocromatin in the formation of G- quadruplexes. They also reasoned that G4 ChIP-seq resulted to have higher sensibility and resolution than BG4 immunostaining because the peaks observed are more than the immunofluorescent foci [113].

All these results demonstrate the presence of G4s in the genome.

However, to understand the biological role of G-quadruplexes it is necessary to know their position and distribution, because the equilibrium between G4 folding and G4 unfolding might act as a regulatory molecular switch.

It has been reported that G4 folding occurs preferentially during DNA replication, transcription and repair because in these processes DNA assumes a transient single stranded form allowing Hoogsteen base paring instead of normal Watson-Crick base paring [114]. In addition, superhelical stress, molecular crowding and specific proteins or transcriptional factors are expected to contribute to the stabilization of the G4 structure [83].

2.3.3 G4 in promoters: implication on transcription

Several studies have demonstrated the presence of G4 structures in telomeric regions. Telomeres are regions made by repetitive (TTAGGG) motifs, located at the end of the chromosomes. G4 DNA protects the chromosomes from degradation and from fusion with other chromosomes [115]. The role of telomeres in tumorigenesis is related to their capability to improve cellular immortalization, and their overexpression is founded in the majority of cancer cells, representing a hallmark of cancer [116,117]. It has been reported that G-quadruplex can affect telomerase activity which is blocked by intramolecular G4 structure [95,118].

In addition to the telomeres, G4 DNA is present also in the promoter of the genes.

Small molecules binding to the G4 promoter show anticancer activity in mouse models, a finding that suggests that targeting critical promoter G4 structures may be a promising strategy to treat human cancers [119–121].

Outside the telomeric regions, G4 is present with an average of about 1 quadruplex every 10.000 bases [122]. Moreover, among all the human genes, about 50% have a PQS (putative quadruplex sequence) in proximity of their promoter regions, suggesting that G-quadruplex could have a role in the regulation of gene expression [83].

In 2007, Huppert and Balasubramanian published an article in which, thanks to an analysis carried out on 19.268 known human genes present in ENSEMBL, they found that more than 40% of the gene promoters contains at least one PQS. Moreover, they

demonstrated that the probability to find a G4 correlates with the distance to TSS: in particular the higher probability to find a PQS region is near the TSS (*Figure 11*) [122].

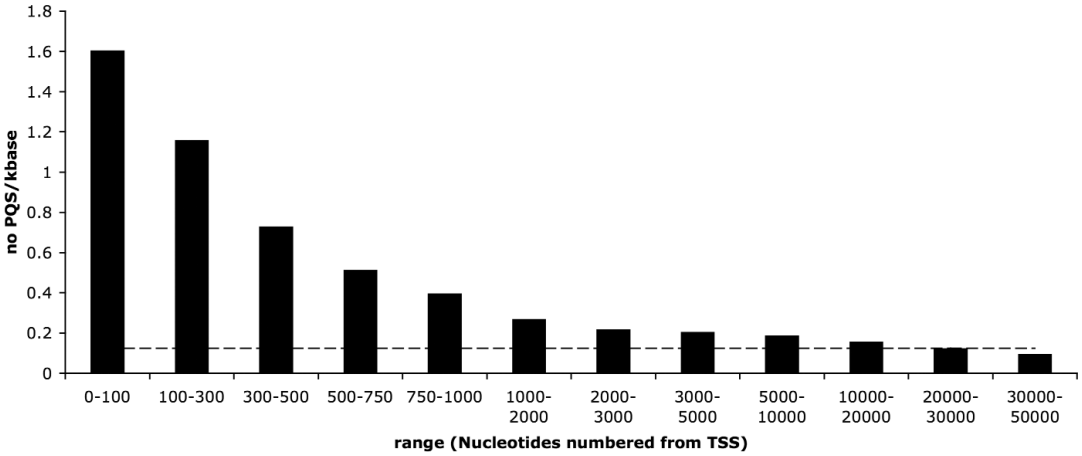

Figure 11. Graphic showing the density of PQS relative to the distance from the TSS. (*Huppert J, 2007*)

Interestingly, other studies demonstrated that the G4 forming sequences are more abundant in oncogene promoters if compared to house-keeping or tumour suppressor genes [123].

The effect of the G4 folded structure in or close to promoter regions could be both positive and negative. Maybe the type of response may be related to the strand position of the G4: on the template or coding strand of DNA. It has been reported that the presence of G4 motifs on the template strand results in the ending of transcription due to the fact that the transcription machinery is blocked; but, if the G-quadruplex is present on the non-template strand, it could maintain the template strand in a single strand conformation promoting gene transcription [124].

G4 structure can also function as a recruitment factor for specific proteins, which can unfold the G- quadruplex and activate transcription [125].

Although several works in literature showed the inhibitory effect of G4 structures on DNA transcription, recently there is a growing amount of data demonstrating the positive effect on transcription induced by G4s [126]. It is clear that is not possible to define a general function for G4 motifs, but we can only analyse each different situation and each G4 in its context. Until now, the most studied G4 motifs are those present in *c- KIT*,

c- MYC and *KRAS* genes [1,127–129], but the evidence of the presence of G- quadruplexes has also been found in other genes such as *VEGF*, *HIF-1α*, *Bcl-2* and *PDGF-A* genes [130– 133]. Balasubramanian and collaborators, studying the *c-KIT* promoter, demonstrated that a G- rich sequence of 21 nucleotides present upstream the transcription start site is able to fold into G4 motif under physiological conditions and is basically conserved between human, mouse, rat and chimpanzee [134]. The *c-KIT* oncogene encodes for a tyrosine kinase receptor and its expression is critical for the development of mast cells, melanocytes and hematopoietic stem cells [135]. It is aberrantly activated in Gastrointestinal Stromal Tumour (GIST) representing the main target of GIST therapies [136]. The discovery that there is a sequence in the *c-KIT* promoter that is able to fold into three different G4 motifs may be an attractive starting point to develop specific targets in order to control c-KIT aberrant expression [137].

C-*MYC* is another critical gene that results to be constitutively expressed in several types of cancer. Its activation leads to the overexpression of many other genes involved in cell proliferation. The regulation of the c-MYC protein level is complex and involves many factors; however, in 2002 the group of Hurley found that is possible to target a G4 motif present in the nuclease hypersensitive element (NHE). This G-quadruplex acts as a repressor element, thus its stabilization using specific ligands may lead to a decrease in transcription resulting in the reduced gene expression. This mechanism may display an alternative way to modulate c-MYC expression in cancers [129].

The third most studied cancer related gene is *KRAS*. In the human and mouse *KRAS* promoters is present a nuclease hypersensitive polypurine/polypirimidine element (NHPPE) containing a G-rich region that is able to assume the G4 conformation. Through circular dichroism and NMR experiments, it has been possible to define that the structure forming in the *KRAS* promoter is an intramolecular parallel G- quadruplex [138,139]. It has been demonstrated that it can adopt two conformations, called Q1 and Q2, which are recognized by different proteins such as PARP-1, Ku-70 and hnRNP A1 [138]. hnRNP A1 is a nuclear ribonucleoprotein which is able to unfold the G4 and can have a role in several biological processes controlled by *KRAS* expression. In a recent work, it has been shown a possible link between KRAS, ILK, a mediator of an aggressive phenotype, and hnRNP A1 in pancreatic cancer. The three proteins seem to

be involved in a loop with a regulatory effect on KRAS expression in pancreatic cancer [140].

2.4 Reactive Oxygen Species

In aerobic organism reactive oxygen species (ROS), which include anion superoxide (O_2^-), hydrogen peroxide (H_2O_2) and hydroxyl radical (·OH), are continuously produced by metabolic reactions. The main sources of ROS are: (i) mitochondria, through electron leakage from the ubiquinone/ubiquinol shuttle; (ii) peroxisome, during β-oxidation of long-chain fatty acids; (iii) cytochrome P-450 enzymes; (iv) nicotinamide adenine dinucleotide phosphate (NADPH) oxidases of the NOX family (*Figure 12*).

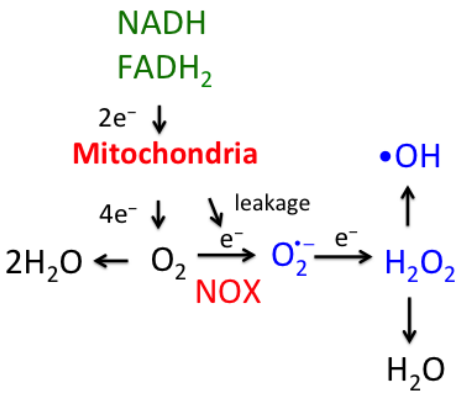

Figure 12. ROS production and regulation in cells.

As high levels of ROS produce a negative impact on proliferation, cancer cells activate several defence mechanisms to keep oxidative stress at non-toxic levels.

In fact, intracellular ROS can oxidize lipids, proteins and nucleic acids and severely damage the cells.

Oxidative stress can act as a double-edge sword in PDAC. From one hand, the initiation of the carcinogenesis process and the malignant transformation of the cells are promoted by the damage to DNA caused by ROS. Moreover, a moderate increase of ROS, typically occurring in cancer cells, facilitates cell survival and cancer progression. On the other hand, an excessive amount of ROS activates apoptosis and leads to cell death.

Therefore, the role of ROS in the development of cancer depends on the concentration of oxidative stress. It is noteworthy that the regulation of redox homeostasis is essential for the promotion of cell proliferation (*Figure 13*).

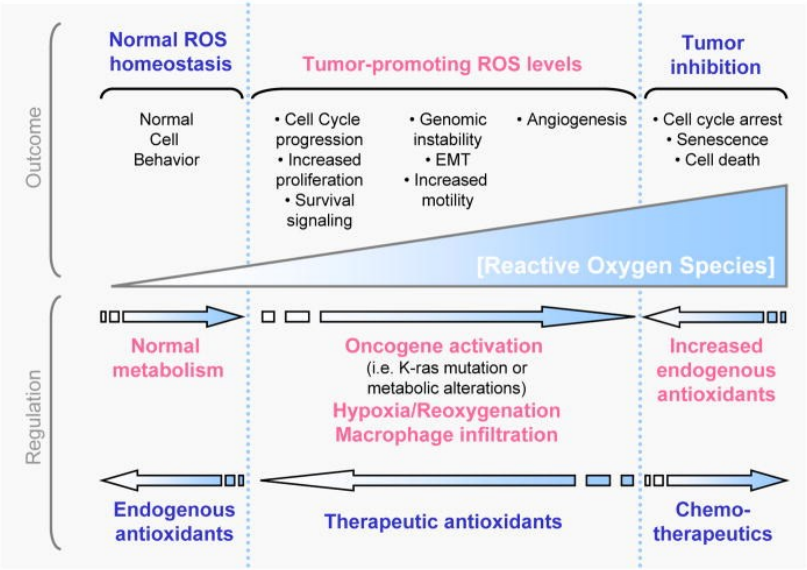

Figure 13. Effects and regulation of ROS production and stimulation on cell viability (*Liou G Y, 2010*)

As stated above, there are different types of ROS among which the most important are represented by O_2^-, H_2O_2 and ·OH.

Anion superoxide is generated by an incomplete reduction of molecular oxygen (O_2) during the flux of electrons through the mitochondrial electron transport chain.

O_2^- is reduced into H_2O_2 by superoxide dismutase and the H_2O_2 is then reduced to water by catalase (*Figure 14*) [141].

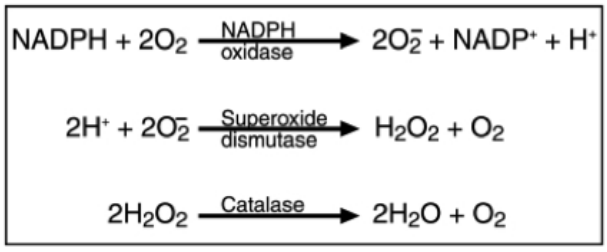

Figure 14. Reactions and enzymes involved in reduction of anion superoxide

Other sources of ROS inside the cells are xanthine oxidase, uncoupled endothelial nitric oxide synthase (eNOS), arachidonic acid and also metabolic enzymes like cytochrome P450 enzymes, lipoxygenase and cyclooxygenase [142,143].

Hydrogen peroxide, which results from protein oxidation in the endoplasmic reticulum or as an end product in peroxisomal oxidation pathways, can diffuse through the membranes and can be also reduce to H_2O by glutathione peroxidase.

H_2O_2 is the most stable form of ROS and can diffuse through membranes presenting a selective reactivity towards the thiol groups of proteins cysteine residues [144,145].

In physiological conditions cysteine residues that exist as anion thiolates (Cys-S^-) are more susceptible to oxidation if compared to the protonated thiol form Cys- SH. Oxidation of this protein residues results into the abundancy of the sulfenic form (SO^-), which causes allosteric modification in protein conformation altering its function. High levels of hydrogen peroxide can lead to the formation of sulfinic (SO_2^-) or sulfonic (SO_3^-) species which, despite sulfenic modification, are irreversible and produce stable protein damage [144–147]. In order to prevent irreversible protein alteration, the sulfenic intermediates react to form disulphide (S-S) bonds with nearby cysteines or are incorporated in sulfenic-amide (S-N) bonds and can be reduced to water by antioxidant systems as glutathione peroxidases (GPXs), peroxiredoxins (PRXs) and catalases [144,146,147].

The third type of ROS is the hydroxyl radical, which is highly reactive and due to its very short half-life can cause oxidation of lipids, proteins and nucleic acids on the site where it is produced [148,149]. In presence of ferrous ions, H_2O_2 is converted to hydroxyl radicals through the Fenton Reaction [142,144,145,148].

Since hydroxyl radicals are deleterious for cell stability and uncontrolled levels of hydrogen peroxide lead to ·OH formation, a tight regulation of ROS detoxification is required [144].

Among the detoxification enzymes mentioned above, the protein's family of peroxiredoxin is considered the ideal hydrogen peroxide scavenger, due to its presence in different cell compartments and its high expression. H_2O_2 oxidizes the cysteine residues of PRXs; then they are reduced by thioredoxins (TRXs), which subsequently return to their reduced form using NADPH [148].

Also GPXs can convert hydrogen peroxide to water and present a high constant rate, but they are less abundant in the cells if compared to PRXs. GPXs function through the reduction of glutathione (GSH) to glutathione disulphide (GSSG) [150]. Thanks to NADPH, which function as an electron donor, glutathione reductase reduces GSSG back to GSH [144,148].

NADPH resulted to be very important in the detoxification process; in fact, it provides the reducing power for the activity of several enzymes. In the cells, there are different

sources of NADPH, which is produced both in the cytosol and in the mitochondria. Its major source in mammalian cells is the oxidative branch of the pentose phosphate pathway (PPP), through the action of the glucose-6-phosphate dehydrogenase [151,152]. Anyway there are other enzymes generating NADPH such as isocitrate dehydrogenases, which catalyse the oxidative decarboxylation of isocitrate and seem to be the main source of NADPH in fat and liver cells, and malic enzymes, which transform malate to pyruvate [148,153].

2.4.1 ROS and diseases

As ROS are more reactive than molecular oxygen (O_2), they are classified as toxic metabolic byproducts that cause damages to lipids, proteins and DNA. However, a lot of studies in the last two decades, found that ROS have a role in cell signalling pathways playing important roles in cell proliferation and growth, differentiation, metabolic adaptation and other biological responses [144,145]. Thus, on one hand ROS are important signalling factors acting through reversible modification to proteins (i.e. kinases, phosphatases); on the other hand oxidative stress can cause cell damages leading to cell death [154].

Several authors reported that ROS have a dual function. Low levels of intracellular ROS are required for normal cellular function and are associated to cell cycle progression and proliferation [142,155]. It is known that H_2O_2 oxidizes the thiol groups of cysteine residues and this represents a critical event for the activation of protein kinase in cells. Some protein kinase involved in important signalling pathways are PTEN, PTP1B and MAPK [156–159]. Other indirect target of ROS are transcription factors like NF-κB, HIF-α, ERK and PI3K [160–163]. Through the regulation of all these factors, ROS can have a role in metabolism, apoptosis, immune signalling and aging [142].

ROS level is tightly controlled in the cells. Aberrant intracellular ROS level associated to an inefficient function of the antioxidant machinery may lead to several disease. In fact, high levels of oxidative stress are implicated not only in carcinogenesis, but also in neurodegeneration, diabetes, aging and atherosclerosis or other cardiovascular disease [142,145].

2.4.2 ROS in cancer cells

Cancer cells produce higher levels of ROS than healthy cells, as they have a higher metabolic rate than the latter. ROS can drive a constitutive activation of growth factors that sustains cellular growth and proliferation.

Elevated ROS levels have been found in several cancers, and they are probably involved in the maintenance of the aggressive phenotype [164].

Cancer cells acquire the ability to induce a new redox balance in order to maintain ROS at levels suitable for optimal cell grown. These adaptations to slightly higher oxidative stress allows cancer cells to proliferate despite enhanced ROS. Oxidative stress is the result of an equilibrium balance between antioxidant and oxidant (ROS) molecules [164,165].

Even if different authors proposed a correlation between ROS and cancer, in the last years there were contradictory evidence about the role of ROS in tumorigenesis. Several studies show that mild-to-moderate increases of ROS promote cancer cell proliferation and metastasis both in human cells and mouse models [166–168]. In contrast, treatments with anti-oxidants, such as N-Acetyl Cysteine (NAC) or vitamins A or E, are not particularly effective in reducing the incidence of cancer, for example the head/ neck cancers and lung cancers [148,169].

However, the higher ROS levels observed in cancer cells cannot be ascribed only to an elevated metabolic rate. Probably, the genetic alterations in certain genes (oncogenes) can be directly or indirectly affected by ROS. In fact, ROS can activate several pathways and genes that have a role in tumour progression and aggressiveness [170]. In particular ROS can (i) promote cellular proliferation through MAPK, activating ERK1/2 and NF-κB key transcription factors [162]; (ii) escape apoptosis by control c-SRC, NF-κB, PI3K/AKT [160]; (iii) support EMT (Epithelial to Mesenchymal Transition) leading to metastasis development [171]; (iv) foster angiogenesis by promoting the release of VEGF [165].

2.4.3 ROS in pancreatic cancer

In PDAC a moderate increase of intracellular ROS is considered a hallmark of cancer and acts as pro-survival and anti-apoptotic factor [142,165,172].

As high ROS levels are detrimental for the cells, in pancreatic cancer cells oncogenic *KRAS* is able to activate expression of several anti-oxidant genes through the Nuclear Factor erythroid 2-like 2 (NFE2L2 or Nrf2) [172,173]. Nrf2 is a member of the Cap' n' collar (CNC) family, a subfamily of basic region-leucine zipper (bZIP) transcription factors. This transcription factor is considered the master regulator of redox homeostasis [148,174–176].

Under physiological unstressed conditions, inactive Nrf2 is sequestered into the cytoplasm bound to the repressor protein Kelch-like ECH-associated protein1 (KEAP1). KEAP1 is an adapter protein for the CUL3/RBX1 E3 ubiquitin ligase complex and mediates the ubiquitination of Nrf2 and its proteolytic degradation in 26S proteasome [173,177].

In normal unstressed conditions, when the ubiquitination is not blocked, the half-life of Nrf2 is very short, from 10 to 30 minutes, and the protein is continuously directed to proteasome for degradation (*Figure 15*) [175,178].

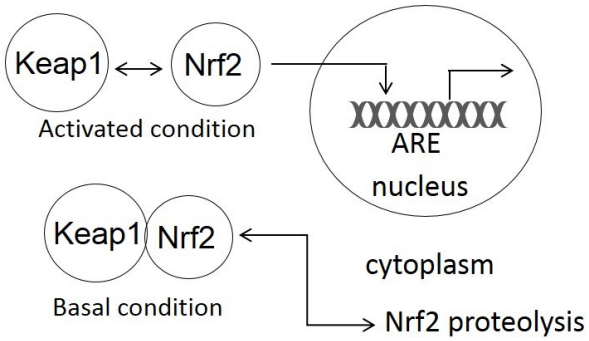

Figure 15. Under basal unstressed conditions Nrf2 is sequestered into the cytoplasm bound to KEAP1. The complex is directed to proteasome for degradation. Under oxidative stress conditions, the activated Nrf2 translocates into the nucleus where it activates the transcription of other antioxidant genes.

On its surface KEAP1 presents some cysteine residues that function as redox sensors. Under oxidative stress conditions, the oxidation of cysteines produces a conformational change in KEAP1 protein resulting in the disruption of the bind with Nrf2. The free protein translocates into the nucleus where it heterodimerizes with small v-maf musculoaponeurotic fibrosarcoma oncogene homolog (Maf) regulator protein [179]. Then the complex binds to the Antioxidant Response Element (ARE) on the DNA and this interaction leads to the transcription of several antioxidant enzymes including phase II

enzymes, as glutathione-S-transferase or NAD(P)H-quinone-oxidoreductase-1 (hNQO- 1) [175,178].

Some authors speculate on the dual role that Nrf2 seems to have in cancer [176,180–182]. This important transcription factor has been considered for a long time as a tumour suppressor for its capacity to activate the antioxidant cellular response through the induction of the transcription of different genes involved in the response to oxidative stress or to xenobiotics [180,183]. In the last years it has been pointed out the possible "dark side" of Nrf2: there are growing evidences that Nrf2 activation is related to progression of tumours and operates as a chemoresistant agent [178,181,184].

In 2011, the Tuveson laboratory demonstrated the correlation between oncogenic *KRAS* and Nrf2, showing that $KRAS^{G12D}$ increases the level of Nrf2 in order to stabilize the redox balance in the cells, lowering intracellular ROS to sustain proliferation (*Figure 16*) [62].

Another study on several pancreatic cancer cell lines reported that the dysregulation of the Nrf2/KEAP1 system leads to enhanced cell proliferation and contributes to the increase of chemo- and radio-resistance in pancreatic cancer cells [173]. Moreover, in the same study, scientists demonstrated that pancreatic tumours are associated with an elevated expression of Nrf2, thanks to Nrf2 staining of both tumour and benign epithelium [173].

Thus, in pancreatic cancer cells Nrf2 is overexpressed and *KRAS* mutations are directly correlated with enhanced expression of Nrf2, resulting in the promotion of the pancreatic intraepithelial neoplasia through the stimulation of proliferation and the suppression of senescence [181,182,184].

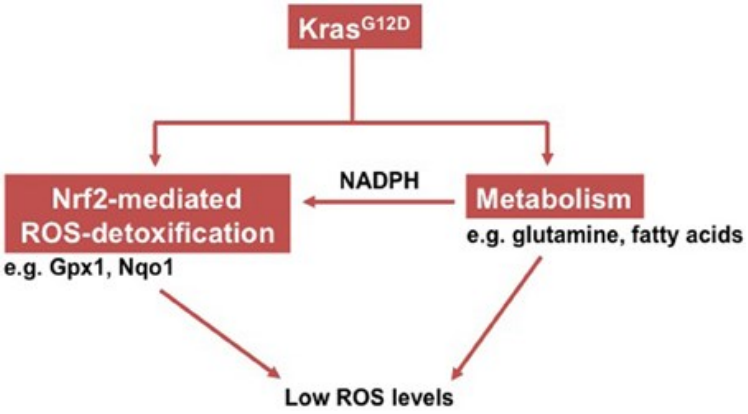

Figure 16. Schematic representation showing how mutated KRAS controls ROS levels through Nrf2 activation and metabolism rewiring (*Kong B, 2013*)

2.5 DNA oxidation

Reactive oxygen species and nitrogen species can damage DNA modifying the bases: an event that can be rather harmful for the cell. Accumulation of DNA lesions can be deleterious for the genome integrity and for all the processes involving DNA. To prevent mutations, the damage caused by ROS must be repaired.

There are two main pathways responsible for DNA repair lesions: NER, nucleotide excision repair pathway, and BER, base excision repair pathway [185,186].

The first process generally recognizes DNA damages or modifications caused by xenobiotic agents. On the contrary, endogenously generated DNA lesions are recognized and removed by specific enzymes belonging to BER. During the process, BER proteins remove the modified base producing an abasic site (AP) that is then cleaved by an AP endonuclease which gives a single strand break. The process continues following two possible pathways: the short patch or the long patch BER. Finally, RNA polymerase and ligase add the missing nucleotides and seal the nick [187,188].

Among the four DNA bases, guanine, having the lowest redox potential, is most prone to oxidation.

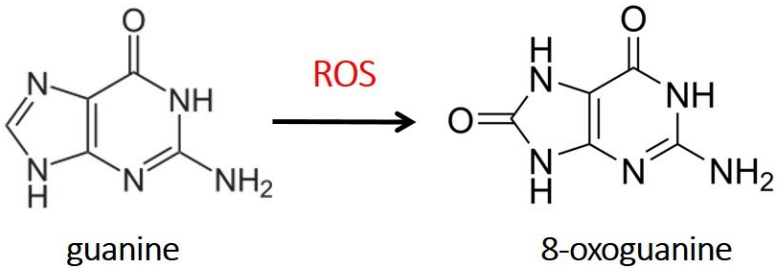

Figure 17. ROS cause the transformation of guanine into 8-oxoguanine

The result of oxidation is the formation of 7,8-dihydro-8-oxoguanine (8OG) which functions as an oxidative stress biomarker inside the cells (*Figure 17*) [189].

The mutagenic effect of this lesion is due to the fact that 8-oxoguanine can coupled with adenine and this leads to a G:C to T:A transversion: a point mutation that can cause cancer [126,190]. Although for a long time oxidative DNA lesions have been seen as mutagenic and detrimental for many cellular processes (in particular transcription), a

large body of data suggest that oxidized bases, such as 8-oxoguanine, act as activators of key signalling pathways [191–193].

It has been reported that the presence of 8OG in the genome may block the advancement of RNA polymerase, leading to a decrease in transcription [194]. In contrast, several studies report a positive correlation between increased 8OG formation and gene expression [126].

In order to better understand the role of 8OG in the genome, scientists performed several studies in which they tried to highlight the position of the lesion in DNA.

Olinski and collaborators demonstrated that 8OG is not disposed randomly in the genome: the quantification of the oxidative lesion in heterochromatin and euchromatin from pig thymus extract showed that 8OG is more abundant in euchromatin [195].

Other studies on the correlation between 8OG and gene expression, reported that the binding of several proteins is reduced when the 8-oxoguanine is present in the protein transcription factor binding sequence. These results are reported for specific protein 1 (SP1), NF-κB and CREB [196–198].

All these findings suggest that 8OG could have an epigenetic role and that its position in the genome may influence several cellular processes.

As reported before, 8OG is a critical lesion for the DNA and must be repaired to avoid damages. The primary enzyme involved in the repair of 8-oxoguanine lesion is the glycosylase hOGG1 (8-oxoguanine DNA glycosylase-1), which recognizes the oxidized DNA base and excises it, leading to the formation of an abasic site [189]. If a defect in OGG1 repair activity occurs, the increased level of 8OG may enhances the raising of DNA mutations. It has been shown that in mice knock-out for OGG1 ($Ogg1^{-/-}$) a reduction in 8-oxoguanine repair machinery lead to lesions accumulation in the genome; this causes an increased frequency of mutations which results to be 2-3 fold higher in liver of null- mice [199,200]. Despite all these events, in the $Ogg1^{-/-}$ mice an increased tumour incidence was not detected, even if in a small number of human tumours has been reported the inactivation of OGG1 repair system [201,202]. Therefore, previous study demonstrated that OGG1 null mice did not show substantial phenotype alterations or problems in embryonic development, and presented only a modest predisposition to tumorigenesis. But the most surprisingly event is that researches demonstrated an enhanced resistance to inflammation [192,203].

In the last years, it has been reported that the hOGG1 glycosylase may have a role going beyond BER.

Boldogh and his co-workers hypothesized that the free 8OG, excised from the DNA, interacts with OGG1 to create an OGG1-8oxoG complex [193,204,205]. They demonstrated that the complex OGG1-8oxoG acts as a guanine nucleotide exchange factor protein (GEF).

This complex shows affinity for all the three RAS proteins and enhances the release of GDP allowing the substitution with GTP, activating RAS protein [193]. Boldogh demonstrated that the addition of supplemental 8OG in MCR5 cells results in an increase of RAS-GTP, the active form of RAS protein, that follows a dose and time response dependent manner. But, when the 8-oxoguanine is added to cells depleted for OGG1 they did not see any significant change in RAS-GTP expression [205].

Furthermore they studied the capability of the OGG1-8oxoG complex to function as a GEF protein also in another cell line (KG-1 cells) which express a mutant OGG1 [193]. KG- 1 cells are human myeloid leukemia cells expressing a 8OG repair deficient OGG1, called $OGG1^{R229Q}$, which resulted to be inactive at the physiological temperature of 37°C either *in vitro* and *in vivo*. In physiological conditions the OGG1 inactivation results in the accumulation of 8OG [206]. When the cells are cultured at lower temperature (25°C) the 8OG excision activity of OGG1 was rescued, showing an increase in p-MEK1/2 and p-ERK1/2 levels confirming the activation of RAS-GTPase [193].

Although these data confirm that 8OG, ones excised from the DNA, can interact with OGG1 and can control RAS activation in cells, the 8-oxoguanine plays important role in gene activation also when it is present as lesion substitution of guanine in the genome. In particular, PQS regions in the DNA are sequences showing a high guanine density, and are therefore potential sites for guanine oxidation.

Studying the sequence of the telomeric quadruplex, Szalai and her collaborators decided to investigate the effect of 8OG in that region through the substitution of different guanines present in the GGG triplet with 8-oxoguanine [207]. As expected, they found that the position of 8OG can influence the formation of the quadruplex and can affect the telomerase activity. If the substitution occurs near the 5'-end, the presence of 8OG permits the G4 folding but stops telomerase activity. On the contrary, if the lesion is

present in the middle of the sequence, the result is an undefined structure which has no impact on telomerase action [207].

In 2011, Sagi presented another study on the effect of 8OG presence in quadruplex folded in telomeric DNA sequence 5'-$dG_3(TTAG_3)_3$, in which he tested the stability of non-canonical structures folded both in NaCl or KCl solutions. Through CD experiments, they demonstrated that almost all the sequences tested fold into a hybrid parallel/antiparallel quadruplex. Analysing the thermal and thermodynamic stability of the sequences modified with 8OG in different positions, they concluded that the presence of a lesion in the middle tetrad destabilizes the quadruplex formation [190].

Beside the studies made on telomeric regions, interesting results were found also in promoter regions of several genes that present G-rich elements able to fold into G4.

G-rich region in the vascular endothelial growth factor (VEGF) gene promoter may fold into a G-quadruplex which is important for the transcriptional regulation of the gene [208,209]. The Gillespie laboratory found that the guanine oxidation in the VEGF promoter induced by hypoxia increases gene expression, speculating that BER may be actively implicated in the process [210]. Working on the same gene promoter, Burrows and colleagues, using a luciferase reporter plasmid, demonstrated that, in the VEGF G- quadruplex promoter region, the presence of 8OG activates the transcription of the gene [126,211].

The role of 8OG in the genome is not completely clear, but all these data show that it can function through different mechanisms: (i) the presence of 8-oxoguanine in the G4 motif can destabilize the structure giving the duplex DNA and leading to gene transcription; (ii) the oxidized guanine may function as a recruitment factor for several protein and transcription factors involved in the regulation of transcription; (iii) excised 8OG can form a complex with OGG1 glycosylase which function as GEF protein favouring the transformation of RAS-GDP into RAS-GTP.

3. AIM OF THE WORK

In this PhD program, I have focused my efforts on studying the biology of oncogenic *KRAS* in PDAC cells from a functional and therapeutic point of view. Many aspects of KRAS regulation are still unclear and this lack of information impedes the design of anticancer strategies against PDAC, a disease that unfortunately does not respond to the conventional therapies.

To rationally design new therapeutic strategies for PDAC, we started from the observation that more than 90% of PDAC patients bear mutation in *KRAS*, in exon 1 at codons 12, 13 and 61. These mutations are detrimental for the patient's health, as mutant KRAS is able to initiate and maintain pancreatic cancer [28,30].

Previous works from our laboratory addressed the question on how KRAS expression is regulated. After years of investigation it has become clear that KRAS is under the control of a critical G-rich sequence located upstream of TSS [1,212,213]. This DNA stretch of 120 nt embeds three G4 motifs – called on the basis of their distance from TSS, G4 near, G4 mid and G4 far – that are sites where DNA is structurally polymorphic. In fact, the purine rich strand of G4 near and G4 far folds into stable G4 structures under physiological conditions. These unusual DNA conformations have drawn the attention of many scientists in the last two decades because compelling evidences that they are present *in vivo* have been provided by three independent methods: NMR [127,214], staining with fluorescent antibody highly specific for G4 DNA [111] and ChIP-Seq analyses of chromatin [113].

The biological function of G4 DNA is still a matter of debate, and the research is still active in this field.

Recent studies indicate that G4 DNA is a key element for transcription and evidence that its function is likely of recruiting transcription factors to the promoter is growing. Indeed, in the case of the *KRAS* gene, we have found that the proteins binding to G4 are transcription factors essential for activating transcription, such as PARP1, MAZ and hnRNP A1. When each protein is suppressed by a specific siRNA, *KRAS* transcription is repressed.

We then asked ourselves if G4 DNA function as a recruiter of proteins is because of its non-canonical folded structure or because the G4 motifs are sites of epigenetic modifications.

In my PhD work, in collaboration with my tutor, I have focused on this important aspect of the KRAS biology in PDAC. To address this point we started from two important observations: first, guanines present in G-clusters, as those that constitute the critical G4 motifs of KRAS, are susceptible to oxidation to 8-oxoguanine due to their low redox potential, compared to the other nucleobases; second, cancer cells, producing higher level of reactive oxygen species than healthy cells, have a high capacity of oxidation and probably a high level of 8-oxoguanine. With these premises, we have investigated the impact of 8-oxoguanine in the promoter of *KRAS*, by addressing important question such as: (i) does 8-oxoguanine alter the folding and the structure of the G4 which acts as an antenna for the transcription factors?; (ii) does 8-oxoguanine in the G4 motif of *KRAS* affects the recruitment of the transcription factors?; (iii) does the glycosidase OGG1 repair the 8-oxoguanine lesion in the folded G4 motif?

Another central point that we have been addressed is how the redox homeostasis is regulated in PDAC and if KRAS is involved in the control of it. In this regard, we have found that KRAS controls the expression of Nrf2, the master regulator that modulates the level of ROS in the cells [62]. Since Nrf2 is enhanced by ROS and is stimulated by KRAS, we wondered if ROS stimulates KRAS too. The results of this research allowed us to propose an axis composed by ROS/Nrf2/KRAS that controls the redox homeostasis in PDAC. We also investigated the intersection of this axis with the survival and apoptosis pathways and found that low ROS levels favour the pro-survival *Snail* gene, while high ROS favours the pro-apoptotic *RKIP* gene.

Another important point on this topic was to examine how ROS activate KRAS. To this regard, we have found that free oxygen radicals stimulates KRAS through a mechanism mediated by G4 DNA. This is quite a new aspect of the research that provides new evidences about the biological role of G4 DNA.

Finally, considering that PDAC cells are addicted to KRAS and that the suppression of the oncogene triggers a cellular response that activates apoptosis, we have pursued a molecular strategy for KRAS inhibition based on the observation that there are several

miRNAs in PDAC that are aberrantly downregulated as they behave as tumour suppressors.

We have identified miR-216b as a strong therapeutic tool for suppressing KRAS in PDAC. We propose some chemical modifications to strengthen the activity of this particular miRNA and we have also tested different strategies for delivering miR-216b in PDAC cells.

In conclusion, my PhD work focuses on oncogenic *KRAS*, as it has a central function on PDAC cells. Our main goal was to explore if KRAS has a role in the redox homeostasis, because the control of oxidative stress has a direct effect on the survival and apoptosis pathways in PDAC, as described in this work. The results of our research ended in three scientific manuscripts, two of which have been already published and one has been submitted.

4. RESULTS

- Section 1
  S. Cogoi, A. Ferino, G. Miglietta, E.B. Pedersen, L.E. Xodo, **The regulatory G4 motif of the Kirsten ras (KRAS) gene is sensitive to guanine oxidation: implications on transcription**, Nucleic Acid Research (2017)

- Section 2
  A. Ferino, G. Cinque, V. Rapozzi, L.E. Xodo, **The ROS-KRAS-Nrf2 axis in the control of the redox homeostasis and the intersection with survival-apoptosis pathways**, submitted.

- Section 3
  A. Ferino, G. Miglietta, R. Picco, S. Vogel, J. Wengel, L.E. Xodo, **MicroRNA therapeutics: design of single-stranded miR-216b mimics to target KRAS in pancreatic cancer cells**, RNA Biology (2018)

Table representing my personal contribution to the papers

Paper	Project Planning	Experimental procedures	Data analysis	Manuscript preparation
The regulatory G4 motif of the Kirsten ras (KRAS) gene is sensitive to guanine oxidation: implications on transcription **Section 1**	30 %	85 %	50 %	30 %
The ROS-KRAS-Nrf2 axis in the control of the redox homeostasis and the intersection with survival-apoptosis pathways **Section 2**	30 %	90 %	60 %	30 %
MicroRNA therapeutics: design of single-stranded miR-216b mimics to target KRAS in pancreatic cancer cells **Section 3**	15 %	50 %	30 %	30 %

Section 1

The regulatory G4 motif of the Kirsten ras (KRAS) gene is sensitive to guanine oxidation: implications on transcription

S. Cogoi, A. Ferino, G. Miglietta, E.B. Pedersen, L.E. Xodo

Nucleic Acid Research (2017)

Published online 20 November 2017 *Nucleic Acids Research, 2018, Vol. 46, No. 2* **661–676**
doi: 10.1093/nar/gkx1142

The regulatory G4 motif of the Kirsten ras (*KRAS*) gene is sensitive to guanine oxidation: implications on transcription

Susanna Cogoi[1,†], Annalisa Ferino[1,†], Giulia Miglietta[1], Erik B. Pedersen[2] and Luigi E. Xodo[1,*]

[1]Department of Medicine, University of Udine, 33100 Udine, Italy and [2]Nucleic Acid Center, Institute of Physics and Chemistry, University of Southern Denmark, DK-5230 Odense, Denmark

Received June 05, 2017; Revised October 13, 2017; Editorial Decision October 27, 2017; Accepted October 31, 2017

ABSTRACT

***KRAS* is one of the most mutated genes in human cancer. It is controlled by a G4 motif located upstream of the transcription start site. In this paper, we demonstrate that 8-oxoguanine (8-oxoG), being more abundant in G4 than in non-G4 regions, is a new player in the regulation of this oncogene. We designed oligonucleotides mimicking the *KRAS* G4-motif and found that 8-oxoG impacts folding and stability of the G-quadruplex. Dimethylsulphate-footprinting showed that the G-run carrying 8-oxoG is excluded from the G-tetrads and replaced by a redundant G-run in the *KRAS* G4-motif. Chromatin immunoprecipitation revealed that the base-excision repair protein OGG1 is recruited to the *KRAS* promoter when the level of 8-oxoG in the G4 region is raised by H_2O_2. Polyacrylamide gel electrophoresis evidenced that OGG1 removes 8-oxoG from the G4-motif in duplex, but when folded it binds to the G-quadruplex in a non-productive way. We also found that 8-oxoG enhances the recruitment to the *KRAS* promoter of MAZ and hnRNP A1, two nuclear factors essential for transcription. All this suggests that 8-oxoG in the promoter G4 region could have an epigenetic potential for the control of gene expression.**

INTRODUCTION

Cancer cells are characterized by high metabolic rates, normally associated with an increased level of reactive oxygen species (ROS) (1,2). Anion superoxide (O_2^-), hydrogen peroxide (H_2O_2) and hydroxyl radical (•OH) are produced by endogenous and exogenous sources (3). Among the endogenous sources, the mitochondrial electron transport chain, which reduces oxygen to water, is the major source of cellular ROS (4). In suspended mitochondria about 0.12–2% of oxygen consumed in the respiration is converted into O_2^- (3,4). However, anion superoxide is also produced enzymatically in essential metabolic pathways, including NADH oxidase, xanthine oxidase, lipo- and cyclo-oxygenases (5). Furthermore, O_2^- is reduced by superoxide dismutase to H_2O_2, which is then converted to •OH via a non-enzymatic Fenton reaction (6). All these chemical and enzymatic reactions push the ROS level more up in high metabolic rate cancer cells than in normal cells. An enhanced ROS level may damage DNA, RNA, lipids and proteins, and may also alter the intracellular signal transduction, for instance through NF-kB (7,8). A key protein of the antioxidant network is Nrf2, a (b-Zip)-type transcription factor that binds to antioxidant response elements in gene promoters and induces the expression of protective genes of the antioxidant response (9–11). Nrf2, being upregulated in pancreatic ductal adenocarcinoma (PDAC) cells, increases the capacity of the cells to control oxidative stress, a necessary condition for optimal cell proliferation (12–14).

The primary genetic lesions causing pancreatic cancer are somatic mutations in the *KRAS* gene. About 90% of PDAC carries *KRAS* G12D, i.e. a *KRAS* allele with a point mutation G→D in exon 1, codon 12 (15–17). The activity of mutant *KRAS* G12D is required in all stages of carcinogenesis (initiation, progression and metastasis) and the inactivation of mutant *KRAS* G12D reverses the transformation process (18–20). Recent studies have reported that *KRAS* G12D reduces the level of ROS in pancreatic cancer cells via Nrf2 (12,14). Since there is a correlation between mutant *KRAS* and Nrf2, we interrogated if in pancreatic cancer cells, the expression of *KRAS* is in some way influenced by oxidative stress. It is well known that oxidation of DNA occurs mainly at guanine, as it has the lowest oxidation energy among nucleobases (21). GG steps are preferred sites for oxidation, with 5′ G being particularly reactive (22). In the promoter of the *KRAS* oncogene there is a G-rich element

*To whom correspondence should be addressed. Tel: +39 043 249 4395; Fax: +39 043 249 4301; Email: luigi.xodo@uniud.it
† These authors contributed equally to the paper as first authors.

called 32R that is critical for transcription and able to fold into a G-quadruplex structure (23). 32R is located between −148 and −116 bp from transcription start site (TSS) and is recognized by several transcription factors including MAZ and hnRNP A1 (24–27). Polymerase-stop assays, footprinting and circular dichroism showed that 32R is highly polymorphic in nature, as it can fold into three alternative G4 structures (28,29). In this study, we have found by chromatin immunoprecipitation (ChIP) combined with quantitative polymerase chain reaction (qPCR) that the 32R region is more oxidized than other G-rich regions that are unable to fold into G4. The presence of 8-oxoG in 32R may lower the stability of the G-quadruplex, depending on where the damage is located inside the sequence. When the oxidation is situated in the major 11-nt loop of the *KRAS* G4, the T_M and folding are practically not affected. But when 8-oxoG is located in a G-tetrad, both T_M and folding are strongly modified. We also investigated how guanine oxidation impacts the binding of the transcription factors to the regulatory G4 motif of *KRAS*. Our data show that 8-oxoG modulates the binding of the nuclear factors to the *KRAS* promoter and also strengthens the recruitment of MAZ and hnRNP A1 to the promoter. Finally, the results are discussed in terms of possible role of 8-oxoG as an epigenetic regulator in the transcription of oncogenic *KRAS*.

MATERIALS AND METHODS

Oligonucleotides and reagents

Unmodified oligonucleotides used in this study have been obtained from Microsynth (CH). 8-oxoG-substituted oligonucleotides were synthesized from 8-oxo-dG CEP from Berry & Associates in 1-μmol scale on solid support by standard procedure, except using concentrated ammonia in the presence of 2-mercaptoethanol (0.25 M) in the deprotection step as described by Bodepudi *et al*. (30). The oligonucleotides were purified by reverse-phase high pressure (or high performance) liquid chromatography on a Water system 600, equipped with a C18 column (XBridge OST C18, 19 ×1000 mm, 5 μm). The composition of the oligonucleotides was verified by Matrix Assisted Laser Desorption Ionisation-Time of Flight (MALDI-TOF) (Supplementary Table S1). Luteolin, was purchased from Alfa Aesar (D), 8-oxoguanine (8-oxoG) and 8-oxodeoxyguanosine from Cayman Chemicals (MI, USA), GTP from Euroclone (I), hydrogen peroxide solution 30% (w/w) from BDH (UK).

Cell cultures

Human pancreatic cancer (Panc-1, MIA PaCa-2, BxPC3) and non-cancer human embryonic kidney 293 cells were maintained in exponential growth in Dulbecco's modified Eagle's medium (DMEM) containing 100 U/ml penicillin, 100 mg/ml streptomycin, 20 mM L-glutamine and 10% foetal bovine serum (Euroclone, I). The cell lines have been genotyped by Microsynth (CH) and their identity confirmed.

Recombinant proteins

Recombinant MAZ and hnRNP A1 were obtained with a high degree of purity as previously described (24,26). Recombinant OGG1 with His-Tag at the *N*-terminus was expressed in *Escherichia coli* bacteria transformed with plasmid pET20 hOGG1. The bacteria were grown for 2 h at 37°C to an absorbance at 600 nm of 0.8–1 units before induction with isopropyl 1-thio-β-d-galactopyranoside (0.4 mM final concentration). The cells were allowed to grow overnight at 25°C, and then centrifuged at 5000 rpm at 4°C. The supernatant was removed and the pellet resuspended in Lysis buffer (50 mM NaH_2PO_4, 300 mM NaCl and 10 mM imidazole) added with 0.2 mM PMSF (phenylmethylsulphonyl fluoride). The bacteria were lysed by sonication [3 ×(30 s sonication/1 min off)], added with 0.05% Tween 20 (Sigma-Aldrich, MO, USA) and the lysate centrifuged for 10 min, 4°C, 10^4 rpm. Ni-NTA resin (Qiagen, D) was added to the supernatant and the mixture was shaken for 1 h, 4°C. The mixture was then centrifuged for 5 min at 1700 rpm and the pellet washed two times with Wash Buffer (50 mM NaH_2PO_4, 300 mM NaCl and 20 mM imidazole). The OGG1 bound to the resin was eluted with a buffer composed by 50 mM NaH_2PO_4, 300 mM NaCl and 600 mM imidazole. OGG1 concentration was determined by Bradford method and the purity was confirmed by sodium dodecyl sulphate-polyacrylamide gel electrophoresis (SDS-PAGE) (Supplementary Figure S1). Finally, the protein was concentrated and desalted by using the Ultracel YM-3 Microcon Centrifugal Filter Devices (Millipore, MA, USA).

Chromatin immunoprecipitation (ChIP) and qPCR analysis

ChIP was carried out as described in ref. 31, by using the ChIP-IT® Express Shearing Kit (Active Motif, CA, USA). In brief, Panc-1 cells (8×10^5) were seeded in 6-well plates and after 24 h some plates were treated with 10 μM luteolin for 24 h in DMEM or with 1 mM hydrogen peroxide for 15 min in serum-free DMEM. The cells were then washed with phosphate buffered saline (PBS) and fixed for 10 min in serum-free DMEM containing 1% formaldehyde. After fixing, the cells were washed with cold PBS and added with Glycine Stop-Fix Solution to arrest the fixing reaction. The cells were washed again with cold PBS, treated with Scraping Solution and centrifuged at 2500 rpm for 10 min at 4°C. The pellet was resuspended in ice-cold lysis buffer supplemented with PMSF, PIC (protease inhibitor cocktail) and incubated for 30 min on ice. The cells were transferred to an ice-cold dounce homogenizer for 20 strokes to release the nuclei. The homogenate was centrifuged for 10 min at 5000 rpm, 4°C, to pellet the nuclei. The nuclei were resuspended in Shearing Buffer and the chromatin sheared by sonication [10 ×(30 s pulse on/30 s pulse off)] on Bioruptor Plus (Diagenode, BG) into DNA fragments of about 300–400 bp. The sheared chromatin was centrifuged at maximum speed for 15 min, 4°C. The chromatin concentration was determined with a spectrophotometer by ultraviolet (UV) absorption (260 nm) and 10 μg treated overnight at 4°C with 1 μg antibody specific for 8-oxoG (Bioss Antibodies, MA, USA) or MAZ or OGG1 (Santa Cruz Biotechnology, TX, USA) or hnRNP-A1 (Sigma-Aldrich, MO, USA). In addition to the antibodies, the mixtures were added with Protein G Magnetic Beads, ChIP buffer-1 and PIC, following the Active Motif Kit protocol. After incubation the mixtures were span and the

chromatin bound to the antibody collected with a magnetic bar. The collected beads were washed once with ChIP buffer-1 and twice with ChIP buffer-2. The beads were then re-suspended in Elution Buffer AM2 and let to incubate on shaking for 15 min at room temperature. The beads were treated with Reverse Crosslinking Buffer and the supernatant with the chromatin was collected. The DNA fragments were amplified by qPCR using primers spe- cific for genomic *KRAS* (accession number NG 007524): *G4*-plus 5′-GTACGCCCGTCTGAAGAAGA-3′ (nucleotides (nt) 4889–4908, 0.2 μM), *G4*-minus 5′-GAGCACACCGATGAGTTCGG-3′ (nt 4958–4977, 0.1 μM), Ctr-1-plus 5′-ACAAAAAGGTGCTGGGTGAGA-3′ (nt 12–32, 0.2 μM), Ctr-1-minus 5′-TCCCCTTCCCGGAGACTTAAT-3′ (nt 248–268, 0.2 μM), Ctr-2-plus 5′-CTCCGACTCTCAGGCTCAAG-3′ (nt 7536–7555, 0.15 μM), Ctr-2-minus 5′-CAGCACTTTGGGAGGCTTAG-3′ (nt 7692–7711, 0.15 μM). Ctr-1 is located in a non-coding region, G4-region is in the promoter, Ctr-2 is in an intron. qPCR reactions were carried out with a CFX-96 real-time PCR apparatus controlled by Optical System software (version 3.1) (Bio-Rad Laboratories, CA, USA) on 1 μl of immunoprecipitated chromatin or input, which were mixed to Sybr Green mix following manufacturer instructions (Kapa Sybr Fast QPCR Mix, Kapa Biosystems, MA, USA) and primers. For G4-region amplification cycles were: 3 min at 95°C, 40 cycles 30 s at 95°C and 40 s at 59°C. For controls amplification cycles were: 3 min at 95°C, 40 cycles 10 s at 95°C and 30 s at 57°C (control-1) or 61°C (control-2). All reactions have been validated before amplification for each target and couple of primers. The Ct-values (number of cycles required for the fluorescent signal to cross the threshold) given by the instrument (Bio-Rad CFX-96) were used to evaluate the difference between sample and input. The adjusted Ct_{input} was obtained by $Ct_{input} - \log_2$ (input dilution factor). Then $\Delta Ct = Ct_{sample} - Adjusted\ Ct_{input}$. The % Input for each sample was calculated as follows: % Input $= 100 \times 2^{(-\Delta Ct)}$. The % Input was obtained for the G4 region and also for the non-G4 regions (Ctr-1 and Ctr-2). The enrichment in 8-oxoG or MAZ or hnRNPA1 or OGG1 of the G4 region respect to the non-G4 regions was determined by the ratio [% Input $_{(G4\ region)}$]/[% Input $_{(non\text{-}G4\ region)}$]. In average, from three to seven samples were used for each experiment. The *t*-test analysis was performed with Sigma Plot 10.1(UK).

Circular dichroism and UV-melting

Circular Dichroism (CD) spectra were obtained on a JASCO J-600 spectropolarimeter, equipped with a thermostated cell holder, with 5 μM oligonucleotides solutions in 50 mM Tris–HCl, pH 7.4, 100 mM KCl. The spectra were recorded in 0.5 cm quartz cuvette at room temperature and 90°C. The spectra are reported as ellipticity (mdeg) versus wavelength (nm). Each spectrum was recorded three times, smoothed and subtracted to the baseline.

UV-melting analysis was performed using the Jasco V-750 UV-visible spectrophotometer equipped with a Peltier temperature control system (ETCS-761) (Jasco, JP). The spectra were analyzed with Spectra Manager (Jasco, JP). Oligonucleotides (5 μM) were annealed in 100 mM KCl, 50 mM Na-cacodylate pH 7.4 (10 min at 95°C, overnight at room temperature). The melting curves were recorded at 295 nm in a 0.5 cm path length quartz cuvette heating (20–90°C) and cooling (90–20°C) at a rate of 0.5°C/min. The thermodynamic parameters for the folding of the wild-type and modified oligonucleotides into G4 were obtained from the UV-melting curves. The 'DNA-Melting Analysis' program (Jasco, JP), which analyzed the melting curves according to a standard *all-or-none* model, gave the ΔH° and ΔS° values. The free energy of quadruplex formation was calculated according to: $\Delta G^\circ = -\mathrm{RT} \ln K = \Delta H^\circ - T\Delta S^\circ$.

PAGE assay

8-OxoG-substituted oligonucleotides end-labeled with [γ-^{32}P]adenosine triphosphate (ATP) (Perkin Elmer) and T4 polynucleotide kinase (Thermo Fisher Scientific, USA), were annealed in duplex or quadruplex as follows: the duplex was obtained annealing (5 min at 95°C, overnight at room temperature) the 8-oxoG-substituted oligonucleotides and 32R with complementary 32Y in 50 mM Tris–HCl, pH 7.4, 100 mM NaCl; the quadruplexes were obtained in 50 mM Tris–HCl, pH 7.4, 100 mM KCl (5 min at 95°C, overnight at room temperature). Radiolabeled duplex and quadruplex (2 nM) were incubated at 37°C with increasing amounts of OGG1 (1 and 5 μM), in 20 mM Tris–HCl pH 8, 50 mM NaCl, 1 mM ethylenediaminetetraaceticacid (EDTA), 0.1 mg/ml bovine serum albumin, 1 mM Na_3VO_4, 5 mM NaF and 0.01% Phosphatase In- hibitor Cocktail. After 15 min, the reactions were stopped by adding to the mixtures 8 μl stop solution (90% for- mamide, 50 mM EDTA). The samples were then denatured for 5 min at 95°C and run for 1 h on a denaturing 20% polyacrylamide gel, prepared in Tris-borate-EDTA (TBE) and 7 M urea, pre-equilibrated at 55°C in an electrophoretic apparatus (C.B.S Scientific Company, CA, USA). After running the gel was fixed in a solution containing 10% acetic acid and 10% methanol, dried and exposed to film for autoradiography (Aurogene, I).

Electrophoresis mobility shift assay (EMSA)

Duplexes and quadruplexes have been prepared as described in previous section. PAGE purified 8-oxoG-substituted oligonucleotides were end-labeled with [γ-^{32}P] ATP and T4 polynucleotide kinase (30 pmol). The corresponding duplexes were obtained by annealing (10 min at 95°C and overnight at room temperature) the modified oligonucleotides with the complementary strand in 50 mM Tris–HCl pH 7.4, 100 mM NaCl. Protein–oligonucleotide interactions were analyzed by electrophoresis mobility shift assays (EMSA). End-labeled duplexes or G-quadruplexes were incubated in 20 μl solutions containing 50 mM Tris–HCl, pH 7.4, 100 mM NaCl (for duplexes) or 100 mM KCl (for G-quadruplexes), 1 mM EDTA, 0.01% Phosphatase Inhibitor Cocktail I (Sigma-Aldrich, MO, USA), 5 mM NaF, 1 mM Na_3VO_4, 2.5 ng/μl poly [dI-dC], 1 mM Dithiothreitol (DTT) and 8% glycerol with increasing amounts of recombinant OGG1 (0.3 and 0.6 μg) or MAZ or hnRNP A1 (2.5–5 μg), time and temperature are indicated in figure legends. The mixtures were analyzed in 5% polyacrylamide gels

prepared in TBE at 20°C. After running, the gels were dried and exposed overnight to auto-radiography (Aurogene, I) at −80°C.

DMS-footprinting experiments

Dimethylsulphate (DMS)-footprinting experiments were performed using PAGE purified 8-oxoG-substituted oligonucleotides (24 nM), end-labeled with [μ-^{32}P] ATP. The oligonucleotides were incubated overnight at 37°C, in 50 mM Tris–HCl, pH 7.4, 1 μg sonicated salmon sperm DNA, 1 mM EDTA, 100 mM KCl or 100 mM LiCl, as specified in the figure legend. DMS dissolved in ethanol (DMS:ethanol, 2/38, vol/vol) was added to the DNA solution (2 μl to a total volume of 50 μl) and left to react for 1 min at room temperature. The reactions were stopped by adding to the mixtures 5 μl of stop solution (1.5 M sodium acetate, pH 5.2, 1 M þ-mercaptoethanol and 16 ng/μl salmon sperm DNA). DNA was precipitated with four volumes of ethanol and resuspended in piperidine 1 M. After cleavage at 90°C for 20 min, the reactions were stopped on ice and the DNA precipitated with 0.3 M sodium acetate, pH 5.2 and three volumes of ethanol. The DNA samples were resuspended in 90% formamide and 50 mM EDTA, denatured at 90°C and run for 2 h on a denaturing 20% polyacrylamide gel, prepared in TBE and 8 M urea, pre-equilibrated at 55°C in a Sequi-Gen GT Nucleic Acids Electrophoresis Apparatus (Bio-Rad, CA, USA), which was equipped with a thermocouple that allows a precise temperature control. After running, the gel was fixed in a solution containing 10% acetic acid and 10% methanol, dried at 80°C and exposed to film (CL-XPosure Thermo scientific, MA, USA) for auto-radiography. Lane scan and analysis was performed with Image Quant TL software (Image Scanner, Amersham, UK).

Pull-down assay with Panc-1 extract

A total of 0.5 mg of nuclear Panc-1 extract (1.3 mg/ml) were incubated for 1.5 h at 37°C with 80 nM biotinylated 32R or **96** in 20 mM Tris–HCl, pH 7.4, 50 mM KCl, 8% glycerol, 1 mM DTT, 0.1 mM ZnAc, 5 mM NaF, 1 mM Na_3VO_4 and 2.5 ng/μl poly[dI-dC]. A total of 100 μg of Streptavidin MagneSphere Paramagnetic Particles (Promega, I) were added and let to incubate for 1 h at 4°C. The beads were captured with a magnet and washed two times. The proteins were denatured and eluted with Laemmli buffer (4% SDS, 20% glycerol, 10% 2-mercaptoethanol, 0.004% bromophenol blue and 0.125 M Tris–HCl). Then they were separated in 10% SDS-PAGE and blotted into nitrocellulose at 70 V for 2 h. The nitrocellulose membrane was blocked for 1 h with 5% fat dried milk in PBS and 0.05% Tween (Sigma-Aldrich, USA) at room temperature. The primary antibodies used were: anti-MAZ (clone 133.7, IgG mouse, Santa Cruz Biotechnology, USA) diluted 1:200, anti-hnRNP A1 (clone 9H10, IgG mouse, Sigma-Aldrich, USA) diluted 1:2000 and anti PARP-1 (polyclonal antibody, IgG rabbit, Cell Signalling Technology, USA) diluted 1:200. The membranes were incubated overnight at 4°C with the primary antibodies, then washed with 0.05% Tween in PBS and incubated for 1 h with the secondary antibodies conjugated to horseradish peroxidase: anti-mouse IgG (diluted 1:5000) and anti-rabbit IgG (diluted 1:5000) (Calbiochem, Merck Millipore, D). The signal was developed with Super Signal ®West PICO, and FEMTO (Thermo Fisher, USA) and detected with ChemiDOC XRS, Quantity One 4.6.5 software (BioRad Laboratories, USA).

RESULTS AND DISCUSSION

8-oxoG in *KRAS* is more abundant in G4 than in non-G4 regions

Cancer cells have relatively high levels of ROS that may damage DNA, RNA and proteins. Oxidative damage to DNA occurs mainly on guanine (21), in particular at the 5′ guanine of GG runs (22). G-rich quadruplex motifs, being composed by several runs of guanines, are effective hotspots for guanine oxidation (32). The formation of 7,8-dihydro-8-oxoguanine (or 8-oxoG) in these sequence motifs may be favored by the particular folded structure that they assume under physiological conditions (23,29). Indeed, four consecutive G-runs separated by few bases can form a G-quadruplex or G4 structure stabilized by tetrads of guanines. A G4-Seq conducted on the human genome found >7 × 10^5 potential G4 motifs, mainly located in functional regions including promoters, 5′-Untranslated region (UTRs) and splicing sites (33). A subsequent G4-ChIP-Seq analysis conducted on chromatin revealed a lower number (about 10^4) of G4 motifs folded into a G-quadruplex. The critical point of these studies is that not all G4 motifs are folded under cellular conditions. Interestingly, many folded G4 motifs are present in oncogenes including *CMYC* and *KRAS* (34). Recently, Burrows and co-workers developed an elegant method, '8-oxoG-Seq', to sequence 8-oxoG in the mouse genome. They found ~10^4 regions of 8-oxoG enrichment in WT mouse embryonic fibroblast, in particular where there are G4 motifs (gene promoters and UTRs) (35). We therefore asked if 8-oxoG has an epigenetic potential in gene regulation and focused on the *KRAS* oncogene, which harbors upstream of the TSS a G-rich sequence with regulatory functions.

Human *KRAS* displays three G4-motifs that, according to their distance from TSS, can be named G4-proximal (previously named 32R, −148/−116), G4-middle (−207/−175) and G4-far (−260/−226) (23,25,28,29,36). Sequence 32R (69% GC), which has been extensively studied in our labo- ratory, is sensitive to nucleases and shows a complex struc- tural polymorphism (23,25,37). DMS-footprinting and CD experiments showed that 32R folds into a parallel G4 with a thymidine bulge in one strand and a (1/1/11) topology (23,25). Moreover, a truncated portion of 32R, comprising the first four G-runs from the 5′-end, folds into a (1/1/4) G-quadruplex (28,38). We reported that 32R is recognized by several nuclear proteins, including MAZ, PARP-1, Ku70 and hnRNP A1 (25–27). The role of MAZ and/or hnRNP A1 on *KRAS* transcription regulation has been investigated in our laboratory and also by Chu *et al*. (24,26,27,39). The data showed that both transcription factors upon binding to 32R unfold the G4 structure and favor the transcription process.

In order to understand, if the guanines of the G4 motifs upstream TSS are prone to oxidation, we carried out

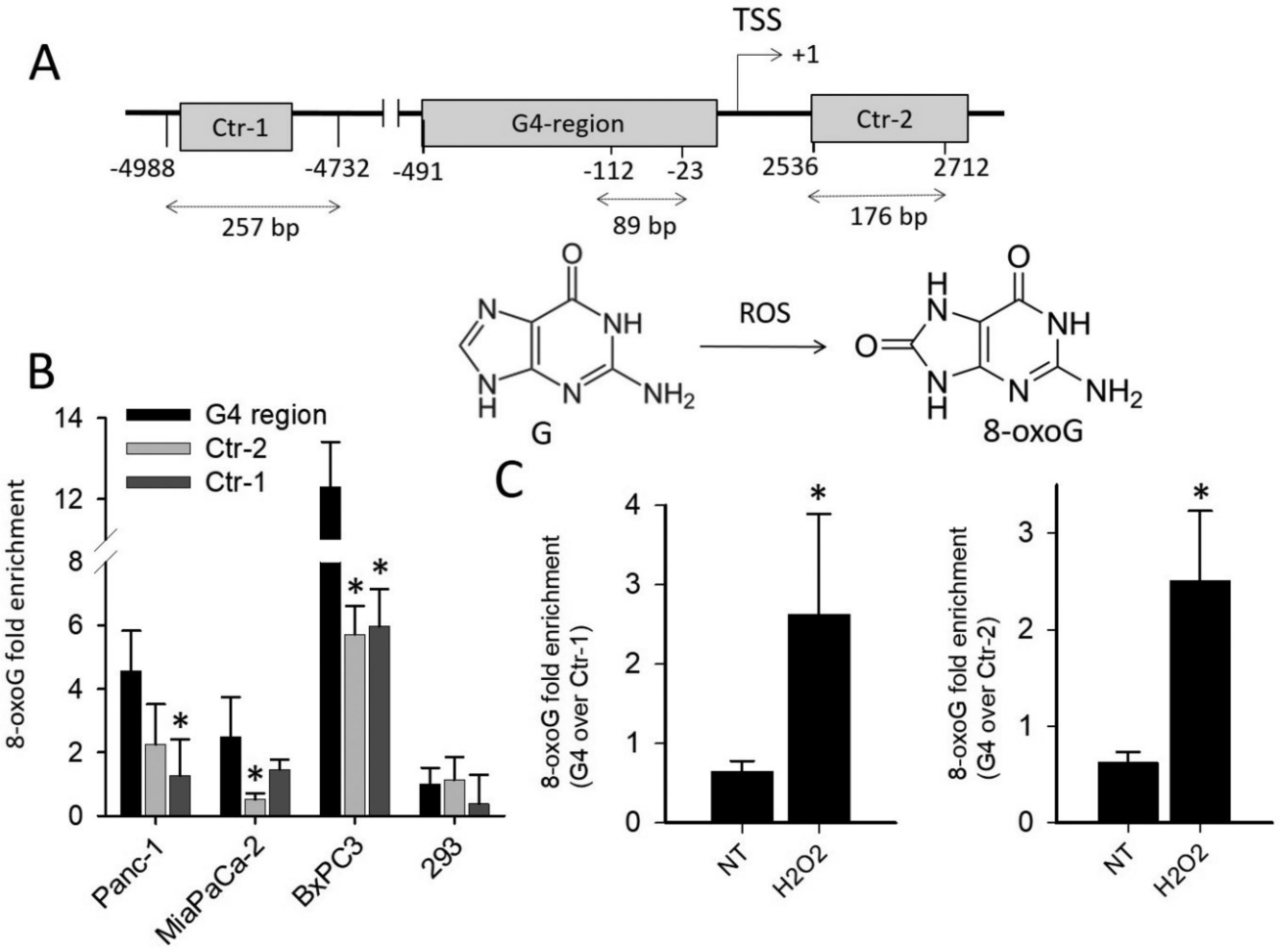

Figure 1. (**A**) Relative distance from TSS of G4 and non-G4 sequences used in quantitative real-time ChIP experiments. The length of each amplified DNA fragment is indicated. The structures of guanine and 8-oxo-7,8-dihydroguanine (8-oxoG) are shown; (**B**) ChIP qPCR showing the basal level of 8-oxoG in G4 and in non-G4 regions Ctr-1 and Ctr-2 in pancreatic cancer cells harboring mutated *KRAS* (Panc-1 and MIAPaCa-2) or wild-type *KRAS* (BxPC3) and in non-cancer HEK-293 cells. The histogram shows the fold enrichment of 8-oxoG in pancreatic cancer cells compared to 8-oxoG in G4 region of 293 cells; (**C**) ChIP qPCR showing the relative level of 8-oxoG in G4 compared to non-G4 regions (Ctr-1 and Ctr-2). The ordinate reports the ratio between the level of 8-oxoG in G4 and in non-G4 region, in Panc-1 cells treated with 1 mM H_2O_2. The asterisk (*) means $P < 0.05$ ($n = 4$), a Student's *t*-test was performed.

ChIP qPCR experiments. We measured the basal level of 8-oxoG in the *KRAS* promoter region including 32R and compared it to other G-rich regions which are unable to fold into G4: Ctr-1 (containing a segment with 56% CG) and Ctr-2 (with 65% CG), both located >2000 bp from 32R (Figure 1A). Preliminary semi-quantitative ChIP PCR experiments carried out with pancreatic Panc-1 cancer cells clearly showed that 8-oxoG is more abundant in G4 than in non-G4 regions (Supplementary Figure S2). However, to determine the difference in guanine oxidation between G4 and non-G4 regions, we performed quantitative ChIP qPCR in three pancreatic cancer cell lines (Panc-1 with *KRAS* G12D, MIA PaCa-2 with *KRAS* G12V and BxPC3 with wild-type *KRAS*) and in one non-tumor cell line (human embryonic kidney 293 cells, HEK-293) (Figure 1B). It turned out that the basal level of 8-oxoG in the cancer cells is up to 12-fold higher than in normal HEK-293 cells. This correlates with the fact that cancer cells have higher levels of ROS than normal cells (1,2). Our analysis also confirmed that in the three cancer cells analyzed, the G4-containing regions are more exposed to guanine oxidation (up to 4-fold) than the non-G4 regions Ctr-1 and Ctr-2. As Ctr-1 and Ctr-2 have a CG content >50% and contain several GG runs, the difference in 8-oxoG between G4 and non-G4 regions cannot be ascribed to a low presence of guanines in the non-G4 regions. Previous studies reported that the secondary structure adopted by DNA affects the reactivity of guanine toward oxidative stress and that the guanines in a G-quadruplex are more keen to oxidation than the guanines in a duplex (40,41). Another interesting observation is the higher level of 8-oxoG in BxPC3 cells compared to Panc-1 and MIA PaCa-2 cells. This can be rationalized with the fact that only the latter cells carry a hyperactivated mutant *KRAS* which is known to constitutively stimulate the expression of Nrf2, a gene that activates the detoxification program bringing down ROS and thus 8-oxoG (9–11). As previously reported (12,14), we also found that there is a direct link between *KRAS* and Nrf2, as the overexpression

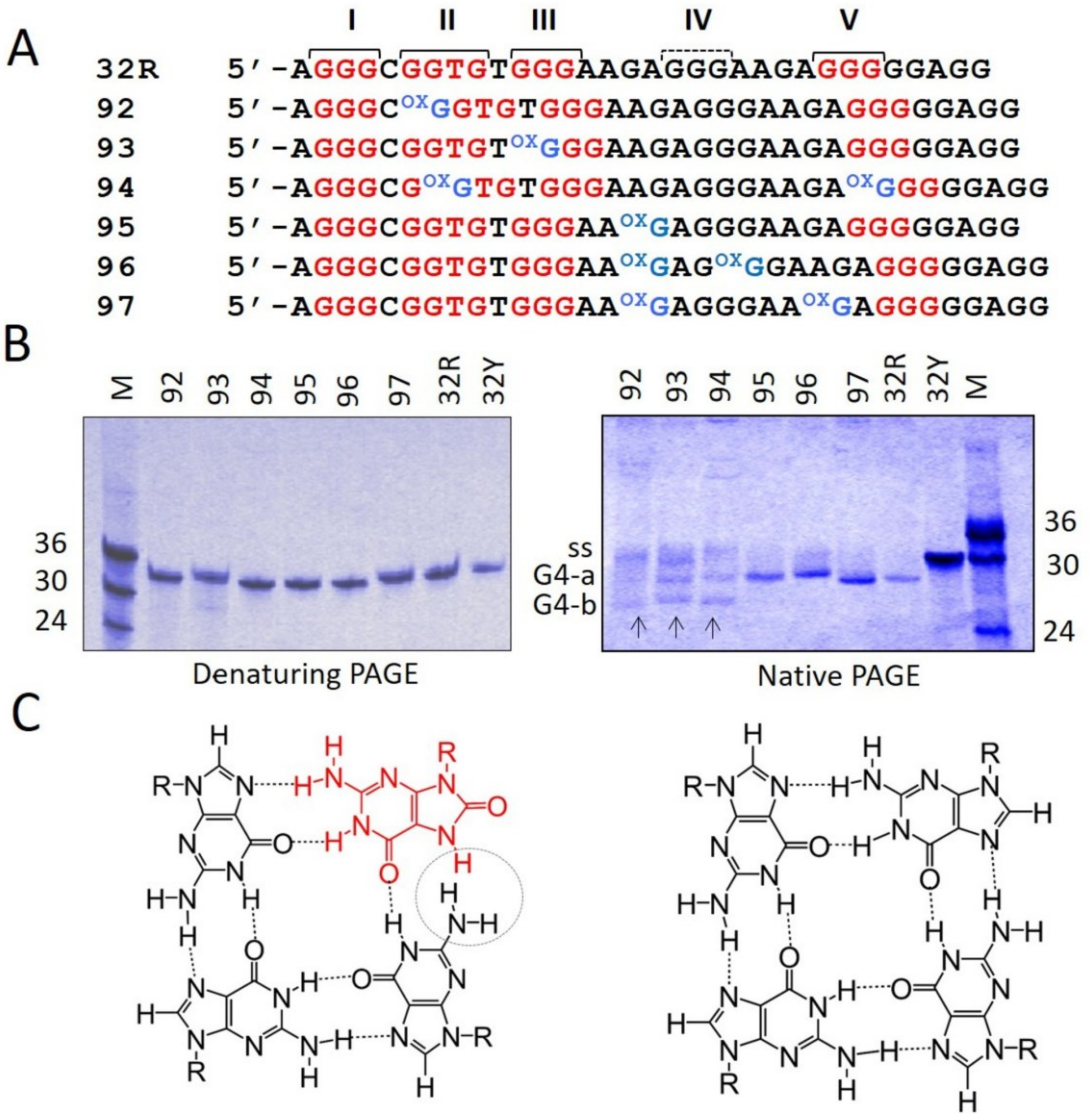

Figure 2. (**A**) Sequences of 32R and of the designed oligonucleotides with one or two 8-oxoG either in the major 11-nt loop of *KRAS* G4 (**92**, **93** and **94**) or in G-tetrads (**95**, **96** and **97**). The G-runs I–V are pointed out; (**B**) 20% PAGE of 32R and 8-oxoG-substituted oligonucleotides in denaturing (left) and native (right) gels. As reference oligonucleotides of 24, 30 and 36 nt have been loaded. G4-a and G4-b are due to G4 structures, ss indicates unstructured oligonucleotides. Gels were repeated three times; (**C**) Structure of a G-tetrad with 8-oxoG (left) and of a canonical G-tetrad (right).

of *KRAS* in Panc-1 cells brought about an increase of Nrf2 (Supplementary Figure S3).

Finally, to make sure that the level of 8-oxoG correlates with the cellular amount of ROS, we performed ChIP qPCR assays with Panc-1 cells treated with H_2O_2. As expected, the treatment with H_2O_2 raised 8-oxoG in the G4 region 4- fold more than in the non-G4 regions Ctr-1 and Ctr-2 (Fig- ure 1C).

8-OxoG affects the folding of the G-rich 32R promoter sequence

DMS-footprinting and CD studies, reported by ourselves (23,25) and others (36), showed that 32R folds into a parallel G4 formed by the G-runs I, II, III and V (Figure 2A). Distinctive features of this G-quadruplex are a large 11-nt loop and a strand with a thymidine bulge (Supplementary Figure S4). On the basis of this putative structure, we designed mimics of 32R, carrying 8-oxoG at specific positions: in the G-tetrads (oligonucleotides **92**, **93** and **94**) or in the 11-nt loop (**95**, **96** and **97**). Under denaturing conditions (7 M urea), the 8-oxoG-substituted oligonucleotides migrated expectedly as wild-type 32R or as its complementary strand 32Y. By contrast, under native conditions (100 mM KCl) the oligonucleotides carrying one or two 8-oxoG in the 11-nt loop (**95**, **96** and **97**) migrated in the same way as 32R, with a single band running faster than the unstructured oligonucleotide 32Y (Figure 2B). This suggests that when the oxidized guanine is in the 11-nt loop, the folding of the G4-motif is not affected [i.e. it is similar to that of wild-type 32R, (1/1/11) G4]. Instead, when 8-oxoG is placed in the G-runs II, III or V, which are involved in the formation

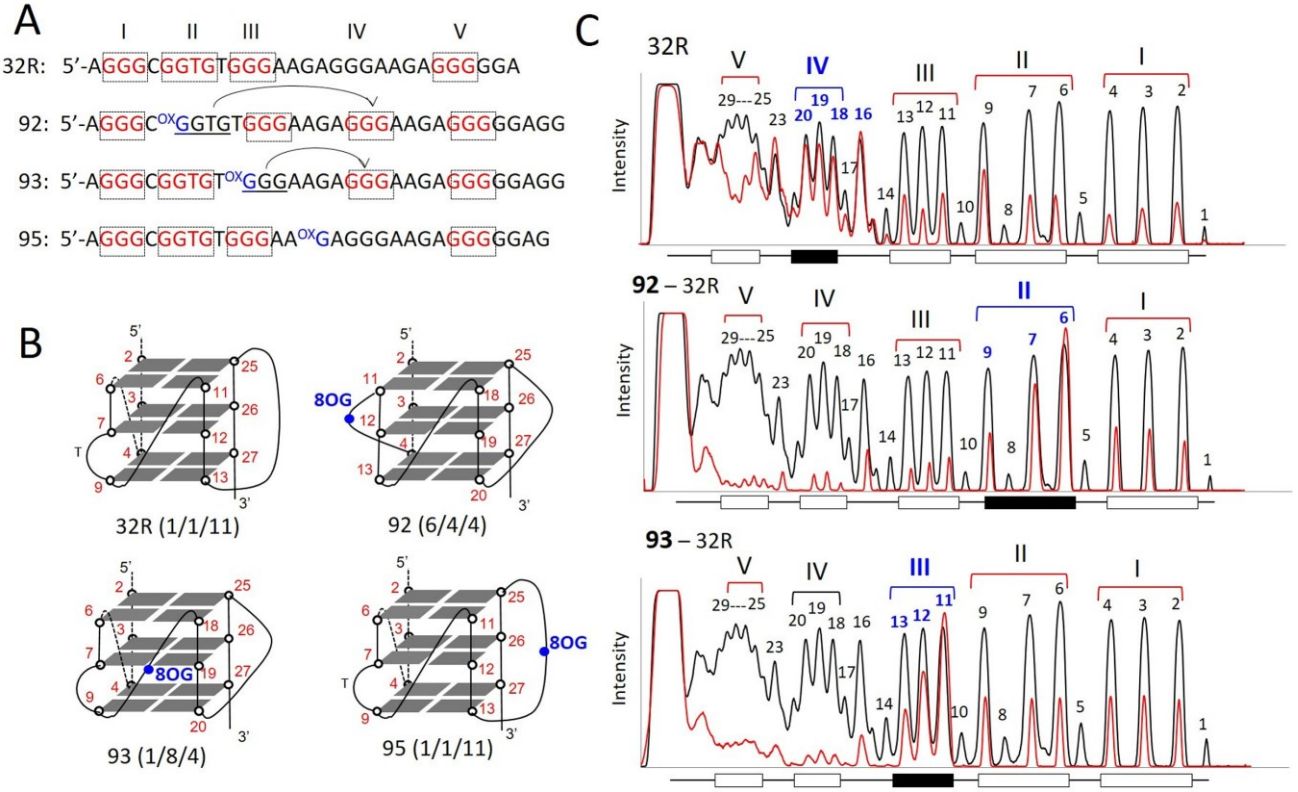

Figure 3. (**A**) Sequences of 32R, **92**, **93** and **95** showing the G-runs involved in G4 formation (indicated in red). Compared to 32R, **92** and **93** undergo a different folding in order to exclude 8-oxoG from a G-tetrad; (**B**) Structure of the putative G-quadruplexes with 8-oxoG; (**C**) Comparison of the DMS-footprinting of unstructured 32R with those of structured 32R and **92**, **93** analogs. Note that the fifth G-run of 32R replaces the G-run with 8-oxoG through an alternative folding. Experiment was repeated three times.

of the G-tetrads (**92**, **93** and **94**), the oligonucleotides migrated with 2-folded structures: one running as the G4 of wild-type 32R (band G4-a) and one running faster (band G4-b) (Figure 2B). It should be borne in mind that 8-oxoG is expected to destabilize the G-tetrad arrangement, as the N7 of diketo 8-oxoG becomes a hydrogen donor and sterically clashes with the amino group of a neighboring guanine (Figure 2C). This means that 8-oxoG can hardly stay in a G-tetrad, as the two H-bonding pattern is replaced by a single H-bonding pattern. It is therefore reasonable to assume that the incorporation of 8-oxoG in a G-tetrad destabilizes the G-quadruplex. Indeed, single substitutions of guanine with 8-oxoG have been reported to do so (42).

An insight into the structure of the human *KRAS* G-quadruplex with 8-oxoG substitutions was obtained by DMS-footprinting. As 32R contains 5 G-runs, it is likely that the G-run carrying 8-oxoG is excluded from the formation of the G-tetrads and replaced by the redundant fifth G-run present in 32R, as observed with G4 motifs found in oncogene promoters and telomeres (Figure 3A and B) (43,44). This occurs through an alternative folding of 32R. As illustrated in Figure 3C, wild-type 32R shows its typical DMS footprinting in 100 mM KCl with all guanines protected from DMS, except G16, G18–20 and G23. This cleavage pattern is consistent with the formation of a (1/1/11)-G4 by the G-runs I, II, III and V (23,25). The DMS-footprinting of oligonucleotide **92**, which was designed with 8-oxoG in G-run II, clearly shows a different cleavage pattern. In keeping with the 'fifth G-run' hypothesis, its folding involves the G-runs I, III, IV and V, giving rise to (6/4/4) G-quadruplex. It can actually be seen that G-run II (G6-G7-G9) is reactive to DMS, while G-run IV (G18-G19-G20) is not. This DMS reactivity pattern demonstrates that the fifth G-run (G-run IV) has indeed replaced G-run II carrying 8-oxoG, through a re-modulation of the folding in order to exclude the oxidized guanine from the G4 scaffold. The resulting (6/4/4) G4, having loops <11 nt, is more compact than wild-type (1/1/11) G4 and that explains why it runs faster in a polyacrylamide gel (band G4-b, Figure 2B). Oligonucleotide **93**, carrying 8-oxoG in G-run III, shows a similar behavior as **92**. In this case, G-run III is more reactive to DMS, suggesting that it is replaced by G-run IV (G18-G19-G20), which appears protected. We also analyzed oligonucleotide **95** with 8-oxoG in the 11-nt loop, that should not impact on the folding. In keeping with this prediction, the footprinting of **95** shows that the bases cleaved are those located in the 11-nt loop, as observed with the wild-type 32R sequence (Supplementary Figure S5). A similar behavior has been observed with the critical G4 motif of *CMYC* (45). DMS footprinting and RNA polymerase stop assays showed that a simple 8-oxoG induces a change in the folding to exclude the oxidized G-run from the formation of the G-tetrads.

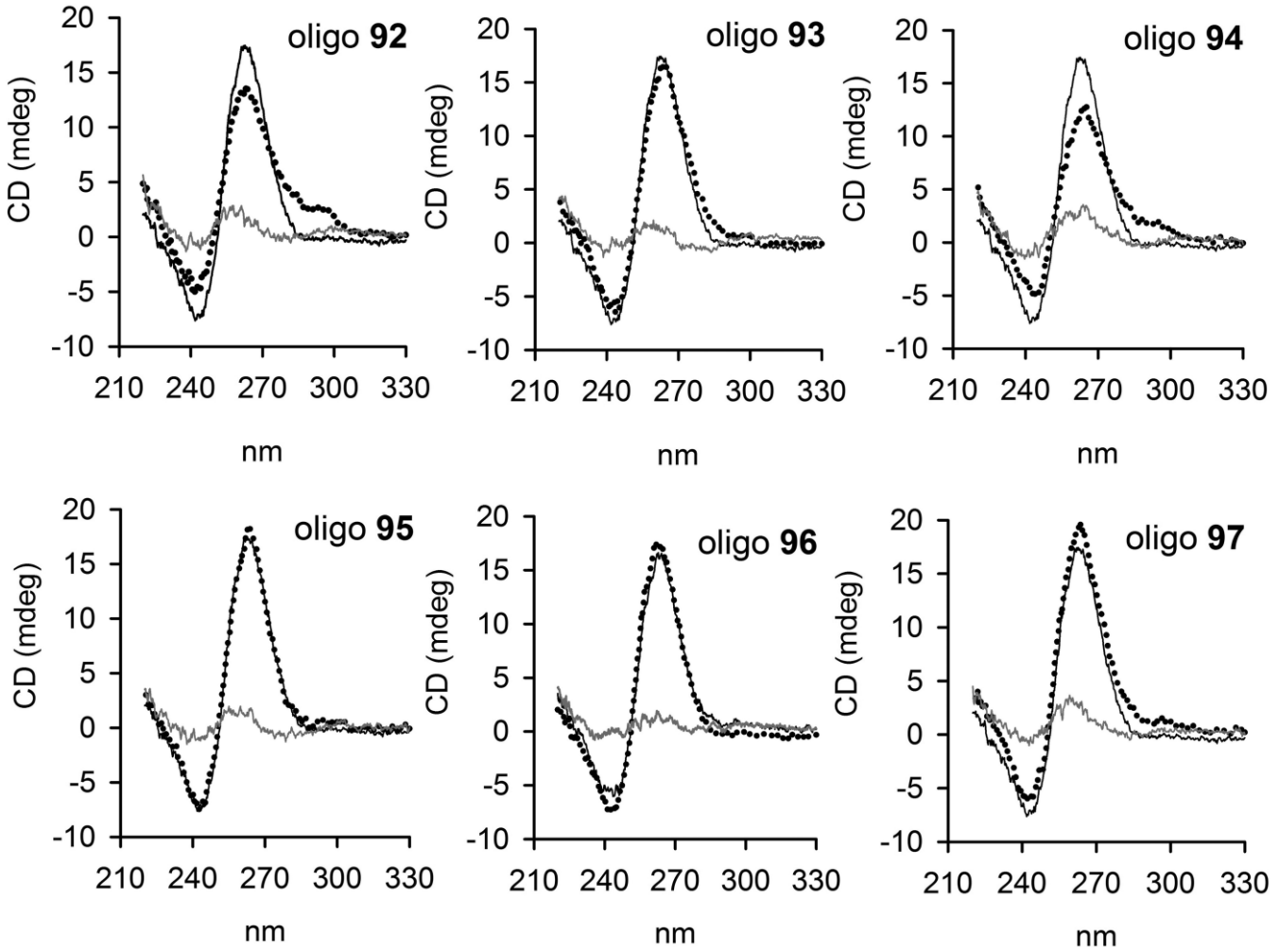

Figure 4. CD spectra of 32R at 20°C (black) and of 8-oxoG-substituted oligonucleotides at 20°C (dotted spectra) and 90°C (gray spectra), in 50 mM Tris–HCl, pH 7.4, 100 mM KCl. Each panel compare the CD spectrum of 32R with that of an oligonucleotide with 8-oxoG. The ordinate reports the ellipticity signal expressed in mdeg.

Fleming and co-workers have observed that there are many oncogenes with G4 motifs carrying an extra G-run that could relieve a damaged guanine through a structural transition (44). The authors hypothesized that the extrusion of the damage into a loop should be necessary for the activation of the base excision repair mechanism. However, the evolutionary selection of a fifth G-run in regulatory G4 motifs recognized by transcription factors might also find its rationale in the fact that 8-oxoG could act as a transcription regulator by modulating the binding and recruitment of transcription factors to promoter sequences (see *infra*).

Circular dichroism and UV-melting of the G4 structures with 8-oxoG

Next, we asked if the presence of 8-oxoG in 32R may affect the strand directionality of the G-quadruplex. To address this question, we performed circular dichroism experiments, as CD is a spectroscopic technique sensitive to DNA secondary structures. In Figure 4, we compared the CD spectra of each 8-oxoG-substituted sequence, obtained at 20 and 90°C, with the CD of 32R. At 20°C, all the spectra are characterized by a strong and positive ellipticity at 264 nm and a negative ellipticity at 245 nm, which are typical of a parallel or type I G-quadruplex (46). At 90°C, the intensity of the 264-nm ellipticity is dramatically reduced, suggesting that at 20°C the 8-oxoG-substituted oligonucleotides are structured. Oligonucleotides **92** (6/4/4) and **94** (6/4/5) show also a weak ellipticity at 295 nm, that may point to the formation of an alternative parallel/antiparallel G4. Instead, the CD spectra of **95**, **96**, **97** and 32R, forming a G4 with the same (1/1/11) topology, exhibit almost identical CD spectra.

As the thermal differential spectra of 32R and 8-oxoG-substituted oligonucleotides show a negative band at 295 nm, we followed their melting by measuring the absorbance at 295 nm as a function of temperature (47). Typical melting curves are shown in Figure 5. At heating/cooling rates of 0.5°C/min, we obtained curves that are superimposable, indicating that the melting/annealing proceeded through equilibrium states. The T_M's, determined by the dAbs/dT versus T plots, are reported in Table 1. The data show that when the oxidized guanine is located in the 11-nt loop (**95**, **96** and **97**), the damage is well tolerated, as the oxidized G4s

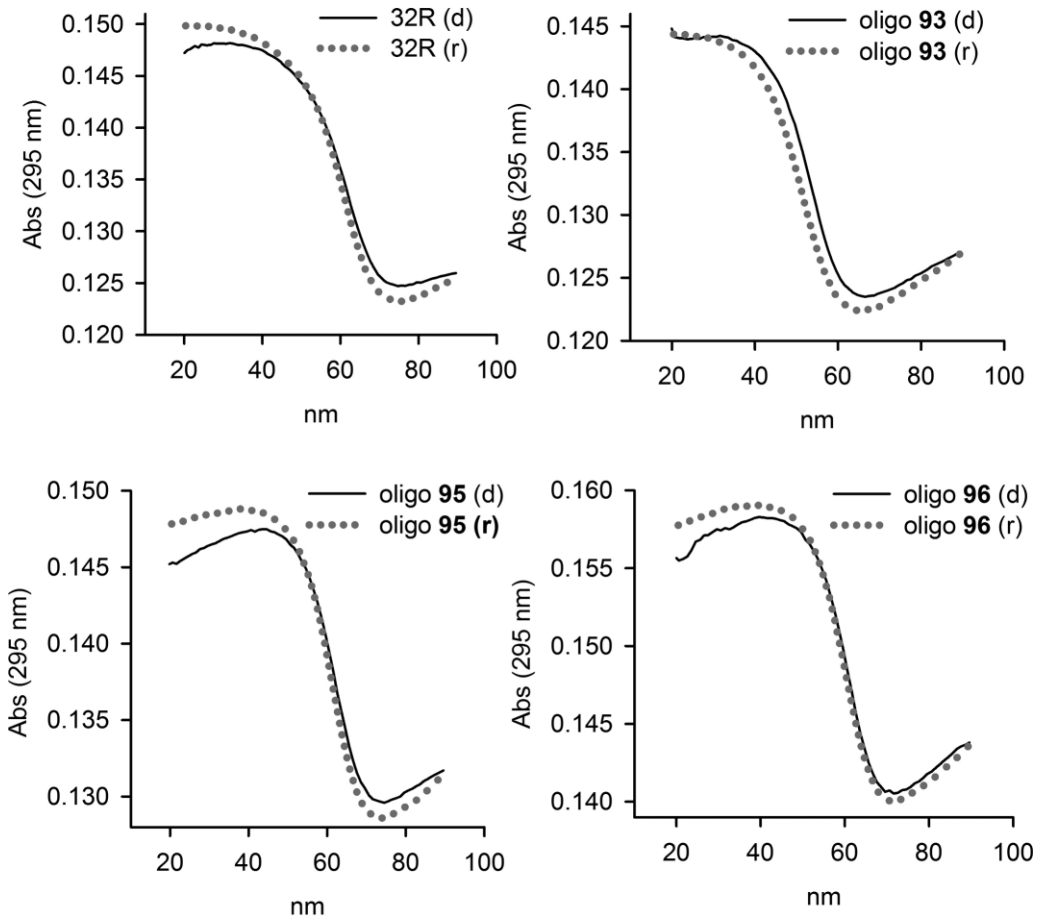

Figure 5. Denaturing and annealing UV-melting curves of 32R and 8-oxoG substituted oligonucleotides in 50 mM cacodylate pH 7.4, 100 mM KCl. The curves have been obtained by measuring the absorbance at 295 nm as a function of temperature, at a heating/cooling rates of 0.5°C/min. Denaturing, black filled curves; renaturing, dotted gray curves.

show T_M values nearly similar to that of 32R ($\Delta T_M \sim 1$–2°C). So, in terms of stability, CD spectra, electrophoretic mobility and DMS-footprinting demonstrate that 32R and **95**, **96** and **97** form the same G-quadruplex. In contrast, when the oxidized guanine is inserted in a G-tetrad, the T_M's of the resulting G4s (**92**, **93**, **94**) are significantly lower than that of the wild-type G4 (ΔT_M 10≈11°C), in agreement with previous data obtained with the telomeric sequence (42). However, in our case, the decrease of the T_M's is not due to altered stacking interactions between the G-tetrads, but to a change in the folding involving the fifth G-run.

The thermodynamic parameters of G-quadruplex formation were obtained from the melting profiles by using a 'DNA Melting Analysis' software (Jasco, JP). As the melting curves proceeded in a two-state manner, we could analyze them with a standard *all-or-none* model. The data reported in Table 1 show that the ΔG of the G-quadruplexes with one or two 8-oxoGs in the major 11-nt loop (**95**, **96** and **97**) is ≈1–2 kcal/mol more favorable than the ΔG of wild-type G4. This increase of stability is enthalpic in origin, and may probably arise from more efficient stacking interactions between 8-oxoG and the surrounding bases in the loop. In contrast, when the damage is inserted in a G-tetrad (**92**, **93** and **94**) the sequences fold into an alternative G-quadruplex with a ΔG about 2 kcal/mol less favorable than the ΔG of wild-type G4.

OGG1 is recruited to the *KRAS* G4 motif region carrying 8-oxoG

The enhanced level of 8-oxoG in the G4 region of *KRAS* upstream of TSS suggested to investigate whether the base-excision repair (BER) pathway is activated. BER is initiated by DNA glycosylases, which recognize and remove the oxidized guanines. The resulting apurinic site is then cleaved and the single-strand break processed by a short- or long-patch BER. The first enzyme of this pathway is OGG1, which behaves *in vitro* as a bifunctional DNA glycosylase excising 8-oxoG and cleaving the abasic site, while *in vivo* it behaves as a monofunctional glycosylase, with APE1 performing the lyase function (48–52). In order to see if OGG1 is recruited to the *KRAS* promoter when the level of 8-oxoG is increased by oxidative stress, we performed ChIP qPCR assays. We found that when Panc-1 cells are treated with H_2O_2 or luteolin, an inhibitor of Nrf2 that causes an increase of cellular ROS (53,54), the recruitment of OGG1 to the *KRAS* promoter increases more in G4 than in the non-G4 regions Ctr-1 and Ctr-2 (Figure 6A). We then pro- duced and purified recombinant OGG1 to test its capac-

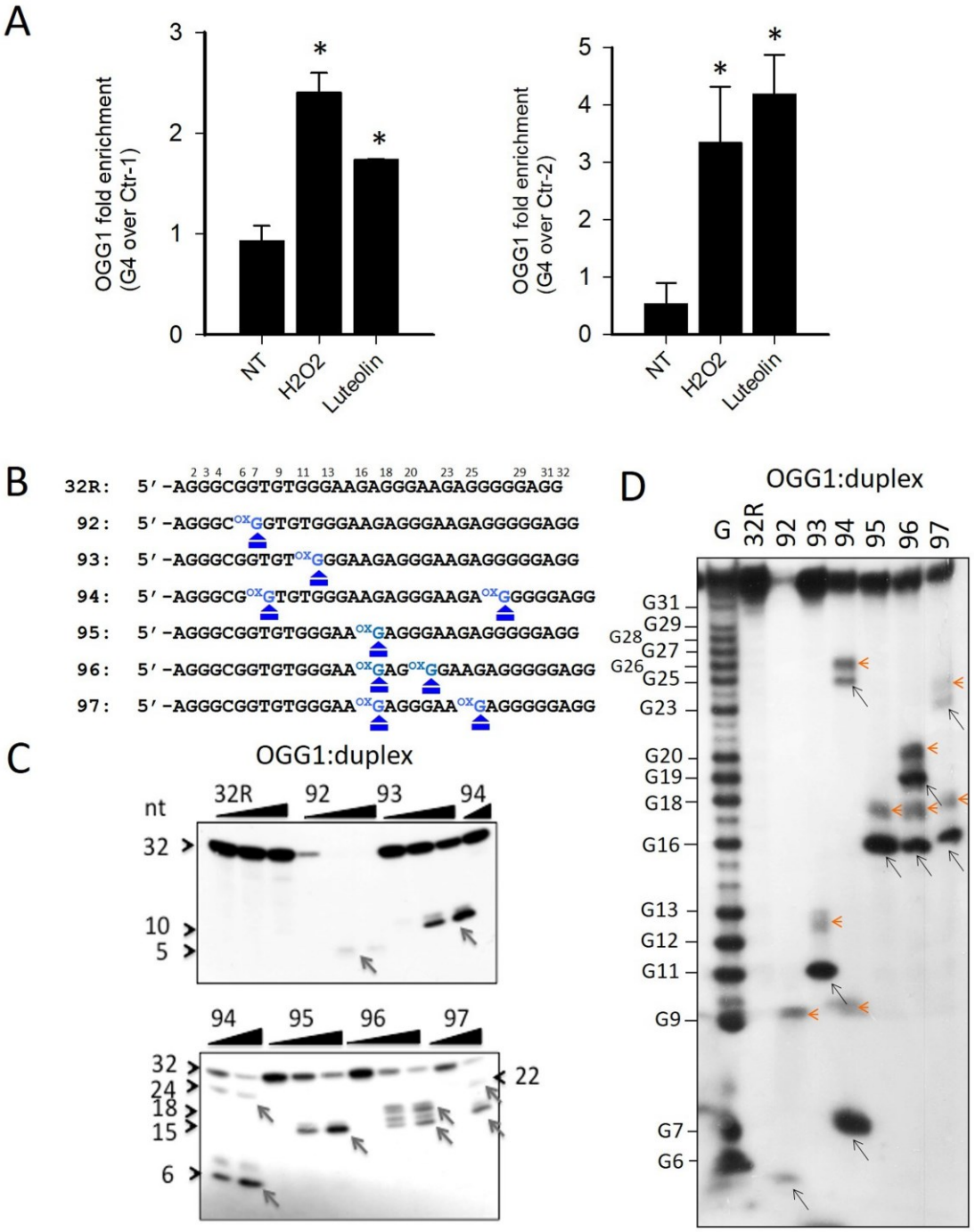

Figure 6. (**A**) ChIP qPCR showing that after treatment of Panc-1 cells with 1 mM H_2O_2 or 10 μM luteolin, the recruitment of OGG1 to the *KRAS* promoter increases more at G4 region than non-G4 regions (Ctr-1 and Ctr-2). Asterisk (*) indicate $P < 0.05$ ($n=4$), a Student's *t*-test was performed; (**B**) Primary sequences of 32R and designed 8-oxoG-substituted oligonucleotides where the positions of 8-oxoG are indicated; (**C**) The panel shows in a denaturing PAGE that OGG1 excises 8-oxoG in the duplexes formed by the designed 8-oxoG oligonucleotides and the complementary strand; (**D**) Sequencing 18% PAGE showing that OGG1 (1 μM) cleaves the radiolabeled duplexes (2 nM) exactly at the positions where there is 8-oxoG. The experiments in (C) and (D) were repeated three times.

Table 1. Thermodynamic parameters for the *KRAS* 8-oxoG substituted oligonucleotides

Oligo	T_M[a] (°C)	ΔT_M[b] (°C)	Number 8-oxoG	ΔH°[c] kcal/mol	ΔS°[c] cal/K mol	ΔG°[c,d] kcal/mol
92	50.7	11.4	1 in G-tetrad	−61.6 ± 0.8	−165 ± 2	−10.4 ± 0.2
93	52.8	9.3	1 in G-tetrad	−74.2 ± 1.3	−202 ± 4	−11.5 ± 0.1
94	52.6	9.5	2 in G-tetrad	−56.0 ± 0.9	−147 ± 3	−10.4 ± 0.2
95	61.5	0.6	1 in 11-nt loop	−78.7 ± 1.0	−208 ± 1	−14.2 ±
96				−80.1 ± 1.3	−215 ± 4	−13.4 ± 0.1
97	63.7	– 1.6	2 in 11-nt loop	−85.1 ± 1.0	−227 ± 3	−14.7 ±
32R				−66.1 ± 1.3	−172 ± 4	−12.8 ± 0.2

[a]data obtained in 50 mM cacodylate pH 7.4, 100 mM KCl.
[b]$\Delta T_M = T_M$ (32R) – T_M (8-oxoG oligo).
[c]Thermodynamic parameters obtained from analysis of melting cuves.
[d]$\Delta G = \Delta H - T\Delta S$, $T = 310$ K.

ity to excise 8-oxoG and cleave the abasic site. Increasing amounts of enzyme were incubated, for 15 min at 37°C, with ^{32}P-ATP labeled 8-oxoG-substituted oligonucleotides, transformed into duplexes with the complementary strand and the products were analyzed in a denaturing PAGE gel (Figure 6B and C). The enzyme did not show any activity on the wild-type 32R duplex, but it cleaved the duplexes carrying one or two 8-oxoGs. With duplexes **92**, **93** and **95**, which have only one 8-oxoG insertion, OGG1 gave only one main cleaved fragment; with duplexes **94, 96** and **97**, designed with two 8-oxoG lesions, it produced two fragments, as expected. Note that the bands are doublets, because after having removed 8-oxoG, OGG1 cleaves the apurinic site by both β and δ eliminations (55). In a native gel, we detected only at 4°C a weak binding of OGG1 to the designed duplexes, because the enzyme destabilizes the complexes (Supplementary Figure S6) by cleaving the substrates. In order to confirm that the cleavage catalyzed by OGG1 occurs exactly at the duplex sites where guanine has been replaced with 8-oxoG, we analyzed the products of the enzymatic reaction in a sequencing gel (Figure 6D). In lane 1, we report a G-reaction that determines the sequence of the duplex substrate. The pattern obtained is in nice agreement with Figure 6B and C. Each duplex substrate gave the fragment of the expected length, indicating that the cleavage occurs exactly at the place where the damaged guanine is. In the sequencing gel, the doublets appear clearer showing that the two fragments differ for two/three nucleotides, as a results of successive β and δ eliminations (55).

Then, we analyzed the catalytic activity of OGG1 on 32R and 8-oxoG- substituted oligonucleotides in the G4 conformation. The radiolabeled oligonucleotides were let to fold in KCl buffer and incubated with OGG1. Almost no cleaved products were detected in a denaturing gel, suggesting that the enzyme does have no or only slight activity against G4, as previously reported by Zhou *et al*. (56) (not shown). However, when we analyzed in a sequencing gel the mixtures between OGG1 and the designed 8-oxoG G-quadruplexes, we observed that the enzyme had a weak activity against specific guanines in the G4s (Figure 7A and B). The G-quadruplexes with 1/1/11 topology showed a small cleavage at G11 (a guanine of an external G-tetrad, Supplementary Figure S4), while G4s with 1/8/4 and 6/4/5 topologies (**93** and **94**) showed a weak cleavage in the loop, at G16/A17. This cleavage activity does not occur at oxidized guanines, is G4 specific and was not detected in the duplexes (see Figure 6C and D). To rule out that the OGG1 cleavage could be due to specific depurinations occurring during oligomer synthesis or handling (57), yielding abasic sites recognized by OGG1, we treated the oligonucleotides with hot piperidine and re-purified them by electrophoresis. The weak activity of OGG1 was detected even after this treatment (Supplementary Figure S7). On a native gel, OGG1 binds to the *KRAS* G-quadruplexes in a non-productive manner, forming stable G4-OGG1 complexes (Figure 7C). It is worth noting that oligonucleotides **92**, **93** and **94**, that fold in two G-quadruplexes (see *infra*), form two OGG1:G4 complexes: one involving the (1/1/11)-G4 and the other the (6/4/4)-G4 (**92**), 1/8/4 G4 (**93**) and (6/4/5) G4 (**94**). Together, these experiments demonstrate that OGG1 recognizes both the duplex and folded conformations of 32R, but only with the duplex substrate the enzyme is able to excise 8-oxoG.

Guanine oxidation and DNA folding modulate the binding of MAZ and hnRNP A1 to the *KRAS* promoter

We previously have demonstrated that 32R in G4 conformation is recognized by several transcription factors including MAZ and hnRNP A1 (25). The consensus sequence of MAZ is 5^j-GGG(A/C)GG (58). There are two binding sites for MAZ at the 5^j and 3^j ends of 32R. We found that MAZ activates the transcription of *KRAS* and *HRAS* (24,59). The *KRAS* G4 is also recognized by hnRNP A1, a protein of 34 kDa that has a wide range of functions including telomere biogenesis, RNA stability and control of transcription (60). The essential role of this nuclear factor in the transcription of *KRAS* has been demonstrated (26,27,39). Both MAZ and hnRNP A1, upon binding to the *KRAS* G4, destabi- lize the structure and facilitate, in the presence of the complementary strand, the transformation of G4 into duplex (26,59). As the guanines in 32R are exposed to oxidation, we asked if 8-oxoG modifies somehow the recruitment and binding of MAZ and hnRNP A1 to the *KRAS* promoter. To address the first point, we performed ChIP qPCR with Panc-1 cells treated with H_2O_2. The results show that the treatment increases the recruitment of MAZ and hnRNP A1 more to G4 than non-G4 regions, as a result of a cellu- lar increase of 8-oxoG (Figure 8A). These data suggest that an increase of oxidation favors the recruitment to the promoter of MAZ and hnRNP A1, two proteins that activate transcription. A ChIP–reChIP assay (61), based on two independent rounds of immunoprecipitations with antibodies specific for MAZ/hnRNP A1 and 8-oxoG, was performed

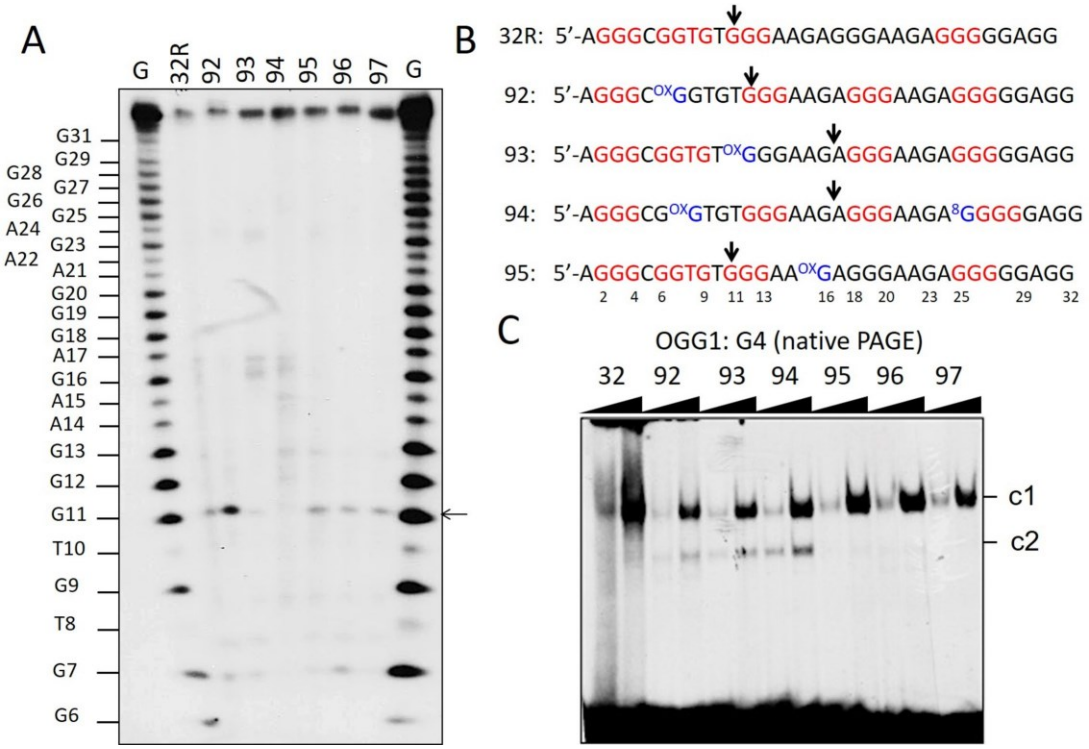

Figure 7. (**A**) Sequencing 18% PAGE showing the effect of OGG1 (1 μM) on the G-quadruplexes. A very weak cleavage activity is detected at specific guanines: G11 in the G4s formed by 32R, **95**, **96** and **97**; G16/A17 in the G4s formed by **93**, G4-(1/8/4) and **94**, G4-(6/4/5). This cleavage activity is not correlated with 8-oxoG; (**B**) Sequences of the G4 motifs 32R, **92**, **93**, **94** and **95** showing the positions where the G4s are cleaved by OGG1 (**96** and **97** behave as **95**); (**C**) Native PAGE showing that OGG1 binds to radiolabeled 32R and 8-oxoG oligonucleotides (20 nM) in the G-quadruplex form. Note that **92**, **93** and **94** form two complexes (c1 and c2) as they form in solution two quadruplexes. OGG1 (0.3 and 0.6 μg) and oligonucleotides (20 nM) have been incubated 45 min at 37°C prior to PAGE. The experiment in A was repeated three times, that in C two times.

to further confirm the co-localization of the transcription factors and 8-oxoG in the chromatinized DNA fragment carrying the G4 motif (Supplementary Figure S8).

To know if the binding of MAZ and hnRNP A1 to the *KRAS* promoter is affected by 8-oxoG, we performed EMSA assays with recombinant proteins and 8-oxoG oligonucleotides in G4 or duplex conformation. Figure 8B reports native gels on the binding of MAZ and hnRNP A1 to wild-type 32R and 8-oxoG-substituted oligonucleotides in the duplex conformation. It shows that the interaction between the proteins and the duplexes carrying one or two 8-oxoG modifications is strongly inhibited. This is in keeping with the finding that the oxidation of both guanines in the consensus sequence of cAMP responsive element-binding protein (CREB) strongly decreased the protein binding (62). In contrast, when 32R and 8-oxoG oligonucleotides are in the G4 conformation, MAZ and hnRNP A1 bind to the DNA target despite it carries 8-oxoG lesions. It is worth noting that the binding of MAZ to 8-oxoG G-quadruplexes with (1/1/11) topology (**95**, **96**, **97**) increases by 5-fold compared to the binding of MAZ to 32R G4. The binding of hnRNP A1 also appears 4-fold more ro- bust with the G-quadruplexes bearing 8-oxoG in the 11-nt loop. To confirm the finding that the transcription factors have more affinity for *KRAS* G4 when it is oxidized in the major loop, we covalently linked biotin to 32R and **96**, car- rying two 8-oxoGs in the 11-nt loop. We used the conjugates as DNA baits in streptavidin–biotin affinity precipitation experiments with a nuclear Panc-1 extract. The presence of MAZ and hnRNP A1 in the proteins binding to the DNA baits was detected and quantified by western blots (Figure 8D). The results are in keeping with those obtained with the recombinant proteins: in the presence of all nuclear proteins, oxidized G4 (**96**) shows ~2-fold higher affinity than wild-type G4 for MAZ and hnRNP A1 [also for PARP-1, a protein that binds to 32R (25)]. Considering the G4 unfolding activity of MAZ and hnRNP A1, these findings are likely to have an impact on the transcription regulation mechanism, as proposed in the following paragraph.

A transcription model for oncogene *KRAS* involving 8-oxoG, OGG1, hnRNP A1 and MAZ

The results of this study, together with previously reported data, add a new element to the molecular mechanism controlling *KRAS* transcription in pancreatic cancer cells: the oxidation of guanine at the critical G4 motif upstream TSS. The high metabolic rate of cancer cells causes an enhanced level of ROS that favors the oxidation of guanine. An increased level of 8-oxoG going beyond the repairing capacity by the cell, would have a negative impact on *KRAS* expression, as the binding of MAZ and hnRNP A1 to the promoter in the duplex conformation would be strongly inhibited. To prevent this, pancreatic cancer cells express high levels of Nrf2: a protein that stimulates the detoxification pathway to keep the oxidative damage at levels compatible with

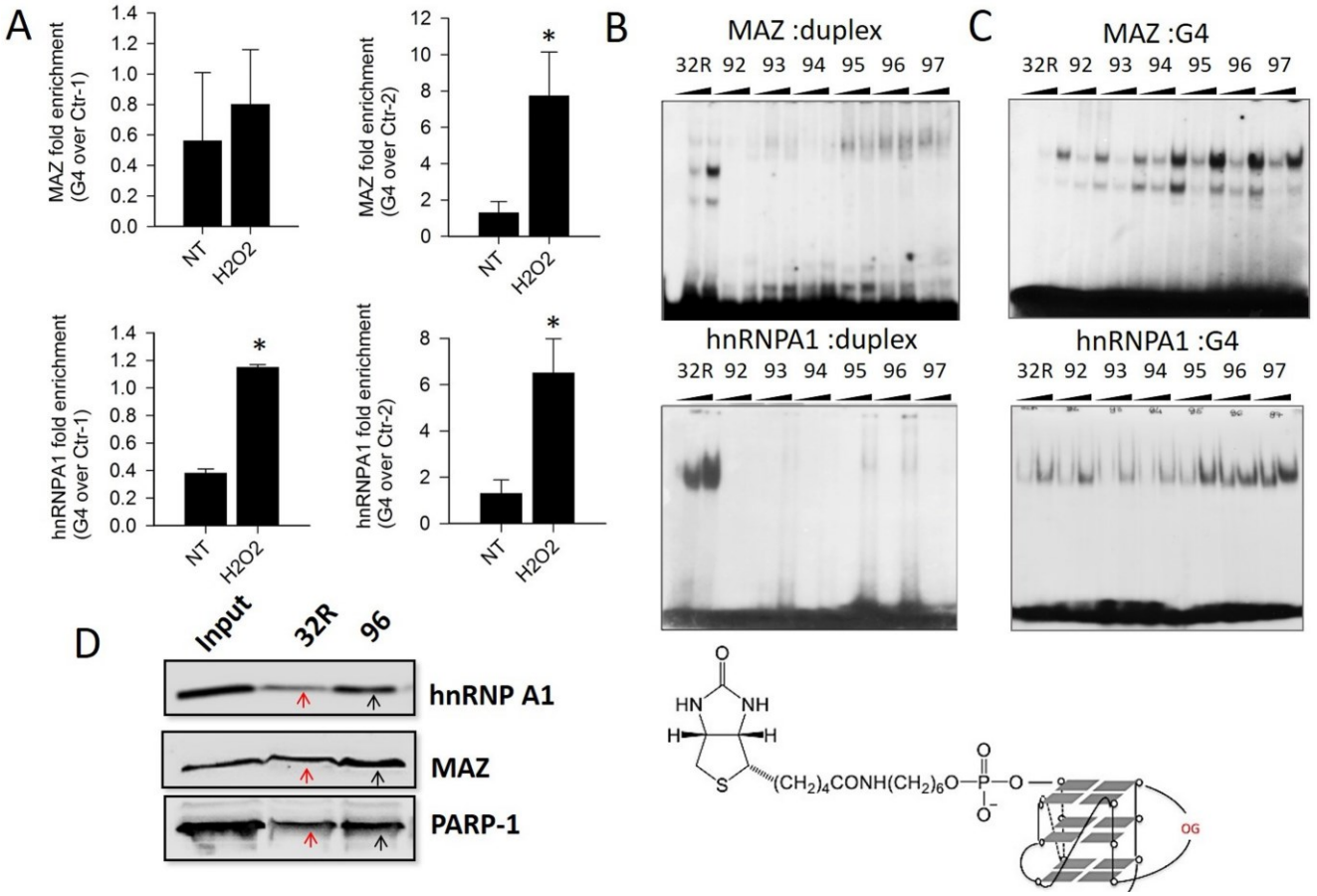

Figure 8. (**A**) ChIP qPCR showing that the recruitment of MAZ and hnRNP A1 to the promoter G4 region is higher than to non-G4 regions (Ctr-1 and Ctr-2), following cell treatment with 1 mM H_2O_2. Asterisk (*) indicates $P < 0.05$ (n 4), a Student's t-test was performed; (**B**) The panels show the binding of MAZ and hnRNP A1 (2.5 and 5 μg) to 20 nM radiolabeled 32R and 8-oxoG oligonucleotides in duplex. The binding of MAZ and hnRNP A1 to the duplexes bearing 8-oxoG is strongly inhibited; (**C**) The panels show the binding of MAZ and hnRNP A1 to G-quadruplexes 32R and analogs bearing 8-oxoG. The proteins bind to the G4s, even though they harbor 8-oxoG. The G4s with 8-oxoG in the 11-nt loop (**95**, **96** and **97**) bind MAZ much more than wild-type G4. Before EMSA, the G4s or duplexes have been incubated with MAZ for 1 h at 37°C and with hnRNP A1 for 30 min at 25°C; (**D**) Streptavidin-biotin pull-down assay with nuclear Panc-1 extract and biotinylated 32R and **96** used as DNA baits (the structure is shown). Cellular proteins bound to G4 were pulled down with streptavidin magnetic beads and analyzed by western blot. The experiments in (B) and (C) were repeated three times.

an optimal cell growth. Indeed, in agreement with previous work (63), we found that the inhibition of Nrf2 brought about an increase of ROS in Panc-1 cells (Supplementary Figure S9). The damage caused to DNA by oxidative stress can modulate gene expression in different ways. While the insertion of a single 8-oxoG in a promoter non-G4 sequence of a reporter gene was found to affect negatively transcription (64), when the oxidized guanine was inserted in the G4-motif of VEGF composed of five G-runs, the expression of *Renilla* luciferase increased by 3-fold. To rationalize this behavior, Fleming *et al*. (65) proposed that gene expression increases because 8-oxoG is excised by OGG1, yielding an abasic site that would favor the folding into a G4 looping out the oxidized G-run. This conformation should facilitate the binding of Ape1 to G4, but without cleaving efficiently the abasic site (66). Finally, the Ref-1 domain of Ape1 would recruit other nuclear factors and stimulate transcription. In addition to this interesting mechanism, Boldogh and co-workers (67) found that in the TNF-a promoter, ROS preferentially oxidizes the guanines in a G-rich region adjacent to a NF-kB-binding site. The authors sustained that the binding of OGG1 to the oxidized G-rich region would promote the recruitment of NF-kB to its binding site, with the consequence of activating transcription. The former mechanism has a more general character and could rationalize also the data of our study. However, also another mechanism can be postulated, in keeping with the original idea that G-quadruplex behaves as a transcription repressor (Figure 9). If we assume that the picture found for *HRAS* (59), based on a mutation analysis of the promoter, also holds for *KRAS*, the promoter G4 motif is normally folded into G4 and transcription is kept to a basal low level. The folding of the G4 motif is favored by DNA supercoiling, which provides sufficient energy to locally unwind the double helix (68,69). This induces the formation of a G-quadruplex on the purine-rich strand and, most likely, an *i*-motif on the pyrimidine strand (70). Although the *i*-motif shows *in vitro* higher stability under slightly acidic conditions, both cellular crowding and supercoiling are expected to stabilize this unusual structure at physiological conditions too (69,71,72). The relatively high oxidative stress in pancreatic cancer cells may induce the oxidation of cer-

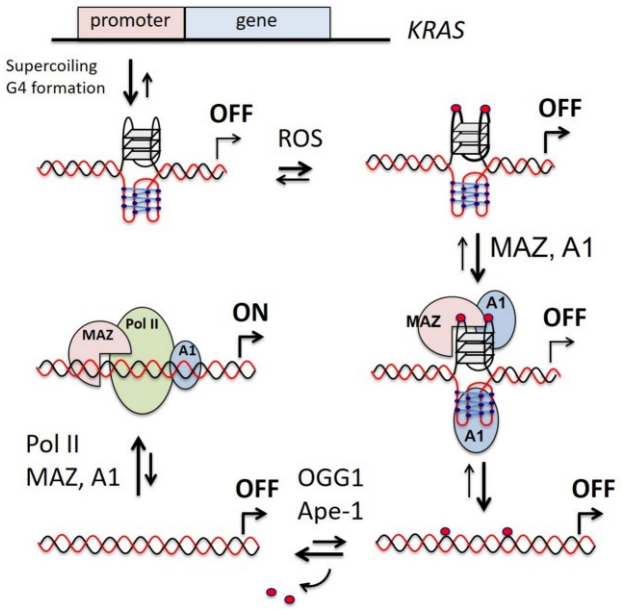

Figure 9. A model for *KRAS* transcription regulation involving 8-oxoG. A1 and Pol II stand for hnRNP A1 and RNA Pol II.

tain guanines, particularly the DNA motifs composed by blocks of guanines (73) and folded into G4 (40). Our data show that the presence of one or two oxidized guanines in the major 11-nt loop of the *KRAS* G-quadruplex increases the binding of MAZ, hnRNP A1 and also PARP-1 to the G-quadruplex. As hnRNP A1 recognizes also the *i*-motif (71), both strands of the G4 motif could interact with nu- clear proteins. The proteins upon binding should destabi- lize the folded structures and facilitate the reconstitution of the double helix (59,71). In this scheme, 8-oxoG would act as an epigenetic marker boosting the recruitment to the promoter of the nuclear factors essential for *KRAS* transcription. The oxidized guanines in the reconstituted duplex will be efficiently repaired via the BER pathway involving OGG1, that excises 8-oxoG, and Ape1, that cleaves the abasic site (48,74). The excision of 8-oxoG from the G4 motif in double helix will increase the affinity of the nuclear factors for the promoter, with the result of activating transcription. This mechanism is supported by the fact that *KRAS* transcription strongly depends on MAZ (24,59) and hnRNP A1 (26,27,39). It also depends on OGG1, as its downregulation in Panc-1 cells by siRNA determines a parallel decrease of *KRAS* transcription (Supplementary Figure S10).

SUPPLEMENTARY DATA

Supplementary Data are available at NAR Online.

ACKNOWLEDGEMENTS

We thank Prof. Magnar Bjorås (University of Oslo) for providing plasmid pET20hOGG1 expressing human OGG1.

FUNDING

Associazione Italiana per la Ricerca sul Cancro (AIRC) [IG 2013, project code 14301]. Funding for open access charge: AIRC [14301].
Conflict of interest statement. None declared.

REFERENCES

1. Liou,G.-Y. and Storz,P. (2010) Reactive oxygen species in cancer. *Free Radic. Res.*, **44**, 1–31.
2. Sosa,V., Moliné,T., Somoza,S., Paciucci,R. and Kondoh,H. (2012) Oxidative stress and cancer: an overview. *Ageing Res. Rev.*, **12**, 376–390.
3. Murphy,M.P. (2009) How mitochondria produce reactive oxygen species. *Biochem. J.*, **417**, 1–13.
4. Giorgio,M., Trinei,M., Migliaccio,E. and Pelicci,P.G. (2007) Hydrogen peroxide: a metabolic by-product or a common mediator of ageing signals. *Nat. Rev. Mol. Cell Biol.*, **8**, 722–728.
5. St-Pierre,J., Buckingham,J., Roebuck,S.J. and Brand,M.D. (2002) Topology of superoxide production from different sites in mitochondrial electron transport chain. *J. Biol. Chem.*, **277**, 44784–44790.
6. Lloyd,R.V., Hanna,P.M. and Mason,R.P. (1997) The origin of the hydroxyl radical oxygen in the Fenton reaction. *Free Radic. Biol. Med.*, **22**, 885–888.
7. Trachootham,D., Lu,W., Ogasawara,M.A., Nilsa,R.D. and Huang,P. (2008) Redox regulation of cell survival. *Antioxid. Redox Signal.*, **10**, 1343–1374.
8. Klaunig,J.E., Kamendulis,L.M. and Hocevar,B.A. (2010) Oxidative stress and oxidative damage in carcinogenesis. *Toxicol. Pathol.*, **38**, 96–109.
9. Jaramillo,M.C. and Zhang,D.D. (2013) The merging role of the Nrf2-Keap1 signaling pathway in cancer. *Genes Dev.*, **27**, 2179–2191.
10. Mitsuishi,Y., Motohashi,H. and Yamamoto,M. (2012) The Keap1–Nrf2 system in cancers: stress response and anabolic metabolism. *Front. Oncol.*, **2**, 1–13.
11. Hayes,J.D., McMahon,M., Chowdhry,S. and Dinkova-Kostova,A.T. (2010) Cancer chemoprevention mechanisms mediated through the Keap1-Nrf2 pathway. *Antioxid. Redox Signal.*, **13**,1713–1748.
12. Tao,S., Wang,S., Moghaddam,S.J., Ooi,A. and Chapman,E. (2014) Oncogenic KRAS confers chemoresistance by upregulating Nrf2. *Cancer Res.*, **74**, 7430–7441.
13. Kong,B., Erkan,M., Kleeff,J. and Michalski,C.W. (2013) Overview on how oncogenic KRAS promotes pancreatic carcinogenesis by inducing low intracellular ROS levels. *Front. Physiol.*, **4**, 1–5.
14. DeNicola,G.M., Karreth,F.A., Humpton,J., Gopinathan,A., Wei,C., Frese,K., Mangal,D., Yu,K.H., Teo,C.J., Calhoun,E.S. *et al.* (2011) Oncogene-induced Nrf2 transcription promotes ROS detoxification and tumorigenesis. *Nature*, **475**, 106–109.
15. Hezel,A.F., Kimmelmann,A.C., Stanger,B.Z., Bardeesy,N. and Depinho,R.A. (2006) Genetic and biology of pancreatic ductal adenocarcinoma. *Genes Dev.*, **20**, 1218–1249.
16. Almoguera,C., Shibata,D., Forrester,K., Martin,J., Arnheim,N. and Perucho,M. (1988) Most human carcinomas of the exocrine pancreas contain mutant c-Ki-ras gene. *Cell*, **53**, 549–554.
17. Yeh,J.J. and Der,C.J. (2007) Targeting signal transduction in pancreatic cancer treatment. *Expert. Opin. Ther. Targets*, **11**, 673–694.
18. Collins,M.A., Bednar,F., Zhang,Y., Brisset,J.C., Galban,S., Galban,C.J., Rakshit,S., Flannagan,K.S., Adsay,N.V. and Pasca di Magliano,M. (2012) Oncogenic KRAS is required for both the initiation and maintenance of pancreatic cancer in mice. *J. Clin. Invest.*, **122**, 639–653.
19. Pasca di Magliano,M and Logsdon,C.D. (2013) Roles of KRAS in panceratic tumor development and progression. *Gastroeneterology*, **144**, 1220–1229.
20. Hingorani,S.R., Petricoin,E.F., Maitra,A., Rajapakse,V., King,C., Jacobetz,M.A., Ross,S., Conrads,T.P., Veenstra,T.D., Hitt,B.A. *et al.* (2003) Preinvasive and invasive ductal pancreatic cancer and its early detection in the mouse. *Cancer Cell*, **4**,437–450.
21. Cadet,J., Douki,T. and Ravanat,J.L. (2008) Oxidatively generated damage to the guanine moiety of DNA: mechanistic aspects and formation in cells. *Acc. Chem. Res.*, **41**, 1075–1083.

22. Kanvah,S., Joseph,J., Schuster,G.B., Barnett,R.N., Cleveland,C.L. and Landman,U. (2009) Oxidation of DNA: damage to nucleobases. *Acc. Chem. Res.*, **43**, 280–287.
23. Cogoi,S. and Xodo,L.E. (2006) G-quadruplex formation within the promoter of the KRAS proto-oncogene and its effect on transcription. *Nucleic Acids Res.*, **34**, 2536–2549.
24. Cogoi,S., Zorzet,S., Rapozzi,V., Géci,I., Pedersen,E.B. and Xodo,L.E. (2013) MAZ-binding G4-decoy with locked nucleic acid and twisted intercalating nucleic acid modifications suppresses KRAS in pancreatic cancer cells and delays tumor growth in mice. *Nucleic Acids Res.*, **41**, 4049–4064.
25. Cogoi,S., Paramasivam,M., Spolaore,B. and Xodo,L.E. (2008) Structural polymorphism within a regulatory element of the human KRAS promoter: formation of G4-DNA recognized by nuclear proteins. *Nucleic Acids Res.*, **36**, 3765–3780.
26. Paramasivam,M., Membrino,A., Cogoi,S., Fukuda,H., Nakagama,H. and Xodo,L.E. (2009) Protein hnRNP A1 and its derivative Up1 unfold quadruplex DNA in the human KRAS promoter: implications for transcription. *Nucleic Acids Res.*, **37**, 2841–2853.
27. Cogoi,S., Rapozzi,V., Cauci,S. and Xodo,L.E. (2016) Critical role of hnRNP A1 in activating KRAS transcription in pancreatic cancer cells: A molecular mechanism involving G4 DNA. *Biochim. Biophys. Acta*, **1861**, 1389–1398.
28. Paramasivam,M., Cogoi,S. and Xodo,L.E. (2011) Primer extension reactions as a tool to uncover folding motifs within complex G-rich sequences: analysis of the human KRAS NHE. *Chem. Commun. (Camb).*, **47**, 4965–4967.
29. Cogoi,S. and Xodo,L.E. (2016) G4 DNA in ras genes and its potential in cancer therapy. *Biochim. Biophys. Acta*, **1859**, 663–674.
30. Bodepudi,V., Shibutani,S. and Johnson,F. (1992) Synthesis of 2^{j}-deoxy-7,8-dihydro-8-oxoguanosine and 2^{j}-deoxy-7,8-dihydro-8-oxoadenosine and their incorporation into oligomeric DNA. *Chem. Res. Toxicol.*, **5**, 608–617.
31. Lin,X., Tirichine,L. and Bowler,C. (2012) Protocol: chromatin immunoprecipitation (ChIP) methodology to investigate histone modifications in two model diatom species. *Plant Methods*, **8**, 48–57.
32. Clark,D.W., Phang,T., Edwards,M.G., Geraci,M.W. and Gillespie,M.N. (2012) Promoter G-quadruplex sequences are targets for base oxidation and strand cleavage during hypoxia-induced transcription. *Free Radic. Biol. Med.*, **53**, 51–59.
33. Chambers,V.S., Marsico,G., Boutell,J.M., Di Antonio,M., Smith,G.P. and Balasubramanian,S. (2015) High-throughput sequencing of DNA G-quadruplex structures in the human genome. *Nat. Biotechnol.*, **33**, 877–881.
34. Hänsel-Hertsch,R., Beraldi,D., Lensing,S.V., Marsico,G., Zyner,K., Parry,A., Di Antonio,M., Pike,J., Kimura,H., Narita,M. *et al.* (2016) G-quadruplex structures mark human regulatory chromatin. *Nat. Genet.*, **48**, 1267–1272.
35. Ding,Y., Fleming,A.M. and Burrows,C.J. (2017) Sequencing the mouse genome for the oxidatively modified base 8-Oxo-7,8-dihydroguanine by OG-seq. *J. Am. Chem. Soc.*, **139**, 2569–2572.
36. Morgan,R.K., Batra,H., Gaerig,V.C., Hockings,J. and Brooks,T.A. (2016) Identification and characterization of a new G-quadruplex forming region within the KRAS promoter as a transcriptional regulator. *Biochim. Biophys. Acta*, **1859**, 235–245.
37. Podbevsek,P. and Plavec,J. (2016) KRAS promoter oligonucleotide with decoy activity dimerazes into a unique topology consisting of two G-quadruplex units. *Nucleic Acids Res.*, **44**, 917–925.
38. Kerkour,A., Marquevielle,J., Ivashchenko,S., Yatsunyk,L.A., Mergny,J.L. and Salgado,G.F. (2017) High-resolution 3D NMR structure of the KRAS proto-oncogene promoter reveals key features of a G-quadruplex involved in transcriptional regulation. *J. Biol. Chem.*, **292**, 8082–8091.
39. Chu,P.C., Yang,M.C., Kulp,S.K., Salunke,S.B., Himmel,L.E., Fang,C.S., Jadhav,A.M., Shan,Y.S., Lee,C.T., Lai,M.D. *et al.* (2016) Regulation of oncogenic KRAS signaling via a novel KRAS-integrin-linked kinase-hnRNPA1 regulatory loop in human pancreatic cancer cells. *Oncogene*, **35**, 3897–3908.
40. Szalai,V.A., Singer,M.J. and Thorp,H.H. (2002) Site-specific probing of oxidative reactivity and telomerase function using 7,8-dihydro-8-oxoguanine in telomeric DNA. *J Am. Chem. Soc.*, **124**, 1625–1631.
41. Fleming,A.M. and Burrows,C.J. (2013) G-quadruplex folds of the human telomere sequence alter the site reactivity and reaction pathway of guanine oxidation compared to duplex DNA. *Chem. Res. Toxicol.*, **26**, 593–607.
42. Vorlícková,M., Tomasko,M., Sagi,A.J., Bednarova,K. and Sagi,J. (2012) 8-oxoguanine in a quadruplex of the human telomere DNA sequence. *FEBS J.*, **279**, 29–39.
43. Fleming,A.M., Zhou,J., Wallace,S.S. and Burrows,C.J. (2015) A role for the fifth G-track in G-quadruplex forming oncogene promoter sequences during oxidative stress: do these sparetires have an evolved function. *ACS Cent. Sci.*, **1**, 226–233.
44. An,N., Fleming,A.M. and Burrows,C.J. (2016) Human telomere G-quadruplexes with five repeats accommodate 8-Oxo-7,8-dihydroguanine by looping out the DNA damage. *ACS Chem. Biol.*, **11**, 500–507.
45. Beckett,J., Burns,J., Broxson,C. and Tornaletti,S. (2012) Spontaneous DNA lesions modulate DNA structural transitions occurring at nuclease hypersensitive element III of the human c-myc proto-oncogene. *Biochemistry*, **51**, 5257–5268.
46. Tran,P.L.T., Mergny,J.L. and Alberti,P. (2011) Stability of telomeric G-quadruplexes. *Nucleic Acids Res.*, **39**, 3282–3294.
47. Mergny,J.L., Phan,A.T. and Lacroix,L. (1998) Following G-quartet formation by UV-spectroscopy. *FEBS Lett.*, **435**, 74–78.
48. Rosenquist,T.A., Zharkov,D.O. and Grollman,A.P. (1997) Cloning and characterization of a mammalian 8-oxoguanine DNA glycosylase. *Proc. Natl. Acad. Sci. U.S.A.*, **94**, 7429–7434.
49. Roldán-Arjona,T., Wei,Y.F., Carter,K.C., Klungland,A., Anselmino,C., Wang,R.P., Augustus,M. and Lindahl,T. (1997) Molecular cloning and functional expression of a human cDNA encoding the antimutator enzyme 8-hydroxyguanine-DNA glycosylase. *Proc. Natl. Acad. Sci. U.S.A.*, **94**, 8016–8020.
50. Radicella,J.P., Dherin,C., Desmaze,C., Fox,M.S. and Boiteux,S. (1997) Cloning and characterization of hOGG1, a human homolog of the OGG1 gene of Saccharomyces cerevisiae. *Proc. Natl. Acad. Sci. U.S.A.*, **94**, 8010–8015.
51. David,S.S., O'Shea,V.L. and Kundu,S. (2007) Base-excision repair of oxidative DNA damage. *Nature*, **447**, 941–950.
52. Allgayer,J., Kitsera,N., Bartelt,S., Epe,B. and Khobta,A. (2016) Widespread transcriptional gene inactivation initiated by a repair intermediate of 8-oxoguanine. *Nucleic Acids Res.*, **44**, 7267–7280.
53. Tang,X., Wang,H., Fan,L., Wu,X., Xin,A., Ren,H. and Wang,X.J. (2011) Luteolin inhibits Nrf2 leading to negative regulation of the Nrf2/ARE pathway and sensitization of human lung carcinoma A549 cells to therapeutic drugs., *Free Radic. Biol. Med.*, **50**, 1599–1609.
54. Chian,S., Thapa,R., Chi,Z., Wang,X.J. and Tang,X. (2014) Luteolin inhibits the Nrf2 signaling pathway and tumor growth in vivo. *Biochem. Biophys. Res. Commun.*, **447**, 602–608.
55. Girard,P.M., Guibourt,N. and Boiteux,S. (1997) The Ogg1 protein of Saccharomyces cerevisiae: a 7,8-dihydro-8-oxoguanine DNA glycosylase/AP lyase whose lysine 241 is a critical residue for catalytic activity. *Nucleic Acids Res.*, **25**, 3204–3211.
56. Zhou,J., Fleming,A.M., Averill,A.M., Burrows,C.J. and Wallace,S.S. (2015) The NEIL glycosylases remove oxidized guanine lesions from telomeric and promoter quadruplex DNA structures. *Nucleic Acids Res.*, **43**, 4039–4054.
57. Amasova,O., Coulter,R. and Fresco,J.R. (2006) Self calalyzed site-specific depurination of guanine residues within gene sequences. *Proc. Natl. Acad. Sci. U.S.A.*, **103**, 4392–4397.
58. Parks,C.L. and Shenk,T. (1996) The serotonin 1a receptor gene contains a TATA-less promoter that responds to MAZ and Sp1. *J. Biol. Chem.*, **271**, 4417–4430.
59. Cogoi,S., Shchekotikhin,A.E. and Xodo,L.E. (2014) HRAS is silenced by two neighboring G-quadruplexes and activated by MAZ, a zinc-finger transcription factor with DNA unfolding property. *Nucleic Acids Res.*, **42**, 8379–8388.
60. Jean-Philippe,J., Paz,S. and Caputi,M. (2013) hnRNP A1: the Swiss Army Knife of Gene Expression. *Int. J. Mol. Sci.*, **14**, 18999–19024.
61. Furlan-Magaril,M., Rincón-Arano,H. and Recillas-Targa,F. (2009) Sequential chromatin immunoprecipitation protocol: ChIP-reChIP. *Methods Mol. Biol.*, **543**, 253–266.
62. Moore,S.P., Toomire,K.J. and Strauss,P.R. (2013) DNA modifications repaired by base excision repair are epigenetic. *DNA Repair (Amst)*, **12**, 1152–1158.

63. Sporn,M.B. and Liby,K.T. (2012) NRF2 and cancer: the good, the bad and the importance of context. *Nat. Rev. Cancer*, **12**, 564–571.
64. Allgayer,J., Kitsera,N., Bartelt,S., Epe,B. and Khobta,A. (2016) Widespread transcriptional gene inactivation initiated by a repair intermediate of 8-oxoguanin. *Nucleic Acids Res.*, **44**, 7267–7280.
65. Fleming,A.M., Ding,Y. and Burrows,C.J. (2017) Oxidative DNA damage is epigenetic by regulating gene transcription via base excision repair. *Proc. Natl. Acad. Sci. U.S.A.*, **114**,2604–2609.
66. Broxson,C., Hayner,J.N., Beckett,J., Bloom,L.B. and Tornaletti,S. (2014) Human AP endonuclease inefficiently removes abasic sites within G4 structures compared to duplex DNA. *Nucleic Acids Res.*, **42**, 7708–7719.
67. Pan,L., Zhu,B., Hao,X., Vlahopoulos,S.A., Hazra,T.K., Hedge,M.L., Rodak,Z., Bacsi,A., Brasier,A.R., Ba,X. *et al.* (1016) Oxidized guanine base lesions Function in 8-oxoguanine DNA glycosylase-1-mediated epigenetic regulation of nuclear factor kB-driven gene expression. *J. Biol. Chem.*, **291**, 25553–25566.
68. Sun,D. and Hurley,L.H. (2009) The importance of negative superhelicity in inducing the formation of G-quadruplex and i-motif structures in the c-Myc promoter: implications for drug targeting and control of gene expression. *J. Med. Chem.*, **52**,2863–2874.
69. Brooks,T.A. and Hurley,L.H. (2009) The role of supercoiling in transcriptional control of MYC and its importance in molecular therapeutics. *Nat. Rev. Cancer*, **9**, 849–861.
70. Manzini,G., Yathindra,N. and Xodo,L.E. (1994) Evidence for intramolecularly folded i-DNA structures in biologically relevant CCC-repeat sequences. *Nucleic Acids Res.*, **22**, 4634–4640.
71. Miglietta,G., Cogoi,S., Pedersen,E.B. and Xodo,L.E. (2015) GC-elements controlling HRAS transcription form i-motif structures unfolded by heterogeneous ribonucleoprotein particle A1. *Sci. Rep.*, **5**, 18097.
72. Kang,H.J., Kendrick,S., Hecht,S.M. and Hurley,L.H. (2014) The transcriptional complex between the *BCL2* i-Motif and hnRNP LL is a molecular switch for control of gene expression that can be modulated by small molecules. *J. Am. Chem. Soc.*, **136**, 4172–4185.
73. Arnold,A.R., Grodick,M.A. and Barton,J.K. (2016) DNA charge transport: from chemical principls to the cell. *Cell Chem. Biol.*, **23**, 183–197.
74. Tell,G., Quadrufoglio,F., Tiribelli,C and Kelley,M.R. (2009) The many functions of APE1/Ref-1: not only a DNA repair enzyme. *Antioxid. Redox Signal*, **11**, 601–620.

Supplementary data

The regulatory G4 motif of the Kirsten ras (*KRAS*) gene is sensitive to guanine oxidation: implications on transcription

Susanna Cogoi,[1] Annalisa Ferino,[1] Giulia Miglietta,[1] Erik B. Pedersen,[2] and Luigi E. Xodo*[1]

[1] Department of Medicine, University of Udine, 33100n Udine, Italy;
[2] Nucleic Acid Center, Institute of Physics and Chemistry, University of Southern Denmark, DK-5230 Odense, Denmark.

Contents

Table S1. 8-oxoG substituted oligonucleotides with the sequence of the regulatory G4-motif of the *KRAS* gene

Oligo [(a)]	5' → 3'	MW Calc.[(b)]	MW Found [(c)]
92	AGGGC^{ox}GGTGTGGGAAGAGGGAAGAGGGGGAGG	10271.7	10275.2
93	AGGGCGGTGT^{ox}GGGAAGAGGGAAGAGGGGGAGG	10271.7	10274.9
94	AGGGCG^{ox}GTGTGGGAAGAGGGAAGA^{ox}GGGGGAGG	10287.7	10291.1
95	AGGGCGGTGTGGGAA^{ox}GAGGGAAGAGGGGGAGG	10271.7	10270.1
96	AGGGCGGTGTGGGAA^{ox}GAG^{ox}GGAAGAGGGGGAGG	10287.7	10290.4
97	AGGGCGGTGTGGGAA^{ox}GAGGGAA^{ox}GAGGGGGAGG	10287.7	10289.4
32R	AGGGCGGTGTGGGAAGAGGGAAGAGGGGGAGG		

(a) ^{ox}G= 8-oxoG; (b) Calculated MW; (c) MW found by MALDI-TOF

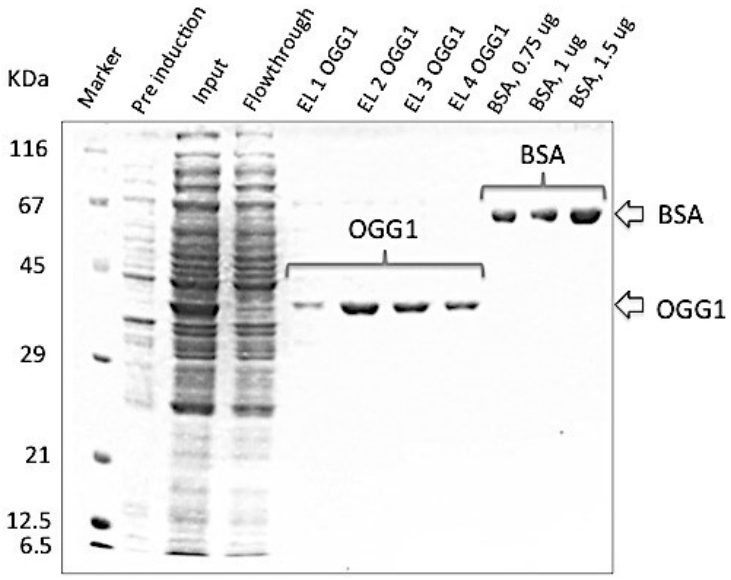

Figure S1. SDS-PAGE showing the degree of purity of recombinant OGG1 used in this work. As for recombinant MAZ and hnRNP A1, we already reported in previous work that these proteins are obtained with a high degree of purity (Ref. 24 and 26).

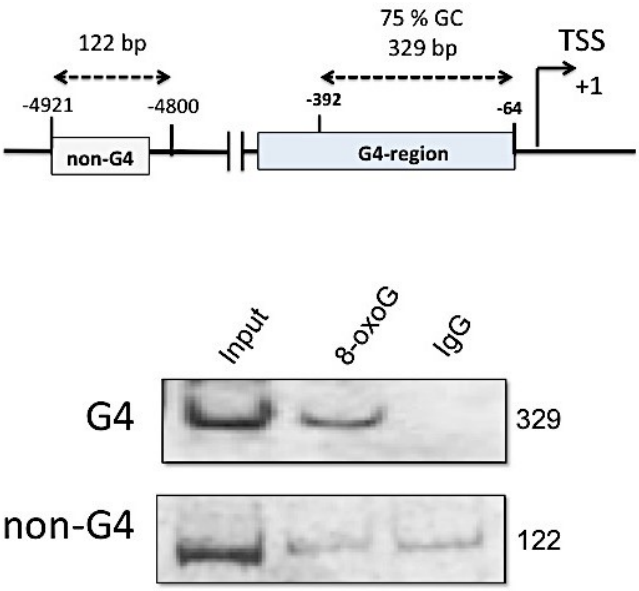

Figure S2: Chromatin immunoprecipitation and PCR showing that the level of 8-oxoG in the G4 region close to TSS is higher than in the non-G4 region located about 4000 bp upstream TSS.

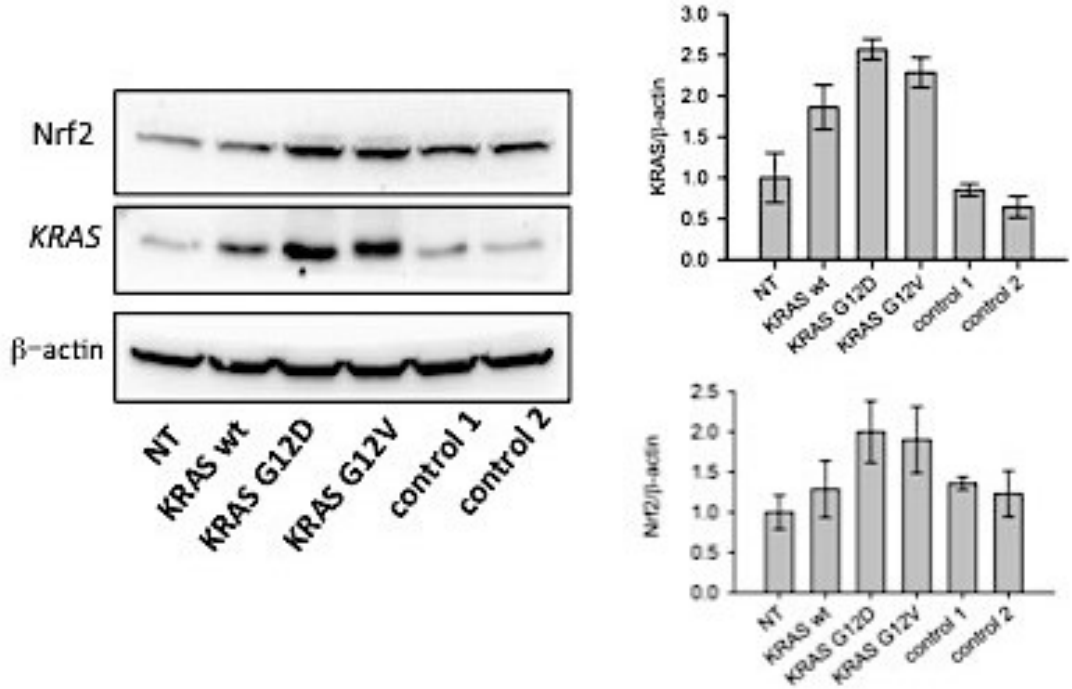

Figure S3: Panc-1 cells transfected with vectors expressing wild-type *KRAS*, mutant KRAS G12D, *KRAS* G12V, empty vectors (control 1, control 2) showed increased levels of KRAS and Nrf2, 96 h after transfection, according to the Western blot analysis. As previously observed, there is a clear correlation between *KRAS* and Nrf2 (Ref. 12, 14).

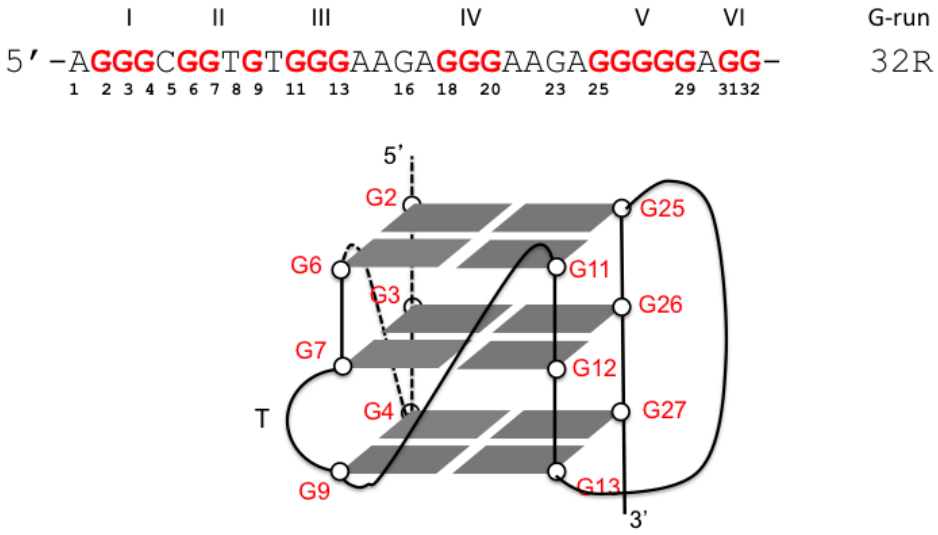

G-quadruplex (1/1/11)

Figure S4. Putative structure of the G-quadruplex assumed by 32R determined by DMS-footprinting experiments (Ref. 23 and 25).

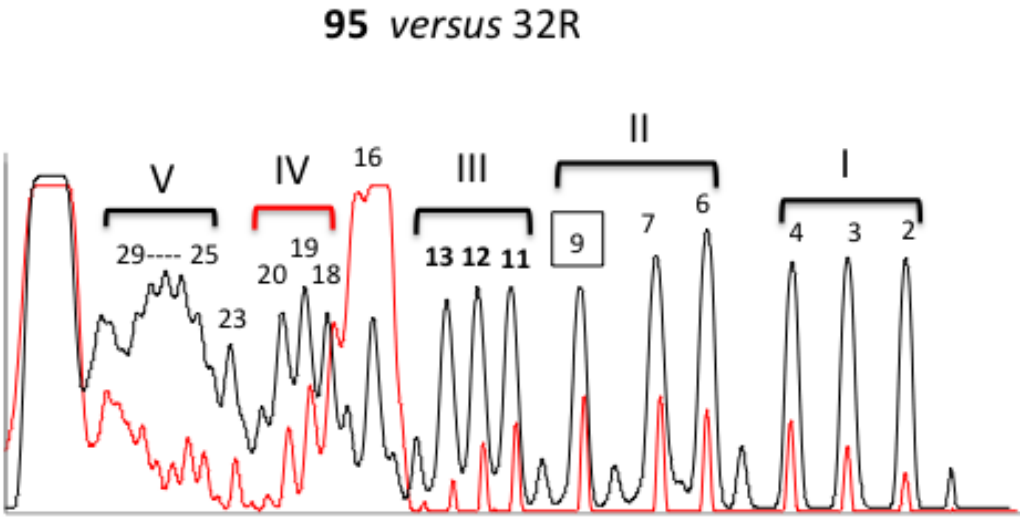

Figure S5. DMS-footprinting of unstructured 32R in LiCl-buffer (black) and 32R with G16 replaced with 8-oxoG (oligonucleotides **95**, Fig. 2, text) annealed in 100 mM KCl (red). It can be seen that, with respect to unstructured 32R, the G-runs I, II, III and V are protected from DMS, while the tract G16-A17-G18-G19-G20 inside the 11-nt loop is highly reactive, in particular the modified 8-oxoG base. The cleavage with piperidine occurs mainly at the modified base and that's why the other guanines of the loop show a lower reactivity to DMS. By comparing these profiles with those reported in Fig. 3 of the text, one can conclude that when 8-oxoG is in the 11-nt loop, the folding of the modified oligonucleotide is similar to that of wild-type 32R.

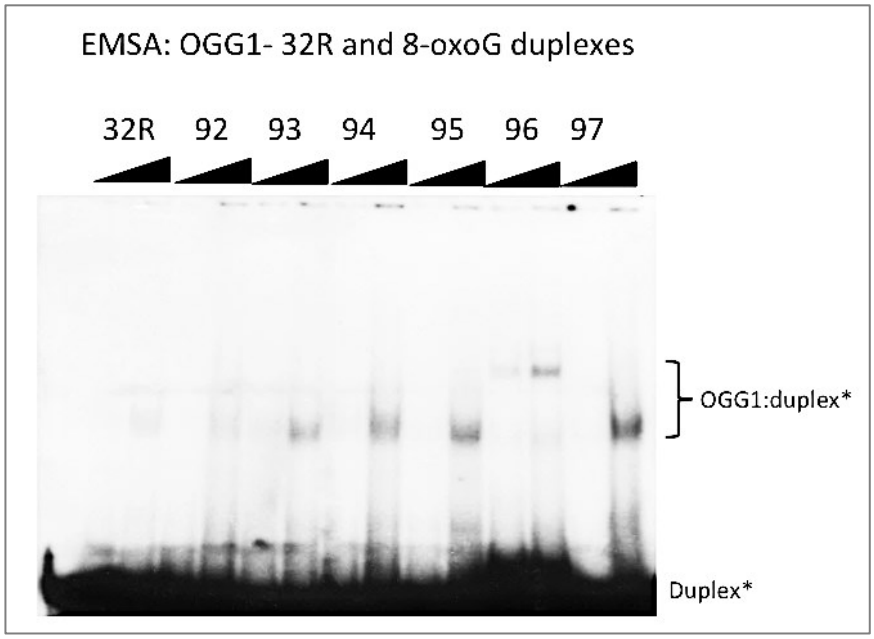

Figure S6: EMSA at 4 °C, under native conditions, showing that the complexes between OGG1 and 8-oxoG duplexes are not so stable and barely detectable in the gel, due to the cleavage activity of the enzyme on the DNA substrates.

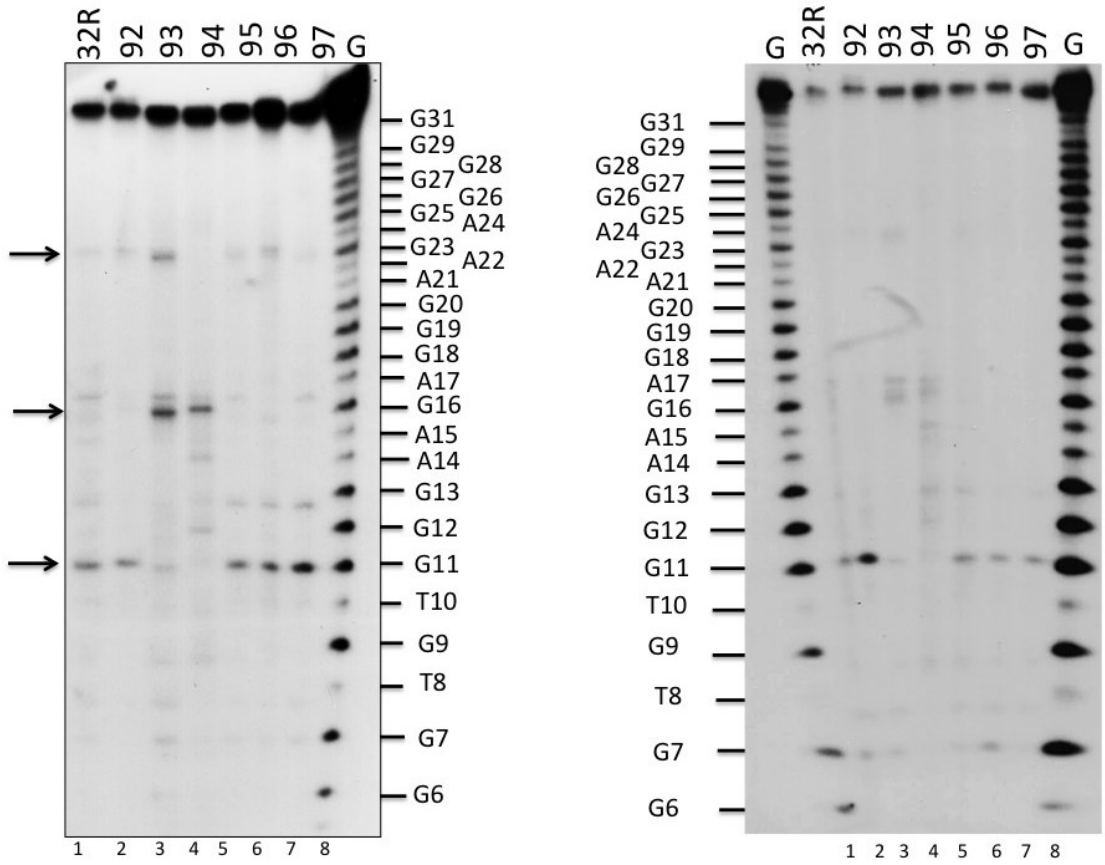

Figure S7. (Left panel) Wild-type and 8-oxoG-substituted oligonucleotides purified by electrophoresis, folded in G4 in 100 mM KC, and treated with OGG1. The reaction products have been run in a sequencing gel. A weak cleavage activity at G11 is detected in the oligonucleotides assuming a (1/1/11) G4. Instead, oligonucleotides **93** and **94**, showed a sligh cleavage at G16 and G23; (Right panel) Purified wild–type and 8-oxoG-substituted oligonucleotides have been treated with hot piperidine, purified again by electrophoresis and folded in 100 mM KCL. The G4 oligonucleotides were used for a OGG1 assay. It can be seen that the piperidine treatment does not remove the cleavages at G11 and G16/A17 by OGG1.

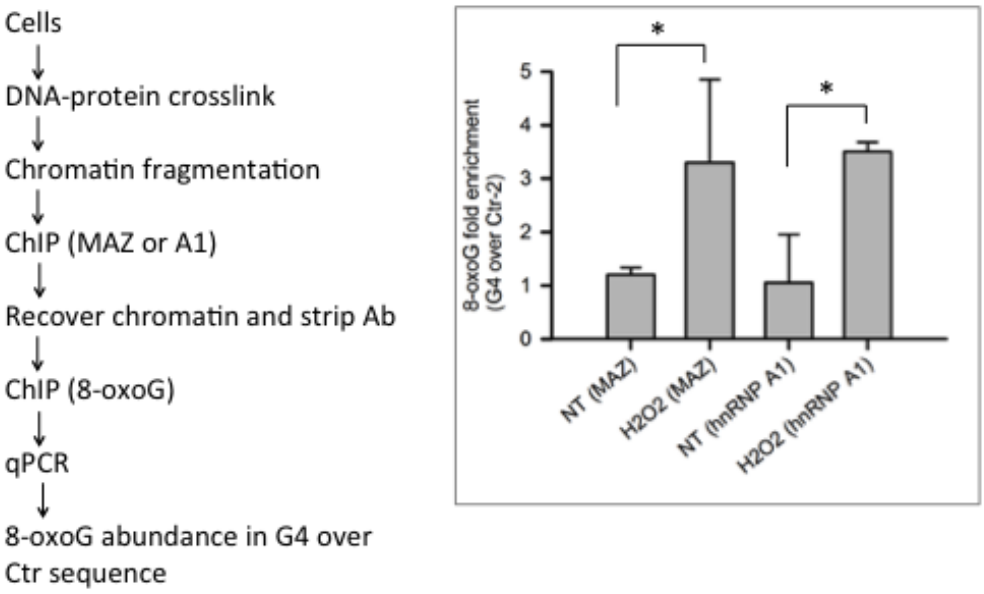

Figure S8: ChiP-reChIP experiment. It is based on two independent rounds of immunoprecipitations with antibodies specific for MAZ/hnRNP A1 and 8-oxoG, was performed to further confirm the co-localization of the transcription factors and 8-oxoG in the chromatinized DNA fragment carrying the G4 motif.

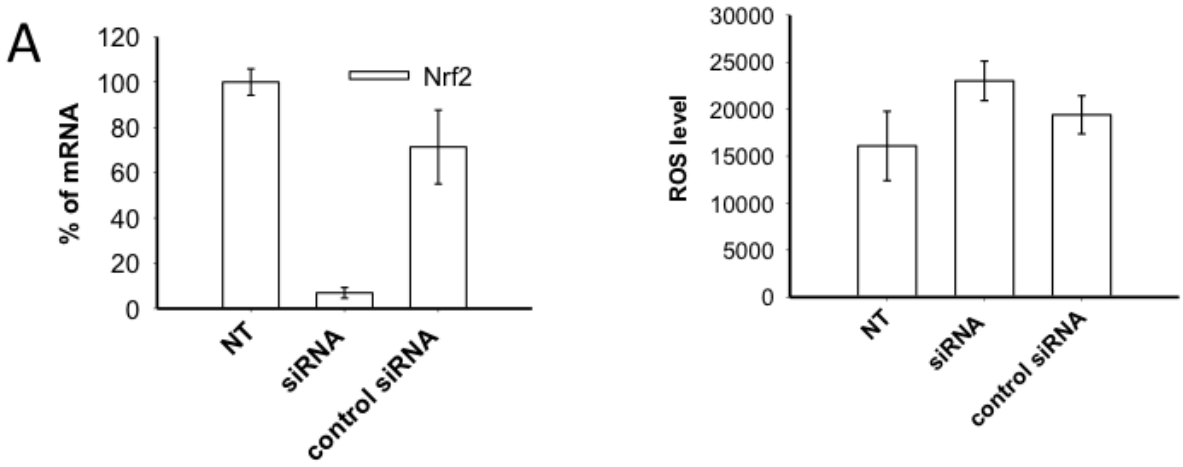

B

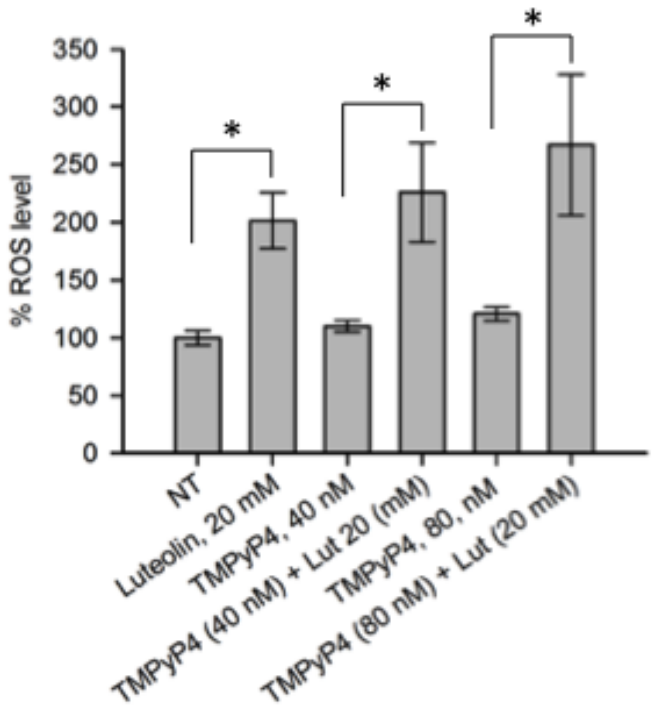

Figure S9. (A) RT qPCR showing that the silencing of Nrf2 with a specific siRNA results in an increase of ROS in Panc-1 cells; (B) Level of ROS in Panc-1 cells treated with 0, 40 and 80 nM of TmPyP4, followed by light treatment (15 min, fluence of 7.2 J/cm^2). Only a slight increase of ROS (~ 30%) is observed as the increased ROS triggers the expression of Nrf2 activating the detoxification genes. When the cells are treated with TMPyP4 and 20 μM luteolin, an inhibitor of Nrf2, the level of ROS increases up to 2.5 fold.

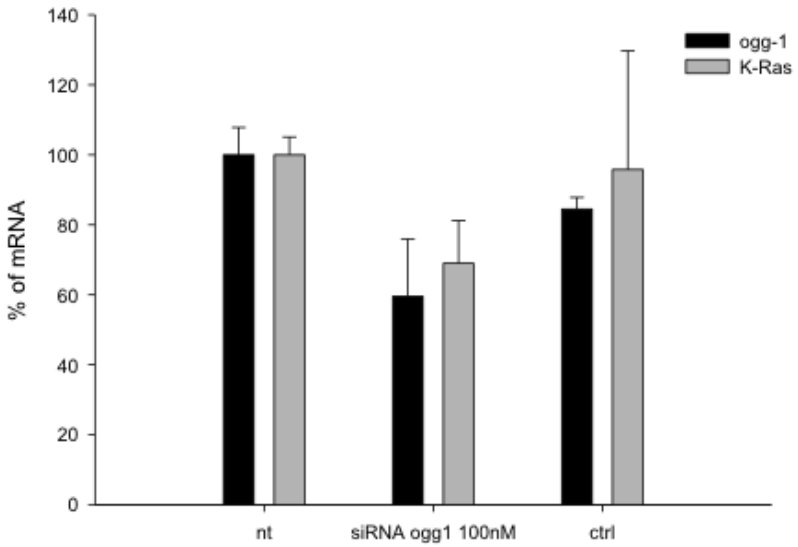

Figure S10. Panc-1 cells treated for 24 h with OGG1 siRNA, then OGG1 and KRAS transcripts were measured by RT qPCR. The downregulation of OGG1 is accompanied by a parallel downregulation of KRAS expression.

Section 2

The ROS-KRAS-Nrf2 axis in the control of the redox homeostasis and the intersection with survival-apoptosis pathways

A. Ferino, G. Cinque, V. Rapozzi and L.E. Xodo

(Submitted)

The ROS-*KRAS*-Nrf2 axis in the control of the redox homeostasis and the intersection with survival-apoptosis pathways

Annalisa Ferino, Giorgio Cinque, Valentina Rapozzi and Luigi E. Xodo*

Department of Medicine, Laboratory of Biochemistry, University of Udine, P.le Kolbe 4, 33100 Udine, Italy

** To whom correspondence should be addressed*: Luigi E. Xodo, Department of Medicine, Laboratory of Biochemistry, P.le Kolbe 4, University of Udine, 33100 Udine, Italy; Tel: (+39) 0432.494395; Fax: (+39) 0432.494301; E-mail: luigi.xodo@uniud.it

Abstract

In highly proliferating cancer cells, oncogenic mutations reprogram the metabolism and increase the production of reactive oxygen species (ROS). Cancer cells prevent ROS accumulation by upregulating antioxidant systems. We found that ROS stimulate the expression of *KRAS*, which in turn upregulates Nrf2, a master regulator of oxidative stress. ROS, *KRAS* and Nrf2 constitute a molecular axis controlling the redox homeostasis and the NF-kB/Snail/RKIP circuitry, which regulates the survival and apoptosis pathways. Our data show that low ROS levels result in the upregulation of prosurvival Snail and simultaneously downregulation proapoptotic RKIP. This gene expression pattern favours cell proliferation. By contrast, high ROS favour apoptosis by upregulating proapoptotic RKIP and downregulating prosurvival Snail. We also discuss the mechanism through which *KRAS* is upregulated by ROS. Lastly, we demonstrate that cancer cells can be sensitized to photodynamic therapy by inhibiting the Nrf2 antioxidant response.

Abbreviations

KRAS, Kirsten ras; Nrf2, Nuclear factor (erythroid-derived 2)-like 2;
G-quadruplex DNA, G4 DNA; PAGE, polyacrylamide gel electrophoresis

Keywords

KRAS, Nrf2, ROS, 8-oxoguanine, G4 DNA, PARP-1, NFkB-Snail-RKIP

Introduction

KRAS is mutated in about 30 % of all human cancers [1] and plays a key role in the pathogenesis of pancreatic ductal adenocarcinoma (PDAC). It has been reported that the ectopic expression of mutant *KRAS* G12D in mice is sufficient to initiate cancer [2, 3]. While the function of *KRAS* in the early steps of tumorigenesis has been addressed [4, 5], its role in later stages of the disease is still poorly understood. Recent studies have demonstrated that PDAC cells are addicted to oncogenic *KRAS* [6, 7]. This means that cancer cells require for proliferation the expression of a single oncogene, although they accumulate multiple genetic lesions [7]. In agreement with this important notion, De Pinho et al. [8] found that oncogenic *KRAS* reprograms the glucose metabolism in PDAC cells, in order to fuel a high anabolic demand, typical of rapidly dividing cells [9,10]. The metabolic rewiring induced by *KRAS* affects the glutamine (Gln) fate too, which does not follow its canonical oxidative pathway through the tricarboxylic acid cycle. By contrast, Gln is transformed into aspartate (Asp) → oxaloacetate → malate → pyruvate: a pathway that is accompanied by an increase of NADPH/$NADP^+$, the reducing power necessary by cancer PDAC cells to maintain the redox homeostasis [11-14].

As cancer cells produce higher levels of reactive oxygen species (ROS) [13], they activate a defence mechanism against oxidative stress. The major cellular response to oxidative stress is the activation of Nrf2 (nuclear factor erythroid 2-related factor 2), a redox-sensitive transcription factor that regulates the expression of antioxidant response element (ARE)-regulated genes [15-18]. While the knockout of Nrf2 in mice increased their susceptibility to a broad range of chemical toxicity, the pharmacological boosting of Nrf2 protected the animals from oxidative damage [19]. Under basal redox conditions,

cytoplasmic Nrf2 is bound to Keap1 and subjected to proteosomal degradation. But, enhanced ROS cause a conformational change in Keap1, due to the oxidation of cysteine residues, resulting in the release of Nrf2 by the Nrf2:Kep1 complex. Free Nrf2 will then translocate into the nucleus and activate ARE-regulated genes [20].

In this work we have analysed the impact of oxidative stress on the expression of *KRAS* and on its intersection with survival and apoptosis pathways. We found that enhanced ROS induce the expression of *KRAS* which, in turn, stimulates Nrf2. *KRAS*-induced Nrf2 brings down the level of ROS, which results in the upregulation of prosurvival Snail and the downregulation of proapoptotic RKIP. By contrast, when ROS are generated and simultaneously Nrf2 is inhibited, proapoptotic RKIP is found upregulated while prosurvival Snail downregulated. Taken together, these data show that *KRAS* controls via Nrf2 the redox homeostasis and, through Snail and RKIP, the survival and apoptosis pathways. Finally, we address the issue of how ROS upregulate *KRAS* and propose a mechanism involving a G-quadruplex structure; we also demonstrate that the inhibition of Nrf2 strengthen the capacity of porphyrin TMPyP4 to act as a PDT photosensitizer for PDAC cells.

Materials and Methods

Oligonucleotides and Reagents

Oligonucleotides used in this study have been obtained from Microsynth (CH). 8-oxoG-substituted oligonucleotides were synthesized using 8-oxo-dG CEP (Berry & Associates) in 1-μmol scale on solid support by standard procedure, except using concentrated ammonia in the presence of 2-mercaptoethanol (0.25 M) in the deprotection step. The oligonucleotides were purified by reverse-phase HLPC equipped with a C18 column (XBridge OST C18, 19 × 1000 mm, 5 μm). Oligonucleotide composition was verified by Matrix Assisted Laser Desorption Ionisation-Time of Flight (MALDI-TOF) (Spectra reported in ref. [21]). Luteolin, was purchased from Alfa Aesar (D), 8-oxoguanine (8-oxoG) and 8-oxodeoxyguanosine from Cayman Chemicals (MI, USA), GTP from Euroclone (I), hydrogen peroxide solution 30% (w/w) from BDH (UK).

Cell Cultures

Human pancreatic (Panc-1, MIA PaCa-2, BxPC3) and bladder T24 cancer cells as well as non-cancer human embryonic kidney 293 cells were maintained in exponential growth in Dulbecco's modified Eagle's medium (DMEM) containing 100 U/ml penicillin, 100 mg/ml streptomycin, 20 mM L-glutamine and 10 % foetal bovine serum (Euroclone, IT).

Western blots

Total protein lysates (15 µg) were electrophoresed on 12 % SDS-PAGE and transferred to a nitrocellulose membrane at 70 V for 2 h. The filter was blocked for 1 h with 5 % nonfat dried milk solution in PBS 0.1 % Tween (Sigma-Aldrich, USA) at room temperature. The primary antibodies used are anti-beta actin (clone JLA20, IgM mouse, $1x10^{-4}$ □g/ml, Calbiochem, Merck Millipore, Germany), anti-KRAS (Sigma Aldrich, clone 3B10-2F2), anti Snail (Cell Signalling, C115D3 Rabbit mAb), anti RKIP (Cell Signalling G38 Ab), anti NF-kB p65 (Santa Cruz, C-20), PARP-1 (Cell Signalling, PARP-1 Ab), MAZ (Santa Cruz, MAZ-133.7) and hnRNP A1 (Sigma, clone 9H10). Membranes with the samples were incubated overnight at 4 °C with primary antibodies. The filters were washed with a 0.1 % Tween in PBS and subsequently incubated for 1 h with the secondary antibodies horseradish peroxidase conjugated: anti-mouse IgM (diluted 1:5000), anti-rabbit IgG (diluted 1:5000) and anti-mouse IgG (1:5000) (Calbiochem, Merck Millipore, Germany). The signal of the proteins was developed with Super Signal ®West PICO, and FEMTO (Thermo Fisher, USA) and detected with ChemiDOC XRS, Quantity One 4.6.5 software (BioRad Laboratories, USA).

RNA extraction and quantitative real-time PCR

Panc-1 and T24 cancer cells were plated in a 96-well plate (18 x 10^3 cells/well). The following day (24 h), we treated the cells with P4/λ (40 or 120 nM P4, 7.2 J/cm^2 white light) and total RNA was extracted using iScript ™ RT-qPCR Sample Preparation Reagent (BioRad, USA) 2, 8 or 33 hours after treatment, following the manufacturer's instructions. For the cDNA synthesis, 1.25 µl of RNA, added with 3.75 ml DEPC water, were heated at 70 °C for 5 min. The solution was added with 7.5 µl of a mix containing: 1x buffer, 0.01 M DTT (Invitrogen, USA), 1.6 µM primer dT [MWG Biotech, Germany; $d(T)_{16}$], 1.6 µM random hexamer primers (Mycrosynth, Switzerland), 0.4 mM dNTPs solution containing equimolar amounts of dATP, dCTP, dGTP and dTTP (Euroclone, Italy), 0.8 U/µl RNase OUT, 8 U/µl of M-MLV reverse transcriptase (Invitrogen, USA). The mixtures were

incubated for 1 h at 37 °C and stopped by heating at 95 °C for 5 min. As a negative control the reverse transcription reaction was performed with a sample containing DEPC-treated water.

To determine the levels of Nrf2, Snail, RKIP, *KRAS* and housekeeping genes hypoxanthine-guanine phosphoribosyltransferase (HPRT) and β2-microglobulin, quantitative real-time multiplex reactions were performed. We used sensi FAST™ syBR (No-ROX kit, Bioline, UK), 2.2 µl of cDNA and primers/probes. The PCR cycle was: 3 min at 95 °C, 50 cycles 10 s at 95 °C, 60 s at 58 °C (RKIP, KRAS, HPRT and β2 microglobulin), 61 °C (Snail) and 62 °C (Nrf2). PCR reactions were carried out with a CFX-96 real-time PCR apparatus controlled by an Optical System software (version 3.1) (Bio-Rad Laboratories, USA). The *KRAS* transcript level was normalized with the housekeeping genes. The primer sequences are reported in Table 1.

As for ChIP experiments, we followed the protocol reported in Ref. [21] and used the ChIP-IT® Express Shearing Kit (Active Motif, CA, USA). qPCR was performed with the following primers specific for genomic *KRAS* (accession number NG_007524): *G4*-plus 5'-GTACGCCCGTCTGAAGAAGA-3' (nucleotides (nt) 4889-4908, 0.2 µM), *G4*-minus 5'-GAGCACACCGATGAGTTCGG-3' (nt 4958-4977, 0.1 µM), Ctr-1-plus 5'-ACAAAAAG-GTGCTGGGTGAGA-3' (nt 12-32, 0.2 µM), Ctr-1-minus 5'-TCCCCTTCCCGGAG-ACTTAAT-3' (nt 248-268, 0.2 µM), Ctr-2-plus 5'-CTCCGACTCTCAGGCTCAAG-3' (nt 7536-7555, 0.15 µM), Ctr-2-minus 5'-CAGCACTTTGGGAGGCTTAG-3' (nt 7692-7711, 0.15 µM). Ctr-1 is located in a non-coding region, G4-region is in the promoter, Ctr-2 is in an intron. A detailed description of the method of analysis is reported in Ref. [21].

Pull-down assay with Panc-1 extract

A total of 150 µg of nuclear Panc-1 extract (1.3 mg/ml) were incubated for 0.5 h at 25°C with 80 nM biotinylated 32R, ODN-**92** and ODN-**96** in 20 mM Tris–HCl, pH 7.4, 50 mM KCl (oligos in G4) 8% glycerol, 1 mM DTT, 0.1 mM ZnAc, 5 mM NaF, 1 mM Na_3VO_4 and 2.5 ng/µl poly[dI-dC]. A total of 80 µg of Streptavidin MagneSphere Paramagnetic Particles (Promega, I), previously washed in buffer, were added and let to incubate for 0.5 h at 25°C. The oligonucleotides were used also in the duplex conformation in the same buffer but in 150 mM NaCl (incubation with extract was carried out at 37°C for 1 h). The beads were captured with a magnet and washed three times. The proteins were denatured and eluted with Laemmli buffer (4% SDS, 20% glycerol, 10% 2-

mercaptoethanol, 0.004% bromophenol blue and 0.125 M Tris–HCl). Then they were separated in 10% SDS-PAGE and blotted into nitrocellulose at 70 V for 2 h. The nitrocellulose membrane was blocked for 1 h with 5 % non fat dried milk in PBS and 0.1% Tween (Sigma-Aldrich, USA) at room temperature. The primary antibodies used were: anti-MAZ (clone 133.7, IgG mouse, Santa Cruz Biotechnology, USA) diluted 1:200, anti-hnRNP A1 (clone 9H10, IgG mouse, Sigma-Aldrich, USA) diluted 1:2000 and anti PARP-1 (polyclonal antibody, IgG rabbit, Cell Signalling Technology, USA) diluted 1:200. The membranes were incubated overnight at 4°C with the primary antibodies, then washed with 0.1% Tween in PBS and incubated for 1 h with the secondary antibodies conjugated to horseradish peroxidase: anti-mouse IgG (diluted 1:5000) and anti-rabbit IgG (diluted 1:5000) (Calbiochem, Merck Millipore, D). The signal was developed with Super Signal ®West PICO, and FEMTO (Thermo Fisher, USA) and detected with ChemiDOC XRS, Quantity One 4.6.5 software (BioRad Laboratories, USA).

Measurement of intracellular ROS

Panc-1 and T24 cells were plated in 6-well plate (2.0 x 10^5 cells/well). The following day we treated the cells with 20 μM luteolin and after 4 h with TMPyP4 (P4) (40 or 80 nM). We irradiated the cells with white light (fluence of 7.2 J/cm^2), 24 h after luteolin treatment. The following day, the medium was removed and the cells washed twice with PBS. After washing, the cells were incubated with 500 μl of 10 μM CM-H_2DCFDA (Invitrogen) in DMEM-free serum for 40 min. After two washes with PBS, the cells were trypsinized and transferred into FACS tubes containing 1 ml of PBS. The suspension was centrifuged at 1200 rpm for 3 min. The pellet was resuspended in 300 μl of PBS and the ROS signal was measured by flow cytometer. In some experiments intracellular ROS levels were determined in a 96-well plate using EnSpire 2300 Multilabel Reader (Perkin Elmer).

Cell transfection with KRAS expression vectors

Panc-1 cells were plated in a 6-well plate (5 x 10^5 cells/well) or in 96-well plate (9 x 10^3 cells/well) and the following day transfected with plasmids encoding WT, G12D, G12V KRAS protein and control plasmid (empty vector) using jetPEI (Polyplus, France) as transfectant reagent. For Western blot total protein lysates were obtained after 96 h in Laemmli Buffer and quantified using a Markwell Test. ROS was determined by treating the

cells with 10 μM H_2DCFDA in DMEM-free serum for 40 min and reading the fluorescence at 515 nm (Ex 495 nm).

PAGE for enzymatic reactions with DNA glycosylases

Oligonucleotides 32R and 8OG-substituted analogues ODN-**92** and ODN-**96** end-labelled with [γ-^{32}P] ATP (Perkin Elmer) and T4 polynucleotide kinase (Thermo Fisher Scientific, USA), were annealed in duplex with complementary 32Y strand in 50 mM Tris-HCl, pH 7.4, 100 mM NaCl (5 min at 95°C, overnight at room temperature). Radiolabelled duplex (2 nM) was incubated at 37 °C with increasing amounts of recombinant hOGG1 or NEIL1 (1 and 5 μM), in 20 mM Tris-HCl pH 8, 50 mM NaCl, 1 mM EDTA, 0.1mg/ml BSA, 1 mM Na_3VO_4, 5 mM NaF and 0.01 % Phosphatase Inhibitor Cocktail. After 15 min the reactions were stopped by adding 2 μl stop solution (90 % formamide, 50 mM EDTA). The samples were then denatured for 5 min at 95 °C and run for 1 h on a denaturing 20 % polyacrylamide gel, prepared in TBE and 7 M urea, pre-equilibrated at 55 °C in an electrophoretic apparatus (C.B.S Scientific Company, CA, USA). After running the gels were fixed in a solution containing 10 % acetic acid and 10 % methanol, dried and exposed to film for autoradiography (Aurogene, IT).

Statistical analysis

Data are reported as the mean ± standard error (SE). Statistical analysis was carried out using Sigma Plot software. Group differences were analyzed by Student's *t*-test or one-way analysis of variance (ANOVA). Groups are considered different when $P< 0.05$.

Results

Oxidative stress in pancreatic cancer cells and role of Nrf2. In aerobic organisms, ROS, which include anion superoxide (O_2^-), hydrogen peroxide (H_2O_2) and hydroxyl radical (·OH), are continuously produced as byproducts of metabolism. Their main sources are: (i) mitochondria, through electron leakage from the ubiquinone/ubiquinol shuttle; (ii) peroxisomes, during β-oxidation of long-chain fatty acids; (iii) cytochrome P-450 enzymes;

(iv) nicotinamide adenine dinucleotide phosphate (NADPH) oxidises of the NOX family [22, 23] [Suppl. Inf. S1]. One of the most injurious consequences of oxidative stress is its impact on DNA. Due to its low redox potential, guanine tends to oxidize to 7,8-dihydro-8-oxoguanine (8OG) [24] [Suppl. Inf. S2]. As there is a direct correlation between 8OG and ROS, the level of 8OG in the genome is a useful cell biomarker for oxidative stress [25]. To evaluate the intrinsic level of oxidative stress in cancer (Panc-1, MIA PaCa-2 and BxPC-3) and non-cancer (embryonic human kidney 293) cells, we measured 8OG by chromatin immunoprecipitation, using an antibody specific for 8OG. Fig. 1A shows that the level of 8OG in cancer cells is significantly higher than in non-cancer 293 cells. This is due to the fact that cancer cells display a higher metabolic rate and thus a higher ROS production than normal cells [10, 13, 14]. A recent study showed that in cancer cells the metabolism is reprogrammed by the *KRAS* oncogene [8, 11]. We measured the basal level of *KRAS* in cancer and non-cancer cells and found that it is expressed more in the former than the latter [Suppl. Inf. S3]. Besides regulating the metabolism, *KRAS* seems to control the redox homeostasis too [15]. A master regulator of the redox homeostasis is Nrf2, a transcription factor that activates the expression of antioxidant response element (ARE)-bearing genes [26, 27]. In response to enhanced ROS, cancer cells strengthen their antioxidant capacity by raising the basal expression of Nrf2 to bring down oxidative stress to levels favouring cell growth [15-17]. To test the response of Nrf2 to an increase of oxidative stress, we used Panc-1 cells, which harbour *KRAS* G12D (G12D, Gly→Asp), the most frequent mutation occurring in PDAC. We treated the cells with porphyrin TMPyP4 (hereafter called P4), a cationic photosensitizer that generates ROS upon light irradiation [28], and measured Nrf2 by Western blot [Fig. 1B]. It can be seen that when the cells are treated with P4 (20, 40 and 80 nM) and light (7.2 J/cm^2), in order to produce ROS through a photodynamic effect (we call the treatment P4/λ), Nrf2 increased in a dose-response manner up to ~ 2-fold compared to untreated cells. A similar result was obtained by quantitative RT-PCR (qRT-PCR), showing that the mRNA of Nrf2 increased ~ 3-fold compared to untreated cells, following a P4/λ treatment (40 nM P4, 7.2 J/cm^2) [Fig. 1C]. A strong inhibitor of Nrf2 is luteolin, a tetrahydroxyflavone that reduces Nrf2 expression [29, 30] [Suppl. Inf. S4]. When Panc-1 cells are treated with P4/λ (40 and 80 nM P4, 7.2 J/cm^2)□ ROS increase in a dose-response manner. However, when the cells are treated with P4/λ and luteolin (20 μM Lu) (treatment called P4/λ/Lu), a higher increase of ROS is observed, as the detoxification program mediated by Nrf2 is inhibited by luteolin (Fig. 1D). This seems to be a general response of cancer cells, as it is observed not only in

pancreatic Panc-1 but also in bladder T24 cancer cells [Fig. 1E]. These data suggest that there is a close correlation between Nrf2 and intracellular ROS.

The ROS-KRAS-Nrf2 axis in the control of the ROS homeostasis. As *KRAS* reprograms the metabolism in pancreatic cancer cells [8], we asked if there is a link between *KRAS*, Nrf2 and ROS. First, we investigated if enhanced ROS stimulates the expression of *KRAS*. We gradually increased ROS in Panc-1 cells with three distinct treatments: luteolin; P4/λ and P4/λ□□u (Fig. 2A). By qRT-PCR we measured *KRAS* mRNA and observed an increase of transcript in a dose response manner: P4/λ□Lu> P4/λ > Lu, i.e proportional to the amount of ROS generated. The increase of *KRAS* expression induced by ROS was confirmed by Western blot, using a monoclonal antibody specific for protein KRAS [Fig. 2B]. The results showed that ROS caused a ~ 2-fold increase of protein in Panc-1. This cellular response was observed also in T24 bladder cancer cells harbouring wild-type *KRAS* [Fig. 2C]. These findings demonstrate that ROS stimulate the expression of *KRAS* in cancer cells bearing either wild type or mutant *KRAS* alleles. A possible mechanism through which *KRAS* is upregulated by ROS will be discussed next.

As Nrf2 is overexpressed in pancreatic cancer cells [16], we interrogated how this redox-sensing factor is upregulated. A first hint that *KRAS* controls the expression of Nrf2 was reported by De Nicola et al. [15], who found that the ectopic expression of *KRAS* G12D in mouse embryonic fibroblasts promoted a 60 % increase of Nrf2. To test if a similar behaviour is observed in pancreatic cancer cells, we transfected Panc-1 cells with a vector expressing either wild-type (pWT) or mutant (pG12D or pG12V) KRAS protein. As a control we used a vector lacking the *KRAS* coding sequence (pEmpty). After transfection, we measured the levels of proteins KRAS and Nrf2 by Western blot [Fig. 2D]. The ectopic expression of *KRAS* G12D or *KRAS* G12V caused a ~ 2-fold increase of Nrf2, while the control vector did not. In agreement with previous data obtained with embryonic fibroblasts [15], our finding supports the notion that in pancreatic cancer cells the expression of Nrf2 is under the control of *KRAS*. The upregulation of Nrf2 induced by the ectopic expression of *KRAS* G12D or KRAS G12V is expected to lower the level of intracellular ROS. To prove this, we transfected Panc-1 cells with the expression vectors pG12D, pG12V and pEmpty and measured ROS with dichlorofluorescein (DCF). Fig. 2E shows that ROS are reduced to 45 % of the control (empty vector), which is in nice accord with our hypothesis. Together our data support the notion that *KRAS* governs the redox state in cancer cells through the ROS/*KRAS*/Nrf2 axis (Fig. 2F).

Intersection between ROS-KRAS-Nrf2 axis and survival/apoptosis pathways. As the ROS-*KRAS*-Nrf2 axis controls the redox homeostasis, we wondered if it also affects the survival and apoptosis pathways. In a previous study we demonstrated that in melanoma B78-H1 cells, a moderate increase of ROS generated by pheophorbide/λ caused the upregulation of NF-kB and prosurvival Snail and the downregulation of proapototic RKIP [31, 32]. NF-kB, Snail and RKIP are interconnected in a circuitry modulated by ROS, that regulates the signalling for cell survival and apoptosis. Pancreatic cancer cells overexpress Snail and Nrf2 [33, 34], therefore we asked if there is a link between Nfr2 and the NF-kB/Snail/RKIP circuitry. To address this question we first measured by qRT-PCR the levels of Nrf2, Snail and RKIP mRNAs in Panc-1 [Fig. 3A)] cancer cells, untreated or treated with two doses of P4/λ (40 and 120 nM P4, light at 7.2 J/cm^2) generating a moderate increase of ROS. The cells responded to the treatment by upregulating Nrf2 (from 20 to 40 %) and prosurvival Snail (up 6-fold), and simultaneously downregulating proapoptotic RKIP (~ 30 %) compared to untreated cells. Snail is a zinc-finger transcription factor with a central role in cell survival and metastasis [35, 36]. When this protein is ectopically expressed in Panc-1 cells, their invasive property increases dramatically [35]. Panc-1 cells, expressing Snail, implanted into nude mice metastasized more efficiently than the unmodified cells [33], thus supporting the notion that Snail plays a key role in PDAC progression. It has been reported that Snail is transcriptionally regulated by NF-kB [37] and capable to induce phenotypic changes in cells. For example, Snail represses the epithelial marker E-cadherin and pushes up the mesenchymal marker Vimentin [38]. Snail is also a potent repressor of the RAF kinase inhibitor protein (RKIP): a metastasis suppressor protein that acts through the inhibition of RAS/MEK/ERK signalling [39, 40]. The effect of ROS on the NF-kB/Snail/ RKIP circuitry was also examined by Western blots [Fig. 3B]. In agreement with qRT-PCR, after P4/λ (80 nM P4, light 7.2 J/cm^2) Nrf2 and Snail were found upregulated while RKIP downregulated. Also NF-kB was strongly upregulated by P4/λ, in accord with previous work [31]. Collectively, these data show that a moderate increase of ROS shifts NF-kB/Snail/ RKIP towards cancer progression. The link between KRAS-Nrf2 and the propapototic/prosurvival NF-kB/Snail/ RKIP circuitry was observed also in T24 bladder cancer cells [Fig. 4A,B].

Next, we investigated how NF-kB/Snail/ RKIP responds to high ROS levels, obtained by generating ROS under conditions in which Nrf2 and thus the detoxification capacity of the cells were repressed. We compared the response of the cells to low ROS generated

by P4/λ and high ROS generated by P4/λ/Lu. Fig. 5A-D shows the expression of prosurvival Snail and proapoptotic RKIP measured by Western blots. The average result of two similar treatments (40 and 80 nM P4, light 7.2 J/cm^2), performed with and without 10 μM luteolin, show that the cells exposed to ROS while Nrf2 is inhibited (high ROS), have prosurvival Snail downregulated and proapoptotic RKIP upregulated. As expected, the NF-kB/Snail/ RKIP circuitry assumes a configuration favouring apoptosis. It has been demonstrated that a decreased level of RKIP in cancer cells is associated with invasion and metastasis, while an increase of RKIP promotes anticancer effects [41]. In PDAC cells RKIP is normally underexpressed and this closely correlates with patient outcomes [42]. The overexpression of RKIP in PDAC cells suppresses proliferation and activates apoptosis [41].

***ROS activate KRAS through a mechanism mediated by G4 DNA*.** To explore how ROS upregulate *KRAS* we focused on the promoter region of the gene which contains between -144 and -117 relative to the transcription start site, a G-rich element called 32R. This sequence is composed of runs of guanines and folds into a G-quadruplex (G4) stabilized by G tetrads, with a T_M of 62.1 °C in 100 mM KCl. The CD spectra of 32R at 25 °C is indicative of the formation of a G4 with a parallel topology [43-45] (Fig. 6A-C) (Suppl. Inf. S5). By streptavidin-biotin pull-down assays and mass spectrometry we found that the G4 formed by 32R is recognized by several transcription factors (TFs) including MAZ, hnRNP A1 and PARP1, which are essential for transcription [44,46-48]. We also found that the guanines in this promoter region, due to their low redox potential, are prone to oxidation to 8OG [21]. ChIP experiments showed that an intracellular increase of ROS boosts the recruitment of the TFs to the 32R promoter region [21] (Fig. 6D). To confirm that the TFs and 8OG co-localize on the same 32R-containing region, we firstly performed a double chromatin immunoprecipitation experiment (ChIP-reChIP) (Suppl. inf. S6) (Fig. 6E). Panc-1 cells were treated with hydrogen peroxide and the chromatin was extracted and sheared into fragments of about 300 bp. Sheared chromatin was immunoprecipitated with an antibody specific for MAZ or hnRNPA1 and the precipitated chromatinized DNA recovered and used for a second immunoprecipitation with an antibody specific for 8OG. After the second ChIP, the DNA was recovered and analysed by qPCR. The results showed that the occupancy of MAZ and hnRNP A1 is higher on the chromatin fragment containing 32R than on the control sequence, in keeping with the co-localization of the TFs and 8OG on the same promoter sequence. Secondly, we demonstrated that there is co-localization also

between 8OG and G4 DNA. Sheared chromatin from hydrogen peroxide-treated cells was pulled down with a biotinylated ligand G4-specific (anthrathiophenedione [49]) (Fig. 7A) (Suppl. Inf. S7). The precipitated chromatin was recovered and then immunoprecipitated with an antibody specific for 8OG. The DNA recovered after the second precipitation was analysed by qPCR. The level of 8OG was higher in the 32R region compared to the control regions. Together, the two immunoprecipitation experiments show that 8OG and TFs co-localize on the same promoter region containing 32R.
Finally, to provide direct evidence that the TFs bind to oxidized G4, we performed pulldown/WB experiments with wild-type 32R or oxidized analogues (ODN-**92** with one 8OG and ODN-**96** with two 8OG) as a bait (Fig. 7B) The presence of 8OG in 32R does not inhibit the folding into a G4 but it can inhibit the topology depending on its position within the sequence. This is described in detail in Ref. [21] (Suppl. Inf. S8). The results show that the G4 structures, either the wild type or those oxidized, form a multiprotein complex with the above TFs. How G4 and ROS favour transcription of *KRAS* will be addressed in Discussion.

Photodynamic treatment in the presence of luteolin: clonogenic assay. Finally, the results of this study may be useful to design efficient photodynamic therapy (PDT) for cancer [50]. PDT is a slightly invasive therapeutic approach involving the administration of a photosensitizer and its activation with light in order to generate ROS killing cancer cells [51]. The treatment can be strengthened if Nrf2, the gene that activates the cellular response to oxidative stress, is inhibited. In fact, the data of Fig. 5 show that when PDT (the P4/λ treatment) □□□combined with an inhibitor of Nrf2 such as luteolin (adjuvant), the cells become more sensitive to PDT by up-regulating proapoptotic RKIP and down-regulating prosurvival Snail: i.e. creating intracellular conditions favouring apoptosis modulated by ROS. To assess the effect of P4 and luteolin on cell growth, we carried out a colony formation assay with pancreatic Panc-1 and BXPC-3 cancer cells. The cells were seeded in a medium containing either P4, luteolin or a mixture between P4 and luteolin and irradiated with light at a fluence of 7.2 J/cm^2. After 8 days of growth the colonies were counted and the results plotted in a histogram. Fig. 8 shows that the number of colonies in the plates treated with only 20 μM luteolin (Lu blocks Nrf2 and increases the basal level of ROS) or P4/λ (40 nM) is 20-25 % lower than the number of colonies in untreated cells. In contrast, the combined treatment, P4/λ + luteolin, reduce the number of colonies to ~ 50 %

of the control. These results strongly support our hypothesis that when Nfr2 is inhibited, the cells are more sensitive to PDT as the Nrf2-directed antioxidant program is inhibited.

Discussion

As any actively dividing cells, cancer cells have a high demand of biomass to fuel their rapid proliferation. To satisfy this requirement, cancer cells reprogram the metabolism and *KRAS* induces the metabolic changes occurring in PDAC (8). A comprehensive review summarizing the metabolic requirements of cancer cells is reported in ref [10]. Cancer cells produce higher amounts of ROS than healthy cells (13). ROS can oxidize lipids, proteins and nucleic acids and their accumulation may severely damage the cells. To protect macromolecules from oxidative damage, cancer cells activate a complex network of enzymatic and non-enzymatic antioxidants [52]. The antioxidant response is regulated by Nrf2, which is activated by ROS. As *KRAS* reprograms the metabolism in PDAC, we asked if there is a correlation between *KRAS* and Nrf2. In agreement with the work of De Nicola et al. [15], we found that the ectopic expression of *KRAS* G12D or G12V in PDAC cells pushes up Nrf2 by nearly 2 folds, thus confirming a direct correlation between *KRAS* and Nrf2. Our data show that ROS, *KRAS* and Nrf2 form a molecular axis preventing ROS accumulation to toxic levels that could inhibit cell cycle progression and proliferation. We also found that the ROS/*KRAS*/Nrf2 axis intersects with survival and apoptosis pathways. By controlling the redzsox homeostasis, the ROS/*KRAS*/Nrf2 axis regulates via NF-kB the expression of prosurvival Snail and proapoptotic RKIP (Fig. 9A,B). Low ROS, occurring when Nrf2 is active, results in upregulation of NF-kB and prosurvival Snail and downregulation of proapoptotic RKIP: survival/proliferation overcomes apoptosis. In contrast, high ROS, occurring when Nrf2 is inhibited, results in downregulation of NF-kB and prosurvival Snail and upregulation of proapoptotic RKIP: in this case apoptosis overcomes proliferation. This behaviour provides an explanation, in terms of molecular pathways, why a combined treatment, PDT and Nrf2 inhibitior, is more effective than only PDT.

Next, an important issue regarding the ROS/*KRAS*/Nrf2 axis is how *KRAS* is upregulated by ROS. To this end, we focused on the *KRAS* promoter containing upstream of TSS a regulatory G-rich element called 32R, which forms a G4 structure recognized by transcription factors MAZ, PARP-1 and hnRNP A1 [43, 44-48, 53]. Due to its low redox potential, guanine in the G4 motif is inclined to oxidation to 8OG. Recent data suggest that

oxidized guanine is likely to be an epigenetic modification stimulating gene expression [54, 55]. ChIP experiments showed that when intracellular ROS is increased with hydrogen peroxide, MAZ, hnRNP A1 and PARP1 are recruited to the promoter 32R region more than in other G-rich regions [21]. PARP1 is likely to play a critical role in the recruitment. This 110 kDa protein has a high affinity for G4 DNA (Kd ~ 10^{-9} M^{-1}) and the tendency to undergo auto poly(ADP-ribosyl)ation following the binding to G4 [56]. So, the protein, displaying on its surface ADP-ribosyl units, becomes anionic and favours the recruitment of MAZ and hnRNP A1, as these TFs having a pI > 7.4 (8.11 and 9.45, respectively) are cationic under physiological conditions. This is consistent with the finding that the G4 structure, with or without 8OG, pulls down from a total Panc-1 extract the three TFs (Fig. 7B).

In conclusion, our data suggest that an increase of cellular ROS favours the oxidation of guanine at the G-rich promoter region of *KRAS* located upstream of TSS. This increases the recruitment of the TFs to the promoter and the subsequent activation of transcription. Our data support the notion that 8OG is not a detrimental by-product of oxidative processes, but an epigenetic modification with gene regulatory functions. A recent study by Fleming et al [57] reported that the presence of 8OG in the *VEGF* G4 motif increases indeed transcription.

Competing interests

Authors declare no conflict of interest and also no financial interests are associated with this manuscript.

Funding

This work was supported by AIRC (the Italian Association for Cancer Research). Grant number: IG 2017, Project Code 19898. Funding for open access charge: AIRC

Authors' contributions

AF and GC have performed the experiments. VR planned some of the experiments. LX conceived the project and wrote the manuscript.

Acknowledgements

We thank Erik Pedersen from the University of Odense (DK) for providing us the oligonucleotides with 8-oxoguanine modifications.

References

1. Niemela JE, Lu L, Fleisher TA, Davis J, Caminha I, Natter M, Beer LA, Dowdell KC, Pittaluga S, Raffeld M, Rao VK, Oliveira JB. Somatic KRAS mutations associated with a human nonmalignant syndrome of autoimmunity and abnormal leukocyte homeostasis. *Blood* 2011, **117**:2883-2886.
2. Collins MA, Bednar F, Zhang Y, Brisset JC, Galbán S, Galbán CJ, Rakshit S, Flannagan KS, Adsay NV, Pasca di Magliano M. Oncogenic Kras is required for both the initiation and maintenance of pancreatic cancer in mice. *J Clin Invest.* 2012, **122**: 639-653.
3. Kong, B., Michalski, C. W., Erkan, M., Friess, H. & Kleeff, J. From tissue turnover to the cell of origin for pancreatic cancer. *Nat Rev Gastroenerol Hepatol*. 2011, **8**: 467-472.
4. Di Magliano MP, Logson CD. Roles of KRAS in panceratic tumor development and progression. *Gastroenterology* 2014, **144**: 1220-1229.
5. Maitra A and Hruban RH. Pancreatic Cancer. *Annu Rev Pathol.* 2008; **3**: 157–188.
6. Weinstein IB and Joe AK. Mechanisms of Disease: oncogene addiction—a rationale for molecular targeting in cancer therapy *Nature Clinical Practice Oncology* 2006, **3**: 448-457.
7. Pagliarini R, Shao W, Sellers WR. Oncogene addiction: pathways of therapeutic response, resistance, and road maps toward a cure. *EMBO Rep*. 2015,**16**:280-96.
8. Ying H. et al. Oncogenic Kras maintains pancreatic tumors through regulation of anabolic glucose metabolism. *Cell* 2012, **149**: 656-670.
9. Vander Heiden MG, Locasale JW, Swanson KD, Sharfi H, Heffron GJ, Amador-Noguez D, Christofk HR, Wagner G, Rabinowitz JD, Asara JM, Cantley LC. Evidence for an alternative glycolytic pathway in rapidly proliferating cells. *Science* 2010, **329**:1492-1499.
10. Vander Heiden MG, Cantley LC, Thompson CB. Understanding the Warburg effect: the metabolic requirements of cell proliferation. *Science* 2009, **324**:1029-1033.
11. Son J, Lyssiotis CA, Ying H, Wang X, Hua S, Ligorio M, Perera RM, Ferrone CR,

Mullarky E, Shyh-Chang N, Kang Y, Fleming JB, Bardeesy N, Asara JM, Haigis MC, DePinho RA, Cantley LC, Kimmelman AC. Glutamine supports pancreatic cancer growth through a KRAS-regulated metabolic pathway. *Nature* 2013, **496**:101-105.

12. Keibler MA, Wasylenko TM, Kelleher JK, Iliopoulos O, Vander Heiden MG, Stephanopoulos G. Metabolic requirements for cancer cell proliferation. *Cancer Metab*. 2016, **4**:1-16.
13. Szatrowski TP, Nathan CF. Production of large amounts of hydrogen peroxide by human tumor cells. *Cancer Res.* 1991, **51**:794-798.
14. Nogueira V, Hay N. Molecular pathways: reactive oxygen species homeostasis in cancer cells and implications for cancer therapy. *Clin Cancer Res*. 2013, **19**:4309-14.
15. DeNicola GM, Karreth FA, Humpton TJ, Gopinathan A, Wei C, Frese K, Mangal D, Yu KH, Yeo CJ, Calhoun ES, Scrimieri F, Winter JM, Hruban RH, Iacobuzio-Donahue C, Kern SE, Blair IA, Tuveson DA. Oncogene-induced Nrf2 transcription promotes ROS detoxification and tumorigenesis. *Nature* 2011, **475**:106-109.
16. Lister A, Nedjadi T, Kitteringham NR, Campbell F, Costello E, Lloyd B, Copple IM, Williams S, Owen A, Neoptolemos JP, Goldring CE, Park BK. Nrf2 is overexpressed in pancreatic cancer: implications for cell proliferation and therapy. *Mol Cancer* 2011, **10**:37.
17. Hong YB, Kang HJ, Kwon SY, Kim HJ, Kwon KY, Cho CH, Lee JM, Kallakury BV, Bae I. Nuclear factor (erythroid-derived 2)-like 2 regulates drug resistance in pancreatic cancer cells. *Pancreas* 2010, **39**:463-472.
18. Buelna-Chontal M, Zazueta C. Redox activation of Nrf2 & NFkB: a double end sword? *Cell Signal* 2013, **25**: 2548-2557.
19. Talalay P, Dinkova-Kostova AT, Holtzclaw WD. Importance of phase 2 gene regulation in protection against electrophile and reactive oxygen toxicity and carcinogenesis. *Adv. Enzyme Regul*. 2003, **43**:121–34.
20. Motohashi H, Yamamoto M. Nrf2-Keap1 defines a physiologically important stress response mechanism. *Trends Mol Med*. 2004;**10**:549–557.
21. Cogoi S, Ferino A, Miglietta G, Pedersen EB, Xodo LE. The regulatory G4 motif of the Kirsten ras (KRAS) gene is sensitive to guanine oxidation: implications on transcription. *Nucleic Acids Res*. 2018, **46**:661-676.
22. Chio IIC, Tuveson DA. ROS in cancer: the burning question. *Trends in Molecular*

Medicine 2017, **23**: 411-429.

23. Geou-Yarh Liou and eter Storz. Reactive oxygen species in cancer. *Free Radic Res.* 2010, **44**:479-496.

24. J. Cadet, J.R. Wagner, V. Shafirovich, N.E.Geacintov. One-electron oxidation reactions of purine and pyrimidine bases in cellular DNA *Int. J. Radiat. Biol.* 2014, **90**:423-432.

25. Gedik CM, Boyle SP, Wood SG, Vaughen NJ, Collins AR. Oxidative stress in humans: validation of biomarkers of DNA damage. *Carcinogenesis* 2002, **23**:1441-1446.

26. Nguyen T, Nioi P, Pickett CB. The Nrf2-Antioxidant Response Element Signaling Pathway and Its Activation by Oxidative Stress. *J Biol Chem*. 2009, **284**:13191-13295.

27. Rushmore TH, Morton MR, Pickett CB. The antioxidant responsive element. Activation by oxidative stress and identification of the DNA consensus sequence required for functional activity. *J. Biol. Chem*. 1991, **266**:11632–11639.

28. Rapozzi V, Zorzet S, Zacchigna M, Della Pietra E, Cogoi S, Xodo LE.Anticancer activity of cationic porphyrins in melanoma tumour-bearing mice and mechanistic in vitro studies. *Mol Cancer* 2014,**13**:75.

29. Tang X, Wang H, Fan L, Wu X, Xin A, Ren H, Wang XJ
Luteolin inhibits Nrf2 leading to negative regulation of the Nrf2/ARE pathway and sensitization of human lung carcinoma A549 cells to therapeutic drugs. *Free Radic Biol Med.* 2011, **50**:1599-609.

30. Chian S, Thapa R, Chi Z, Wang XJ, Tang X.Luteolin inhibits the Nrf2 signaling pathway and tumor growth in vivo. *Biochem Biophys Res Commun*. 2014, **447**:602-608.

31. Rapozzi V, Umezawa K, Xodo LE Role of NF-κB/Snail/RKIP loop in the response of tumor cells to photodynamic therapy. *Lasers Surg Med*. 2011, **43**: 575-585.

32. Wu K, Bonavida B. The activated NF-kappaB-Snail-RKIP circuitry in cancer regulates both the metastatic cascade and resistance to apoptosis by cytotoxic drugs. *Crit Rev Immunol*. 2009, **29**:241-54.

33. Tao Yin, Chunyou Wang, Tao Liu, Gang Zhao, Yunhong Zha, and Ming Yang. Expression of Snail in Pancreatic Cancer Promotes Metastasis and Chemoresistance. *J Surg Res* 2007, **141:** 196–203.

34. Wang Z, Zhao L, Xiao Y, Gao Y, Zhao C. Snail transcript levels in diagnosis of pancreatic carcinoma with fine-needle aspirate. *Br J Biomed Sci*. 2015;**72**:107-10.
35. Nieto MA, The snail superfamily of zinc-finger transcription factors. *Nat Rev Mol Cell Biol.* 2002*,* **3**:155-66.
36. Yadi Wu and Binhua P. Zhou· Snail. More than EMT. *Cell Adhesion & Migration*, 2010, **4**:199-203.
37. Julien S, Puig I, Caretti E, Bonaventure J, Nelles L, van Roy F, Dargemont C, de Herreros AG, Bellacosa A, Larue L. Activation of NF-kappaB by Akt upregulates Snail expression and induces epithelium mesenchyme transition. *Oncogene* 2007, **26**:7445-7456.
38. Batlle E, Sancho E, Francí C, Domínguez D, Monfar M, Baulida J, García De Herreros A. The transcription factor snail is a repressor of E-cadherin gene expression in epithelial tumour cells. *Nat Cell Biol*. 2000, **2**:84-89.
39. S Beach, H Tang, S Park, AS Dhillon, ET Keller, W Kolch, and KC Yung. Snail is a repressor of RKIP transcription in metastatic prostate cancer cells. *Oncogene,* 2008, **27**:2243–2248.
40. Eva Karamitopoulou, Inti Zlobec, Beat Gloor, Agathi Kondi-Pafiti, Alessandro Lugli and Aurel Perren. Loss of Raf-1 kinase inhibitor protein (RKIP) is strongly associated with high-grade tumor budding and correlates with an aggressive phenotype in pancreatic ductal adenocarcinoma (PDAC). *J Transl Med*. 2013, **11**: 311.
41. Dai H, Chen H, Liu W, You Y, Tan J, Yang A, Lai X, Bie P. Effects of Raf kinase inhibitor protein expression on pancreatic cancer cell growth and motility: an in vivo and in vitro study. *J Cancer Res Clin Oncol*. 2016, **142**:2107-2117.
42. Song SP, Zhang SB, Li ZH, Zhou YS, Li B, Bian ZW, Liao QD, Zhang YD. Reduced expression of Raf kinase inhibitor protein correlates with poor prognosis in pancreatic cancer. *Clin Transl Oncol*. 2012, **14**:848-52.
43. Cogoi S, Rapozzi V, Cauci S, **Xodo** LE. Critical role of **hnRNP A1** in activating KRAS transcription in pancreatic cancer cells: A molecular mechanism involving G4 DNA. *Biochim Biophys Acta* 2017, **1861**:1389-1398.
44. Cogoi S[1], Paramasivam M, Spolaore B, Xodo LE. Structural polymorphism within a regulatory element of the human KRAS promoter: formation of G4-DNA recognized by nuclear proteins. *Nucleic Acids Res*. 2008, **36**:3765-80.

45. Cogoi S, Xodo LE. G-quadruplex formation within the promoter of the KRAS proto-oncogene and its effect on transcription. *Nucleic Acids Res*. 2006, **34**:2536-2549.
46. Paramasivam M, Membrino A, Cogoi S, Fukuda H, Nakagama H, Xodo LE. Protein hnRNP A1 and its derivative Up1 unfold quadruplex DNA in the human KRAS promoter: implications for transcription. *Nucleic Acids Res*. 2009, **37**:2841-2853.
47. Chu PC, Yang MC, Kulp SK, Salunke SB, Himmel LE, Fang CS, Jadhav AM, Shan YS, Lee CT, Lai MD, Shirley LA, Bekaii-Saab T and Chen CS. Regulation of oncogenic KRAS signaling via a novel KRAS-integrin-linked kinase-hnRNPA1 regulatory loop in human pancreatic cancer cells. *Oncogene*. 2016, **35**, 3897-3908.
48. Cogoi S, Zorzet S, Rapozzi V, Géci I, Pedersen EB, Xodo LE. MAZ-binding G4-decoy with locked nucleic acid and twisted intercalating nucleic acid modifications suppresses KRAS in pancreatic cancer cells and delays tumor growth in mice. *Nucleic Acids Res*. 2013, **41**:4049-64.
49. Miglietta G, Cogoi S, Marinello J, Capranico G, Tikhomirov AS, Shchekotikhin A, Xodo LE. RNA G-Quadruplexes in Kirsten Ras (KRAS) Oncogene as Targets for Small Molecules Inhibiting Translation. *J Med Chem*. 2017, **60**:9448-9461.
50. van Straten D, Mashayekhi V, de Bruijn HS, Oliveira S and Robinson DJ. Oncologic Photodynamic Therapy: Basic Principles, Current Clinical Status and Future Directions. *Cancer* 2017, **9**, 19.
51. Rapozzi V, Zacchigna M, Biffi S, Garrovo C, Cateni F, Stebel M, Zorzet S, Bonora GM, Drioli S, XodoLE. Conjugated PDT drug: photosensitizing activity and tissue distribution of PEGylated pheophorbide a. Cancer Biol Ther. 2010 Sep 1;10(5):471-82.
52. Kobayaski M, Yamamoto M. Nrf2-keap-1 regulation of cellular defence mechanisms against electrophilesand reactive oxygen species. *Adv Enzyme Regul.* 2006, **46**: 113-140.
53. Cogoi S, Paramasivam M, Membrino A, Yokoyama KK, Xodo LE. The KRAS promoter responds to Myc-associated zinc finger and poly(ADP-ribose) polymerase 1 proteins, which recognize a critical quadruplex-forming GA-element. *J Biol Chem*. 2010, **285**:22003-22016.
54. Fleming AM, Ding Y, Burrows CJ. Oxidative DNA damage is epigenetic by regulating gene transcription via base excision repair. *PNAS*. 2017, **114**: 2604-2609.

55. Ba X, Boldogh **I**. 8-Oxoguanine DNA glycosylase 1: Beyond repair of the oxidatively modified base lesions. *Redox Biol.* 2018, 14:669-678.
56. Soldatenkov VA, Vetcher AA, Duka T, Ladame S. First evidence of a functional interaction between DNA quadruplexes and poly(ADP-ribose) polymerase-1. *ACS Chem Biol*. 2008, **3**: 214-219.
57. Fleming AM, Burrows CJ. DNA Repair (Amst). 2017 Aug;568-Oxo-7,8-dihydroguanine, friend and foe: Epigenetic-like regulator versus initiator of mutagenesis. *DNA Repair (Amst)*. 2017, **56**:75-83.

Table 1: DNA primers and oligonucleotides used in this study

*KRAS f*orward	5'-CGAATATGATCCAACAATAGAG
KRAS reverse	5'-ATGTACTGGTCCCTCATT
β2-microgobuline forward	5'-CCCCACTGAAAAAGATGA
β2-microglobuline reverse	5'-CCATGATGCTGCTTACAT
HPRT forward	5'-CTTGATTGTGGAAGATATAATTG
HPRT reverse	5'-TATATCCAACACTTCGTGG
Nrf2 forward	5' TCAGCGACGGAAAGAGTATGA
Nrf2 reverse	5'-CCACTGGTTTCTGACTGGATGT
Snail forward	5'-GAGGCGGTGGCAGACTAG
Snail reverse	5'-GACACATCGGTCAGACCA
RKIP forward	5'-AGACCCACCAGCATTTCGTG
RKIP reverse	5'-GCTGATGTCATTGCCCTTCA
G4 near	b-AGGGCGGTGTGGGAAGAGGGAAGAGGGGGAGG
ODN-92*	b-AGGGC**G**GTGTGGGAAGAGGGAAGAGGGGGAGG
ODN-96*	b-AGGGCGGTGTGGGAA**G**AG**G**GAAGAGGGGGAGG

* **G**= 8-oxoguanine

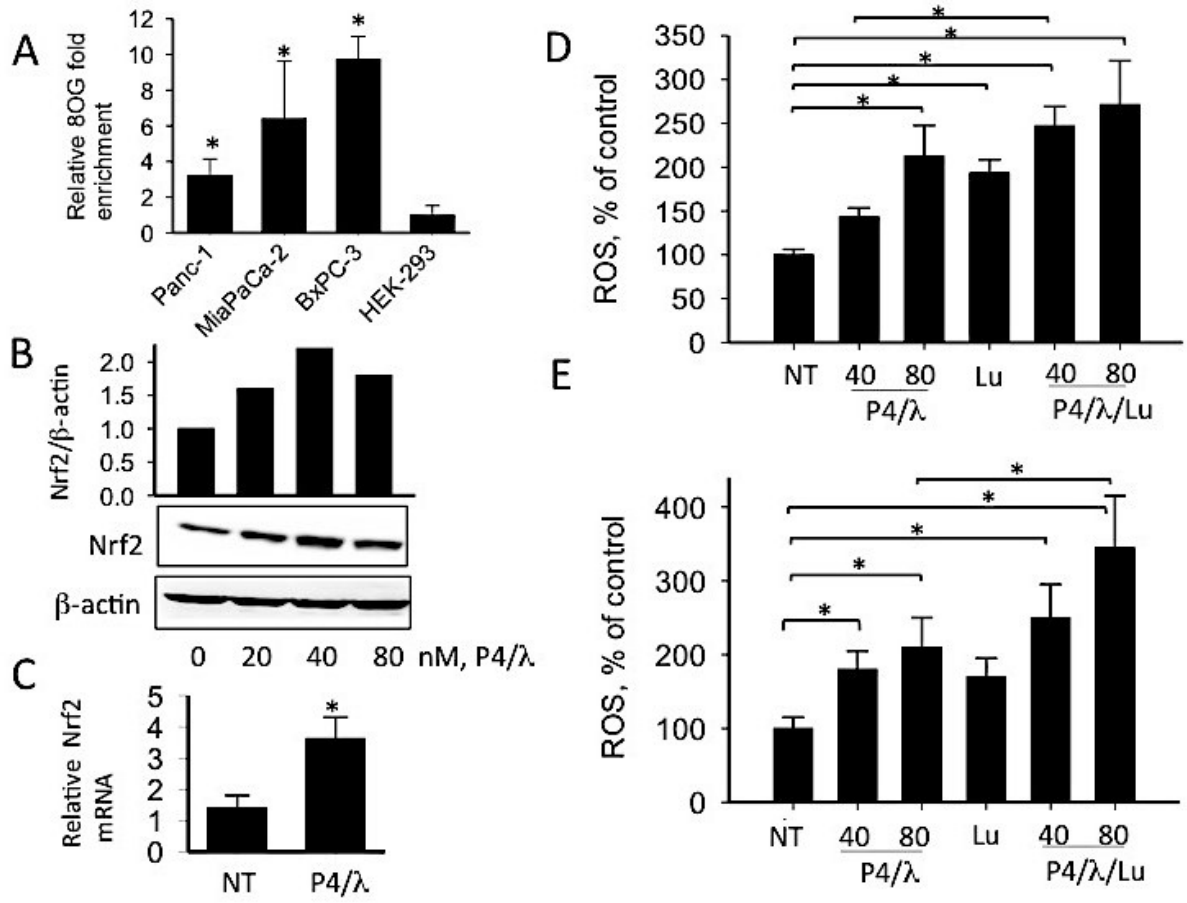

Figure 1. (A) Level of 8-oxoguanine (8OG), determined by ChIP-qPCR assays, in PDAC cells (Panc-1, MIA PaCa-2, BxPC-3) and non-cancer 293 cells. Error bars (± SE) obtained from 3 experiments. Student's *t*-test, (*)= P< 0.05; (B) Level of Nrf2 in Panc-1 cells 48 h after treatment with P4/λ (P4= 0, 20, 40 and 80 nM, light 7.2 J/cm^2); (C) Levels of Nrf2 mRNA respect to HPRT and β2 microglobulin mRNA in untreated cells (NT) and in cells treated with 40 nM P4 and light 7.2 J/cm^2 (P4/λ); (D, E) Levels of ROS in Panc-1 (D) and T24 (E) cells untreated (NT) or treated with P4□λ (P4, 40 and 80 nM, light 7.2 J/cm^2) or 20 μM Lu or P4/λ/Lu (P4, 40 and 80 nM, 20 μM Lu, 7.2 J/cm^2). Analysis performed 24 h after treatment. Error bars (± SE) obtained from 3 experiments. One-way ANOVA test (*)= P< 0.05.

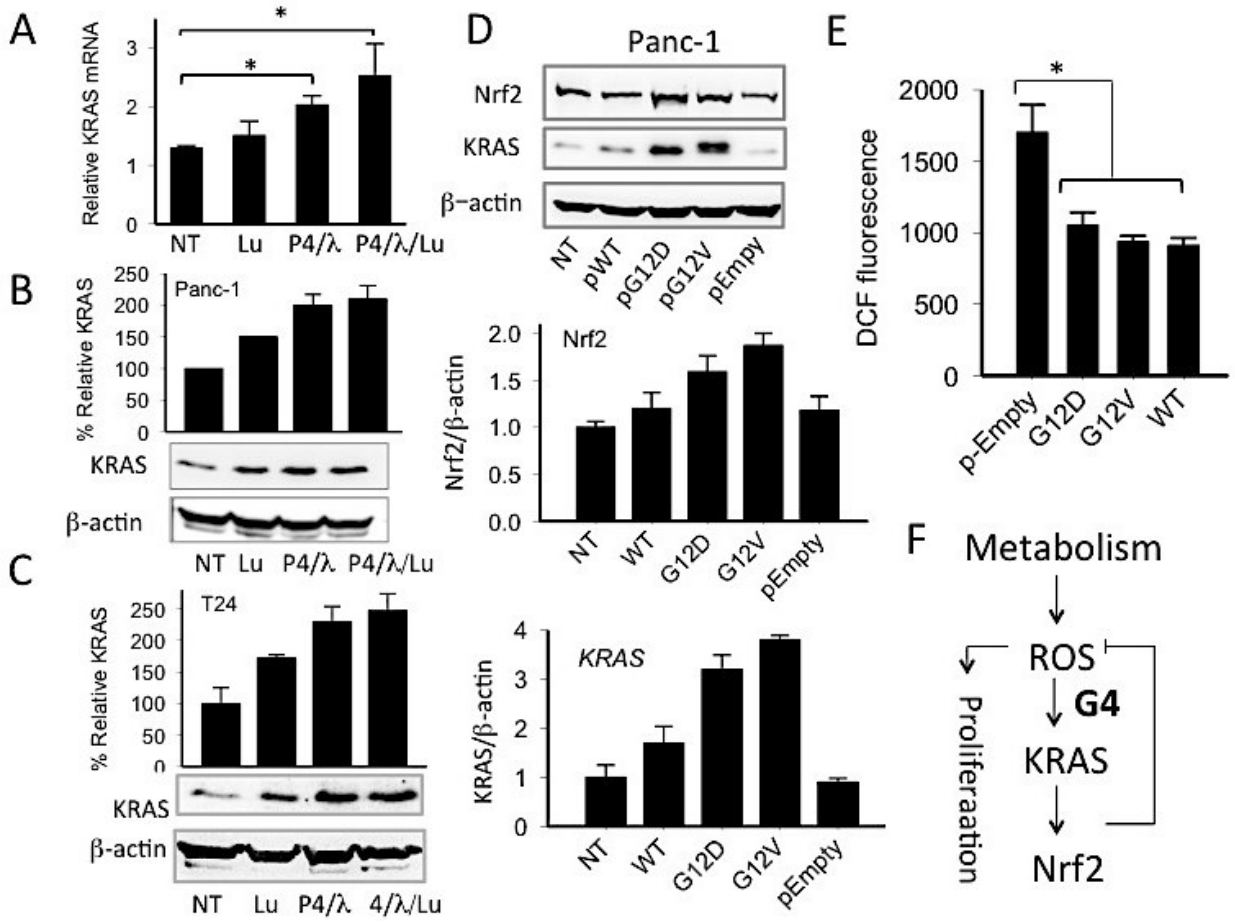

Figure 2. (A) Levels of *KRAS* mRNA in Panc-1 cells untreated (NT) or treated for 1 h with 20 μM Lu, P4/λ (40 nM P4, light 7.2 J/cm^2), P4/λ/Lu (40 nM P4, 20 μM Lu, light 7.2 J/cm^2). Student's *t*-test, (*)= P< 0.05, error bars (± SE) obtained from 3 experiments; (B and C) Western blots showing the level of KRAS in Panc1 (B) and T24 (C) cancer cells ~ 2 days after treatment. Error bars (± SE) obtained from 2 experiments, Student's *t*-test, (*)= P< 0.05; (D) Western blot showing the expression of *KRAS* in Panc-1 cells untreated (NT) or treated with vectors encoding WT, G12D, G12V KRAS protein and a control vector, pEmpty (a vector without *KRAS* coding sequence). The histograms show the relative levels of KRAS and Nrf2. Error bars (± SE) obtained from 2 experiments; (E) Fluorescence of 2',7'-dichlorofluorescein (DCF) in Panc-1 cells treated with pEmpty and vectors pG12D and pG12V encoding for KRAS protein. Student's *t*-test, (*)= P< 0.05, error bars (± SE) obtained from 3 experiments; (F) The ROS-KRAS-Nfr2 axis which regulates the ROS homeostasis in PDAC cells.

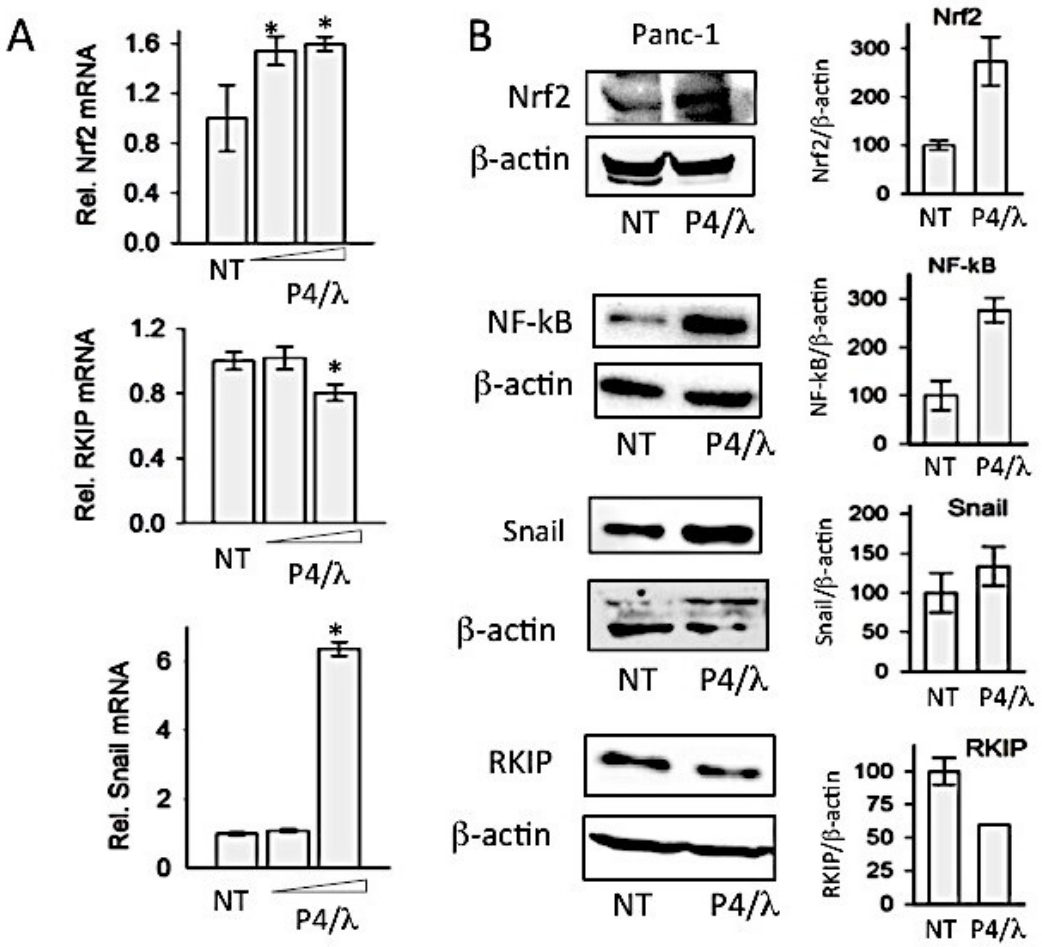

Figure 3. (A) Quantitative RT-PCR determination of Nrf2, Snail and RKIP mRNAs in Panc-1 cells treated for 8 h with P4/λ (40 and 120 nM P4, light 7.2 J/cm^2). Student's *t*-test, (*)= P< 0.05, error bars (± SE) obtained from 3 experiments; (B) Western blot determination of Nrf2, NF-kB, Snail, RKIP and β-actin in Panc-1 cells treated with P4/λ (80 nM P4, light 7.2 J/cm^2). Analysis was carried out 48 h after treatment. The histograms report the levels of proteins Nrf2, NF-kB, Snail and RKIP in untreated (NT) and P4/λ treated cells compared to β-actin. Errors have been estimated from two experiments.

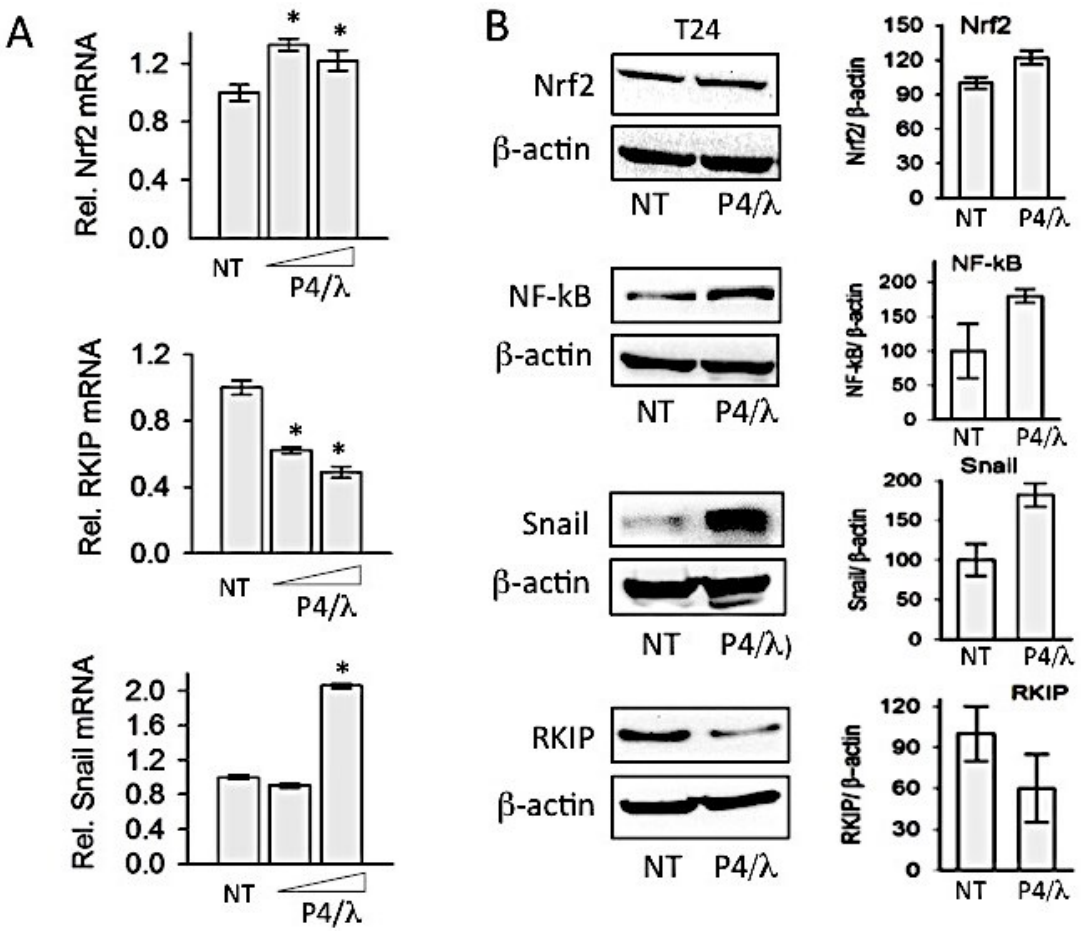

Figure 4. (A) Quantitative RT-PCR determination of Nrf2, Snail RKIP mRNAs in T24 bladder cancer cells treated for 8 h with PS/λ (40 and 120 nM P4, light 7.2 J/cm^2). Student's *t*-test, (*)= P< 0.05, error bars (± SE) obtained from 3 mRNA experiments; (B) Western blot determination of Nrf2, NF-kB, Snail, RKIP and β-actin in T24 cells treated with P4/λ (80 nM P4, light 7.2 J/cm^2).). Analysis was carried out 48 h after treatment; (C) Histograms reporting the levels of proteins Nrf2, NF-kB, Snail and RKIP in untreated (NT) and P4/λ treated cells compared to β-actin. Errors have been estimated from two experiments.

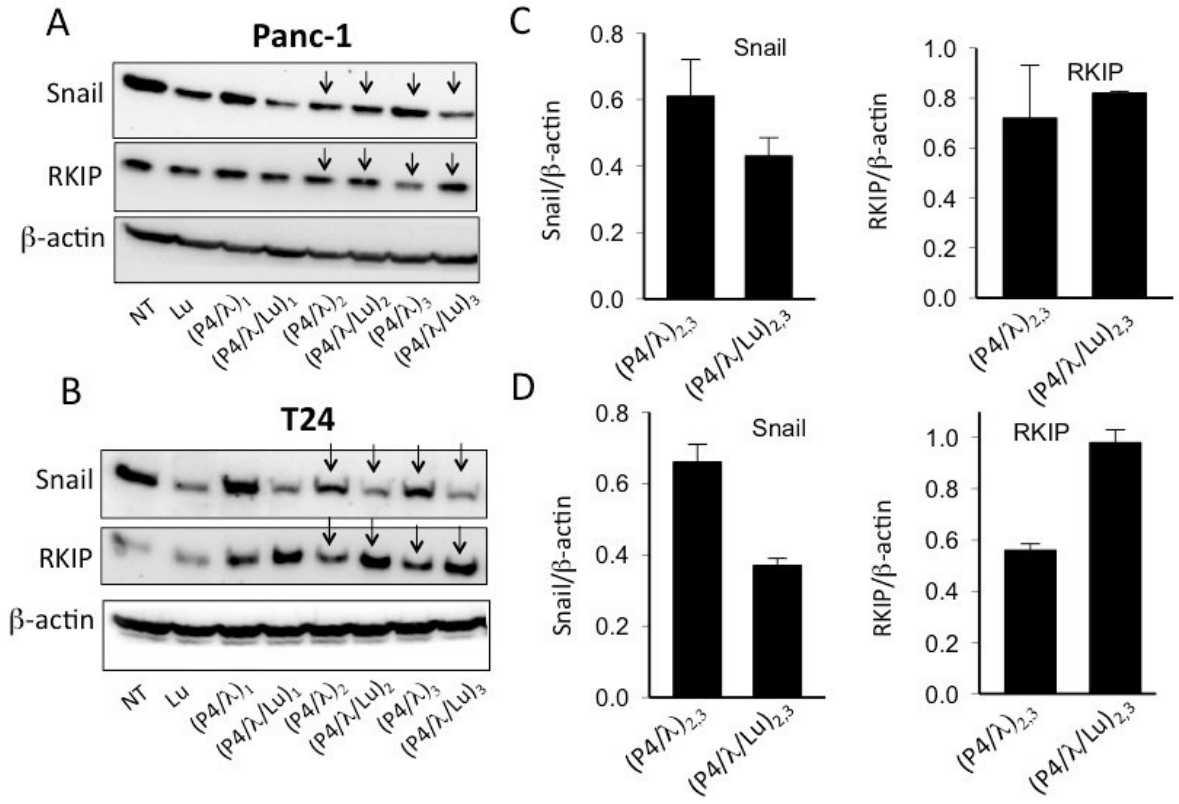

Figure 5. (A, B) Western blots showing the levels of Snail, RKIP and β-actin in Panc-1 (A) and T24 (B) cancer cells treated with three doses of P4/λ (20, 40 and 80 nM P4, light 7.2 J/cm^2) or P4/λ/Lu (20, 40 or 80 nM P4, light 7.2 J/cm^2, 20 μM Lu).). The analysis was carried out 48 h after days after treatment; (C, D) The histograms report the levels of RKIP and Snail compared to β-actin in cells treated P4/λ and P4/λ/Lu (80 nM P4, 20 μM Lu, light 7.2 J/cm^2).

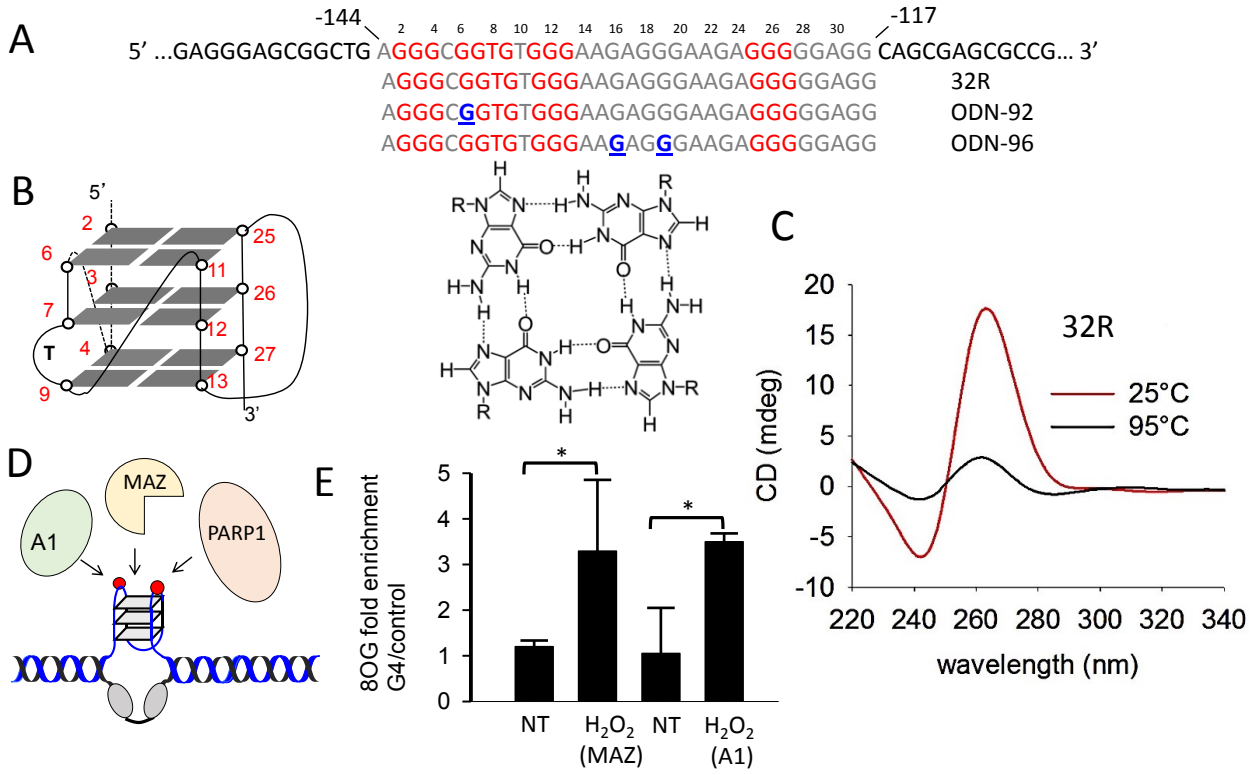

Figure 6. (A) Sequence of the *KRAS* G-rich motif located upstream of TSS, embedding the 32R sequence (signed with a solid line), forming a G4 with the G-runs shown in red. The sequences of oligonucleotides 32R, ODN-92 and ODN-96 with 8OG modifications (indicated with underlined G in blue) are shown; (B) Structure of KRAS G4 characterized by two 1-nt and one 11-nt loops and a T-bulge in one strand (Suppl. Inf. S5); (C) CD spectra for 32R in 50 mM cacodylate pH 7.4, 100 mM KCl at 25 and 95 °C; (D) ChIP and EMSA experiments showed that hnRNP A1 (abbreviated A1), MAZ and PARP-1 are recruited to the G4 motif; (E) Double chromatin immunoprecipitation (ChIP-reChIP) and qPCR showing that MAZ and hnRNPA1 co-localize on the G4 region harbouring 8OG. Student's *t*-test, (*)= P< 0.05, error bars (± SE) obtained from one experiment in triplicate.

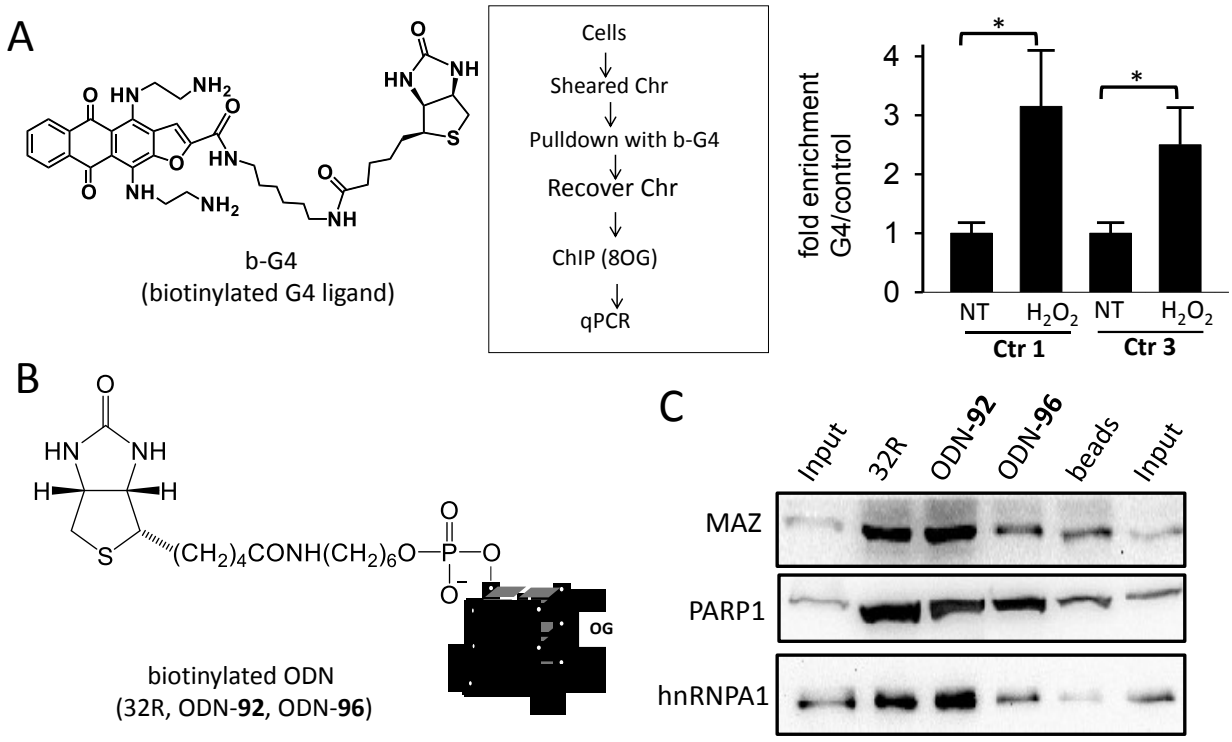

Figure 7. (A) Pull-down chromatin with a G4-ligand and immunoprecipitation with 8OG Ab show that 8OG and G4 DNA co-localize on the G4 region located in the KRAS promoter. Student's *t*-test, (*)= P< 0.05, error bars (± SE) obtained from one experiment in triplicate; (B) Pulldown/Western blot assay carried out with a Panc-1 extract and 32R conjugated to biotin. Sequence 32R was also designed with one (ODN-**92**) or two (ODN-**96**) 8OGs. The pulldown proteins were analysed by Western blot with specific Ab for MAZ, hnRNP A1 and PARP1. G4 32R and the oxidized analogues form a multiprotein complex with the transcription factors;

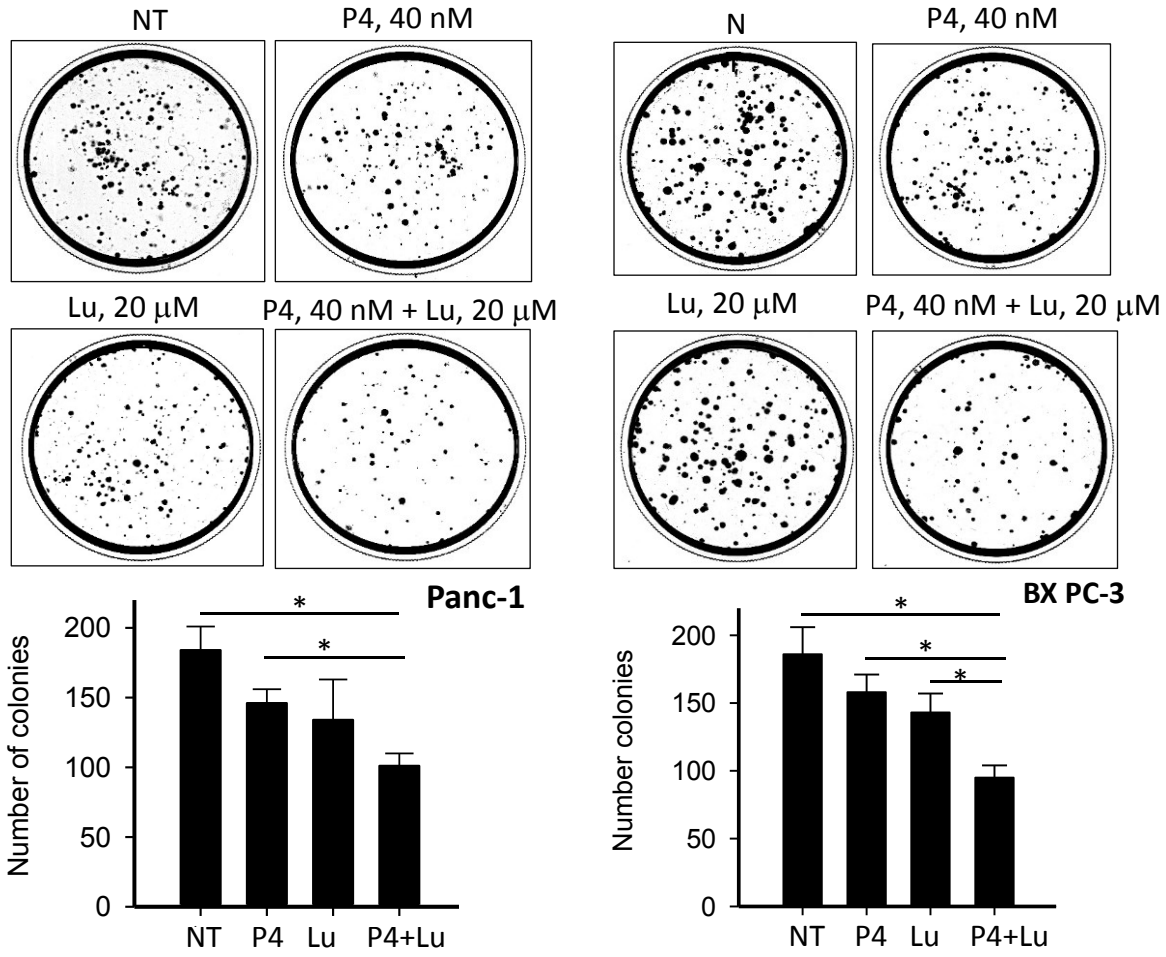

Figure 8. Clonogenic assays. (A) Pancreatic Panc-1 and BXPC3 cancer cells were treated with P4/λ (40 nM P4, light 7.2 J/cm^2), luteolin (20 μM) and P4/λ/Lu (40 nM P4, light 7.2 J/cm^2, 20 μM Lu). The histogram shows the % colonies in untreated and treated cells. Error bars have been obtained from three independent experiments. A Student's *t*-test was performed, (*)= $P < 0.05$.

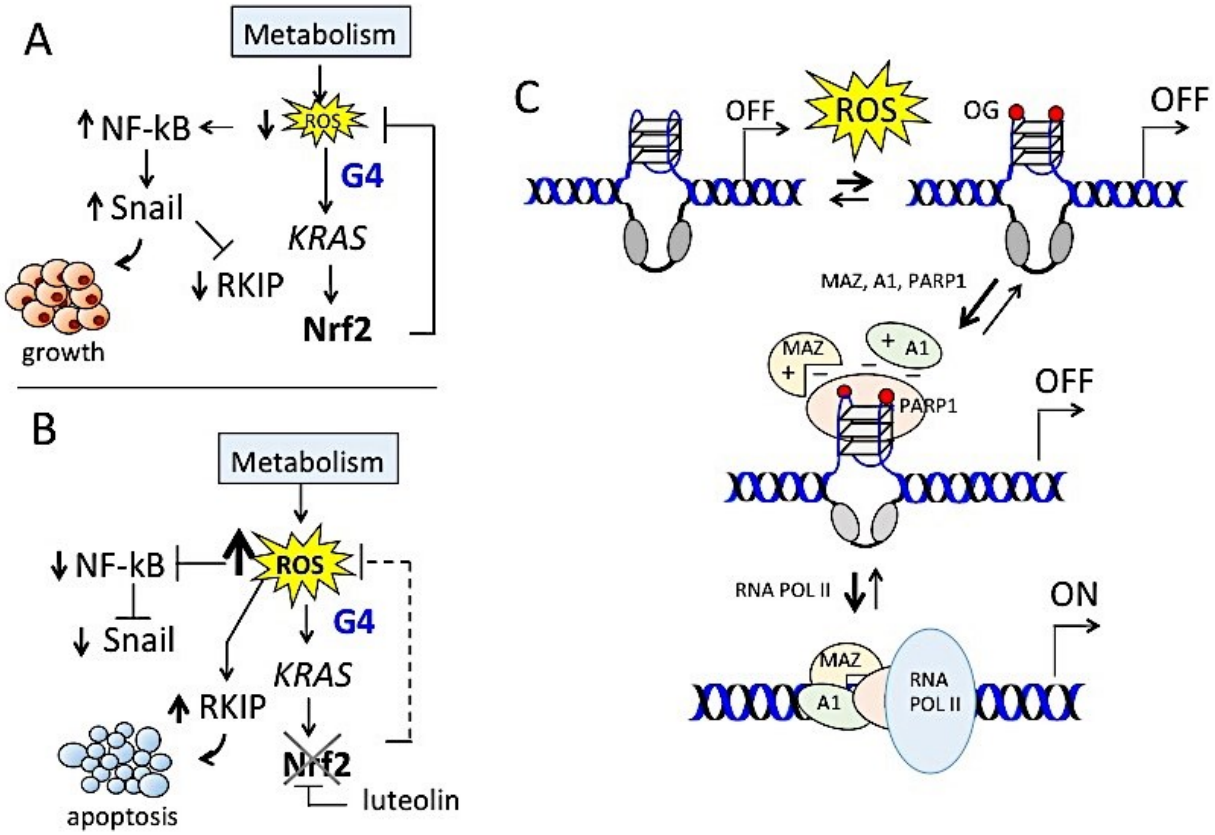

Figure 9. (A and B) The ROS-KRAS-Nrf2 axis and its intersection with NFkB-Snail-RKIP. When Nrf2 is upregulated by *KRAS*, the ROS level is low and NF-kB and Snail are upregulated while RKIP is downregulated. This expression profile favour cell growth. In contrast, when Nrf2 is inhibited by luteolin, the ROS level is increased. This results in downregulation of NF-kB and Snail and upregulation of RKIP. This expression profile favours apoptosis; (C) Proposed mechanism for *KRAS* transcription activation by ROS. The promoter G-rich G4 motif undergoes oxidation and folding. Oxidized G4 favours the recruitment of TFs (PARP1, hnRNP A1 and MAZ). PARP1 binds to G4 with a high affinity and becomes anionic through auto poly(ADP-ribosyl)ation. Anionic PARP1 stimulates the recruitment of cationic MAZ and hnRNPA1, TFs essential for transcription.

Supplementary Information

The ROS-*KRAS*-Nrf2 axis in the control of the redox homeostasis and the intersection with survival-apoptosis pathways

Annalisa Ferino, Giorgio Cinque, Valentina Rapozzi and Luigi E. Xodo*

Department of Medicine, Laboratory of Biochemistry, University of Udine, P.le Kolbe 4, 33100 Udine, Italy

Suppl. Inf. S1: In aerobic organisms, ROS – including anion superoxide (O_2^-), hydrogen peroxide (H_2O_2) and hydroxyl radical (·OH) – are continuously produced by metabolic reactions. The main sources of ROS are: (i) mitochondria, through electron leakage from the ubiquinone/ubiquinol shuttle; (ii) peroxisomes, during β-oxidation of long-chain fatty acids; (iii) cytochrome P-450 enzymes; (iv) nicotinamide adenine dinucleotide phosphate (NADPH) oxidises of the NOX family.

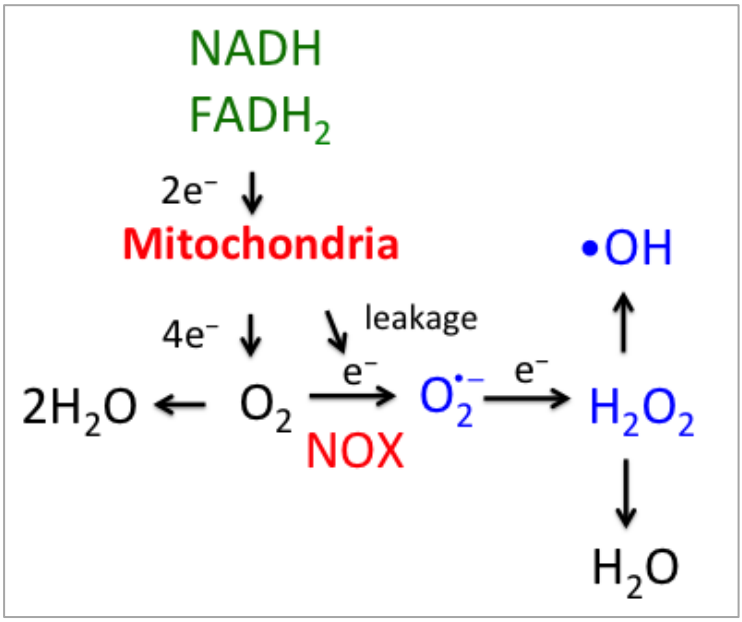

Suppl. Inf. S2: Due to its low redox potential, guanine is prone to oxidation to 7,8-dihydro-8-oxoguanine (8OG). The presence of 8OG in the G4 motif and in control G-rich sequences Ctr-1 and Ctr-2, unable to form a G-quadruplex, was analysed by ChiP assays with an antibody specific for 8OG.

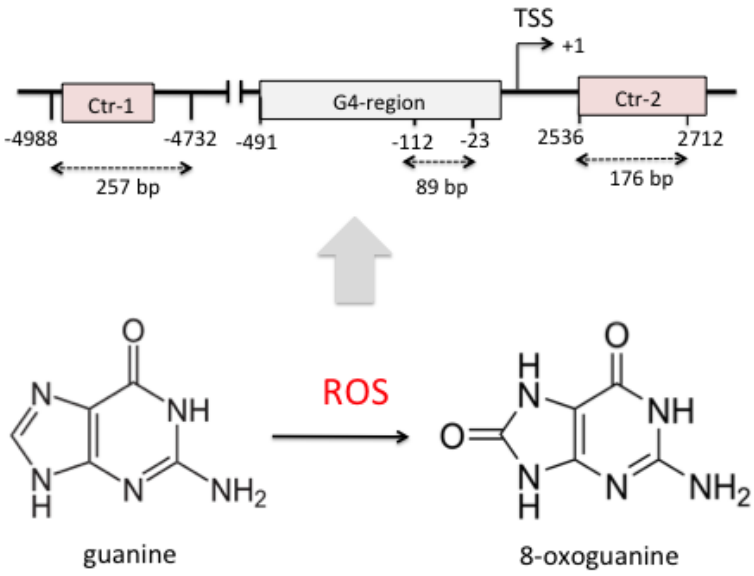

Suppl. Inf. S3: Western blot showing the basal level of KRAS protein in cancer (pancreatic Panc-1, MIA PaCa-2, BSPC-3; bladder T24) cells and in non-cancer 293 cells.

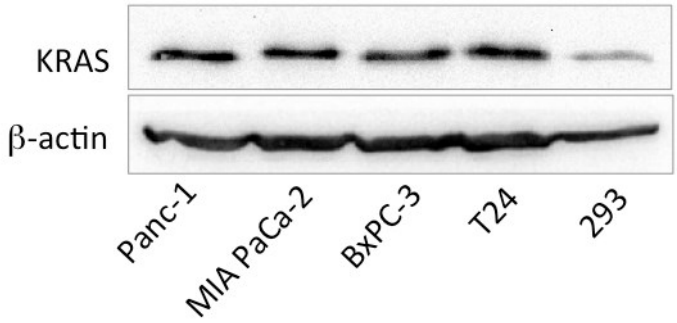

Suppl. Inf. S4: Luteolin is a tetrahydroxyflavone that reduces Nrf2 expression. When Panc-1 cells are treated with luteolin, the expression of Nrf2 is significantly reduced, as shows by the western blot reported below. In this experiment the cells were treated with 20 μM luteolin (lane 2) and Nrf2 is significantly reduced. Luteolin downregulates Nrf2 also when it is stimulated by a P4/λ treatment that pro
duces ROS: lane 3, 20 nM P4 and light (8 J/cm^2); lane 4, 20 nM P4, light 8 J/cm^2, 20 μM luteolin; lane 5, 40 nM P4 and light 8 J/cm^2; lane 6, 40 nM P4, light 8 J/cm2, 20 μM luteolin.

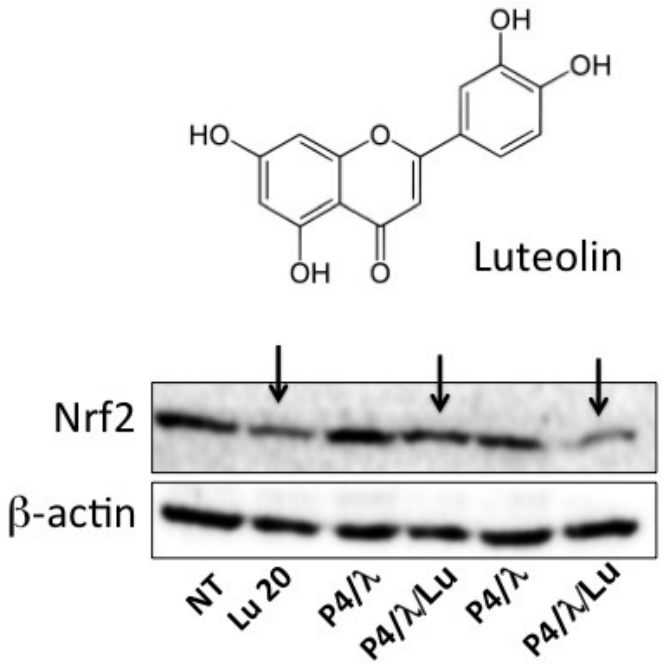

Suppl. Inf. S5: The G4 structure formed by 32R. DMS footprinting and CD support a G-quadruplex with a parallel topology and a strand containing a T-bulge. Typical melting curves of 32R in 50 mM cacodylate pH 7.4 and 100 mM KCl. The heating and cooling curves show that the melting and annealing are reversible, with T_M is 61.6 °C.

32R 5'-AGGGCGGTGTGGGAAGAGGGAAGAGGGGGAGG

2 4 6 8 10 12 14 16 18 20 22 24 26 28 30 32

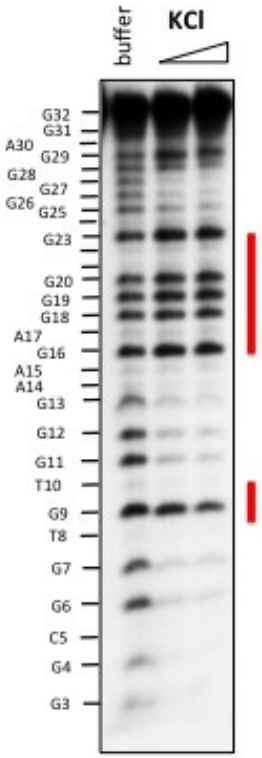

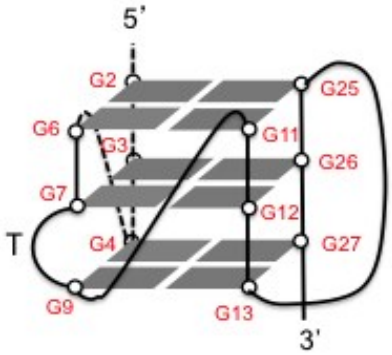

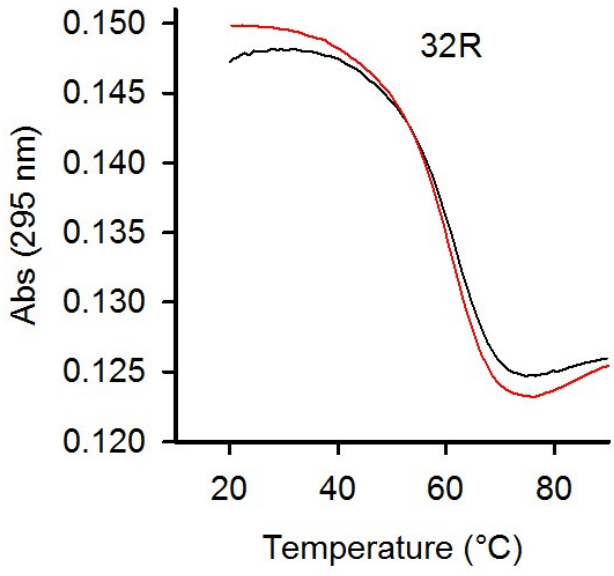

Suppl. Inf. S6. ChiP-reChIP is a strategy useful to determine *in vivo* the co-localization of proteins in a chromatinized DNA fragment on the basis of two independent immunoprecipitations with specific antibodies. In our experiment we first obtained the chromatin from Panc-1 cells treated with hydrogen peroxide. Then the chromatin was fragmented into pieces of about 300 bp by sonication. The sonicated chromatin was immunoprecipitated with an antibody specific for MAZ or hnRNPA1. The precipitated chromatinized DNA was recovered and used for a second immunoprecipitation with an antibody specific for 8-oxoG. After the second ChIP, the DNA was recovered and analysed by qPCR, in order to see if an enhanced level of 8-oxoG was present in the G4 motif region compared to control region. The ChIP-reChIP showed that MAZ and hnRNP A1 are localized in the same chromatin fragment harbouring a higher level of 8-oxoG compared to control region. A scheme of the experiment is shown below.

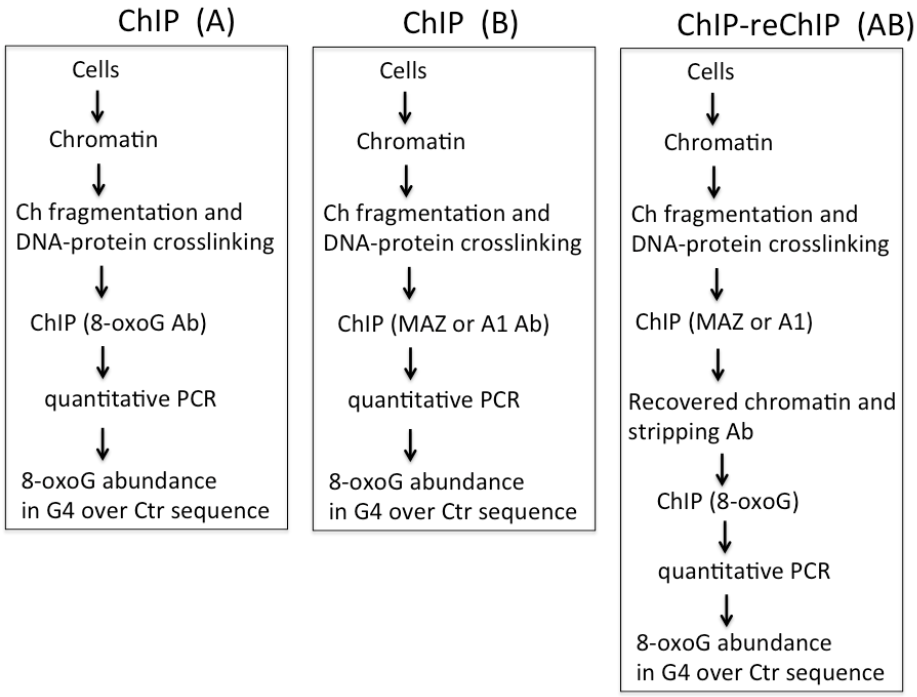

Suppl. Inf. S7. To demonstrate that there is co-localization between 8OG and the G4 structure we carried out a pull-down/ChIP experiment.

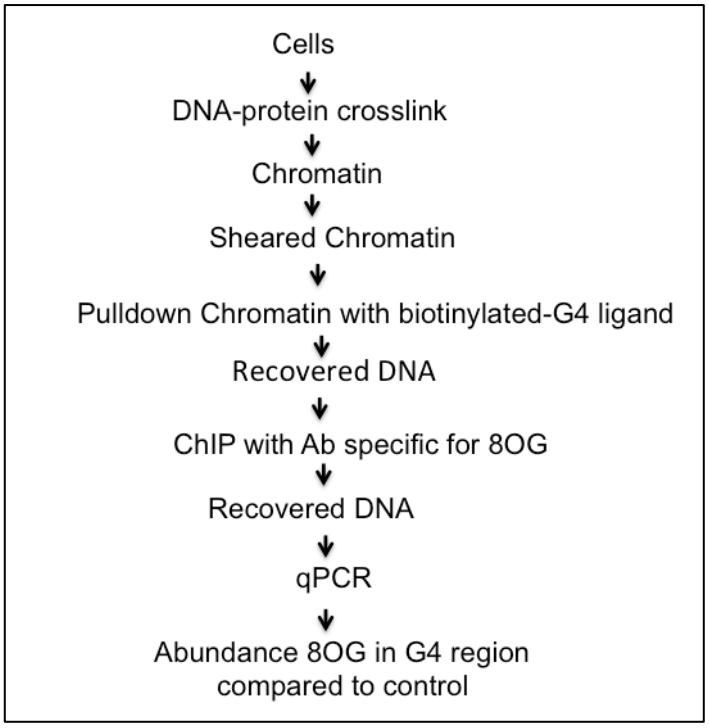

(A) Pull-Down Panc-1 chromatin with biotin-streptavidin technology. Panc-1 cells (8 x 10^5) were seeded in a 6-well plate and after 24 h some wells treated with 1mM H_2O_2 for 30 min in serum-free DMEM. The chromatin was collect by using the ChIP-IT® Express Shearing Kit (Active Motif, USA), following the manufacturer instructions.
Then 20 □g of chromatin were incubated for 6 h at 4 °C with 0.8 □M biotinylated ligand (anthrafuranedione **2a**, J Med Chem 2017, 60, 9448-61) in water. A total of 40□□g of Streptavidin MagneSphere Paramagnetic Particles (Promega, Italy), previously washed in 50 mM Tris-HCl, pH 7.4, 50 mM KCl and incubated with Salmon Sperm DNA in a thermomixer for 30 min at 25 °C and 600 rpm, was added and let to incubate for 30 min at 25 °C. The beads were captured with a magnet and the DNA was eluted by an incubation for 30 min at 25 °C with 0,8 M NaCl.

Chromatin Immunoprecipitation (ChIP)

The concentration of DNA eluted from the Pull-down assay was determined on a NanoDrop2000 Spectrophotometer (Thermo Scientific, USA) and 1 □g was treated overnight at 4 °C with 1 □g of antibody specific for 8-oxoG (Bioss Antibodies, USA). In addition to the antibody the mixtures were added with Protein G Magnetic Beads, ChIP Buffer-1 and PIC, as indicated in the Active Motif Kit protocol. After incubation, the mixtures were span and the chromatin bound to the antibody collected with a magnetic bar. The collected beads were washed once with ChIP Buffer-1 and twice with ChIP Buffer-2. The beads were then re-suspended in Elution Buffer AM2 and let to incubate on shaking for 15 min at room temperature. The Reverse Crosslinking Buffer was added to the mixture and the supernatant with the chromatin was collected. The DNA fragments were amplified by qPCR.

In *J Med Chem 2017, 60, 9448-61*, we have demonstrated that the biotinylated G4 ligand **2a** efficiently pulls down a G4 DNA in a streptavidin-biotin assay.

Suppl. Inf.S8

CD spectra at 20 and 90 °C of 32R and oxidized analogues ODN-92 and ODN-96 in 50 mM Tris-HCl, pH 7.4, 100 mM KCl. Melting curves of 32R, ODN-**92** and ODN-**96** in 50 mM cacodylate pH 7.4, 100 mM KCl.

When 8OG is located in the major 11-nt loop, the topology of the G-quadruplex does not change, neither the T_M (see 32R and ODN-96). In contrast, when 8OG is in a G-run, the topology of the G4 changes, as well as the T_M which decreases from 61.6 to 50.7 °C.

5'-AGGGCGGTGTGGGAAGAGGGAAGAGGGGGAGG 32R
5'-AGGGCGGTGTGGGAAGAGGGAAGAGGGGGAGG ODN-**92**
5'-AGGGCGGTGTGGGAAGAGGGAAGAGGGGGAGG ODN-**96**

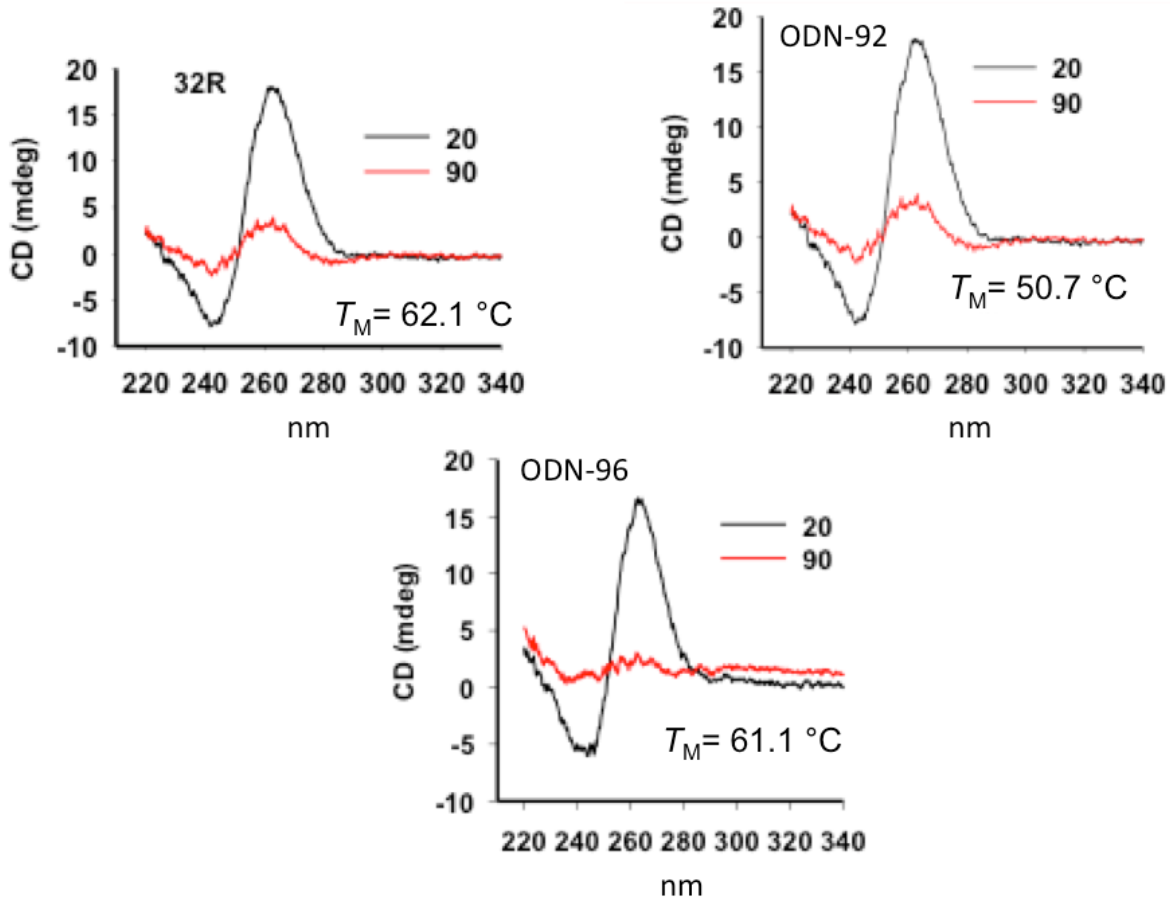

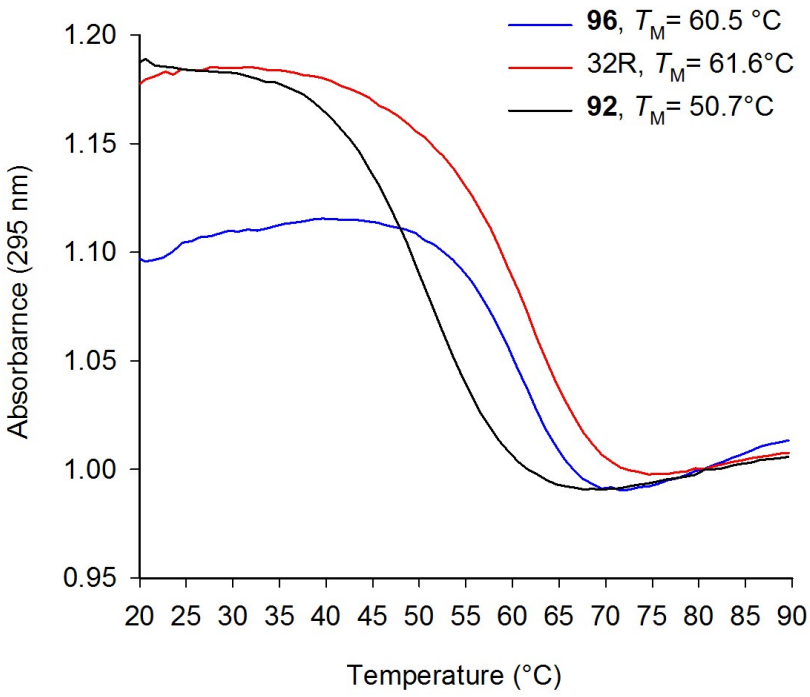
96, T_M= 60.5 °C
32R, T_M= 61.6°C
92, T_M= 50.7°C
Absorbarnce (295 nm)
1.20
1.15
1.10
1.05
1.00
0.95
20 25 30 35 40 45 50 55 60 65 70 75 80 85 90
Temperature (°C)

Section 3

MicroRNA therapeutics: design of single-stranded miR-216b mimics to target KRAS in pancreatic cancer cells

A. Ferino, G. Miglietta, R. Picco, S. Vogel, J. Wengel, L.E. Xodo

RNA Biology (2018)

RNA BIOLOGY
https://doi.org/10.1080/15476286.2018.1526536

RESEARCH PAPER

OPEN ACCESS Check for updates

MicroRNA therapeutics: design of single-stranded miR-216b mimics to target *KRAS* in pancreatic cancer cells

Annalisa Ferino [a&], Giulia Miglietta [a&$], Raffaella Picco [a], Stefan Vogel [b], Jesper Wengel [b], and Luigi E. Xodo [a]

[a]Department of Medicine, Laboratory of Biochemistry, University of Udine, Italy; [b]Nucleic Acids Centre, University of Southern Denmark, Odense, Denmark

ABSTRACT

Datasets reporting microRNA expression profiles in normal and cancer cells show that miR-216b is aberrantly downregulated in pancreatic ductal adenocarcinoma (PDAC). We found that *KRAS*, whose mutant G12D allele drives the pathogenesis of PDAC, is a target of miR-216b. To suppress oncogenic *KRAS* in PDAC cells, we designed single-stranded (ss) miR-216b mimics with unlocked nucleic acid (UNA) modifications to enhance their nuclease resistance. We prepared variants of ss-miR-216b mimics with and without a 5′ phosphate group. Both variants strongly suppressed oncogenic *KRAS* in PDAC cells and inhibited colony formation in pancreatic cancer cells. We observed that the designed ss-miR-216b mimics engaged AGO2 to promote the silencing of *KRAS*. We also tested a new delivery strategy based on the use of palmityl-oleyl-phosphatidylcholine (POPC) liposomes functionalized with ss-miR- 216b conjugated with two palmityl chains and a lipid-modified cell penetrating peptide (TAT). These versatile nanoparticles suppressed oncogenic *KRAS* in PDAC cells.

Received 16 May 2018
Revised 21 August 2018
Accepted 11 September 2018

KEYWORDS
KRAS; PDAC cells; miR-216b; AGO2; POPC liposome

Introduction

Pancreatic ductal adenocarcinoma (PDAC) is one of the major causes of death in western countries [1,2]. As current treatments are not effective, there is an urgent need to develop new therapies [3]. The main genetic lesion present in > 90% of PDAC patients is a mutation in the *KRAS* proto-oncogene, mainly in exon 1 at codon 12, G12D (Gly→Asp) or G12C (Gly→Cys) [4]. It has been demonstrated that mutant *KRAS* is the major driver of PDAC and that the expression of $KRAS^{G12D}$ in transgenic mice pancreas causes intraepithelial neoplastic lesions progressing into full malignancy [4–6]. The expression of $KRAS^{G12D}$ is necessary for tumour maintenance and its extinction leads to a rapid tumor regression [6]. Recent work has demonstrated that pancreatic cancer cells are 'addicted' to mutant *KRAS*, as this oncogene reprograms the metabolism of tumor cells, in particular the glucose and glutamine pathways, in order to fuel a higher proliferation rate [7,8].

It is known that several properties of cancer cells, including proliferation, migration, invasion and gene expression, are regulated by small noncoding microRNAs [9–14]. These molecules are synthesized as long RNA strands folding into hairpin-loop structures processed by Drosha and Dicer into mature duplexes ranging from 17 to 26 nt in length [9–14]. The guide strand of the mature RNA duplexes forms a complex with argonaute proteins that bind to a 3'-untraslated region (3'-UTR) mRNA target. This mediates two modes of gene silencing: translation repression and/or RNA decay [12–15]. Synthetic double-stranded (ds) miRNAs have given encouraging results as antigene molecules [16] and recent studies have demonstrated that single-stranded (ss) RNAs, mimicking the guide strand of miRNAs, can also mediate an Ago-dependent inhibition of the target gene [17–21]. These findings provided new perspectives on the use of synthetic miRNAs as therapeutic agents.

In an attempt to inhibit *KRAS* in pancreatic cancer cells, we started from the observation that certain small noncoding RNAs are aberrantly expressed in cancer tissues [22]. In cancer, miRNAs inhibiting the expression of tumor suppressor genes are often upregulated, and this favors the development of the tumor. Instead, miRNAs behaving as tumor suppressors are downregulated and inhibit cancer growth [22–27]. Two miRNA-based therapeutic approaches have been developed: miRNA antagonists and miRNA mimics. MiRNA antagonists are single-stranded oligonucleotides that bind to oncogenic miRNAs and ablate their function. MiRNA mimics instead are used to restore a miRNA that is downregulated in the tumor, normally behaving as a tumor suppressor (replacement strategy) [23].

In our study we focused on a miRNA aberrantly downregulated in PDAC, miR-216b, in order to design therapeutic agents suppressing *KRAS* in these tumor cells [28]. We designed single-stranded (ss) miR-216b mimics with unlocked nucleic-acid modifications, with or without a 5' phosphate,

CONTACT LuigiE. Xodo luigi.xodo@uniud.it Department of Medicine, Laboratory of Biochemistry, University of Udine, Italy
[&]AF and GM have equally contributed to this work
[$]LEX dedicates this paper to the memory of Susanna Cogoi, a wonderful colleague with whom he collaborated for two decades
Supplemental data for this article can be accessed here.

and found that they strongly suppress oncogenic *KRAS* in PDAC cells. We also tested the activity of miR-216b conjugated to two palmityl chains and fixed on the surface of palmityl-oleyl-phosphatidylcholine (POPC) liposomes, functionalized with the trans-activator of transcription of the human immune-deficiency virus (TAT) cell penetrating peptide [29–32]. The results of our study may have relevance in cancer therapy, for designing single-stranded UNA-modified miRNA mimics against therapeutically important genes.

Results and discussion

We consulted miRNA expression profiles relative to PDAC and adjacent non-tumor tissues, deposited in the Array Express Archive of Functional Genomics. The three datasets analyzed, whose accession number are E-MTAB-753, GSE43796 and GSE41372 [28], showed that several miRNAs are differently expressed when the tumor PDAC tissue was compared with adjacent non-tumor tissue. Among the abnormally downregulated miRNAs, miR-216b showed an expression fold change of 27.95 (GSE43796) (Figure 1). Similar data were observed with E-MTAB-753 and GSE41372 (Fig. S1). In keeping with these data, Liu et al [33] have recently reported that the level of miR-216b in PDAC cells (Panc-1, BxPC3 and SW 1990) is 3- to 4-fold lower than in non-cancer cells. The targets of miR-216b in PDAC cells include TPT1, a gene encoding for the translationally-controlled tumor protein [34], and ROCK1, the ρ-associated coiled-coil containing protein kinase 1 [33]. In addition, miR-216b targets the *KRAS* oncogene in nasopharyngeal tumor cells [35]. MiR-216b plays a critical role in PDAC, as in a transgenic mouse model this miRNA is downregulated in all steps of tumorigenesis, suggesting that it behaves as a tumor suppressor [36]. Considering that PDAC cells are addicted to *KRAS*, we asked if *KRAS* is a target of miR-216b even in this lethal cancer and if miR-216b mimics, properly modified, may be a valuable therapeutic tool to suppress mutant *KRAS* in PDAC cells.

Design of single-stranded miRNA mimics specific for oncogenic KRAS

Synthetic miRNA mimics are normally double-stranded RNA molecules imitating mature microRNA duplexes [16]. Synthetic double-stranded miRNA mimics are incorporated into the miRNA-induced silencing complex (miRISC) that directs miRNA to its mRNA target in a sequence-specific manner for translation inhibition or mRNA degradation. Interestingly, previous studies have showed that both double- and ss-siRNAs act through the RNAi pathway and silence gene expression [20,21]. This led to the hypothesis that ss-miRNAs might also suppress gene expression. Indeed, ss-miRNAs are loaded into miRISC and inhibit gene expression [18]. Against this background, we designed synthetic ss-miRNA mimics to attempt *KRAS* suppression in pancreatic cancer cells. One might wonder why to use ss-miRNAs, considering that ds-miRNAs are potent tools for gene silencing. Two reasons have been put forward [18]: (i) ds-miRNAs, being more complex molecules than ss-miRNAs, are expected to be transported into the cells less efficiently than the single-stranded analogues [37]; (ii) ds-miRNAs are composed of the guide and passenger strands, and the latter may be a source of undesired off-target effects [38]. Figure 2(a) shows the primary sequence of the designed miR-216b mimics and their target in the 3'-UTR of *KRAS* mRNA. At the 5'-end the miR-216b sequence, UCUCUAAA-5', is perfectly complementary to mRNA and represents the 'seed region'. Some complementarity with the target is also present at the 3'-end of miR-216b, where 5'-UAAAC is base-paired with mRNA. This should improve the interactions between miRNA and the target gene [39,40]. To increase their nuclease stability, we designed miR-216b mimics with one or two unlocked nucleic acid (UNA) modifications [41,42]. The key feature of UNA is the loss of C2'-C3' bond of the ribose, a modification that increases the flexibility of the RNA strand [43] (Figure 2(b)). A single UNA modification in the middle of a RNA/RNA duplex can lower the T_m by 5–10 °C, but when the UNA modification is placed near the duplex end, it causes a rather modest drop in T_m of 1–3 °C [43,44].

We designed two UNA-modified miR-216b mimics: compound U1 with one modified adenine (uA) at the 3'-end; compound U2 with two uAs, at the 3'-end and in the middle of the oligoribonucleotide, but outside the seed sequence (Figure 2(a)). The uA at the 3'-end is also located in a portion of miR-216b that does not pair with the mRNA target. Therefore, these modifications should not affect the hybridization of the UNA-modified mimics to the RNA target. Previous studies have reported that: (i) ss-miRNAs with 2'-methyl, 2'-fluoro, 2'-O-methoxyethyl and with a phosphorothioate backbone are fairly active [17,45]; (ii) the binding of Argonaute 2 (AGO2) to modified siRNAs (including UNA-modified siRNAs) is not affected by chemical modifications [18,21]. Another important element in designing synthetic ss-miRNAs is the presence of a phosphate at the 5'-end. Lima et al. found that a 5' phosphate is a critical determinant for ss-siRNAs [17,18,21]. Yet, ss-siRNAs function through the RNAi pathway and require protein AGO2 [21]. Recently, Chorn et al. have compared the activity of ss-2'F-miRNAs against ss-2'OH-miRNAs [17]. They observed that the former had a higher capacity to suppress CD164 in HCT-116 cells than the latter. Moreover, with both types of miRNA the phosphorylation at the 5' end was irrelevant. In contrast, when the ss-miRNAs contained both 2'-F and 2'-OH riboses, the 5' phosphorylated analogues showed higher activity [17]. This suggests that the 5' phosphorylation has a complex effect on miRNA activity. We thus designed UNA-modified ss-miRNAs with and without a 5' phosphate group (Figure 2(a)). To investigate the gain in stability obtained with the UNA insertions, we treated the wild-type and UNA-modified miRNA mimics with cellular nucleases from a total Panc-1 extract. Figure 3(a) shows the integrity of the designed ss-miRNA mimics with a 5' phosphate after incubation with a total Panc-1 extract for 1, 2 and 4 h, at 37°C. After 4 h, only ~ 10% of miR-216b-P was still intact. This percentage increased to ~ 20 and ~ 65%, respectively, when one or two UNA modifications were introduced in the oligonucleotide. Figure 3(b) shows that the non-phosphorylated analogues are slightly more resistant: after 4 h,

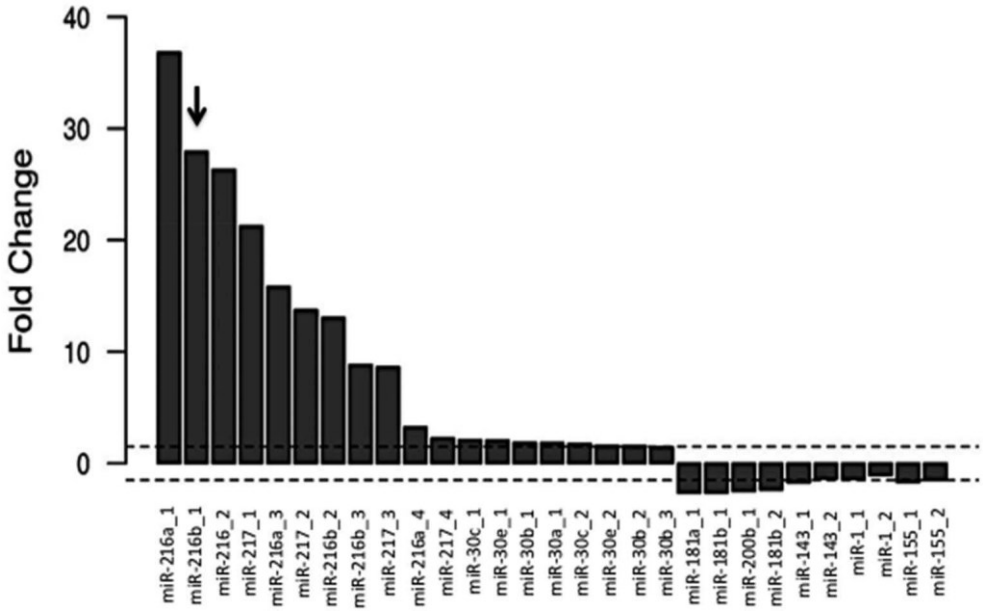

Figure 1. Fold change [FC = $\log_2(F_{non\text{-}tumour}/F_{tumour})$] of miRNAs in normal tissue over cancer PDAC tissue. Data have been obtained from GSE43796.

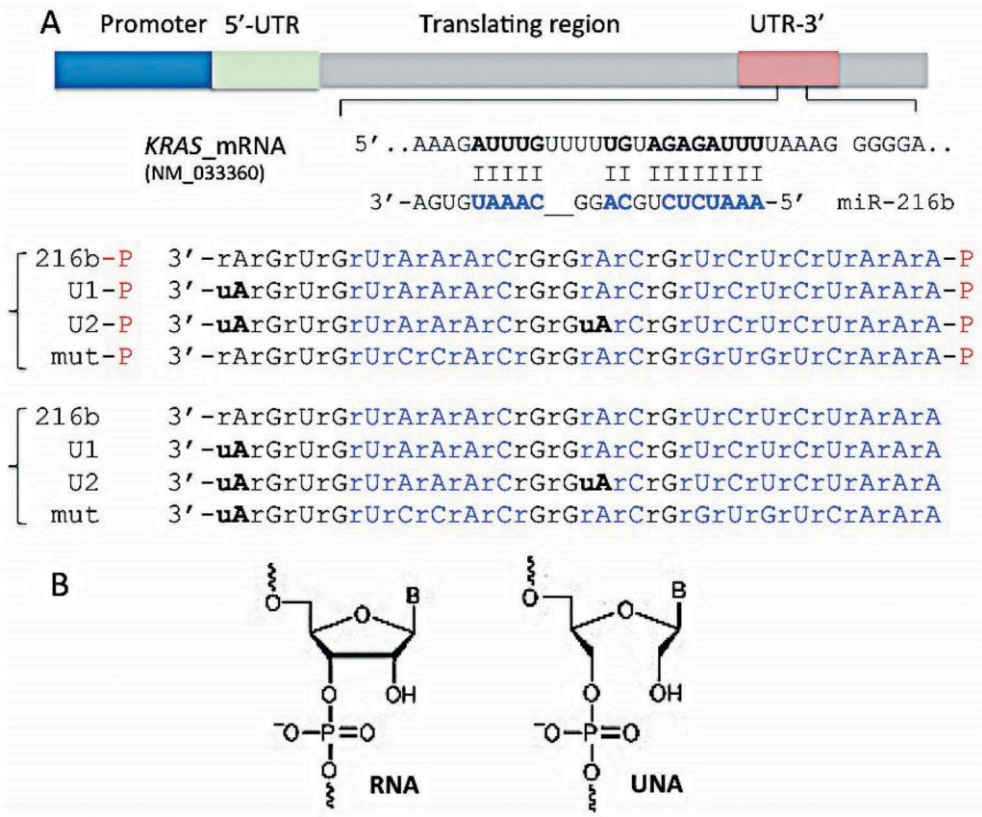

Figure 2. (a) Sequence of the *KRAS* 3′-UTR recognized by miR-216b. We designed single-stranded UNA-modified miR-216b mimics with and without a 5′ phosphate: wild-type miR-216b and miR-216b-P; miR-216b with one UNA (U1 and U1-P) or two UNAs (U2 and U2-P). Mutated miRNAs with and without a 5′ phosphate (mut-P, mut) were used as a control (Supplementary S3); (b) The structures of RNA and UNA, lacking the covalent bond between C2′ and C3′ of the ribose, are shown.

~ 27% of miR-216b was intact, while the percentage of undigested U1 and U2 was ~ 30 and ~ 80%, respectively. This proves that UNA insertions at the 3' end and in the middle of the sequence boost the resistance of the designed mimics to PDAC cellular nucleases.

Anti KRAS activity of UNA-modified miR-216b mimics in PDAC cells

To suppress oncogenic *KRAS* in Panc-1 cells we employed a replacement strategy. A previous study reported that miR-

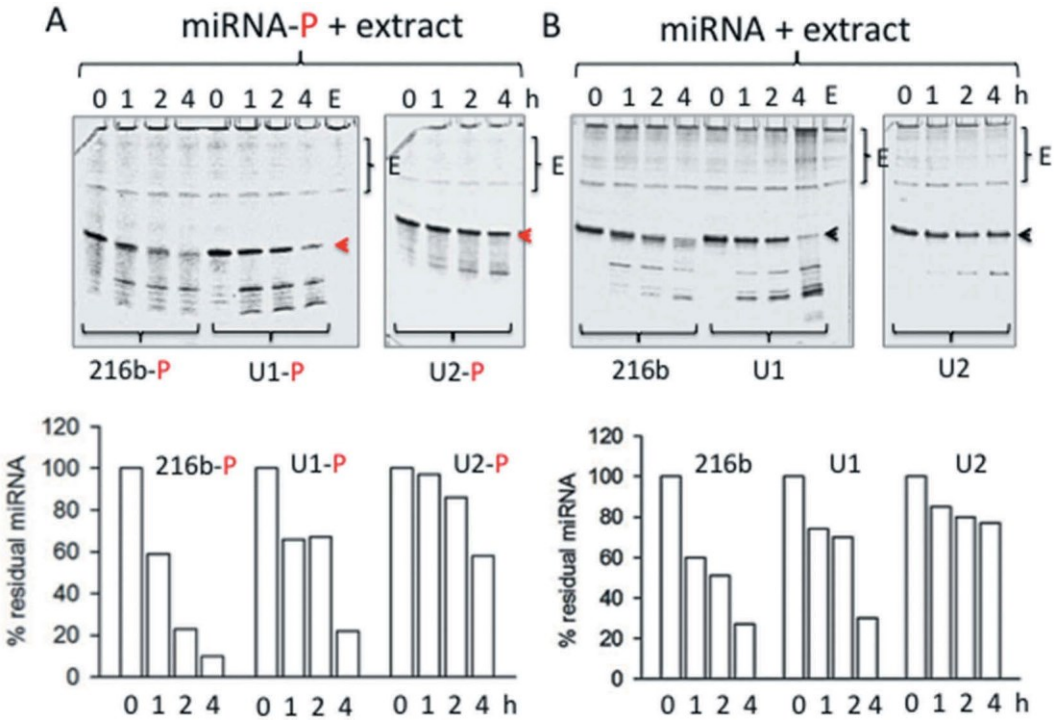

Figure 3. Denaturing (7 M urea) polyacrylamide gel showing the integrity of wild-type and UNA-modified mimics with (a) and without (b) a 5′ phosphate, after incubation for 1, 2 and 4 h with 2 µg Panc-1 cellular extract (E) at 37 °C. The mobility of E is shown in each panel. The arrow shows the undegraded miRNA. The % of undegraded miRNA at the various times is shown in the histograms.

216b down-regulates *KRAS* in nasopharyngeal cancer cells [35]. Although miR-216b is aberrantly downregulated in PDAC, its therapeutic potential in pancreatic cancer cells has not yet been investigated. Our first step was to demonstrate that miR-216b is indeed *KRAS*-specific in PDAC. To this end, we hybridized wild-type and UNA-modified miR-216b mimics to their complementary sequence and obtained 22-mer ds-mimics with or without UNA insertions and 5' phosphate in the guide strand (ds-216b, ds-U1, ds-U2 and ds-U2-P) (Figure 4). We also obtained a mutated ds-UNA-modified miRNA that was used as a control. Panc-1 cells were transfected two times with the duplexes and after an incubation of 48 h, a Western blot was performed to measure the level of KRAS protein (Figure 4). Duplexes ds-U1 and ds-U2 dramatically reduced the level of KRAS protein to ~ 10% of the control (ds-mut). Instead, duplex wild-type (ds-216b) produced a weaker protein suppression (~ 35% of the control). Duplex ds-U2-P, in which the guide strand bears a 5' phosphate, reduced protein KRAS to ~ 40% of the control. This experiment clearly demonstrates that in PDAC cells oncogenic *KRAS* is a target of miR-216b.

Next, we designed ss-miR-216b mimics, with and without a 5' phosphate, and examined their capacity to suppress *KRAS* in Panc-1 cells. As miRNAs inhibit gene expression either by translation repression and/or by mRNA decay [12–14], we measured by quantitative RT-PCR the level of *KRAS* transcript in Panc-1 cells treated with the designed ss-miR-216b mimics. As in the case of nasopharyngeal cells [35], we did not notice any significant reduction of *KRAS* mRNA at 16, 40 or 72 h (Fig. S2). Instead, when we measured by Western blot the level of the KRAS protein in Panc-1 cells treated the ss-miRNAs, we observed a dramatic suppression of the protein (Figure 5(a,b)). In keeping with the nuclease stability data, the compound showing the highest capacity to suppress protein KRAS was U2, the ss-miRNA with two UNA modifications. We found that both 5' phosphorylated and non-phosphorylated single-stranded mimics caused a strong suppression of translation. UNA modifications turned out to be essential for the activity of the ss-miRNA mimics, which brought the protein down to < 10% of the control. The phosphorylation at the 5' end did not seem to be an essential determinant, at least with these miRNAs containing UNA modifications. As a next issue, we wondered what the specificity of miR-216b for *KRAS* is, since this oncogene is highly homologous to *HRAS* and *NRAS*. As illustrated in Figure 5(c,d) none of the designed miR-216b mimics had any impact on HRAS and NRAS proteins. This was expected, as the matching between the seed region of the designed mimics and the 3'-UTR sequence in these genes is suboptimal. In these cases, the base pairing in the miRNA 3' half would have importance for stabilizing the interaction [12–14]. The lack of complementarity at the 3' end makes the mimics ineffective against *HRAS* and *NRAS*. We can therefore conclude that, at least in pancreatic cancer cells, miR-216b regulates only the *KRAS* member of the ras family.

Single-stranded miR-216b without 5′ phosphate is AGO-dependent

Previous studies have demonstrated that AGO2 is a protein involved in RNAi gene silencing activated by ss-siRNAs [46] or ss-miRNA mimics with a 5' phosphate [18]. On this basis,

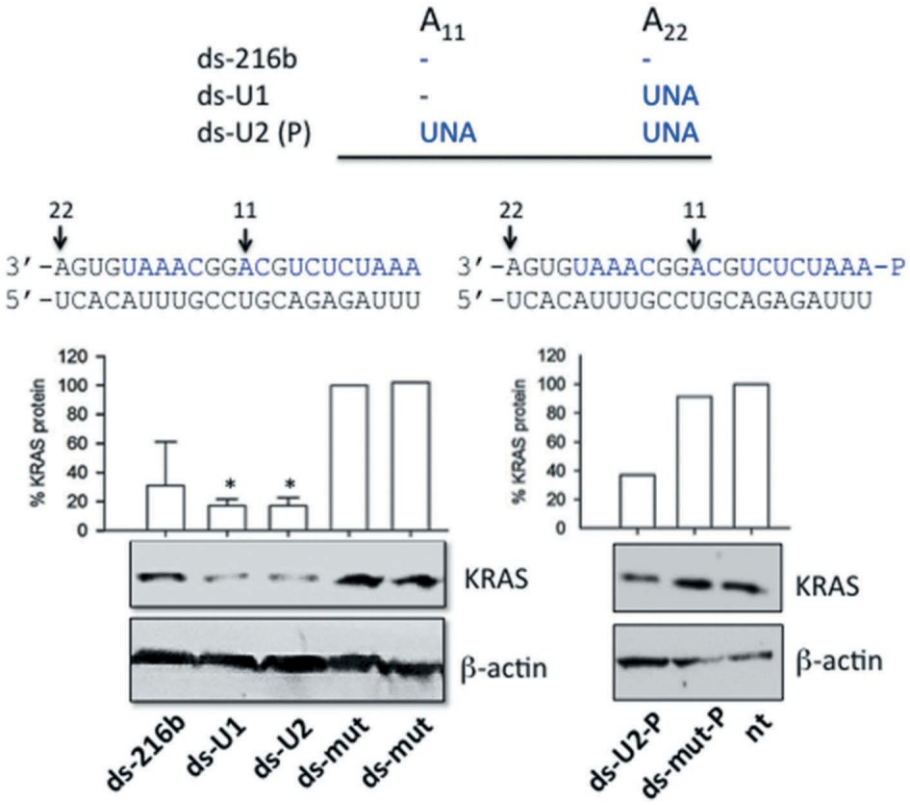

Figure 4. Effect of double-stranded UNA-modified mimics (ds-216b, ds-U1, ds-U2, ds-mut, ds-U2-P, ds-mut-P) on *KRAS* expression in Panc-1 cells. MiR-216b, U1, U2 and mut were hybridized to the complementary strand; Western blots were performed 48 h after the second transfection. The histogram shows the % KRAS protein determined as T/C x 100 where T = (KRAS/β-actin) in cells treated with ds-216b, ds-U1, ds-U2 and ds-U2-P, C = (KRAS/β-actin) in cells treated with ds-mut. The values are the average of three independent Western blot experiments, error bars represent ± SE. A Student's *t*-test was performed, the asterisk (*) means P < 0.05 (n = 3).

we asked if the activity of UNA-modified ss-miR-216b without a 5' phosphate is also mediated by AGO2. To address this point, we silenced in Panc-1 cells AGO2 by siRNA and one day after we treated the cells with the designed ss-miR-216b mimics. The levels of proteins AGO2 and KRAS were measured by Western blot (Figure 6(a,b)). The results show that when protein AGO2 is suppressed, the designed miR-216b mimics are unable to knock out *KRAS*. In contrast, when the designed ss-miRNA mimics suppressed *KRAS*, AGO2 was expressed in the cells, as expected (Figure 6(c)). Together these results suggest that the silencing mechanism promoted by the ss-miR-216b mimics lacking a 5' phosphate is clearly AGO2 dependent. The crystal between AGO2 and miR-20a showed that besides the 5' phosphate, also the phosphates and ribose 2'-OHs of the seed sequence promote contacts with the protein [46]. This suggests that in the absence of a 5' phosphate, ss-miR-216b will only have more freedom to adopt a position within the binding site of AGO2.

Luciferase and clonogenic assays

To obtain further experimental evidence that the designed UNA-modified ss-miR-216b mimics lacking a 5' phosphate are active and specific for *KRAS*, we tested them in a luciferase assay (Figure 7(a,b)). We used plasmid pGL4.75-KRAS LCS6m, carrying *Renilla* luciferase driven by the CMV promoter and the human *KRAS* 3' UTR (3200 bp) containing downstream of luciferase the *KRAS* 3' UTR. Panc-1 cells were treated with 10 nM miRNA mimics (complexed with *Interferin*), with 30 ng pGL4.75-KRAS LCS6m and 70 ng pGL3-Control Vector carrying *Firefly* luciferase driven by the SV40 promoter. When the cells were transfected only once with the miRNA mimics, the reduction of luciferase was proportional to the modifications introduced in ss-miR-216b. The molecule with the strongest anti-*KRAS* activity was U2, which decreased luciferase to ~ 60% of the control (luciferase expressed in mut-treated Panc-1 cells). Instead, when the cells were transfected twice with the single-stranded miR-216b, U1 and U2 (one treatment 24 h after the other) the suppression of luciferase was stronger: it was reduced to ~ 60, ~ 50 and ~ 40% by miR-216b, U1 and U2, respectively. A roughly similar result was obtained with the 5' phosphorylated mimics (not shown). The luciferase experiment unambiguously proved that oncogenic *KRAS* can be downregulated by miR-216b. The luciferase assay gave a weaker effect than the western blot assay, probably because CMV is a stronger promoter than the *KRAS* promoter, and also because in the luciferase assay the target is not in its natural context.

Since *KRAS* stimulates the pathway controlling cell growth, the suppression of protein KRAS should result in the inhibition of proliferation. To assess the effect of miR-216b, U1 and U2 on the growth of PDAC cells, we carried out a colony formation assay with Panc-1 and MIA PaCa-2 cells, carrying the *KRAS* mutations G12D and G12C, respectively. The PDAC cells were seeded in a medium after being diluted in

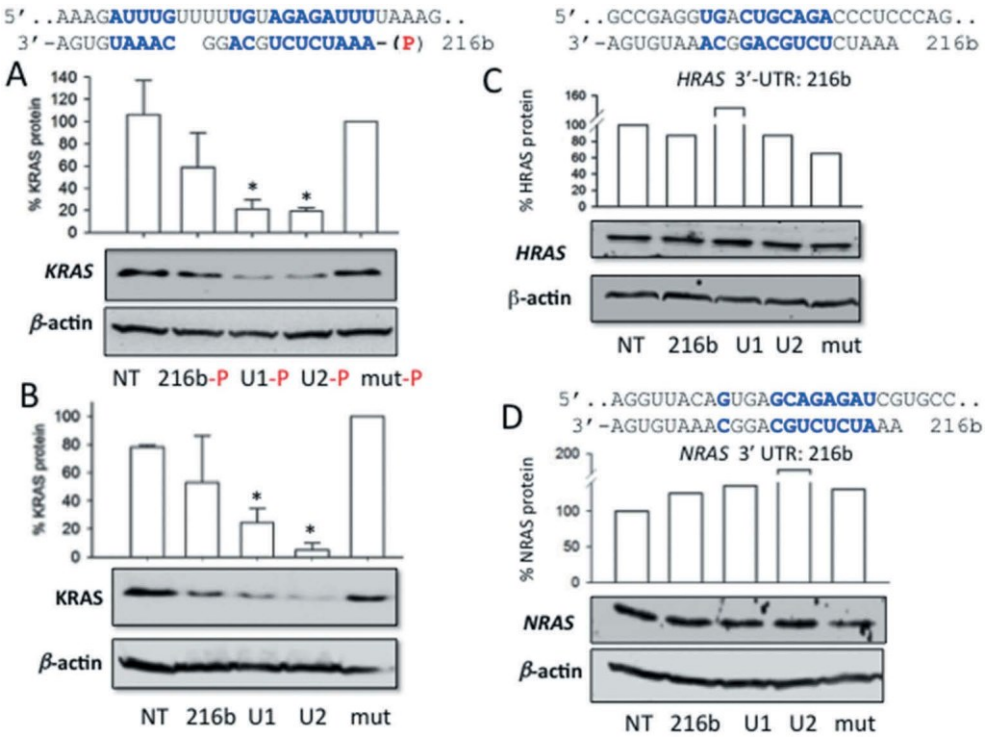

Figure 5. (a, b) Effect of single-stranded miRNA mimics with and without a 5′ phosphate on the expression of *KRAS* in Panc-1 cells. The cells, 24 h after seeding, were treated with the mimics, using *Interferin*. A second treatment was carried out 24 h after the first treatment. A Western blot was carried out 48 h after the second treatment; (a) Base-pairing between *KRAS* 3′-UTR mRNA and miR-216b. The Western blot shows the impact on protein KRAS of the designed ss-miR-216b mimics with a 5′ phosphate. Histograms show the % KRAS protein in miRNA-treated cells compared to mut-treated cells is reported; (b) as in a but with single-stranded mimics without a 5′ phosphate; (c) and (d) match between *HRAS* and *NRAS* 3′-UTR mRNA and miR-216b. The Western blots show the levels of HRAS and NRAS proteins in Panc-1 cells treated with the designed ss-miR-216b mimics. Results obtained from three independent Western blot experiments, error bars represent ± SE. A Student's *t*-test was performed, the asterisk (*) means $P < 0.05$ ($n = 3$).

a way that a single colony could be formed by each cell. After 10 days of growth, the colonies of at least 50 cells were counted and the results plotted in a histogram. Figure 8(a, b), show the data of a typical colony-formation assay obtained with Panc-1 and MIA PaCa-2 cells. The number of colonies on the untreated plate shows to be similar to the number on the plate treated with the control single-stranded mut sequence, which does not suppress oncogenic *KRAS*. In contrast, miR-216b and the UNA-analogues strongly reduced the number of colonies with both types of cells. U2 reduced the number of MIA PaCa-2 colonies to ~ 40% of the control. As *KRAS* controls cell adhesion via the integrin-linked kinase (ILK) [47–49], its suppression in Panc-1 cells resulted in cell aggregation and reduction of the number of colonies by ~ 50%.

Lipid-modified miR-216d and POPC liposomes

In the experiments described above, the miRNA mimics were delivered to the cells complexed with *Interferin*, a commercial polyethyleneimine-based transfectant agent. To improve miRNA delivery, we used as a transporter palmityl-oleyl-phosphatidylcholine (POPC) liposomes in combination with surface attached functionalities [29,30]. POPC liposomes were functionalized with a cell-penetrating peptide, the trans-activator of transcription of the human immune-deficiency virus (TAT), and with miR-216b, as previously reported [29,30,50,51]. Both miR-216b and TAT were chemically modified with a palmityl membrane anchor to allow their rapid attachment to the liposome surface. This strategy, illustrated in Figure 9(a), has been recently adopted to suppress *KRAS* in Panc-1 cells with POPC liposomes functionalized with G4-decoy oligonucleotides and TAT [29]. In the present work, bioactive nanoparticles were obtained by treating POPC liposomes with lipid-modified miR-216b (216b-Pal) and TAT (TAT-Pal). The effector molecules spontaneously anchored to the liposome surface. Oligonucleotide 216b-Pal being not covalently attached to the liposomes can move freely on the lipid surface and interact efficiently with the mRNA target. The membrane anchor of miR-216b consists of a 3-amino-1,2-propanediol unit with two saturated palmityl chains (membrane anchor X) [29,30]. We treated two pancreatic cancer cells (Panc-1 and MIA PaCa-2) twice with POPC liposomes functionalized with TAT-Pal and 216b-Pal and then measured the level of KRAS protein by Western blot. It was observed that KRAS protein is reduced to about ~ 30–40% of the control (cells treated with empty liposomes or with 216b-mut) (Figure 9(b)). This supports the conclusion that POPC liposomes are an attractive vehicle to deliver miR-26b. Lastly, the bioactivity of 216b-Pal delivered via POPC liposomes was tested in a colony formation assay. The lipid-modified 216b-Pal fixed on POPC

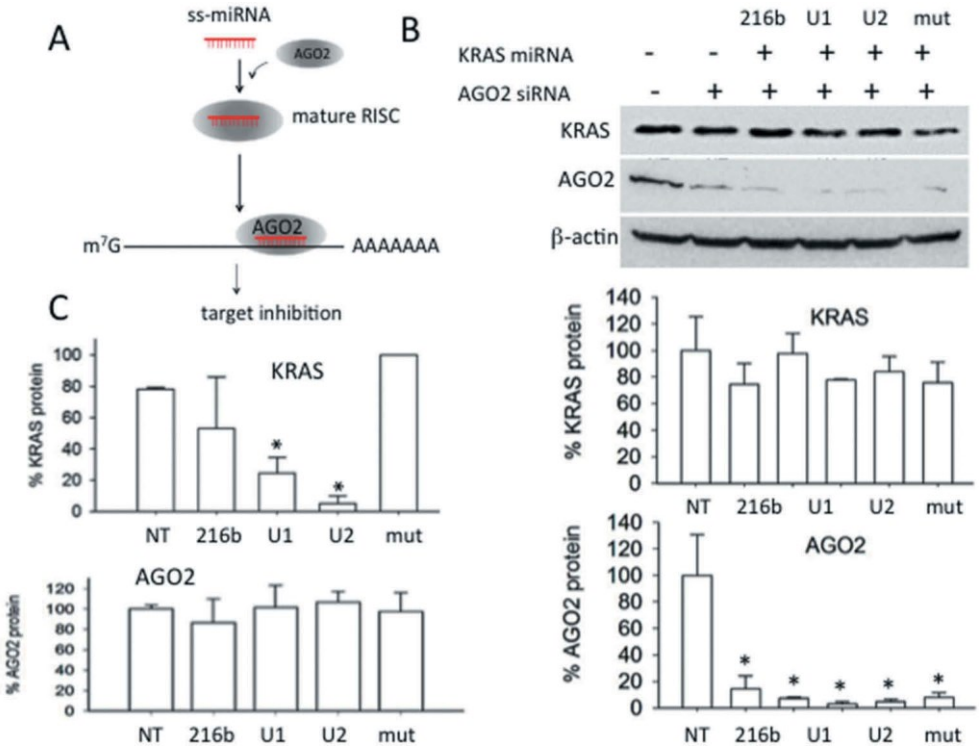

Figure 6. (a) Scheme showing the function of AGO2 in the silencing mechanism mediated by ss-miRNA; (b) Western blot showing that the silencing of AGO2 by a specific siRNA, results in the inactivation of the designed ss-miR-216b mimics. The histograms show the % of KRAS and AGO2 proteins in the cells treated with the designed ss-miR-216b mimics lacking a 5′ phosphate and with AGO2 siRNA as indicated; (c) histograms show the levels of AGO2 and KRAS proteins in Panc-1 cells treated with the designed ss-miR-216b mimic lacking a 5′ phosphate. Results obtained from two independent Western blot experiments, error bars represent ± SE.

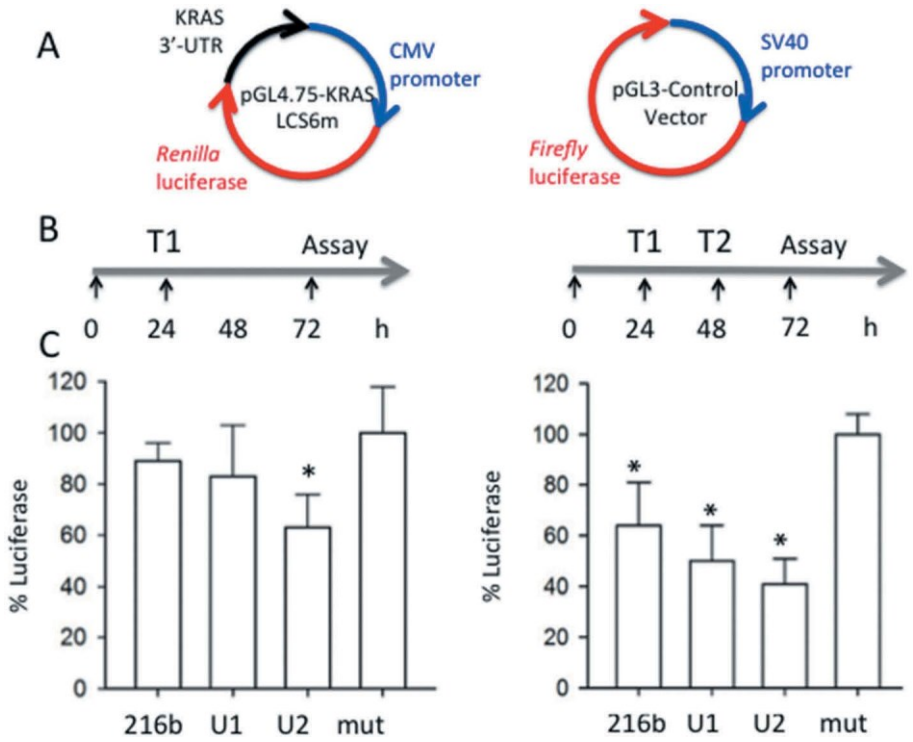

Figure 7. (a) Plasmids used for the luciferase experiments; (b) Outline of the luciferase experiments. T1: plasmids transfection and first miRNA treatment; T2: second miRNA treatment; (c) Histograms show the levels of *Renilla* luciferase in Panc-1 cells treated with miRNAs mut, 216-b, U1 and U2. The histograms report the % luciferase in Panc-1 cells treated with the designed ss-miRNAs (% luciferase = T/C x 100 where T = Renilla/Firefly in miRNA treated cells, C = Renilla/Firefly luciferase in controlled miRNA treated cells (mut)). Error bar is obtained from three independent experiments. A Student's *t*-test was performed, the asterisk (*) means $P < 0.05$ (n = 3).

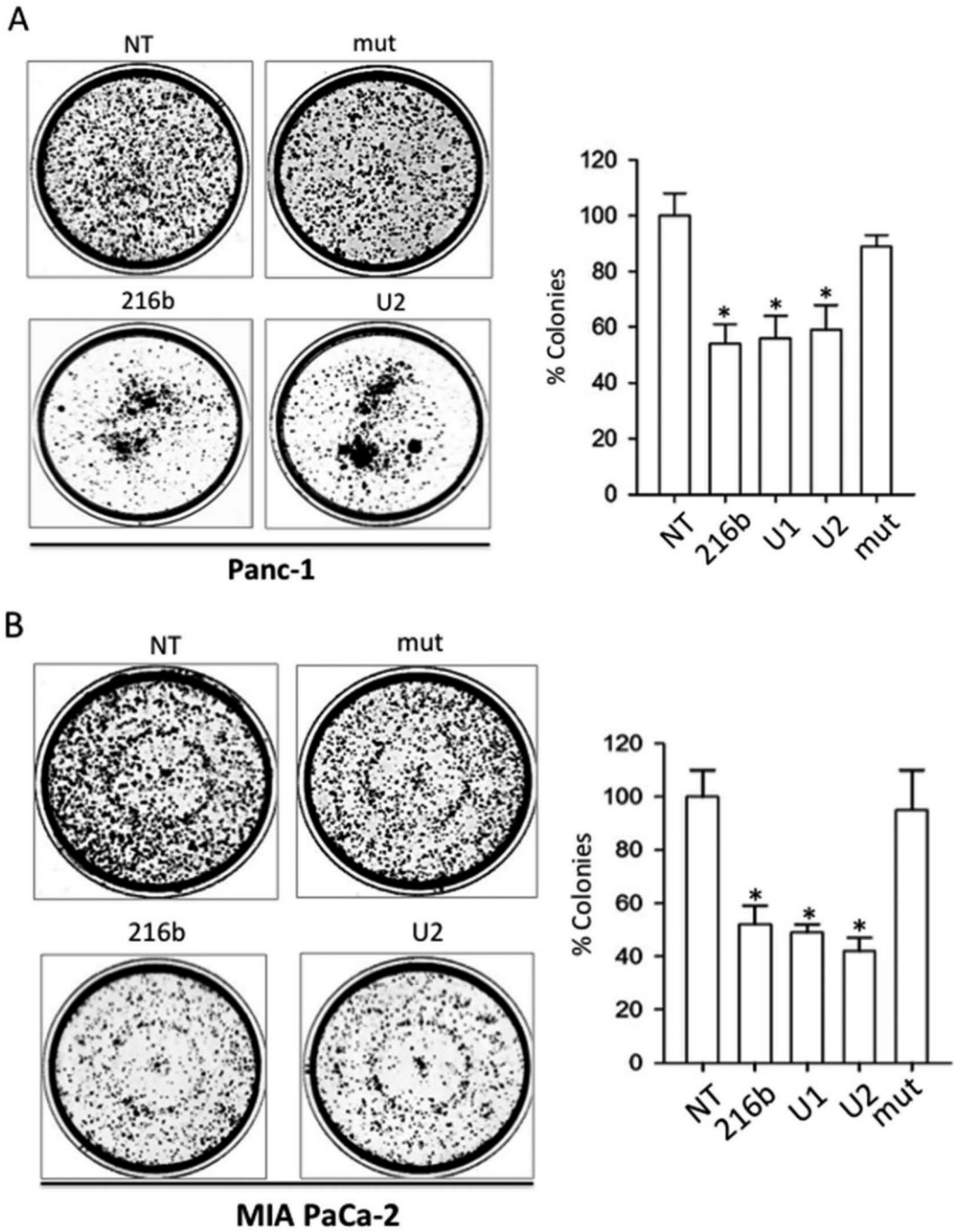

Figure 8. Clonogenic assays. MiRNAs 216-b, U1 and U2 decrease the % of colonies in Panc-1 (a) and Mia PaCa-2 (b) pancreatic cancer cells, while miRNA mut did not. NT = untreated cells. Histogram shows the % colonies in miRNA-treated cells compared to NT. Error bar is obtained from three independent experiments. A Student's *t*-test was performed, the asterisk (*) means $P < 0.05$ (n = 3).

liposomes reduced Panc-1 and MIA PaCa-2 colony formation to about 60% of the control (Figure 10).

Conclusion

The aim of this study was to design oligoribonucleotides combining the potency of the RNAi pathway with the versatility of single-stranded RNA, in order to prepare antigene molecules specific for the *KRAS* oncogene, the main causative agent for pancreatic cancer. To this purpose we focused on miR-216b, a miRNA that is aberrantly downregulated in PDAC. We found that double–stranded miR-26b mimics, with UNA-modifications in the guide strand, specifically down regulate the *KRAS* gene but not the *NRAS* and *HRAS* analogues. We also observed that UNA-modified single-stranded miR-216b mimics exhibit a formidable inhibitory activity against oncogenic *KRAS* in pancreatic cancer cells. The designed ss-miRNAs acted through an AGO2-dependent mechanism, in keeping with the results of a recent study [18]. There are two earlier

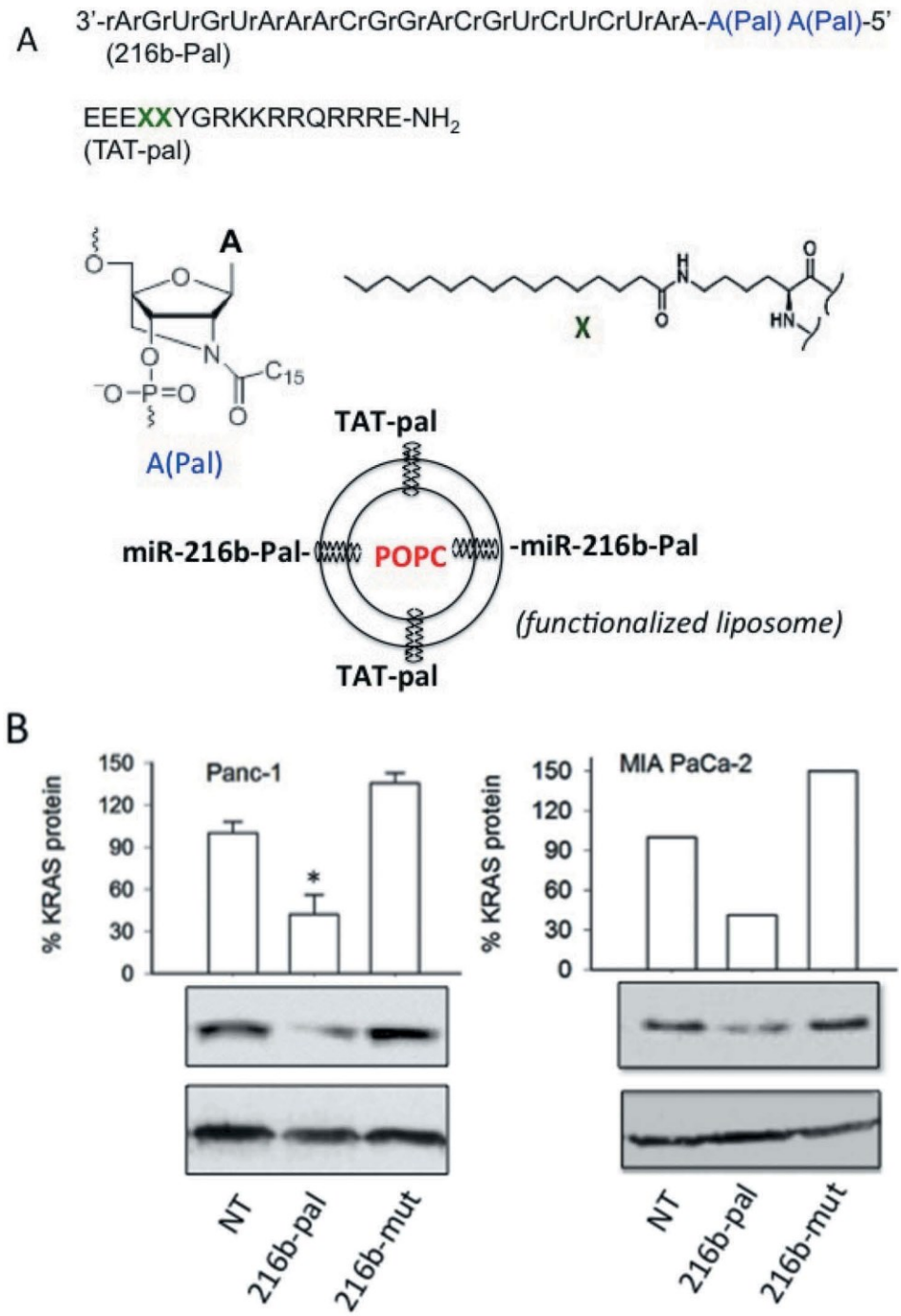

Figure 9. (a) Sequence of miR-216b with two palmityl chains (216b-pal) and of TAT peptide with two X insertions containing two saturated palmityl chains (TAT-pal). MiRNA 216b-pal and TAT-pal attached through their lipid modifications to the surface of POPC liposomes; (b) Western blot showing the reduction of KRAS protein in Panc-1 and MIA PaCa-2 cells treated with the POPC liposomes functionalized with TAT-pal and miR-216b-pal.

studies showing that ss-miRNAs may act as gene silencing agents [17,18]. Our study provides further evidence in support of this conclusion. We designed ss-miRNAs with and without a 5' phosphate: in both cases the effector molecules suppressed the *KRAS* target gene with similar strength. Western blots showed that the designed ss-miR-216b mimic with two UNA modifications reduced dramatically (by 90%) the KRAS protein in Panc-1 cells as well as the capacity of colony formation (by 50%). To our knowledge, this is the first report showing that miR-216b targets oncogenic *KRAS* in PDAC cells. As a proof-of-principle we conjugated miR-216b with two palmityl chains and fixed it on the surface of POPC liposomes, functionalized with the TAT cell-penetrating peptide, which was also conjugated with two palmityl chains. The results obtained with two PDAC cell lines showed that the nanoparticle functionalized with TAT-Pal and 216b-Pal caused ~ 70% decrease of protein KRAS and ~ 40% inhibition of colony formation. This delivery strategy may have a interesting potential for *in vivo* studies

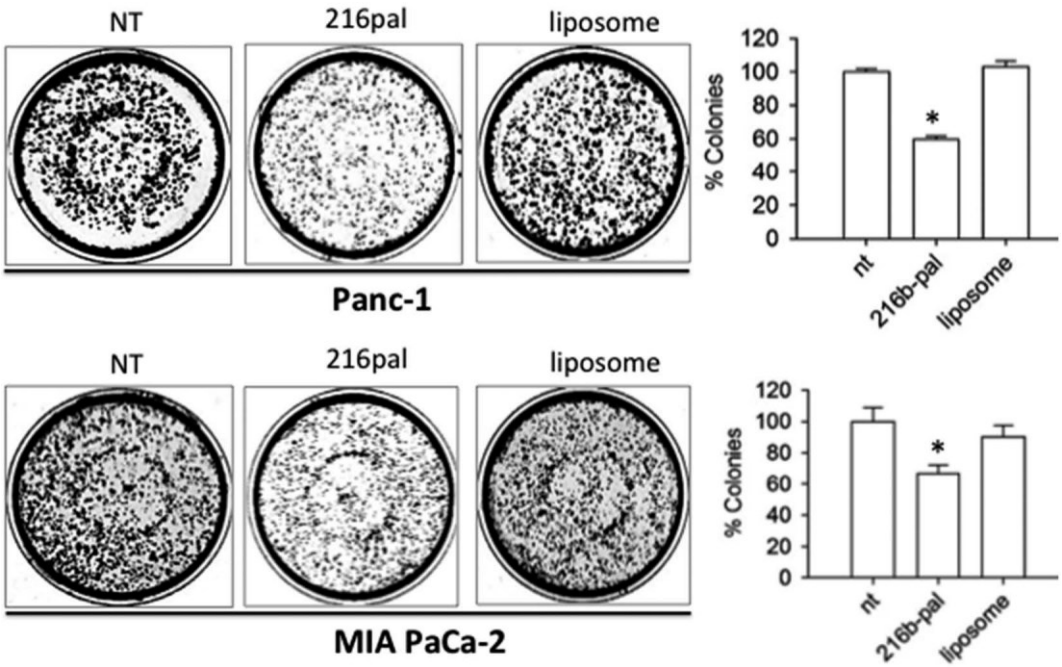

Figure 10. Clonogenic assays. Effect of functionalized POPC liposomes on colony formation in Panc-1 and Mia PaCa-2 pancreatic cancer cells. NT = untreated cells, 216-pal = cells treated with POPC liposomes functionalized with 216b-pal and TAT-pal; Liposome = cells treated with POPC non-functionalized with the effector molecules. Histogram shows the % colonies in miRNA-treated, liposome-treated and non-treated (NT) cells. Error bar is obtained from three independent experiments. A Student's *t*-test was performed, the asterisk (*) means $P < 0.05$ (n = 3).

Experimental

Synthesis of UNA-modified miRNAs

The synthesis of the UNA-modified miRNA miR-216b mimics (216b, U1, U2, mut, U1-P, U2-P) was performed on an automated nucleic acid synthesizer as previously reported. The oligonucleotides were purified by HPLC by using a C18 3 µm 300 Å reversed phase column. Maldi MS analyses were carry out to confirm the structure of the designed UNA-modified miRNAs and evaluate their purity. Calculated and experimental masses were almost identical for all the oligonucleotides (Fig. S3 and S4).

Synthesis of lipid-conjugated TAT and miR-216b

The oligonucleotide was synthesized on an ExpediteTM 8900 nucleic acid synthesis system (Perceptive Biosystems Inc.). The synthesis was performed on a 1.0 µmol scale on GE Healthcare Custom Primer Support™ T40s using standard conditions for automated synthesis with DCI as activator. However, the lipid modified phosphor amidite was dissolved in 2:1 DCE:MeCN at a concentration of 0.1 M, 42® was used as activator (Proligo reagent/Sigma-Aldrich) and the coupling time was increased to 20 min. The DMT protecting group on the last nucleotide in the sequence was removed. After deprotection and cleavage from the solid support using standard conditions (conc. NH_3(aq.) over night at 55 °C), the oligonucleotides were purified by HPLC.

TAT was synthesized on a Liberty 1 Microwave Peptide Synthesizer using a Rink Amide resin and an amino acid concentration of 0.2 M for unmodified amino acids and 0.1 M for the lipid-modified amino acids. After synthesis, the peptide was cleaved from the resin, deprotected and purified by HPLC using a C18 5 µm 10 × 150 mm column.

Cell cultures

The cells used in this study are the human pancreatic adenocarcinoma cells Panc-1 with a *KRAS* G12D (12 Gly→Asp) mutation and MIA PaCa- 2 with a *KRAS* G12C (12 Gly→Cys) mutation. The cell lines have been genotyped by Microsynth (CH) to verify their identity. As expected, they matched 100% to the DNA-profiles of the cell line of Panc-1 (ATCC® CRL-1469TM) and MIA PaCa-2 (ATCC® CRM-CRL-1420TM).

Preparation of POPC liposomes

Liposomes were prepared as previously described [31]. They were extruded on a LIPIX Extruder, Northern Lipids. 114 mg 1-palmityl-2-oleyl-*sn*-glycero-3-phosphocholine (POPC) was suspended in 1.5 mL 10 mM phosphate buffer (10 mM NaH2PO4. 2 H2O, 5 mM Na2HPO4, 140 mM Na^+, pH 7.4) (100 mM POPC) and the resulting solution was extruded 10 times through two stacked polycarbonate filters with a pore size of 50 nm using compressed N2 (~ 30 bar). The size of the

liposomes, determined using Nanoparticle Tracking Analysis, was about 80 nm.

Transfection experiments

The cells were transfected twice with the designed ds- or ss-miRNAs. When the cells were about 65% confluent, 10 nM ss- or ds-miRNAs were transfected in the cells in the presence of Interferin (Polyplus, France), following the manufacturing instructions. After 24 h of incubation a second transfection was performed. The double-stranded miRNA mimics have been prepared in DEPC water containing 100 mM NaCl, 50 mM Tris-HCl pH 7.4, heating the solution for 5 min at 80 °C and let the molecules to anneal overnight at room temperature.

Transfections with POPC liposomes were carried out as previously reported [29]. Briefly, Liposomes (2.8 µl, liposome stock solution ~ 10^{-12} moles/L) were mixed with 110 pmol ss/ds-miRNA in 200 µl phosphate buffer (10 mM NaH2PO4, 5 mM Na2HPO4, 140 mM NaCl pH 7.4). After overnight incubation at room temperature, 2.3 µg of peptide were added to the solution and let to incubate for 30 minutes (liposome mix). For all liposome formulations a statistic distribution of miRNA and CPPs during membrane anchoring to the surface of the liposomes was assumed. Finally, the liposome mix (200 µl) was added to the cells in 2 ml DMEM.

As for the clonogenic assays, the liposome mix was obtained by adding 100 pmol miRNA in 50 µl buffer (liposome and peptide were scaled down accordingly). Then 50 µl of liposome mix were in this case added to 120 µl cell medium. A second transfection was performed 24 h following the first. Then, 48 h after the second transfection the cells in each well were divided in 3 parts and seeded again in 3 wells.

Anti AGO2 siRNA (10 nM, OriGene, USA) were transfected in Panc-1 cells using Interferin (PolyPlus, France) according to manufacturing instructions.

Stability of miRNAs in cellular environment

To determine their nuclease resistance, the designed miRNAs (3 µM) have been incubated for 1, 2 and 4 h in a total extract from Panc-1 cancer cells (2 µg). After incubation the oligonucleotides have been run in a denaturing 20% polyacrylamide gel (7 M urea, 1 x TBE), which was stained with 'stains all'.

Dual luciferase assays

Panc-1 cells were plated (15 x 10^3) in 96-well plate and after one day transfected with miR-216b or UNA-analogues and with plasmids pGL4.75-KRAS LCS6m (a gift from Frank Slack, Plasmid # 44,571, Addgene) and pGL3 Control Vector (Promega, USA). Transfection was performed by mixing 70 ng of pGL3 Control Vector (*Firefly luciferase)* with 30 ng of pGL4.75-KRAS LCS6m (*Renilla luciferase)*, by using jet-PEI (Polyplus) as a transfectant agent. A second miRNA transfection was performed 24 h after the first transfection and the luciferase assays were performed 48 h after the second transfection. A Dual-Glo Luciferase Assay System (Promega, USA) was used. Samples were read on a Turner Luminometer and the relative luminescence expressed as T/C x 100, where T = *Renilla* luciferase/*Firefly* luciferase in miRNA treated cells and C = *Renilla* luciferase/*Firefly* luciferase in mut-treated cells.

Western blots

Total cell protein lysates (15–20µg) extracted from Panc-1 cells were sonicated for 10 minutes and the lysates were electrophoresed on 12% SDS-PAGE and transferred into a nitrocellulose membrane, at 70 V for 2 h. The filter was blocked for 1 h with 5% nonfat dry milk solution in PBS 0.05% Tween (Sigma-Aldrich, Italy) at room temperature. Membranes were incubated overnight at 4 °C with the primary antibodies: monoclonal anti-KRAS (clone 3B10-2F2, IgG1 mouse, 2.5 µg/mL, Sigma-Aldrich, USA), polyclonal anti-HRAS (IgG rabbit, diluted 1:300, Santa Cruz Biotechnology Inc, USA), monoclonal anti-NRAS (clone F155-227, IgG_1 mouse, 2.5 µg/mL) and monoclonal anti-actin (clone JLA20, IgM mouse, 1x10^{-4} µg/mL, Calbiochem, Merck Millipore, Germany). The membranes were washed with a 0.05% Tween in PBS and then incubated 1 h with the secondary antibodies horseradish peroxidase conjugated: anti-mouse IgG (diluted 1:5000) and anti-mouse IgM (diluted 1:2000) (Calbiochem, Merck Millipore, Germany) and anti-rabbit IgG (diluted 1:5000) (Calbiochem, Merck Millipore, Germany). To detect the protein we used Super signal ® West PICO and FEMTO (ThermoFisher Scientific Pierce, USA). The exposure time depended on the antibody used and was usually between 30 s and 5 min. The protein levels were quantified by the Image Quant TL Version 2003 software (Amersham).

Colony forming assay

To assess the effect of miR-216b, U1 and U2 on the growth of PDAC cells we carried out colony formation assays with Panc-1 and MIA PaCa-2 cells, carrying the *KRAS* mutations G12D and G12C, respectively. The PDAC cells, treated with the designed miRNAs, were seeded in a medium after being diluted in a way that a single colony could be formed from each cell. After 7–13 days of growth, the colonies of at least 50 cells were counted and the results plotted in a histogram. NT = untreated cells. Histogram shows the % colonies in miRNA-treated cells compared to NT. Values obtained from three independent experiments. A Student's *t*-test was performed, (*) = P < 0.05.

RNA Extraction and Real-time PCR (see Fig. S2).

Abbreviations

PDAC pancreatic ductal adenocarcinoma
KRAS Kirsten ras
UTR untranslated region
POPC palmityl-oleyl-phosphatydilcholine
TAT trans-activator of transcription

Author Contributions

The manuscript was written by LEX, through the contributions of all authors. All authors have given approval to the final version of the manuscript.

Disclosure statement

No potential conflict of interest was reported by the authors.

Funding

This work has been carried out with the financial support of AIRC (Italian association for cancer research, IG 2017, Project Code 19898).

Supporting Information

The following information is available free of charge:

(i) Array Express Archive of Functional genomics E-MTAB-753, GSE41372; (ii) Levels of *KRAS* mRNA in miRNA treated Panc-1 cells measured by quantitative real-time PCR; (iii) Molecular masses of UNA-modified RNAs by MALDI MS and Maldi spectra; (iv) Further Materials and methods information.

ORCID

Annalisa Ferino http://orcid.org/0000-0003-2524-7192
Giulia Miglietta http://orcid.org/0000-0001-5186-6603
Raffaella Picco http://orcid.org/0000-0002-6132-6333
Stefan Vogel http://orcid.org/0000-0002-0587-719X
Jesper Wengel http://orcid.org/0000-0001-9835-1009
Luigi E. Xodo http://orcid.org/0000-0003-3344-7207

References

[1] Jemal A, Siegel R, Ward E, et al. Cancer statistics. Cancer J Clin 2007; 57:43–66.
[2] Jemal A, Siegel R, Ward E, et al. Cancer statistics. Cancer J Clin 2010; 60:277–300.
[3] Kleeff J, Reiser C, Hinz U, et al. Surgery for recurrent pancreatic ductal adenocarcinoma. Ann Surg 2007, 245:566–572.
[4] Bryant KL, Mancias JD, Kimmelman AC, et al. KRAS: feeding pancreatic cancer proliferation. Trends Biochem Sci. 2014; 39:91–100.
[5] Collins MA, Bednar MA, Zhang F, et al. Oncogenic Kras is required for both the initiation and maintenance of pancreatic cancer in mice. J Clin Invest 2012;122:639–653.
[6] Kong B, Michalski CW, Erkan M, et al., From tissue turnover to the cell of origin for pancreatic cancer Nat Rev Gastroenterol Hepatol2011; 8: 467–472.
[7] Ying H, Kimmelman AC, Lyssiotis CA, et al., Oncogenic Kras maintains pancreatic tumors through regulation of anabolic glucose metabolism. Cell 2012; 149: 656–670.
[8] Son J, Lyssiotis CA, Ying H, et al., Glutamine supports pancreatic cancer growth through a KRAS-regulated metabolic pathway. Nature 2013; 496: 101–105.
[9] Jonas S, Izaurralde E Towards a molecular understanding of microRNA-mediated gene silencing. Nat Rev Genet 2015; 16: 421–433.
[10] Stefani G, Slack FJ Small non-coding RNAs in animal development. Nat Rev Mol Cell Biol 2008; 9: 219–230.
[11] Krol J, Loedige I, Filipowicz W, The widespread regulation of microRNA biogenesis, function and decay. Nat Rev Genet 2010; 11: 597–610.
[12] Filipowicz W, Bhattacharyya SN, Sonenberg N, Mechanisms of post-transcriptional regulation by microRNAs: are the answers in sight? Nat. Rev Genet 2008; 9: 102–114.
[13] Huntzinger E, Izaurralde E Gene silencing by microRNAs: contributions of translational repression and mRNA decay. Nat Rev Genet 2011; 12:99–110.
[14] Izaurralde E Gene regulation. Breakers blockers-miRNAs Sci 2015; 349: 380–382.
[15] Iwakawa HO, Tomari Y, The functions of microRNAs: mRNA decay and translational repression. Trends Cell Biol. 2015; 25:651–665.
[16] Goldgraben MA, Russell R, Rueda OM, et al. A double-stranded microRNA mimics can induce length- and passenger strand–dependent effects in a cell type–specific manner. Rna 2016; 22:193–203.
[17] Chorn G, Klein-McDowell M, Zhao L, et al. Single-stranded microRNA mimics. Rna 2012; 18:1796–1804.
[18] Matsui M, Prakash TP, Corey DR, Argonaute 2-dependent regulation of gene expression by single-stranded miRNA mimics. Mol Ther 2016; 24:946–955.
[19] Schirle NT, Kinberger GA, Murray HF, et al. Structural analysis of human Argonaute-2 bound to a modified siR-NA guide. J Am Chem Soc 2016;138:8694–8697.
[20] Yu D, Pendergraff H, Liu J, et al. Single-stranded RNAs use RNAi to potently and allele-selectively inhibit mutant huntingtin expression. Cell 2012; 150: 895–908.
[21] Lima WF, Prakash TP, Murray HM, et al. Single-stranded siRNAs activate RNAi in animals, Cell 2012;150:883–894.
[22] Di Leva G, Croce C, miRNA profiling of cancer. Curr Opin Genet Dev 2013; 23: 3–11.
[23] Ling H, Fabbri M, Ga C, MicroRNAs and other non-coding RNAs as targets for anticancer drug development. Nat Rev Drug Discov 2013; 12: 847–865.
[24] Lin S, Gregory RI, MicroRNA biogenesis pathways in cancer. Nat Rev Cancer 2015; 15: 321–333.
[25] Matsui M, Corey DR, Non-coding RNAs as drug targets. Nat Rev Drug Discov 2017; 16: 167–179.
[26] Seux M, Iovanna J, Dagorn JC et al. MicroRNAs in pancreatic ductal adenocarcinoma: new diagnostic and therapeutic clues. Pancreatology 2009; 9: 66–72.
[27] Ling H. Non-coding RNAs: therapeutic strategies and delivery systems.Adv Exp Med Biol. 2016; 937:229–237.
[28] Barrett T, Troup DB, Wilhite SE, et al., NCBI GEO: archive for functional genomics data sets—10 years on. Nucleic Acids Res. 2011; 39: 1005–1010.
[29] Cogoi S, Jakobsen U, Pedersen EB, et al., Lipid-modified G4-decoy oligonucleotide anchored to nanoparticles: delivery and bioactivity in pancreatic cancer cells. Sci Rep. 2016 6:38468.
[30] Jakobsen U, Vogel S Assembly of liposomes controlled by triple helix formation. Bioconjug 2013; 24, 1485–1495.
[31] Jakobsen U, Vogel S, DNA-controlled assembly of liposomes in diagnostics. Methods Enzymol 2009; 464: 233–248.
[32] Jakobsen U, Simonsen AC, Vogel S, DNA-controlled assembly of soft nanoparticles. J Am Chem Soc 2008; 130: 10462–10463.
[33] Liu Y-A, Zhang Y, Zheng Z, et al., MicroRNA-216b reduces growth, migration and invasion of pancreatic ductal adenocarcinoma cells by directly targeting β–associated coiled-coil protein kinase 1. Oncol 2018; 15:6745–6751.
[34] You Y, Tan J, Gong Y, et al., MicroRNA-216b-5p functions as a tumor-suppressive RNA by targeting TPT1 in pancreatic cancer cells. J Cancer 2017; 8: 2854–2865.
[35] Deng M, Tang H, Zhou Y, et al., MiR-216b suppresses tumor growth and invasion by targeting KRAS in nasopharyngeal carcinoma. J Cell Sci 2011; 124: 2997–3005.
[36] Azevedo-Pouly AC, Sutaria DC, Jiang J, et al., MiR-216 and miR-217 expression is reduced in transgenic mouse models of pancreatic adenocarcinoma, knockout of miR-216/miR-217 host gene is embryonic lethal. Funct Integr Genomics 2017; 17: 203–212.
[37] Koller E, Vincent TM, Chappell A, Mechanisms of single-stranded phosphorothioate modified antisense oligonucleotide accumulation in hepatocytes. Nucleic Acids Res. 2011; 39: 4795–4807.

[38] Jackson AL, Bartz SR, Schelter J, et al., Expression profiling reveals off-target gene regulation by RNAi. Nat Biotecnol 2003; 21: 635–637.
[39] Brennecke J, Stark A, Russell RA, et al., Principles of microRNA–Target recognition. Plos Biol. 2005; 3 e85.
[40] Grimson A, Farh KK, Johnston KW, MicroRNA targeting specificity in mammals: determinants beyond Seed Pairing. Mol Cell 2007; 27: 91–105.
[41] Bramsen JB, Laursen MB, Nielsen AF, et al., A large-scale chemical modification screen identifies design rules to generate siRNAs with high activity, high stability and low toxicity. Nucleic Acids Res. 2009; 37: 2867–2881.
[42] Snead NM, Escamilla-Powers JR, Rossi JJ, et al., 5′-unlocked nucleic acid modification improves siRNA targeting. Mol Ther Nucleic Acids 2013; 2 e103.
[43] Langkjaer N, Pasternak A, Wengel J, UNA (unlocked nucleic acid): a flexible RNA mimic that allows engineering of nucleic acid duplex stability. Bioorg Med Chem 2009; 17: 5420–5425.
[44] Pasternak A, Wengel J, Unlocked nucleic acid – an RNA modification with broad potential. Bioorg Med Chem 2011; 9: 3591–3597.
[45] Watts JK, Yu D, Charisse K et al., Effect of chemical modifications on modulation of gene expression by duplex antigene RNAs that are complementary to non-coding transcripts at gene promoters. Nucleic Acids Res. 2010, 38: 5242–5259.
[46] Elad Elkayam E, Kuhn CD, Tocilj A, et al., The structure of human argonaute-2 in complex with miR-20. Cell 2012; 150: 100–110.
[47] Novak A, Hsu S, Leung-Hagesteijn C et al., Cell adhesion and the integrin-linked kinase regulate the LEF-1 and β-catenin signaling pathways. Proc Natl Acad Sci U S A 1998; 95: 4374–4379.
[48] Cogoi S, Rapozzi V, Cauci S et al., Critical role of hnRNP A1 in activating KRAS transcription in pancreatic cancer cells: a molecular mechanism involving G4 DNA. Biochim Biophys Acta 2017; 1861: 1389–1398.
[49] Chu PC, Yang MC, Kulp SK, et al., Regulation of oncogenic KRAS signaling via a novel KRAS-integrin-linked kinase-hnRNPA1 regulatory loop in human pancreatic cancer cells. Oncogene 2016; 35: 3897–3908.
[50] Green M, Loewenstein PM, Autonomous functional domains of chemically synthesized human immunodeficiency virus tat transactivator protein. Cell 1988; 55: 1179–1188.
[51] Frankel AD, Pabo CO, Cellular uptake of the tat protein from human immunodeficiency virus. Cell 1988; 55: 1189–1193.

SUPPLEMENTARY DATA

MicroRNA Therapeutics: Design of single-stranded miR-216b mimics to target *KRAS* in pancreatic cancer cells †

Annalisa Ferino,[a,&] *Giulia Miglietta,*[a,& †] *Raffaella Picco,*[a] *Stefan Vogel,*[b] *Jesper Wengel and Luigi E. Xodo*[a *]

(a) Department of Medicine, Laboratory of Biochemistry, University of Udine, Italy; luigi.xodo@uniud.it;

(b) Nucleic Acids Centre, University of Southern Denmark, DK 5230, Odense, Denmark

(c) .

Supplementary data, S1. miRNA and FC values calculated for three dataset (GSE43796, E-MTAB-753 and GSE41372).

GSE43796

miRNA	FC
hsa-miR-216a	36.83
hsa-miR-216a	26.34
hsa-miR-216a	15.82
hsa-miR-216a	3.25
hsa-miR-216b	**27.95**
hsa-miR-216b	**13.03**
hsa-miR-216b	**8.83**
hsa-miR-217	21.26
hsa-miR-217	13.73
hsa-miR-217	8.61
hsa-miR-217	2.25
hsa-miR-30c	2.09
hsa-miR-30c	1.76
hsa-miR-30e	2.05
hsa-miR-30e	1.59
hsa-miR-30b	1.86
hsa-miR-30b	1.56
hsa-miR-30b	1.44
hsa-miR-30a	1.85
hsa-miR-181a	-2.64
hsa-miR-181b	-2.63
hsa-miR-181b	-2.35
hsa-miR-200b	-2.49
hsa-miR-143	-1.71
hsa-miR-143	-1.37
hsa-miR-1	-1.40
hsa-miR-1	-1.06
hsa-miR-155	-1.69
hsa-miR-155	-1.47

E-MTAB-753

miRNA	FC
hsa-miR-217	2.95
hsa-miR-216b	**2.27**
hsa-miR-30a	1.77
hsa-miR-30b	1.76
hsa-miR-30d	1.59
hsa-miR-143	-6.33
hsa-miR-1	-1.24
hsa-miR-199b-3p	-4.79
hsa-miR-199a-3p	-4.61
hsa-miR-181a	-4.37
hsa-miR-155	-3.90

GSE41372

miRNA	FC
hsa-miR-217	14.67
hsa-miR-216a	8.96
hsa-miR-30d	1.67
hsa-miR-30a	1.63
hsa-miR-30e	1.60

$$\text{Fold Change} = FC = \log_2 (F\ ctrl\ /F\ tumor)$$

Three miRNA expression datasets (GSE41372, GSE43796, E-MTAB-753) of pancreatic cancer were retrieved from GEO (Barrett, 2011) and ArrayExpress (Parkinson, 2007). The available raw files have been downloaded. As for the affymetrix platform, the CEL files were processed using standard tools

available within the *affy* package in R (Gautier, 2004), they were normalized using the standard RMA algorithm (Irizarry, 2003). The Agilent raw data text files were normalized between arrays by quantile normalization using the *limma* library (Ritchie, 2015). A statistical analysis was performed using the standard *t*-test for unpaired samples (tumour samples and non-tumour samples were unrelated). Differentially expressed miRNAs in the malignant tissues were defined as those characterized by a $P < 0.05$ and a fold change FC >1.5 or FC < -1.5. We searched for a correlation between KRAS and the differentially expressed miRNAs by using miRGate (Andrés-León et al., 2015), Targetscan (Lewis et al., 2005) and Miranda (Betel et al., 2010).

Supplementary data, S2. Levels of *KRAS* mRNA in Panc-1 cells measured by quantitative real-time PCR. The assay has been performed 16, 40 and 72 h after the second treatment with 10 nM single-stranded miR-216b and UNA-modified miRNA mimics with and without a phosphate at the 5' end. .

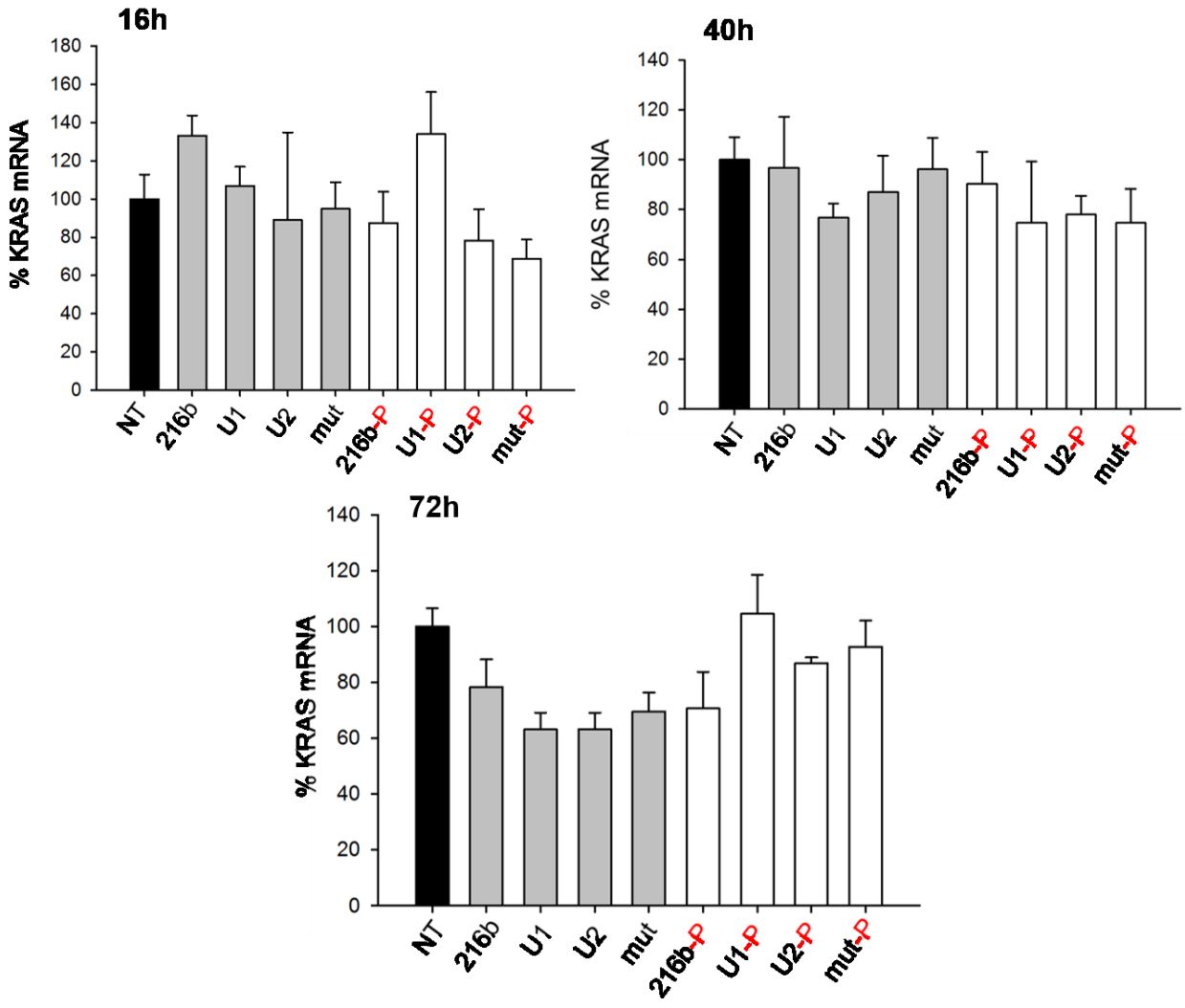

RNA Extraction and Real-time PCR

Panc-1 cells ($15x10^3$) were transfected in a 96-well plate with 10 nM miRNA 216b as described above. RNA was extracted 16, 40 and 72 h after the second transfection by using iScript™ RT-qPCR Sample Preparation Reagent (Bio Rad) following the manufacturer's instructions. For cDNA synthesis 1.25 µl of RNA (extracted from about 10^3 cells) was heated at 55 °C and placed in ice. The solution was added to 11.25 µl of mix containing (final concentrations) 1 x buffer, 0.01 M DTT (Invitrogen), 1.6 µM primer dT (MWG Biotech, Ebersberg, Germany; d(T)16), 1.6 µM Random hexamer primers (Microsynth), 0.4 mM dNTPs solution containing equimolar amounts of dATP, dCTP, dGTP, and dTTP (Euroclone, Pavia, Italy), 0.8 units/µl RNase OUT, and 8 units/µl of Maloney

murine leukemia virus reverse transcriptase (Invitrogen). The reactions were incubated for 1 h at 37 °C and stopped with heating at 95 °C for 5 min.

Real-time PCR multiplex reactions were performed with 1 x Kapa Probe fast qPCR kit (KAPA Biosystems, Wilmington, MA, USA) for *KRAS* and housekeeping genes β2-microglobulin and HPRT, 1.0 µl of cDNA in 10 µl final and primers/probes at the following concentrations: for *KRAS*, the probe was FAM-TACTCCTCTTGACCTGCTGTG-BHQ1 (accession No. NM_033360, from 352 to 372, 90 nM), the sense primer was 5′-CGAATATGATCCAACAATAGAG (from 271 to 292, 180 nM) and the antisense primer was 5′-ATGTACTGGTCCCTCATT (from 379 to 396, 180 nM). For β2-microglobulin accession n. NM_004048 probe ROX-TATGCCTGCCGTGTGAACC-BHQ2 (from 352 to 370, 60 nM), the primer sense was 5′-CCCCACTGAAAAAGATGA (from 333 to 350, 100 nM), the primer antisense was 5′-CCATGATGCTGCTTACAT (from 415 to 432, 100 nM). For HPRT accession n. NM_000194 probe 5′-Cy5-CTTGCGACCTTGACCATCTT-BHQ2 (from 633 to 652, 180 nM), the primer sense was 5′-CTTGATTGTGGAAGATATAATTG (from 557 to 575, 210 nM), the primer antisense was 5′-TATATCCAACACTTCGTGG (from 672 to 690, 230 nM). The PCR cycle was: 3 min at 95 °C, 50 cycles 10 s at 95 °C, 60s at 58 °C. PCR reactions were carried out with a CFX-96 real-time PCR apparatus controlled by an Optical System software (version 3.1) (BioRad Laboratories, CA, USA). *KRAS* mRNA was normalized with the two housekeeping genes.

Supplementary S3

Table 1. Molecular masses of UNA-modified RNAs by MALDI MS

miRNA sequence*	Name	Calculated	Found
5’-rArArArUrCrUrCrUrGrCrArGrGrCrArArArUrGrUrGuA	U1	7051,4	7051,3
5’-rArArArUrCrUrCrUrGrCuArGrGrCrArArArUrGrUrGuA	U2	7053,4	7053,4
5’-rArArArCrUrGrUrGrGrCrArGrGrCrArCrCrUrGrUrGuA	mut	7082,4	7082,7

5’P-rArArArUrCrUrCrUrGrCrArGrGrCrArArArUrGrUrGuA	U1-P	7131,3	7131,3
5’P-rArArArUrCrUrCrUrGrCuArGrGrCrArArArUrGrUrGuA	U2-P	7133,3 /	7133,6

* uA= unlocked nucleic acid

Maldi spectrum of miR-216b with one UNA modification (U1)

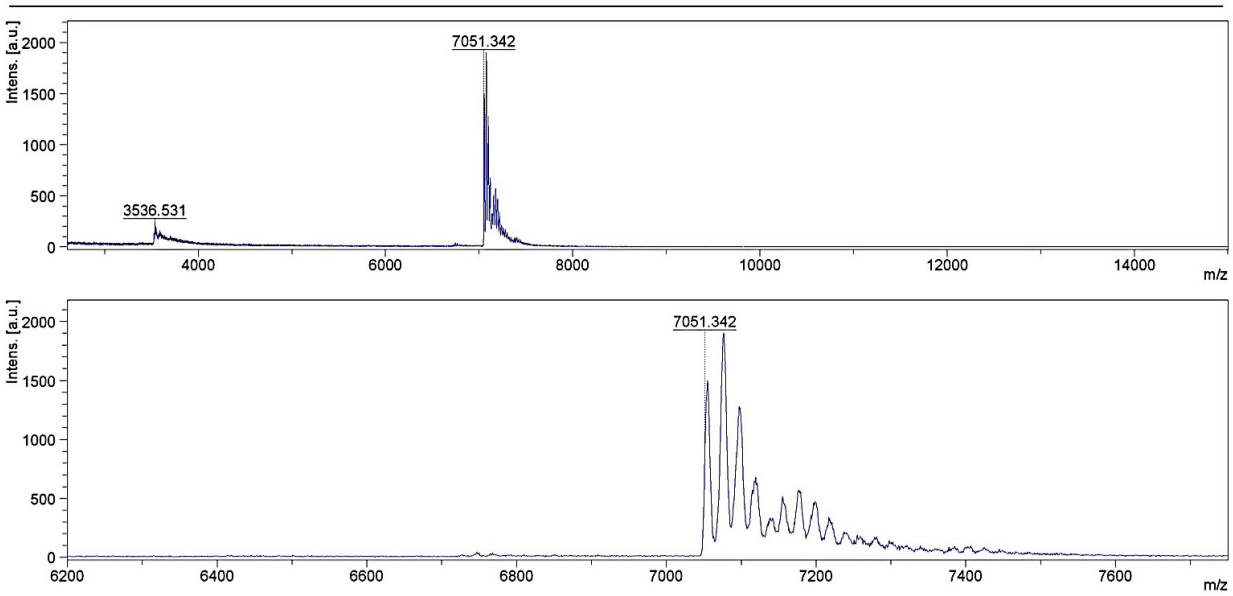

Maldi spectrum of miR-216b with two UNA modification (U2)

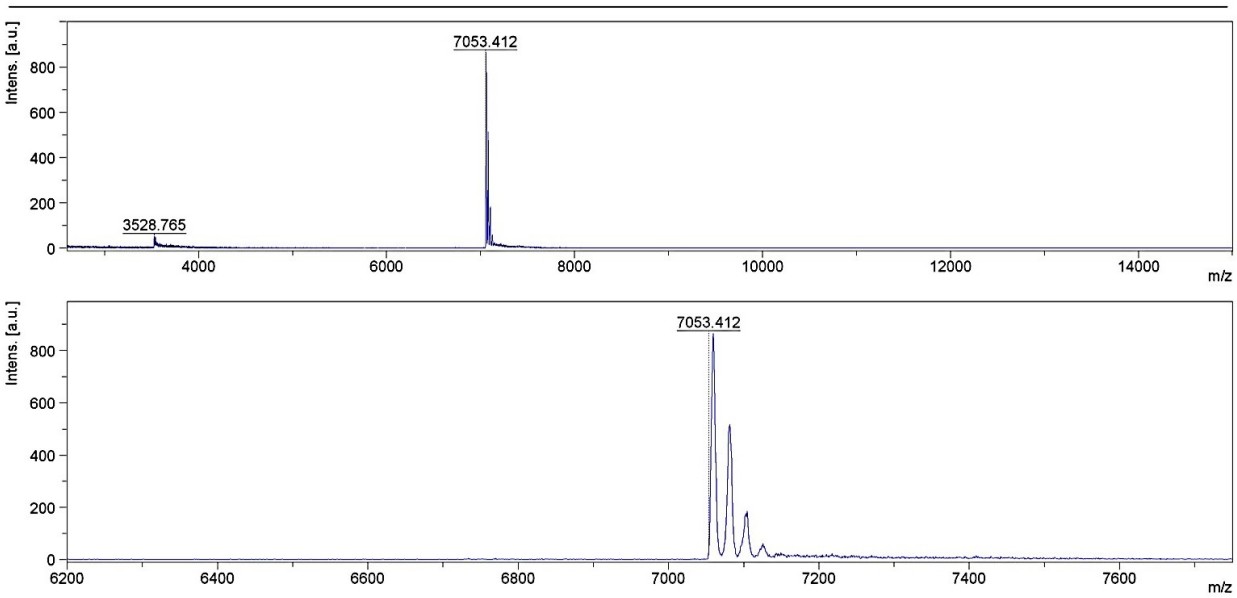

Maldi spectrum of mut with one UNA modification (U1)

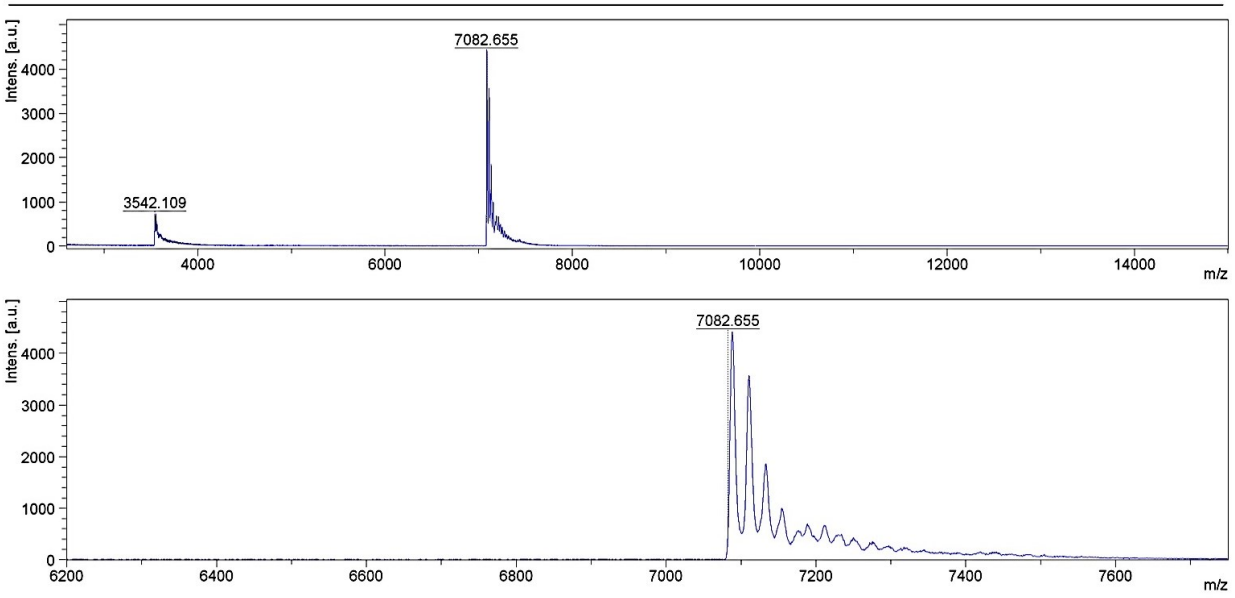

Maldi spectrum of miR-216b with one UNA modification and 5’-phosphate (U1-P)

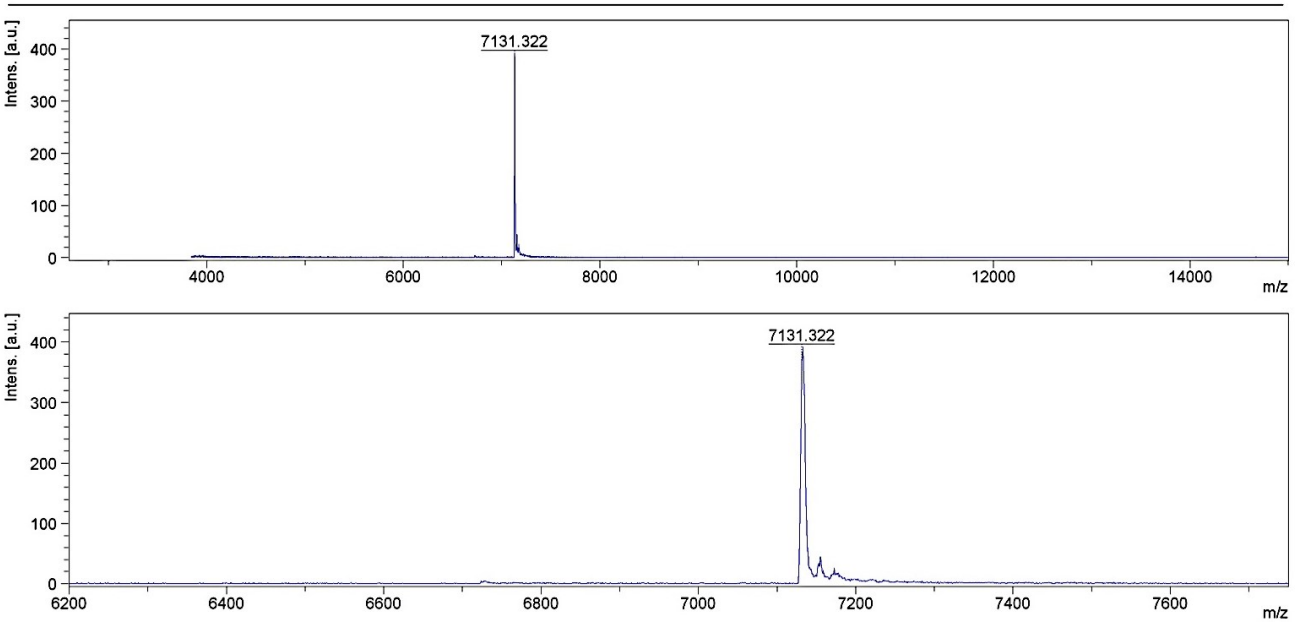

Maldi spectrum of miR-216b with two UNA modifications and 5’-phosphate (U2-P)

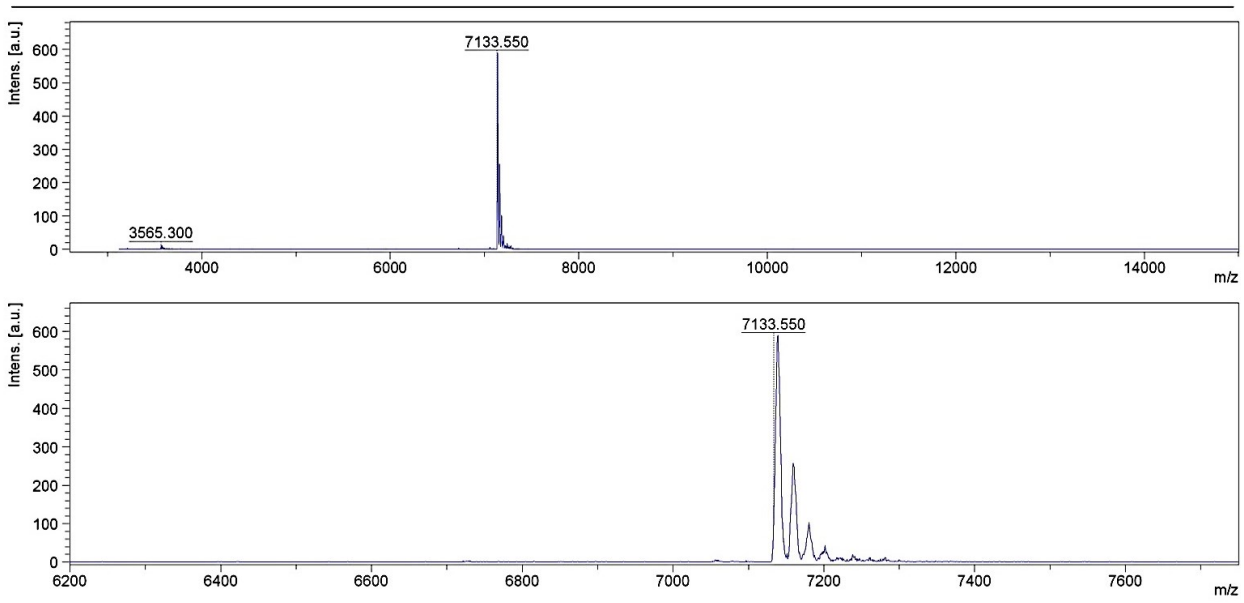

Supplementary S4

Table 2. Oligonucleotides used in this study.

216b	5'-rArArArUrCrUrCrUrGrCrArGrGrCrArArArUrGrUrGrA
U1	5'-rArArArUrCrUrCrUrGrCrArGrGrCrArArArUrGrUrGuA
U2	5'-rArArArUrCrUrCrUrGrCuArGrGrCrArArArUrGrUrGuA
mut	5'-rArArArCrUrGrUrGrGrCrArGrGrCrArCrCrUrGrUrGuA
216b-P	5'P-rArArArUrCrUrCrUrGrCrArGrGrCrArArArUrGrUrGrA
U1-P	5'P-rArArArUrCrUrCrUrGrCrArGrGrCrArArArUrGrUrGuA
U2-P	5'P-rArArArUrCrUrCrUrGrCuArGrGrCrArArArUrGrUrGuA
mut-P	5'P-rArArArCrUrGrUrGrGrCrArGrGrCrArCrCrUrGrUrGrA
complementary-216b	5'-rCrArCrArUrUrUrGrCrCrUrGrCrArGArGrArUrUrUrU
complementary-mut:	5'-rCrArCrArGrGrUrGrCrCrUrGrCrCrArCrArGrUrUrUrU

uA= unlocked nucleic acid modification;

Bibliography

Barrett T, Troup DB, Wilhite SE, et al. NCBI GEO: archive for functional genomics data sets—10 years on. Nucleic Acids Res. 2011 Jan; 39: D1005–1010.

Parkinson H, Kapushesky M, Shojatalab M, et al. Array Express a public database of microarray experiments and gene expression profiles. Nucleic Acids Res. 2007; 35:D747–750.

Gautier L, Cope L, Bolstad BM, et al., Affy--analysis of Affymetrix GeneChip data at the probe level. Bioinformatics. 2004; 20:307-315.

Irizarry RA, Bolstad BM, Collin F, et al., Summaries of Affymetrix GeneChip probe level data. Nucleic Acids Res. 2003; 31:e15.

Ritchie ME, Phipson B, Wu D, et al. limma powers differential expression analyses for RNA-sequencing and microarray studies. Nucleic Acids Res. 2015; 43:e47.

Andrés-León E, González Peña D, Gómez-López G, et al., MiRGate: a curated database of human, mouse and rat miRNA-mRNA targets. Database (Oxford) 2015; 2015:bav035.

Lewis BP, Burge CB, Bartel DP. Conserved seed pairing, often flanked by adenosines, indicates that thousands of human genes are microRNA targets. Cell 2005; 120:15-20.

Betel D, Koppal A, Agius P, et al. Comprehensive modeling of microRNA targets predicts functional non-conserved and non-canonical sites. Genome Biol. 2010;11:R90.

5. CONCLUSION

Mutant KRAS is present in more than 90% of pancreatic tumours where it plays an important role in the initiation and progression of the disease. Despite the important achievements of the last years, several aspects on KRAS biology are not yet clear and further studies are needed to develop targeted strategies against this oncogene for the treatment of PDAC.

Previous work from our laboratory showed that the KRAS promoter contains a G- rich region located upstream of the transcription start site (TSS). This sequence being composed by runs of guanines (G4 motif) folds into a G-quadruplex (or G4) structure that, according to recent studies, is present in the cell [1]. This unusual conformation is recognized by several transcription factors such as MAZ, PARP-1 and hnRNP A1 and the most likely function of the G4 structure is to recruit to the KRAS promoter the nuclear proteins essential for activating transcription.

Recent studies have reported that pancreatic cancer cells are addicted to KRAS because it reprograms the metabolism in order to sustain a high metabolic rate, typical of cancer. An interesting byproduct of the metabolism are the so-called ROS species: free radical reactive oxygen species that are cytotoxic. Because of the rapid metabolism of cancer cells, their level of ROS is higher than in normal cells. ROS are strong oxidizing agents and may affect the cellular biomolecules including DNA. It is worth noting that, among the nucleobases, guanine, in particular when present in a G- rich sequence, is the most oxidizable of the nucleobases, due to its low redox potential. The main product of guanine oxidation is 8-oxoguaine (8OG).

We discovered by ChIP experiments performed with an antibody specific for 8OG, that this oxidized base is more abundant in the KRAS G4 region than in genomic non- G4 regions. Starting from this finding, we investigated if 8OG in the promoter G4 motif of KRAS can somehow affect the transcription of the gene. To address this point we start by designing oligonucleotides mimicking the KRAS G4 motif, carrying 8OG modifications in different positions, either in the G- tetrads or in the 11-loop. The synthesis of these modified oligonucleotides was carried at the University of Odense (DK), with which we had a collaboration.

We discovered that 8OG can modulate the folding of the KRAS G4 motif. Circular dichroism experiments and UV-melting curves showed that 8OG strongly destabilizes G4 when the lesion is present in a G-tetrad, whereas, if it is located in a loop, it does not affect the stability of the structure. Moreover, DMS-footprinting assays confirmed that when 8OG is located in a G-run, the oxidized G-run is excluded from the formation of the G4 structure and replaced by the extra G-run present in the G4 motif (the KRAS G4 motif is composed by 5 runs of guanines). The reason why the oxidized G-run is excluded is due to the fact that N7 of 8OG becomes a donor of H-bond, whereas in wild type guanine is an acceptor. So, the presence and position of the oxidized guanine plays a crucial role in the folding of the G4 motif and in the topology of the G4 structure, which can affect its stability, interaction with transcription factors and gene transcription.

In addition to its impact on DNA folding, 8OG affects the recruitment and binding of the transcription factors to the *KRAS* promoter, as stated above. ChIP assays showed that, when the cells are treated with hydrogen peroxide (H_2O_2) - a molecule that increases the oxidative stress in the cells – the level of 8OG increases more in the G4 motif than in non-G4 motif regions. We also found that the recruitment of the above transcription factors to the promoter is increased, suggesting that 8OG can be an important marker for transcription. Together our data suggest that in pancreatic cancer cells a moderate increment in the level of ROS affects favourably transcription in the sense that ROS stimulate the expression of KRAS, which is necessary for cell growth.

So, we can conclude that ROS may be an important player in KRAS expression and tumour progression. However, high levels of ROS can be cytotoxic and even if ROS are upregulated in cancer cells, their level is strictly controlled by the cells to avoid cellular conditions that may favour apoptosis instead of proliferation. It is known that the redox homeostasis is regulated by Nrf2 which maintains the ROS equilibrium at levels suitable with cell growth. In the light of data reported in literature [62], we investigated the response of Nrf2 expression from ROS and found that there is a strict correlation between ROS and Nrf2 in pancreatic cancer cells. Interestingly, we also found that KRAS controls the expression of Nrf2 as the ectopic expression of mutant KRAS upregulates Nrf2. Since Nrf2 is stimulated by both ROS and KRAS, we asked if ROS upregulates KRAS as well. We discovered by Western blots and RT-PCR experiments that when the level of ROS in the cells is increased by H_2O_2, the expression of KRAS is also increased,

suggesting that ROS function as KRAS stimulators. In the light of these data, we asked how ROS upregulate KRAS. We have hypothesized that this occurs through a mechanism involving oxidation at the G4 motif, which is known to play an essential role in the transcription of the gene. We reasoned that the relatively high level of oxidative stress present in pancreatic cancer cells favours the oxidation of guanine, in particular in the G-runs of the G4 motif, as supported by ChIP data. This oxidative event stimulates the recruitment to the promoter of the transcription factors essential for transcription, suggesting that 8OG may function as an epigenetic marker for transcription. But it should be noted that 8OG is a mutagenic DNA lesion that is repaired by glycosylase hOGG1 when the G4 motif leaves the G4 conformation and assumes the canonical duplex conformation. This occurs when the transcription factors binds to the oxidized G4 structure. We surprisingly found that upon binding they unfold the structure and promote the transition of the G4 motif from the folded to the duplex form. In the duplex form, hOGG1 excises 8OG creating an apurinic site that is repaired by BER system. After BER, a transcription machinery involving RNA Pol II is formed at the promoter and transcription is activated. As proposed by Boldogh and co-workers [205,215], hOGG1 excises 8OG and binds tightly to it, forming a complex that acts as a guanine nucleotide exchange factor. This complex contributes to the activation of protein KRAS by promoting the transformation of KRAS-GDP to KRAS-GTP. It is possible that this mechanism play an important role in KRAS activation in tumour cells, but further work is necessary to fully address this issue.

In addition to the control of the redox homeostasis, we found that the ROS/KRAS/Nrf2 axis is also linked to survival and apoptosis pathways. This involves NF-κB, Snail and RKIP. The expression of these proteins are sensitive to ROS. In fact, our data show that low ROS levels result in the upregulation of NF-κB and pro-survival Snail and in the simultaneous downregulation of pro-apoptotic RKIP. This gene expression pattern favours cell proliferation. By contrast, high ROS favour apoptosis by upregulating pro-apoptotic RKIP and downregulating NF-κB and pro-survival Snail. There is a clear interconnection between the ROS-KRAS-Nrf2 axis and the NF κB-Snail-RKIP pathway. Considering that KRAS controls the ROS homeostasis via Nrf2 and that the ROS-homeostasis controls, in turn, the survival and apoptosis pathways, KRAS is a key gene for the proliferation of pancreatic cancer cells. Indeed, the suppression of this oncogene

results in the inhibition of cell proliferation and activation of apoptosis. Now we can understand the molecular basis of this behaviour. When KRAS is inhibited, Nrf2 is not stimulated and endogenous ROS increases to higher levels. Enhanced ROS inhibits NF-κB which in turn downregulates Snail and simultaneously upregulate RKIP. As RKIP is a pro-apoptotic gene, the gene expression profile activated by enhance ROS is consistent with apoptosis.

Finally, the data of this PhD work are useful in the design of effective PDT treatments for pancreatic cancer. PDT is a treatment modality involving a photosensitizer that, upon irradiation at a given wavelength, generates ROS that can kill cancer cells. Since ROS stimulates Nrf2, the ROS produced by PDT are partly detoxified by the anti-ossification programs activated by Nrf2. In the presence of active Nrf2, PDT will be effective if it overcomes the action of Nrf2. In the light of this behaviour, the generation of ROS in the presence of an inhibitor of Nrf2, i.e. under conditions in which the cellular defences against oxidative stress are suppressed, may render PDT more efficient. To support this prove-of-concept we performed some preliminary experiments by treating photodynamically (fluence 7.2 J/cm^2) Panc-1 and BX-PC3 cells with a cationic porphyrin (TMPyP4) or with TMPyP4 and luteolin, an inhibitor of Nrf2. We found indeed that when PDT is combined with luteolin (adjuvant), the cells become more sensitive to PDT treatment. By measuring the number of cell colonies after 8 days of growth, TMPyP4 + Luteolin reduced the colonies by 50 %, while TMPyP4 alone by only 25 %. These results strongly support our hypothesis that when Nfr2 is inhibited, the cells are more sensitive to PDT as the Nrf2-directed antioxidant program is inhibited. These results provide the molecular basis for the design of innovative PDT treatment by using a photosensitizer and an adjuvant molecule that reduces the detoxification pathways of cancer cells.

Another topic of this PhD program was to find out molecules that specifically suppress KRAS. I have investigated the capacity of a miRNA aberrantly downregulated in PDAC (miR-216b) to inhibit the expression of KRAS in pancreatic cancer cells. We focused on miR-216b, which has been identified in three different databases. In collaboration with the University of Odense (DK), we designed single-stranded miRNA mimics modified with unlocked nucleic acid (UNA) in order to improve their resistance in the cells. We demonstrated that designed miRNAs strongly suppress KRAS in pancreatic cancer cells

through on AGO dependent mechanism. We also modified miR- 216b with a palmityl chain in order to anchor it to the surface of palmitoyl- oleyl- phosphatidylcholine (POPC) liposomes, which in turn were functionalized with cell penetrating peptides. These nanoparticles were tested in two different pancreatic cancer cell lines and efficiently decreased colony formation: a promising result for further studies.

BIBLIOGRAPHY

1. Cogoi, S. & Xodo, L. E. G-quadruplex formation within the promoter of the KRAS proto-oncogene and its effect on transcription. *Nucleic Acids Res.* **34,** 2536–2549 (2006).

2. Siegel, R. L., Miller, K. D. & Jemal, A. Cancer statistics, 2018. *CA. Cancer J. Clin.* **68,** 7–30 (2018).

3. Vincent, A., Herman, J., Schulick, R., Hruban, R. H. & Goggins, M. Pancreatic cancer. *Lancet* **378,** 607–620 (2011).

4. Kamisawa, T., Wood, L. D., Itoi, T. & Takaori, K. Pancreatic cancer. *Lancet* **388,** 73–85 (2016).

5. Mohammed, S., Van Buren, G. & Fisher, W. E. Pancreatic cancer: Advances in treatment. *World J. Gastroenterol.* **20,** 9354–9360 (2014).

6. Del Chiaro, M., Segersvärd, R., Löhr, M. & Verbeke, C. Early detection and prevention of pancreatic cancer: Is it really possible today? *World J. Gastroenterol.* **20,** 12118–12131 (2014).

7. Cox, A. D. & Der, C. J. Ras history: The saga continues. *Small GTPases* **1,** 2–27 (2010).

8. Harvey, J. J. An Unidentified Virus which causes the Rapid Production of Tumours in Mice. *Nature* **204,** 1104 (1964).

9. Kirsten, W. H. & Mayer, L. A. Morphologic responses to a murine erythroblastosis virus. J. Natl Cancer Inst. 39 , 311 – 335 (1967). **335,** 1967 (1967).

10. Malumbres, M. & Barbacid, M. RAS oncogenes: The first 30 years. *Nat. Rev. Cancer* **3,** 459–465 (2003).

11. Scolnick, E. M., Rands, E., Williams, D. & Parks, W. P. Studies on the nucleic acid sequences of Kirsten sarcoma virus: a model for formation of a mammalian RNA-containing sarcoma virus. *J. Virol.* **12,** 458–63 (1973).

12. Willingham, M. C., Pastan, I., Shih, T. Y. & Scolnick, E. M. Localization of the src gene product of the Harvey strain of MSV to plasma membrane of transformed cells by electron microscopic immunocytochemistry. *Cell* **19,** 1005–1014 (1980).

13. Scolnick, E. M., Papageorge, A. G. & Shih, T. Y. Guanine nucleotide-binding activity as an assay for src protein of rat-derived murine sarcoma viruses. *Proc. Natl. Acad. Sci.* **76,** 5355–5359 (1979).

14. Scolnick, E. M. & Parks, W. P. Harvey sarcoma virus: a second murine type C sarcoma virus with rat genetic information. *J. Virol.* **13,** 1211–9 (1974).

15. Der, C. J., Krontiris, T. G. & Cooper, G. M. Transforming genes of human bladder and lung carcinoma cell lines are homologous to the ras genes of Harvey and Kirsten sarcoma viruses. *Proc. Natl. Acad. Sci. U. S. A.* **79,** 3637–40 (1982).

16. Chang, E. H., Gonda, M. A., Ellis, R. W., Scolnick, E. M. & Lowy, D. R. Human genome contains four genes homologous to transforming genes of Harvey and Kirsten murine sarcoma viruses. *Proc. Natl. Acad. Sci.* **79,** 4848–4852 (1982).

17. Takashima, A. and Faller, D. V. Targeting the RAS oncogene. *Expert Opin. Ther. Targets* **17,** 507–531 (2013).

18. Lowy, D. R. & Willumsen, B. M. Function and Regulation of Ras. *Annu. Rev. Biochem.* **62,** 851–891 (1993).

19. Goldfinger, L. E. & Michael, J. V. Regulation of Ras signaling and function by plasma membrane microdomains. *Biosci. Trends* **11,** 23–40 (2017).

20. Moores, S. L., Schaber, M. D., Mosser, S. D., Rands, E., O'Hara, M. B., Garsky, V. M., Marshall, M. S., Pompliano, D. L. and Gibbs, J. B. Sequence dependence of protein isoprenylation. *J. Biol. Chem.* **266,** 14603–14610 (1991).

21. Zeitouni, D., Pylayeva-Gupta, Y., Der, C. J. & Bryant, K. L. KRAS mutant pancreatic cancer: No lone path to an effective treatment. *Cancers* **8,** (2016).

22. Maertens, O. & Cichowski, K. An expanding role for RAS GTPase activating proteins (RAS GAPs) in cancer. *Adv. Biol. Regul.* **55,** 1–14 (2014).

23. Rajalingam, K., Schreck, R., Rapp, U. R. & Albert, Š. Ras oncogenes and their downstream targets. *Biochim. Biophys. Acta - Mol. Cell Res.* **1773,** 1177–1195 (2007).

24. Scheffzek, K., Ahmadian, M. R., Kabsch, W., Wiesmüller, L., Lautwein, A., Schmitz, F. and Wittinghofer, A. The Ras-RasGAP complex: Structural basis for GTPase activation and its loss in oncogenic ras mutants. *Science* **277,** 333–338 (1997).

25. Bos, J., Rehmann, H. & Wittinghofer, A. GEFs and GAPs : Critical Elements in the Control of Small G Proteins. *Cell* **129,** 865–877 (2007).

26. Vetter, I. R. & Wittinghofer, A. The Guanine in Switch Three Dimensions. *Science (80-.).* **294,** 1299–1304 (2001).

27. Boriack-Sjodin, P. A., Margarit, S. M., Bar-Sagi, D. & Kuriyan, J. The structural basis of the activation of Ras by Sos. *Nature* **394,** 337–343 (1998).

28. Bryant, K. L., Mancias, J. D., Kimmelman, A. C. & Der, C. J. KRAS: Feeding pancreatic cancer proliferation. *Trends Biochem. Sci.* **39,** 91–100 (2014).

29. Tuveson, D. A., Shaw, A. T., Willis, N. A., Silver, D. P., Jackson, E. L., Chang, S., Mercer, K. L., Grochow, R., Hock, H., Crowley, D., Hingorani, S. R., Zaks, T., King, C., Jacobetz, M. A., Wang, L., Bronson, R. T., Orkin, S. H., DePinho, R. A. and Jack, T. Endogenous oncogenic K-ras G12D stimulates proliferation and widespread neoplastic and developmental defects. *Cancer Cell* **5,** 375–387 (2004).

30. Collins, M. A, Bednar, F., Zhang, Y., Brisset, J., Galbán, S., Galbán, C. J., Rakshit, S., Flannagan, K. S., Adsay, N. V. and Pasca di Magliano, M. Oncogenic Kras is required for both the initiation and maintenance of pancreatic cancer in mice. *J. Clin. Invest.* **122,** 639–653 (2012).

31. Ying, H., Kimmelman, A. C., Lyssiotis, C. A., Hua, S., Chu, G. C., Fletcher-Sananikone, E., Locasale, J. W., Son, J., Zhang, H., Coloff, J. L., Yan, H., Wang, W., Chen, S., Viale, A., Zheng, H., Paik, J., Lim, C., Guimaraes, A. R., Martin, E. S., Chang, J, R. A. Oncogenic Kras Maintains Pancreatic Tumors through Regulation of Anabolic Glucose Metabolism. *Cell* **149,** 656–670 (2012).

32. Di Magliano, M. P. & Logsdon, C. D. Roles for KRAS in pancreatic tumor development and progression. *Gastroenterology* **144,** 1220–1229 (2013).

33. Morris IV, J. P., Cano, D. A., Sekine, S., Wang, S. C. & Hebrok, M. β-catenin blocks Kras-dependent reprogramming of acini into pancreatic cancer precursor lesions in mice. *J. Clin. Invest.* **120,** 508–520 (2010).

34. Fisher, G. H., Wellen, S. L., Klimstra, D., Lenczowski, J. M., Tichelaar, J. W., Lizak, M. J., Whitsett, J. A., Koretsky, A. and Varmus, H. E. Induction and apoptotic regression of lung adenocarcinomas by regulation of a K-Ras transgene in the presence and absence of tumor suppressor genes. *Genes Dev.* **15,** 3249–3262 (2001).

35. Chin, L., Tam, A., Pomerantz, J., Wong, M., Holash, J., Bardeesy, N., Shen, Q., O'Hagan, R., Pantginis, J., Zhou, H., Horner, J. W., Cordon-Cardo, C., Yancopoulos, G. D. and DePinho, R. A. Essential role for oncogenic Ras in tumour maintenance. *Nature* **400,** 468–472 (1999).

36. Heiden, M. G. V., Cantley, L. C. and Thompson, C. B. Understanding the Warburg Effect : The Metabolic Requirements of Cell Proliferation. *Science* **324,** 1029–1033 (2009).

37. Liberti, M. V. & Locasale, J. W. The Warburg Effect: How Does it Benefit Cancer Cells? *Trends Biochem Sci* **41,** 211–218 (2016).

38. Luengo, A., Gui, D. Y. & Vander Heiden, M. G. Targeting Metabolism for Cancer Therapy. *Cell Chem. Biol.* **24,** 1161–1180 (2017).

39. Son, J., Lyssiotis, C. A., Ying, H., Wang, X., Hua, S., Ligorio, M., Perera, R. M., Ferrone, C. R., Mullarky, E., Shyh-Chang, N., Kang, Y., Fleming, J. B., Bardeesy, N., Asara, J. M., Haigis, M. C., DePinho, R. A., C. L. C. and K. A. C. Glutamine supports pancreatic cancer growth through a Kras-regulated metabolic pathway. *Nature* **496,** 101–105 (2013).

40. Cantor, J. R. & Sabatini, D. M. Cancer cell metabolism: One hallmark, many faces. *Cancer Discov.* **2,** 881–898 (2012).

41. DeBerardinis, R. J. & Cheng, T. The diverse functions of glutamine in metabolism, cell biology and cancer. *Oncogene* **29,** 313–324 (2010).

42. Prior, I. A., Lewis, P. D. & Mattos, C. A comprehensive survey of ras mutations in cancer. *Cancer Res.* **72,** 2457–2467 (2012).

43. Cox, A. D., Fesik, S. W., Kimmelman, A. C., Luo, J. & Der, C. J. Drugging the undruggable RAS: Mission Possible? *Nat. Rev. Drug Discov.* **13,** (2014).

44. Grant, B. J., Lukman, S., Hocker, H. J., Sayyah, J., Brown, J. H., McCammon, J. A. and Gorfe, A. A. Novel Allosteric Sites on Ras for Lead Generation. *PLoS One* **6,** 1–10 (2011).

45. Buhrman, G., O'Connor, C., Zerbe, B., Kearney, B. M., Napoleon, R., Kovrigina, E. A., Vajda, S., Kozakov, D., Kovrigin, E. L. and Mattos, C. Analysis of Binding Site Hot Spots on the Surface of Ras GTPase. *J. Mol. Biol.* **413,** 773–789 (2011).

46. Fuhrman, S., Hendrickson, T., Kissinger, C. and Love, R. Ras Oncoprotein Inhibitors: the Discovery of Potent, Ras Nucleotide Exchange Inhibitors and the Structural Determination of a Drug-Protein Complex. *Bioorg. Med. Chem.* **5,** 125–133 (1997).

47. Herrmann, C., Block, C., Geisen, C., Haas, K., Weber, C., Winde, G., Möröy, T. and Müller, O. Sulindac sulfide inhibits Ras signaling. *Oncogene* **17,** 1769–1776 (1998).

48. González-pérez, V., Reiner, D. J., Alan, J. K., Mitchell, C., Edwards, L. J., Khazak, V., Der, C. J. and & Cox, A. D. Genetic and functional characterization of putative Ras / Raf interaction inhibitors in C . elegans and mammalian cells. *J. Mol. Signal.* **5,** 1–14 (2010).

49. Kato-Stankiewicz, J., Hakimi, I., Zhi, G., Zhang, J., Serebriiskii, I., Guo, L., Edamatsu, H., Koide, H., Menon, S., Eckl, R., Sakamuri, S., Lu, Y., Chen, Q. Z., Agarwal, S., Baumbach, W. R., Golemis, E. A., Tamanoi, F. and Khazak, V. Inhibitors of Ras/Raf-1 interaction identified by two-hybrid screening revert Ras-dependent transformation phenotypes in

human cancer cells. *Proc. Natl. Acad. Sci.* **99,** 14398–14403 (2002).

50. Maurer, T., Garrenton, L. S., Oh, A., Pitts, K., Anderson, D. J., Skelton, N. J., Fauber, B. P., Pan, B., Malek, S., Stokoe, D., Ludlam, M. J. C., Bowman, K. K., Wu, J., Giannetti, A. M., Starovasnik, M. A., Mellman, I., Jackson, P. K., Rudolph, J., Wang, G. Small-molecule ligands bind to a distinct pocket in Ras and inhibit SOS-mediated nucleotide exchange activity. *Proc. Natl. Acad. Sci.* **109,** 5299–5304 (2012).

51. Appels N. M. G. M., B. J. H. and S. J. H. M. Development of Farnesyl Transferase Inhibitors: A Review. *Oncologist* **10,** 565–578 (2005).

52. Cox, A. D. & Der, C. J. Farnesyltransferase inhibitors: Promises and realities. *Curr. Opin. Pharmacol.* **2,** 388–393 (2002).

53. Berndt, N., Hamilton, A. D. & Sebti, S. M. Targeting protein prenylation for cancer therapy. *Nat. Rev. Cancer* **11,** 775–791 (2011).

54. Whyte, D. B., Kirschmeier, P., Hockenberry, T. N., Nunez-Oliva, I., James, L., Catino, J. J., Bishop, W. R. and Pai, J. K. K- and N-Ras are Geranylgeranylated in Cells Treated with Farnesyl Protein Transferase Inhibitors. *J. Biol. Chem.* **272,** 14459–14464 (1997).

55. Lobell, R. B., Omer, C. A., Abrams, M. T., Bhimnathwala, H. G., Brucker, M. J., Buser, C. A., Davide, J. P., DeSolms, S. J., Dinsmore, C. J., Ellis-Hutchings, M. S., Kral, A. M., Liu, D., Lumma, W. C., Machotka, S. V., Rands, E., Williams, T. M., Graham, N. E. Evaluation of Farnesyl:Protein Transferase and Geranylgeranyl:Protein Transferase Inhibitor Combinations in Preclinical Models. *Cancer Res.* **61,** 8758–8768 (2001).

56. Wilhelm, S. M., Carter, C., Tang, L. Y., Wilkie, D., McNabola, A., Rong, H., Chen, C., Zhang, X., Vincent, P., McHugh, M., Cao, Y., Shujath, J., Gawlak, S., Eveleigh, D., Rowley, B., Liu, L., Adnane, L., Lynch, M., Auclair, D., Taylor, I., Gedrich, R., Vo, P. A. BAY 43-9006 exhibits broad spectrum oral antitumor activity and targets the RAF/MEK/ERK pathway and receptor tyrosine kinases involved in tumor progression and angiogenesis. *Cancer Res.* **64,** 7099–7109 (2004).

57. Engelman, J. A., Chen, L., Tan, X., Crosby, K., Guimaraes, A. R., Upadhyay, R., Maira, M., McNamara, K., Perera, S. A., Song, Y., Chirieac, L. R., Kaur, R., Lightbown, A., Simendinger, J., Li, T., Padera, R. F., García-Echeverría, C., Weissleder, R., Mahm, K.-K. Effective use of PI3K and MEK inhibitors to treat mutant Kras G12D and PIK3CA H1047R murine lung cancers. *Nat. Med.* **14,** 1351–1356 (2008).

58. Freeman, A. K., Ritt, D. A. & Morrison, D. K. Effects of Raf Dimerization and Its Inhibition on Normal and Disease-Associated Raf Signaling. *Mol. Cell* **49,** 751–758 (2013).

59. Muller, F. L., Aquilanti, E. A. & Depinho, R. A. Collateral Lethality: A New Therapeutic Strategy in Oncology. *Trends in Cancer* **1,** 161–173 (2015).

60. Shukla, K., Ferraris, D. V., Thomas, A. G., Stathis, M., Duvall, B., Delahanty, G., Alt, J., Rais, R., Rojas, C., Cao, P., Xiang, Y., Dang, C. V., Slusher, B. S. and Tsukamoto, T. Design, synthesis, and pharmacological evaluation of bis-2-(5- phenylacetamido-1,2,4-thiadiazol-2-yl)ethyl sulfide 3 (BPTES) analogs as glutaminase inhibitors. *J. Med. Chem.* **55,** 10551–10563 (2012).

61. Amaravadi, R. K., Lippincott-schwartz, J., Yin, X., Weiss, W. A., Takebe, N., Timmer, W., Dipaola, R. S., Lotze, M. T. and W. E. Principles and Curret Strategies for Targeting Autophagy for Cancer Treatment. *Clin. Cancer Res.* **17,** 654–666 (2011).

62. DeNicola, G. M., Karreth, F. A., Humpton, T. J., Gopinathan, A., Wei, C., Frese, K.,

Mangal, D., Yu, K. H., Yeo, C. J., Calhoun, E. S., Scrimieri, F., Winter, J. M., Hruban, R. H., Iacobuzio-Donahue, C., Kern, S. E., Blair, I. A. and Tuveson, D. A. Oncogene-induced Nrf2 transcription promotes ROS detoxification and tumorigenesis. *Nature* **475,** 106–110 (2011).

63. Yu, S., Lu, Z., Liu, C., Meng, Y., Ma, Y., Zhao, W., Liu, J., Yu, J. and Chen, J. miRNA-96 Suppresses KRAS and Functions as a Tumor Suppressor Gene in Pancreatic Cancer. *Cancer Res.* **70,** 6015–6025 (2010).

64. Chen, X., Guo, X., Zhang, H., Xiang, Y., Chen, J., Yin, Y., Cai, X., Wang, K., Wang, G. & Ba, Y., Zhu, L., Wang, J., Yang, R., Zhang, Y., Ren, Z., Zen, K., Zhang, J., Zhang, C. Y. Role of miR-143 targeting KRAS in colorectal tumorigenesis. *Oncogene* **28,** 1385–1392 (2009).

65. Lavrado, J., Brito, H., Borralho, P. M., Ohnmacht, S. A., Kim, N., Leitão, C., Pisco, S., Gunaratnam, M., Rodrigues, C. M. P., Moreira, R., Neidle, S. and Paulo, A. KRAS oncogene repression in colon cancer cell lines by G-quadruplex binding indolo[3,2-c]quinolines. *Sci. Rep.* **5,** 1–10 (2015).

66. Garzon, R., Calin, G. A. & Croce, C. M. MicroRNAs in Cancer. *Annu. Rev. Med.* **60,** 167–179 (2009).

67. Iwakawa, H. oki & Tomari, Y. The Functions of MicroRNAs: mRNA Decay and Translational Repression. *Trends Cell Biol.* **25,** 651–665 (2015).

68. Jonas, S. & Izaurralde, E. Towards a molecular understanding of microRNA-mediated gene silencing. *Nat. Rev. Genet.* **16,** 421–433 (2015).

69. Johnson, S. M., Grosshans, H., Shingara, J., Byrom, M., Jarvis, R., Cheng, A., Labourier, E., Reinert, K. L., Brown, D. and Slack, F. J. RAS is regulated by the let-7 microRNA family. *Cell* **120,** 635–647 (2005).

70. Deng, M., Tang, H., Zhou, Y., Zhou, M., Xiong, W., Zheng, Y., Ye, Q., Zeng, X., Liao, Q., Guo, X., Li, X., Ma, J. and Li, G. miR-216b suppresses tumor growth and invasion by targeting KRAS in nasopharyngeal carcinoma. *J. Cell Sci.* **124,** 2997–3005 (2011).

71. Ling, H., Fabbri, M. & Calin, G. A. MicroRNAs and other non-coding RNAs as targets for anticancer drug development. *Nat. Rev. Drug Discov.* **12,** 847–865 (2013).

72. Saini, N., Zhang, Y., Usdin, K. & Lobachev, K. S. When secondary comes first-The importance of non-canonical DNA structures. *Biochimie* **95,** 117–123 (2013).

73. Kamenetskii, M. D. F. Triplex DNA Structures. *Annu. Rev. Biochem.* **64,** 65–95 (1995).

74. Maruyama, A., Mimura, J., Harada, N. & Itoh, K. Nrf2 activation is associated with Z-DNA formation in the human HO-1 promoter. *Nucleic Acids Res.* **41,** 5223–5234 (2013).

75. Miglietta, G., Cogoi, S., Pedersen, E. B. & Xodo, L. E. GC-elements controlling HRAS transcription form i-motif structures unfolded by heterogeneous ribonucleoprotein particle A1. *Sci. Rep.* **5,** 1–13 (2015).

76. Nadel, J., Athanasiadou, R., Lemetre, C., Wijetunga, N. A., Ó Broin, P., Sato, H., Zhang, Z., Jeddeloh, J., Montagna, C., Golden, A., Seoighe, C. and Greally, J. M. RNA:DNA hybrids in the human genome have distinctive nucleotide characteristics, chromatin composition, and transcriptional relationships. *Epigenetics and Chromatin* **8,** 1–19 (2015).

77. Qin, T., Liu, K., Song, D., Yang, C., Zhao, H. and Su, H. Binding interactions of zinc cationic porphyrin with duplex DNA: From B-DNa to Z-DNA. *Int. J. Mol. Sci.* **19,** 1–12

(2018).

78. Brázda, V., Laister, R. C., Jagelská, E. B. & Arrowsmith, C. Cruciform structures are a common DNA feature important for regulating biological processes. *BMC Mol. Biol.* **12,** 33 (2011).

79. Kaushik, M., Kaushik, S., Roy, K., Singh, A., Mahendru, S., Kumar, M., Chaudhary, S., Ahmed, S. and Kukreti, S. A bouquet of DNA structures: Emerging diversity. *Biochem. Biophys. Reports* **5,** 388–395 (2016).

80. Wang, G. and Vasquez, K. M. Impact of alternative DNA structures on DNA damage, DNA repair, and genetic instability. *DNA Repair* **19,** 143–151 (2014).

81. Bang, I. Investigations on guanylic acid. *Biochem Z.* **26,** 293–311 (1910).

82. Gellert, M., Lipsett, M. N. & Davies, D. R. Helix Formation By Guanylic Acid. *Proc. Natl. Acad. Sci.* **48,** 2013–2018 (1962).

83. Rhodes, D. & Lipps, H. J. Survey and summary G-quadruplexes and their regulatory roles in biology. *Nucleic Acids Res.* **43,** 8627–8637 (2015).

84. Lane, A. N., Chaires, J. B., Gray, R. D. & Trent, J. O. Stability and kinetics of G-quadruplex structures. *Nucleic Acids Res.* **36,** 5482–5515 (2008).

85. Piazza, A., Adrian, M., Samazan, F., Heddi, B., Hamon, F., Serero, A., Lopes, J., Teulade-Fichou, M.-P., Phan, A. T. and Nicolas, A. Short loop length and high thermal stability determine genomic instability induced by G-quadruplex-forming minisatellites. *EMBO J.* **34,** 1718–1734 (2015).

86. Burge, S., Parkinson, G. N., Hazel, P., Todd, A. K. & Neidle, S. Quadruplex DNA: Sequence, topology and structure. *Nucleic Acids Res.* **34,** 5402–5415 (2006).

87. Cogoi, S. & Xodo, L. E. G4 DNA in ras genes and its potential in cancer therapy. *Biochim. Biophys. Acta* **1859,** 663–674 (2016).

88. Balasubramanian, S., Hurley, L. H. & Neidle, S. Targeting G-quadruplexes in gene promoters: A novel anticancer strategy? *Nat. Rev. Drug Discov.* **10,** 261–275 (2011).

89. Huppert, J. L. & Balasubramanian, S. Prevalence of quadruplexes in the human genome. *Nucleic Acids Res.* **33,** 2908–2916 (2005).

90. Maizels, N. G4 motifs in human genes. *Ann N Y Acad Sci* **1267,** 53–60 (2012).

91. Lam, E. Y. N., Beraldi, D., Tannahill, D. & Balasubramanian, S. G-quadruplex structures are stable and detectable in human genomic DNA. *Nat. Commun.* **4,** (2013).

92. Du, Z., Zhao, Y. and Li, N. Genome-wide analysis reveals regulatory role of G4 DNA in gene transcription. *Genome Res.* **18,** 233–241 (2008).

93. Lipps, H. J. & Rhodes, D. G-quadruplex structures: in vivo evidence and function. *Trends Cell Biol.* **19,** 414–422 (2009).

94. Brooks, T. A., Kendrick, S. & Hurley, L. Making sense of G-quadruplex and i-motif functions in oncogene promoters. *FEBS J.* **277,** 3459–3469 (2010).

95. Zahler, A. M., Williamson, J. R., Cech, T. R. & Prescott, D. M. Inhibition of telomerase by G-quartet DMA structures. *Nature* **350,** 718–720 (1991).

96. Neidle, S. & Read, M. A. G-quadruplexes as therapeutic targets. *Biopolymers* **56,** 195–

208 (2000).

97. Patel, D. J., Phan, A. T. & Kuryavyi, V. Human telomere, oncogenic promoter and 5′-UTR G-quadruplexes: diverse higher order DNA and RNA targets for cancer therapeutics. *Nucleic Acids Res.* **35,** 7429–7455 (2007).

98. Bedrat, A., Lacroix, L. & Mergny, J. L. Re-evaluation of G-quadruplex propensity with G4Hunter. *Nucleic Acids Res.* **44,** 1746–1759 (2016).

99. Risitano, A. & Fox, K. R. Influence of loop size on the stability of intramolecular DNA quadruplexes. *Nucleic Acids Res.* **32,** 2598–2606 (2004).

100. Hazel, P., Huppert, J., Balasubramanian, S. & Neidle, S. Loop-length-dependent folding of G-quadruplexes. *J. Am. Chem. Soc.* **126,** 16405–16415 (2004).

101. Todd, A. K. Bioinformatics approaches to quadruplex sequence location. *Methods* **43,** 246–251 (2007).

102. Hänsel-Hertsch, R., Di Antonio, M. & Balasubramanian, S. DNA G-quadruplexes in the human genome: Detection, functions and therapeutic potential. *Nat. Rev. Mol. Cell Biol.* **18,** 279–284 (2017).

103. Takahashi, H., Nakagawa, A., Kojima, S., Takahashi, A., Cha, B. Y., Woo, J. T., Nagai, K., Machida, Y. and Machida, C. Discovery of novel rules for G-quadruplex-forming sequences in plants by using bioinformatics methods. *J. Biosci. Bioeng.* **114,** 570–575 (2012).

104. Mullen, M. A., Olson, K. J., Dallaire, P., Major, F., Assmann, S. M. and Bevilacqua, P. C. RNA G-Quadruplexes in the model plant species Arabidopsis thaliana: prevalence and possible functional roles. *Nucleic Acids Res.* **38,** 8149–8163 (2010).

105. Griffin, B. D. & Bass, H. W. Review: Plant G-quadruplex (G4) motifs in DNA and RNA; abundant, intriguing sequences of unknown function. *Plant Sci.* **269,** 143–147 (2018).

106. Metifiot, M., Amrane, S., Litvak, S. & Andreola, M.-L. G-quadruplexes in viruses: function and potential therapeutic applications. *Nucleic Acids Res.* **42,** 12352–12366 (2014).

107. Beaume, N., Pathak, R., Yadav, V. K., Kota, S., Misra, H. S., Gautam, H. K. and Chowdhury, S. Genome-wide study predicts promoter-G4 DNA motifs regulate selective functions in bacteria: radioresistance of D. radiodurans involves G4 DNA-mediated regulation. *Nucleic Acids Res.* **41,** 76–89 (2013).

108. Hershman, S. G., Chen, Q., Lee, J. Y., Kozak, M. L., Yue, P., Wang, L. S. and Johnson, F. B. Genomic distribution and functional analyses of potential G-quadruplex-forming sequences in Saccharomyces cerevisiae. *Nucleic Acids Res.* **36,** 144–156 (2008).

109. Zhao, Y., Du, Z. & Li, N. Extensive selection for the enrichment of G4 DNA motifs in transcriptional regulatory regions of warm blooded animals. *FEBS Lett.* **581,** 1951–1956 (2007).

110. Schaffitzel, C., Berger, I., Postberg, J., Hanes, J., Lipps, H. J. and Pluckthun, A. In vitro generated antibodies specific for telomeric guanine-quadruplex DNA react with Stylonychia lemnae macronuclei. *Proc. Natl. Acad. Sci.* **98,** 8572–8577 (2001).

111. Biffi, G., Tannahill, D., McCafferty, J. & Balasubramanian, S. Quantitative visualization of DNA G-quadruplex structures in human cells. *Nat. Chem.* **5,** 182–186 (2013).

112. Chambers, V. S., Marsico, G., Boutell, J. M., Di Antonio, M., Smith, G. P. and Balasubramanian, S. High-throughput sequencing of DNA G-quadruplex structures in the human genome. *Nat. Biotechnol.* **33,** 877–881 (2015).

113. Hänsel-Hertsch, R., Beraldi, D., Lensing, S. V., Marsico, G., Zyner, K., Parry, A., Di Antonio, M., Pike, J., Kimura, H., Narita, M., Tannahill, D. and Balasubramanian, S. G-quadruplex structures mark human regulatory chromatin. *Nat. Genet.* **48,** 1267–1272 (2016).

114. Li, W., Wu, P., Ohmichi, T. & Sugimoto, N. Characterization and thermodynamic properties of quadruplex / duplex competition. *FEBS Lett.* **526,** 77–81 (2002).

115. Moyzis, R. K., Buckingham, J. M., Cram, L. S., Dani, M., Deaven, L. L., Jones, M. D., Meyne, J., Ratliff, R. L. and Wu, J. R. A highly conserved repetitive DNA sequence, (TTAGGG)n, present at the telomeres of human chromosomes. *Proc. Natl. Acad. Sci.* **85,** 6622–6626 (1988).

116. Greider, C. W. & Blackburn, E. H. Identification of a specific telomere terminal transferase activity in tetrahymena extracts. *Cell* **43,** 405–413 (1985).

117. Kim, N.W., Piatyszek, K. R., Prowse, Karen R., Harley, C. B., West, M. D., Ho, P. L., Coviello, G. M., Wright, W. E., Weinrich, S. L. and Shay, J. W. Specific Association of Human Telomerase Activity with Immortal Cells and Cancer. *Science* **226,** 2011–2015 (1994).

118. Oganesian, L., Moon, I. K., Bryan, T. M. & Jarstfer, M. B. Extension of G-quadruplex DNA by ciliate telomerase. *EMBO J.* **25,** 1148–1159 (2006).

119. Burger, A. M., Dai, F., Schultes, C. M., Burger, A. M., Dai, F., Schultes, C. M., Reszka, A. P., Moore, M. J., Double, J. A. and Neidle, S. The G-Quadruplex-Interactive Molecule BRACO-19 Inhibits Tumor Growth , Consistent with Telomere Targeting and Interference with Telomerase Function Growth , Consistent with Telomere Targeting and Interference with Telomerase Function. *Cancer Res.* **65,** 1489–1496 (2005).

120. Zhou, G., Liu, X., Li, Y., Xu, S. & Ma, C., Wu, X., Cheng, Y., Yu, Z., Zhao, G. and Chen, Y. Telomere targeting with a novel G-quadruplex-interactive ligand BRACO-19 induces T-loop disassembly and telomerase displacement in human glioblastoma cells. *Oncotarget* **7,** 14925–14939 (2016).

121. Neidle, S. Human telomeric G-quadruplex: The current status of telomeric G-quadruplexes as therapeutic targets in human cancer. *FEBS J.* **277,** 1118–1125 (2010).

122. Huppert, J. L. & Balasubramanian, S. G-quadruplexes in promoters throughout the human genome. *Nucleic Acids Res.* **35,** 406–413 (2007).

123. Eddy, J. & Maizels, N. Gene function correlates with potential for G4 DNA formation in the human genome. *Nucleic Acids Res.* **34,** 3887–3896 (2006).

124. Bochman, M. L., Paeschke, K. & Zakian, V. A. DNA secondary structures: Stability and function of G-quadruplex structures. *Nat. Rev. Genet.* **13,** 770–780 (2012).

125. Paramasivam, M., Membrino, A., Cogoi, S., Fukuda, H., Nakagama, H. and Xodo, L. E. Protein hnRNP A1 and its derivative Up1 unfold quadruplex DNA in the human KRAS promoter: implications for transcription. *Nucleic Acids Res.* **37,** 2841–2853 (2009).

126. Fleming, A. M. & Burrows, C. J. 8-Oxo-7,8-dihydroguanine, friend and foe: Epigenetic-like regulator versus initiator of mutagenesis. *DNA Repair* **56,** 75–83 (2017).

127. Rankin, S., Reszka, A. P., Huppert, J., Zloh, M., Parkinson, G. N., Todd, A. K., Ladame, S., Balasubramanian, S. and Neidle, S. Putative DNA quadruplex formation within the human c-kit oncogene. *J. Am. Chem. Soc.* **127,** 10584–10589 (2005).

128. Simonsson, T., Pecinka, P. and Kubista, M. DNA tetraplex formation in the control region of c-myc. *Nucleic Acids Res.* **26,** 1167–1172 (1998).

129. Siddiqui-Jain, A., Grand, C. L., Bearss, D. J. & Hurley, L. H. Direct evidence for a G-quadruplex in a promoter region and its targeting with a small molecule to repress c-MYC transcription. *Proc. Natl. Acad. Sci.* **99,** 11593–11598 (2002).

130. De Armond, R., Wood, S., Sun, D., Hurley, L. H. & Ebbinghaus, S. W. Evidence for the presence of a guanine quadruplex forming region within a polypurine tract of the hypoxia inducible factor 1α promoter. *Biochemistry* **44,** 16341–16350 (2005).

131. Sun, D., Guo, K. & Shin, Y.-J. Evidence of the formation of G-quadruplex structures in the promoter region of the human vascular endothelial growth factor gene. *Nucleic Acids Res.* **39,** 1256–1265 (2011).

132. Sun, D., Guo, K., Rusche, J. J. & Hurley, L. H. Facilitation of a structural transition in the polypurine/polypyrimidine tract within the proximal promoter region of the human VEGF gene by the presence of potassium and G-quadruplex-interactive agents. *Nucleic Acids Res.* **33,** 6070–6080 (2005).

133. Dai, J., Dexheimer, T. S., Chen, D., Carver, M., Ambrus, A., Jones, R. A. and Yang, D. An intramolecular G-quadruplex structure with mixed parallel/antiparallel G-strands formed in the human BCL-2 promoter region in solution. *J. Am. Chem. Soc.* **128,** 1096–1098 (2005).

134. Fernando, H., Reszka, A. P., Huppert, J., Ladame, S., Rankin, S., Venkitaraman, A. R., Neidle, S. and Balasubramanian, S. A conserved quadruplex motif located in a transcription activation site of the human c-kit oncogene. *Biochemistry* **45,** 7854–7860 (2006).

135. Yarden, Y., Kuang, W. J., Yang-Feng, T., Coussens, L., Munemitsu, S., Dull, T. J., Chen, E., Schlessinger, J., Francke, U. and Ullrich, A. Human proto-oncogene c-kit: a new cell surface receptor tyrosine kinase for an unidentified ligand. *EMBO J.* **6,** 3341–51 (1987).

136. Heinrich, M. C., Griffith, D. J., Druker, B. J., Wait, C. L., Ott, K. A., Zigler, A. J. Inhibition of c-kit receptor tyrosine kinase activity by STI 571, a selective tyrosine kinase inhibitor. *Blood* **96,** 925–32 (2000).

137. McLuckie, K. I. E., Waller, Z. A. E., Sanders, D. A., Alves, D., Rodriguez, R., Dash, J., McKenzie, G. J., Venkitaraman, A. R. and Balasubramanian, S. G-Quadruplex-Binding benzo[a]phenoxazines down-regulate c-KIT expression in human gastric carcinoma cells. *J. Am. Chem. Soc.* **133,** 2658–2663 (2011).

138. Cogoi, S., Paramasivam, M., Spolaore, B. & Xodo, L. E. Structural polymorphism within a regulatory element of the human KRAS promoter: Formation of G4-DNA recognized by nuclear proteins. *Nucleic Acids Res.* **36,** 3765–3780 (2008).

139. Morgan, R. K., Batra, H., Gaerig, V. C., Hockings, J. & Brooks, T. A. Identification and characterization of a new G-quadruplex forming region within the kRAS promoter as a transcriptional regulator. *Biochim. Biophys. Acta* **1859,** 235–245 (2016).

140. Chu, P. C., Yang, M. C., Kulp, S. K., Salunke, S. B., Himmel, L. E., Fang, C. S., Jadhav, A. M., Shan, Y. S., Lee, C. T., Lai, M. D., Shirley, L. A., Bekaii-Saab, T. and Chen, C. S. Regulation

of oncogenic KRAS signaling via a novel KRAS-integrin-linked kinase-hnRNPA1 regulatory loop in human pancreatic cancer cells. *Oncogene* **35,** 3897–3908 (2016).

141. Bedard, K. & Krause, K.-H. The NOX Family of ROS-Generating NADPH Oxidases: Physiology and Pathophysiology. *Physiol. Rev.* **87,** 245–313 (2007).

142. Zhang, L. *et al.* Reactive Oxygen Species and Targeted Therapy for Pancreatic Cancer. *Oxid. Med. Cell. Longev.* **2016,** 1–9 (2016).

143. Kang, S. W., Lee, S. & Lee, E. K. ROS and energy metabolism in cancer cells: Alliance for fast growth. *Arch. Pharm. Res.* **38,** 338–345 (2015).

144. Reczek, C. R. & Chandel, N. S. ROS-dependent signal transduction. *Curr. Opin. Cell Biol.* **33,** 8–13 (2015).

145. Glasauer, A. & Chandel, N. S. Ros. *Current Biology* **23,** 100–102 (2013).

146. Schieber, M. & Chandel, N. S. ROS function in redox signaling and oxidative stress. *Curr. Biol.* **24,** R453–R462 (2014).

147. Ray, P. D., Huang, B. W. & Tsuji, Y. Reactive oxygen species (ROS) homeostasis and redox regulation in cellular signaling. *Cell. Signal.* **24,** 981–990 (2012).

148. Chio, I. I. C. & Tuveson, D. A. ROS in Cancer: The Burning Question. *Trends Mol. Med.* **23,** 411–429 (2017).

149. Dizdaroglu, M. & Jaruga, P. Mechanisms of free radical-induced damage to DNA. *Free Radic. Res.* **46,** 382–419 (2012).

150. Beer, S. M., Taylor, E. R., Brown, S. E. & Dahm, C. C., Costa, N. J., Runswick, M. J. and Murphy, M. P. Glutaredoxin 2 catalyzes the reversible oxidation and glutathionylation of mitochondrial membrane thiol proteins. *J. Biol. Chem.* **279,** 47939–47951 (2004).

151. Minard, K. I., Jennings, G. T., Loftus, T. M., Xuan, D. & McAlister-Henn, L. Sources of NADPH and expression of mammalian NADP+-specific isocitrate dehydrogenases in Saccharomyces cerevisiae. *J. Biol. Chem.* **273,** 31486–31493 (1998).

152. Lewis, C. A., Parker, S. J., Fiske, B. P., McCloskey, D., Gui, D. Y., Green, C. R., Vokes, N. I., Feist, A. M., Vander Heiden, M. G. and Metallo, C. M. Tracing Compartmentalized NADPH Metabolism in the Cytosol and Mitochondria of Mammalian Cells. *Mol. Cell* **55,** 253–263 (2014).

153. Hanukoglu, I. & Rapoport, R. Routes and regulation of NADPH production in steroidogenic mitochondria. *Endocr. Res.* **21,** 231–241 (1995).

154. Acharya, A., Das, I., Chandhok, D. & Saha, T. Redox regulation in cancer A double-edged sword with therapeutic potential. *Oxid. Med. Cell. Longev.* **3,** 23–34 (2010).

155. Schumacker, P. Reactive Oxygen Species in Cancer: A Dance with the Devil. *Cancer Cell* **27,** 156–157 (2015).

156. Denu, J. M. & Tanner, K. G. Specific and reversible inactivation of protein tyrosine phosphatases by hydrogen peroxide: Evidence for a sulfenic acid intermediate and implications for redox regulation. *Biochemistry* **37,** 5633–5642 (1998).

157. Lee, S. R., Yang, K. S., Kwon, J., Lee, C., Jeong, W. and & Rhee, S. G. Reversible inactivation of the tumor suppressor PTEN by H2O2. *J. Biol. Chem.* **277,** 20336–20342 (2002).

158. Yang, M., Haase, A. D., Huang, F. K., Coulis, G., Rivera, K. D., Dickinson, B. C., Chang, C. J., Pappin, D. J., Neubert, T. A., Hannon, G. J., Boivin, B. and Tonks, N. K. Dephosphorylation of Tyrosine 393 in Argonaute 2 by Protein Tyrosine Phosphatase 1B Regulates Gene Silencing in Oncogenic RAS-Induced Senescence. *Mol. Cell* **55,** 782–790 (2014).

159. Kamata, H., Honda, S., Maeda, S., Chang, L., Hirata, H. and Karin, M. Reactive oxygen species promote TNFα-induced death and sustained JNK activation by inhibiting MAP kinase phosphatases. *Cell* **120,** 649–661 (2005).

160. Morgan, M. J. & Liu, Z. G. Crosstalk of reactive oxygen species and NF-κB signaling. *Cell Res.* **21,** 103–115 (2011).

161. Movafagh, S., Crook, S. & Vo, K. Regulation of hypoxia-inducible Factor-1a by reactive oxygen species: New developments in an old debate. *J. Cell. Biochem.* **116,** 696–703 (2015).

162. Son, Y., Kim, S., Chung, H. T. & Pae, H. O. Reactive oxygen species in the activation of MAP kinases. *Methods Enzymol.* **528,** 27–48 (2013).

163. Vasudevan, K. M., Barbie, D. A., Davies, M. A., Rabinovsky, R., McNear, C. J., Kim, J. J., Hennessy, B. T., Tseng, H., Pochanard, P., Kim, S. Y., Dunn, I. F., Schinzel, A. C., Sandy, P., Hoersch, S., Sheng, Q., Gupta, P. B., Boehm, J. S., Reiling, J. H., E. S. & Mills, G. B., Hahn, W. C., Sellers, W. R. and Garraway, L. A. AKT-Independent Signaling Downstream of Oncogenic PIK3CA Mutations in Human Cancer. *Cancer Cell* **16,** 21–32 (2009).

164. Sosa, V., Moliné, T., Somoza, R., Paciucci, R., Kondoh, H. and & LLeonart, M. E. Oxidative stress and cancer: An overview. *Ageing Res. Rev.* **12,** 376–390 (2013).

165. Martinez-Useros, J., Li, W., Cabeza-Morales, M. & Garcia-Foncillas, J. Oxidative Stress: A New Target for Pancreatic Cancer Prognosis and Treatment. *J. Clin. Med.* **6,** 29 (2017).

166. Gupta, A., Rosenberger, S. F. & Bowden, G. T. Increased ROS levels contribute to elevated transcription factor and MAP kinase activities in malignantly progressed mouse keratinocyte cell lines. *Carcinogenesis* **20,** 2063–2073 (1999).

167. Kundu, N., Zhang, S. & Fulton, A. M. Sublethal oxidative stress inhibits tumor cell adhesion and enhances experimental metastasis of murine mammary carcinoma. *Clin. Exp. Metastasis* **13,** 16–22 (1995).

168. Pelicano, H., Lu, W., Zhou, Y., Zhang, W., Chen, Z., Hu, Y. and Huang, P. Mitochondrial dysfunction and reactive oxygen species imbalance promote breast cancer cell motility through a CXCL14-mediated mechanism. *Cancer Res.* **69,** 2375–2383 (2009).

169. Zandwijk, N., Dalesio, O., Pastorino, U., Vries, N. & Tinteren, H. EUROSCAN, a randomized trial of vitamin A and N-acetylcysteine in patients with head and neck cancer or lung cancer. *J. Natl. Cancer Inst.* **92,** 977–986 (2000).

170. Vurusaner, B., Poli, G. & Basaga, H. Tumor suppressor genes and ROS: Complex networks of interactions. *Free Radic. Biol. Med.* **52,** 7–18 (2012).

171. Cichon, M. & Radisky, D. ROS-induced epithelial-mesenchymal transition in mammary epithelial cells is mediated by NF-κB-dependent activation of Snail. *Oncotarget* **5,** 2827–38 (2014).

172. Durand, N. & Storz, P. Targeting reactive oxygen species in development and progression of pancreatic cancer. *Expert Rev. Anticancer Ther.* **17,** 19–31 (2017).

173. Lister, A., Nedjadi, T., Kitteringham, N. R., Campbell, F., Costello, E., Lioyd, B., Copple, I. M., Williams, S., Owen, A., Neoptolemos, J. P., Goldring, C. E. and Park, B. K. Nrf2 is overexpressed in pancreatic cancer: implications for cell proliferation and therapy. *Mol. Cancer* **10,** 1–13 (2011).

174. Hayes, J. D. & Dinkova-Kostova, A. T. The Nrf2 regulatory network provides an interface between redox and intermediary metabolism. *Trends Biochem. Sci.* **39,** (2014).

175. Hayes, A. J., Skouras, C., Haugk, B. & Charnley, R. M. Keap1-Nrf2 signalling in pancreatic cancer. *Int. J. Biochem. Cell Biol.* **65,** 288–299 (2015).

176. Moon, E. J. & Giaccia, A. Dual roles of NRF2 in tumor prevention and progression: Possible implications in cancer treatment. *Free Radic. Biol. Med.* **79,** 292–299 (2015).

177. Buelna-Chontal, M. & Zazueta, C. Redox activation of Nrf2 & NF-κB: A double end sword? *Cell. Signal.* **25,** 2548–2557 (2013).

178. Arlt, A., Schäfer, H. & Kalthoff, H. The 'n-factors' in pancreatic cancer: Functional relevance of NF-κB, NFAT and Nrf2 in pancreatic cancer. *Oncogenesis* **1,** (2012).

179. Nguyen, T., Nioi, P. & Pickett, C. B. The Nrf2-antioxidant response element signaling pathway and its activation by oxidative stress. *J. Biol. Chem.* **284,** 13291–13295 (2009).

180. Lau, A., Villeneuve, N. F., Sun, Z., Wong, P. K. & Zhang, D. D. Dual roles of Nrf2 in cancer. *Pharmacol. Res.* **58,** 262–270 (2008).

181. Wang, X. J., Sun, Z., Villeneuve, N. F., Zhang, S., Zhao, F., Li, Y., Chen, W., Yi, X., Zheng, W., Wondrak, G. T., Wong and P. K., Zhang, D. D. Nrf2 enhances resistance of cancer cells to chemotherapeutic drugs, the dark side of Nrf2. *Carcinogenesis* **29,** 1235–1243 (2008).

182. Kong, B., Qia, C., Erkan, M., Kleeff, J. & Michalski, C. W. Overview on how oncogenic Kras promotes pancreatic carcinogenesis by inducing low intracellular ROS levels. *Front. Physiol.* **4 SEP,** 1–5 (2013).

183. Soini, Y., Eskelinen, M., Juvonen, P., Kärjä, V., Haapasaari, K. M., Saarela, A. and Karihtala, P. Nuclear Nrf2 expression is related to a poor survival in pancreatic adenocarcinoma. *Pathol. Res. Pract.* **210,** 35–39 (2014).

184. Chio, I. I. C., Jafarnejad, S. M., Ponz-Sarvise, M., Park, Y., Rivera, K., Palm, W., Wilson, J., Sangar, V., Hao, Y., Öhlund, D., Wright, K., Filippini, D., Lee, E. J., Da Silva, B., Schoepfer, C., Wilkinson, J. E. and Buscaglia, J. M. *et al.* NRF2 Promotes Tumor Maintenance by Modulating mRNA Translation in Pancreatic Cancer. *Cell* **166,** 963–976 (2016).

185. Melis, J. P. M., van Steeg, H. & Luijten, M. Oxidative DNA Damage and Nucleotide Excision Repair. *Antioxid. Redox Signal.* **18,** 2409–2419 (2013).

186. Maynard, S., Schurman, S. H., Harboe, C., de Souza-Pinto, N. C. and Bohr, V. A. Base excision repair of oxidative DNA damage and association with cancer and aging. *Carcinogenesis* **30,** 2–10 (2009).

187. Kim, Y.-J. & M. Wilson III, D. Overview of Base Excision Repair Biochemistry. *Curr. Mol. Pharmacol.* **5,** 3–13 (2012).

188. Krokan, H. E. & Bjørås, M. Base excision repair. *Cold Spring Harb. Perspect. Biol.* **5,** 1–22 (2013).

189. David, S. S., O'Shea, V. L. & Kundu, S. Base-excision repair of oxidative DNA damage.

Nature **447,** 941–950 (2007).

190. Vorlícková, M., Tomasko, M., Sagi, A. J., Bednarova, K. & Sagi, J. 8-Oxoguanine in a quadruplex of the human telomere DNA sequence. *FEBS J.* **279,** 29–39 (2012).

191. Seifermann, M. & Epe, B. Oxidatively generated base modifications in DNA: Not only carcinogenic risk factor but also regulatory mark? *Free Radic. Biol. Med.* **107,** 258–265 (2017).

192. Pandita, T. K. Unraveling the novel function of the DNA repair enzyme 8-oxoguanine-DNA glycosylase in activating key signaling pathways. *Free Radic. Biol. Med.* **73,** 439–440 (2014).

193. German, P., Szaniszlo, P., Hajas, G., Radak, Z., Bacsi, A., Hazra, T. K., Hegde, M. L., Ba, X. and Boldogh, I. Activation of cellular signaling by 8-oxoguanine DNA glycosylase-1-initiated DNA base excision repair. *DNA Repair* **12,** 856–863 (2013).

194. Tornaletti, S., Maeda, L. S., Kolodner, R. D. & Hanawalt, P. C. Effect of 8-oxoguanine on transcription elongation by T7 RNA polymerase and mammalian RNA polymerase II. *DNA Repair (Amst).* **3,** 483–494 (2004).

195. Zarakowska, E., Gackowski, D., Foksinski, M. & Olinski, R. Are 8-oxoguanine (8-oxoGua) and 5-hydroxymethyluracil (5-hmUra) oxidatively damaged DNA bases or transcription (epigenetic) marks? *Mutat. Res.* **764–765,** 58–63 (2014).

196. Ramon, O., Sauvaigo, S., Gasparutto, D., Faure, P., Favier, A. and Cadet, J. Effects of 8-oxo-7,8-dihydro-2'-deoxyguanosine on the binding of the transcription factor Sp1 to its cognate target DNA sequence (GC box). *Free Radic. Res.* **31,** 217–229 (1999).

197. Hailer-Morrison, M. K., Kotler, J. M., Martin, B. D. & Sugden, K. D. Oxidized guanine lesions as modulators of gene transcription. Altered p50 binding affinity and repair shielding by 7,8-dihydro-8-oxo-2'-deoxyguanosine lesions in the NF-κB promoter element. *Biochemistry* **42,** 9761–9770 (2003).

198. Moore, S. P. G., Toomire, K. J. & Strauss, P. R. DNA modifications repaired by base excision repair are epigenetic. *DNA Repair* **12,** 1152–1158 (2013).

199. Klungland, A., Rosewell, I. & Hollenbach, S., Larsen, E., Daly, G., Epe, B., Seeberg, E., Lindahl, T. and Barnes, D. E. Accumulation of premutagenic DNA lesions in mice defective in removal of oxidative base damage. *Proc. Natl. Acad. Sci. U. S. A.* **96,** 13300–5 (1999).

200. Minowa, O., Arai, T., Hirano, M., Monden, Y., Nakai, S., Fukuda, M., Itoh, M., Takano, H., Hippou, Y., Aburatani, H., Masumura, K., Nohmi, T., Nishimura, S. and Noda, T. Mmh/Ogg1 gene inactivation results in accumulation of 8-hydroxyguanine in mice. *Proc. Natl. Acad. Sci.* **97,** 4156–4161 (2000).

201. Shinmura, K., Kohno, T., Kasai, H., Koda, K., Sugimura, H. and Yokota, J. Infrequent mutations of the hOGG1 gene, that is involved in the excision of 8-hydroxyguanine in damaged DNA, in human gastric cancer. *Japanese J. Cancer Res.* **89,** 825–828 (1998).

202. Chevillard, S., Radicella, J. P., Levalois, C., Lebeau, J., Poupon, M. F., Oudard, S., Dutrillaux, B. and Boiteux, S. Mutations in OGG1, a gene involved in the repair of oxidative DNA damage, are found in human lung and kidney tumours. *Oncogene* **16,** 3083–3086 (1998).

203. Mabley, J. G., Pacher, P., Deb, A., Wallace, R., Elder, R. H. and S. C. Potential role for 8-

oxoguanine DNA glycosylase in regulating inflammation. *FASEB J.* **18,** 1–18 (2004).

204. Luo, J., Hosoki, K., Bacsi, A., Radak, Z., Hegde, M. L., Sur, S., Hazra, T. K., Brasier, A. R., Ba, X. and Boldogh, I. 8-Oxoguanine DNA glycosylase-1-mediated DNA repair is associated with Rho GTPase activation and α-smooth muscle actin polymerization. *Free Radic. Biol. Med.* **73,** 430–438 (2014).

205. Boldogh, I., Hajas, G., Aguilera-Aguirre, L., Hegde, M. L., Radak, Z., Bacsi, A., Sur, S., Hazra, T. K. and Mitra, S. Activation of Ras signaling pathway by 8-oxoguanine DNA glycosylase bound to its excision product, 8-oxoguanine. *J. Biol. Chem.* **287,** 20769–20773 (2012).

206. Hill, J. W. & Evans, M. K. A novel R229Q OGG1 polymorphism results in a thermolabile enzyme that sensitizes KG-1 leukemia cells to DNA damaging agents. *Cancer Detect. Prev.* **31,** 237–243 (2007).

207. Szalai, V. A., Singer, M. J. & Thorp, H. H. Site-specific probing of oxidative reactivity and telomerase function using 7,8-dihydro-8-oxoguanine in telomeric DNA. *J. Am. Chem. Soc.* **124,** 1625–1631 (2002).

208. Sun, D., Liu, W.-J., Guo, K., Rusche, J. J., Ebbinghaus, S., Gokhale, V. and Hurley, L. H. The proximal promoter region of the human vascular endothelial growth factor gene has a G-quadruplex structure that can be targeted by G-quadruplex-interactive agents. *Mol. Cancer Ther.* **7,** 880–889 (2008).

209. Guo, K., Gokhale, V., Hurley, L. H. & Sun, D. Intramolecularly folded G-quadruplex and i-motif structures in the proximal promoter of the vascular endothelial growth factor gene. *Nucleic Acids Res.* **36,** 4598–4608 (2008).

210. Pastukh, V. M., Roberts, J., Clark, D. W., Bardwell, G. C., Patel, M., Al-Mehdi, A., Borchert, G., and Gillespie, M. N. An Oxidative DNA 'Damage' and Repair Mechanism Localized in the VEGF Promoter is Important for Hypoxia-induced VEGF mRNA Expression. *Am. J. Physiol. Lung Cell. Mol. Physiol.* **309,** 1367–1375 (2015).

211. Fleming, A. M., Ding, Y. & Burrows, C. J. Oxidative DNA damage is epigenetic by regulating gene transcription via base excision repair. *Proc. Natl. Acad. Sci.* **114,** 2604–2609 (2017).

212. Cogoi, S., Paramasivam, M., Spolaore, B. & Xodo, L. E. Structural polymorphism within a regulatory element of the human KRAS promoter: Formation of G4-DNA recognized by nuclear proteins. *Nucleic Acids Res.* (2008). doi:10.1093/nar/gkn120

213. Cogoi, S., Paramasivam, M., Filichev, V., Géci, I., Pedersen, E. B. and Xodo, L. E. Identification of a new G-quadruplex motif in the KRAS promoter and design of pyrene-modified G4-decoys with antiproliferative activity in pancreatic cancer cells. *J. Med. Chem.* **52,** 564–568 (2009).

214. Kerkour, A., Marquevielle, J., Ivashchenko, S., Yatsunyk, L. A., Mergny, J. and Salgado, G. F. High-resolution three-dimensional NMR structure of the KRAS proto-oncogene promoter reveals key features of a G-quadruplex involved in transcriptional regulation. *J. Biol. Chem.* **292,** 8082–8091 (2017).

215. Aguilera-Aguirre, L., Bacsi, A., Radak, Z., Hazra, T. K., Mitra, S., Sur, S., Brasier, A. R., Ba, X., Boldogh, I. Innate Inflammation Induced by the 8-Oxoguanine DNA Glycosylase-1 − KRAS − NF- κB Pathway. *J. Immunol.* **193,** 4643–4653 (2014).

ACKNOWLEDGEMENTS

Firstly, I would like to thank my supervisor Prof. Luigi Xodo for the support of my PhD studies and related research and for his great knowledge. His guidance helped me in the time of research and in writing this thesis.

Beside my tutor, I would like to express my sincere gratitude to Valentina Rapozzi, for her encouragement in several situations, for her insightful comments, but also for hard questions which let me widen my research from different perspectives. Thanks to her, I learn to assess the results that I obtain from a critical point of view.

My sincere thanks also goes to my colleagues, especially Giulia, with whom I started my PhD, and Giorgio and another Giulia, who have been worked with me during this last year. We spent a lot of time working together and we discuss about our experiments, comparing ourselves. During my PhD I have been found not only knowledgeable collegues, but also a lot of new friends.

Finally, my thought goes to Susanna, who left us too soon. She taught to me a lot of things about how working with cells and about methodology for several experiments. But, apart from all this, she was a special person that I will certainly never forget.
I will always remember her contagious joy, her desire to smile at life even in the most difficult moments and the passion she put into everything she did. My greatest special thanks goes to her, for being part of my life journey.
I miss you, Susanna.